

NASA's Fuel-Cell Program

Ernst M. Cohn

Head, Electrochemical Technology Projects

NASA, Code RPP, Washington 25, D.C.

The goal of NASA's fuel-cell program is to obtain light-weight, dependable power sources to supply a variety of needs. These may include, for example, communication; command and control; guidance; radar; image acquisition, processing, and transmission; data handling and storage; life support; experiments on environments and planetary surfaces; and motive power for surface-exploration vehicles.

Among the major factors to be considered in the design of space-type fuel cells are (1) the need for very high reliability, because chances for repair are extremely limited even on manned missions; (2) high energy and power densities, because it costs between \$1,000 and \$5,000 to put a pound of substance into space, and our lift capabilities are limited while power requirements keep increasing; (3) the space environment, where gravity is absent or, on the surface of planets, varies from that on earth; where radiation and meteoroids present hazards; where temperatures can fluctuate widely; and where there is no atmosphere to provide oxygen and act as a heat sink.

As this is being written, work is in progress on the low-temperature fuel cell, with an ion-exchange membrane as electrolyte, which will power the Gemini spacecraft and on the intermediate-temperature modified Bacon fuel cell for the Apollo vehicle. The former, estimated to cost \$10 million, and the latter (\$28 million) represent the first functional uses of fuel cells. At the time of this presentation, it will have been decided whether a fuel cell will also power the lunar excursion module of Apollo. These multi-million dollar programs for developing flight equipment far eclipse the much more moderate research and development program of NASA. The former are the responsibility of the Office of Manned Space Flight, the latter of the Office of Advanced Research and Technology (OART).

In fiscal year 1963, OART spent about \$1.25 million on fuel-cell projects ranging from "basic" research to prototype development. On this occasion, I can only select a few examples of our work to illustrate the range of problems it covers and to give you some of the reasons for undertaking these projects.

On a NASA grant, Professor Bockris and his co-workers at the University of Pennsylvania are studying the dynamic behavior of porous electrodes, potentials of zero charge, and differences between chemical and electrochemical catalysis, among other topics. As part of a grant for work on energy conversion in general, this

group is also working on the fundamentals of bioelectrochemistry. We thus hope to acquire basic information that will be useful for all kinds of fuel-cell systems. I shall return to biochemical fuel cells later.

An interesting hybrid between conventional batteries and fuel cells is represented by an idea advanced by Bernard Gruber, who proposes to impregnate a dry tape with anodic and cathodic material, one on each side, and adding electrolyte just before running the tape through two current collectors. By operating in this manner, one can activate the ingredients immediately before use, thus making possible indefinite storage as well as combinations of normally incompatible materials. This work is well underway at Monsanto and promises to yield high-energy-density electrochemical power sources that may compete with both primary batteries and primary fuel cells. The need for storable reactants -- for emergency use or energy-depot purposes -- may also be met by development of fuel cells that have multi-chemical capability and might utilize residual or excess amounts of rocket propellants, such as UDMH and nitrogen tetroxide.

In devising space power systems, we must consider not only the power source but also the equipment that is to be run from it. As a crude rule of thumb, we may assume 25% of the output will be needed as alternating current, 25% as direct current, and the remainder as either AC or DC. Furthermore, various devices will be operated at different voltages. Thus, power "conditioning" is an important factor in considering the electrical system as a whole. Mechanical and/or electric pulsing of fuel cells -- now being studied on grant as well as contract -- may yield advantages of several kinds: Longer operating life, improved resistance to poisoning of catalysts, lower concentration polarization, and greater power output from the fuel-cell battery; and better circuit control and higher conversion efficiency from the over-all system may be obtained by quasi-AC operation. Needless to say, such benefits, particularly as concerns the fuel cell proper, might be even greater in ground applications where hydrocarbons or alcohols are used directly as anodic fuels.

Another task that should benefit both earth and space applications is research on high-performance, thin electrodes that promise drastic cuts in fuel-cell weight and volume. Over the last two years or so we have progressed from perhaps 150 lbs. per kilowatt to about 70 lbs., exclusive of fuel and fuel tankage; 30 to 40 lbs. per kilowatt for fuel cell plus auxiliaries now appears to be in sight.

Work under way at Allis-Chalmers is directed not only at obtaining a space-type, low-temperature, hydrogen-oxygen fuel cell, with an asbestos retainer for the electrolyte; it is also concerned with finding a simple and reliable method for removing heat and water with the least number of mechanical moving parts and minimum need for parasitic power. This goal should be attained by evaporating water through a capillary membrane adjacent to the electrodes, the cavity behind the membrane being evacuated to a pressure corresponding to that of the vapor pressure of the KOH electrolyte at its operating temperature of about 200° F. Operability of such an

arrangement has been demonstrated, control is simple, and temperature is not a critical factor.

Primary fuel cells, i.e., those through which reactants are passed once only, are useful in space only for limited periods. That is because the product of power and duration (=energy) determines the amount of fuel and oxidant that must be carried aloft. For extended missions, therefore, other primary sources of energy must be used. In connection with solar and nuclear energy sources and conversion devices, fuel cells may be used for energy storage, as secondary power sources during periods of darkness (solar primary power), during emergencies, and during periods of peak-power demand. Among the several methods of possible regeneration of reactants from products, only electrolysis and thermal treatment have proven practical thus far. Even so, it is not yet clear whether regenerative fuel cells will be competitive with secondary batteries or other secondary conversion devices.

At present, we have two efforts under way on secondary or regenerative fuel cells. One concerns improvements for a low-temperature hydrogen-oxygen cell, with electrolytic decomposition of water. The other is a K^+ diffusion cell, in which potassium ions are transported through the electrolyte and form an amalgam at the mercury cathode. The amalgam is then decomposed, by heating, into its more or less pure components. Whereas the former device appears particularly suitable for use in connection with solar energy, the latter could receive its primary energy from either solar or nuclear heat.

Biochemical fuel cells captured the public imagination some time ago. Meanwhile, further exploration of this 50-year-old concept has indicated rather severe limitations of power density and energy density for such devices. Nevertheless, they are likely to find specialty uses, even if these limitations cannot be overcome. One such possibility is to consider biocells as energy-saving waste disposals for extended space flights, during which human waste must be reprocessed for attaining a closed or nearly closed ecology. In addition to the grant mentioned earlier, NASA is supporting a three-fold attack on this problem by sponsoring basic, applied, and developmental studies, aimed at finding materials and conditions conducive to degradation of human waste. Since the power consumed in such a device will undoubtedly exceed the theoretical -- let alone the realizable -- power output, this use of bioelectrochemistry is obviously not aimed at power production. If feasible, however, it may prove to require less net energy input than any other approach to waste reutilization. Similarly, biocells might profitably be considered as possible means for solving problems of water pollution, the power produced being a welcome byproduct.

What do we expect from space-type fuel cells? Our immediate, prime considerations are for high power density and reliability. The Gemini and Apollo fuel cells, for example, will have perhaps 1/6 to 1/10 the weight of the best available primary batteries that are capable of delivering the same total amount of energy. Furthermore, the product water will be used by the astronauts, an additional bonus not available from batteries.

Other requirements may become as important or even more so for different space applications. Longevity and ease of maintenance, for example, could well be the desiderata for fuel cells used at a lunar station or depot. Ease of packaging, storing, and converting chemicals to active species (say, hydrogen and oxygen) may determine what types of fuel cell will look most promising for propulsion on the moon or for powering space suits.

Apart from requiring a variety of fuel, each optimized for a particular task, we expect to see a much higher degree of sophistication in the mode of operation of fuel-cell systems. Increasing attention is already being directed toward optimization of controls and operating conditions. Each system must be optimized in such a way as to take advantage of the leeway permitted by its size, components, and operating variables.

Fuel cells will have to become truly integrated into the systems of which they will be parts. I already mentioned biochemical fuel cells as being primary chemical reactors, and the Gemini and Apollo fuel cells as being sources of potable water. Not only byproduct chemicals, but also byproduct heat could be useful in some cases. Once we have reliable information about the composition of the lunar surface, we may need to develop fuel cells particularly suited for lunar purposes and independent of supplies from earth.

This necessarily incomplete discussion of NASA's fuel-cell program will give you a feeling for the difficulties we face and the methods we use in attempting to overcome them. Virtually all of the information thus obtained should be equally as useful for earthbound as for space-type fuel cells. Thus, we hope not only to solve a part of the space power problem, but also to contribute directly to the advancement of fuel-cell technology that will benefit our economy. We are very much interested in your comments on our program and welcome your ideas and suggestions for fulfilling our task, which is to provide NASA with reliable, optimized fuel-cell power that will be applicable to many different jobs under a great variety of space and planetary conditions.

FUEL CELL ELECTRODES FOR ACID MEDIA

Walter G. Taschek

U. S. Army Electronics Research and Development Laboratories
Fort Monmouth, N. J.

The long range goal of fuel cell research is the development of fuel cell batteries operating directly or indirectly on inexpensive fuels, e.g., hydrocarbons, and air as the oxidant. The batteries must operate at high efficiency at practical current densities and have long operational life if they are to compete with present forms of power generation. The batteries must employ electrolytes which are not affected by carbon dioxide. For this approach, acid electrolytes are mandatory. Consequently, a part of our program is concerned with liquid acid electrolytes. Also, the development of an efficient air cathode operating under these conditions is necessary.

Original work was conducted on "Hydrogen and Oxygen Electrodes for Acid Media," and was reported at the 16th Annual Power Sources Conference in 1962.⁽¹⁾ It was found that by means of a new preparation technique for catalyzed, activated carbon electrodes, wetproofed with paraffin, high performance of hydrogen anodes and oxygen cathodes could be obtained. The effect of electrolyte concentration on performance was investigated with 3N, 6N, and 10N sulphuric acid. Little change in performance was observed. In measuring the electrochemical characteristics of the oxygen electrodes, a peculiar effect was observed. This effect is shown in Figure 1. By increasing the current density over 8 mA/cm², a decrease in polarization was observed. However, tests with careful temperature control eliminated this behavior termed "Heat Effect". The life of the paraffin wetproofed electrodes was short. Initial tests made with Teflon wetproofed electrodes showed performances close to that of paraffin wetproofed electrodes.

In continuation of this work, investigations have been conducted on hydrogen, oxygen, and air electrodes operating in liquid, acid media. Various electrode preparation techniques have been used, employing paraffin and Teflon as wetproofing agents. The electrochemical performance of the electrodes has been measured over extended periods of operation.

The carbon electrodes used in these investigations were supplied by Speer Carbon Company, grade 7716, dimensions 1 x 1 x 1/8 inch.

The preparation techniques used most extensively were:

A. Paraffin Treated Electrodes

(1) Activation: The raw carbon electrodes were weighed and then fired in a carbon dioxide atmosphere at 800°C for 8 minutes. After that, the electrodes were cooled in a stream of carbon dioxide to prevent air oxidation of the hot carbon. Finally, the electrodes were weighed and their weight loss calculated. A 7 - 10% weight loss was desired.

(2) Wetproofing: The activated carbon electrodes were immersed in a wetproofing solution for 1/2 hour. The wetproofing solution contained 2 g of paraffin per 100 ml of petroleum ether. The electrodes were then dried by drawing air through the pores for several hours. This was accomplished by means of a

water aspirator. The activated and wetproofed electrodes were then ready for catalyzation with platinum.

(3) Catalyzation: A solution of $H_2PtCl_6 \cdot nH_2O$ was prepared containing from 50 - 100 mg of platinum per ml of solution. The volume of solution which was necessary to cover the electrodes with 2 mg platinum per sq cm of geometric electrode surface was measured. The electrodes were heated in an oven at $200^\circ C$. The solution was then applied to the surface of the hot electrodes with a brush. Finally, the electrodes were placed in a vacuum oven at $150 - 175^\circ C$ for several hours.

B. Teflon Treated Electrodes (Teflon Applied by Immersion)

(1) Activation: Same as with paraffin treated electrodes.

(2) Wetproofing: The activated electrodes were immersed for 15 minutes in a dispersion of Teflon in water, containing 10 ml of Teflon 41-BX per 100 ml of water. Prior to drying, the excess of Teflon resin was rinsed from the carbon surface with distilled water. The electrodes were then dried like in the case of paraffin wetproofing. Teflon 41-BX is a Fluorocarbon resin of hydrophobic negatively charged particles in an aqueous medium of $pH = 10$. The average size of the resin particles is about 0.2 microns. The dispersion was obtained from E. I. DuPont de Nemours, Inc. (2)

(3) Catalyzation: Same as with paraffin treated electrodes.

C. Teflon Treated Electrodes (Teflon Applied by Electrodeposition)

(1) Activation: Same as with paraffin treated electrodes.

(2) Wetproofing: An activated electrode was placed in the electrodeposition bath containing 4 ml Teflon 41-BX per 100 ml water. Figure 2 shows a diagram of the electrodeposition apparatus. A DC power supply connected to a variable resistor served as the source of current. The electrode to be wetproofed was the anode (+) and a platinum strip was the cathode (-). A potential of 6 V was applied across the electrodes and the resulting current was about 65 mA. The distance between the anode and cathode was 1 to 2 inches. Direct current passing through the dispersion of Teflon 41-BX caused the negatively charged dispersed particles to migrate toward the positive carbon anode by electrophoresis. The particles were discharged and deposited there. The only occurrence at the platinum cathode was the evolution of hydrogen gas. It was observed that a heavier deposit of Teflon was formed at the carbon surface facing away from the cathode.

(3) Catalyzation: Same as with paraffin electrodes. The carbon surface lean of Teflon deposits was catalyzed.

A diagram of the cell used to test electrodes is shown in Figure 3. The electrolyte used in all tests was 5N sulphuric acid. All cells were operated at room temperature. Gas pressures of hydrogen, oxygen, and air were maintained at the bubble pressure of the electrode. The bubble pressure was defined as the minimum pressure required to maintain visible bubbling at the electrode-electrolyte interface. The interrupter technique described by Kordesch and Marko was used to eliminate the IR drop in potential measurements. (3) A saturated calomel electrode was used as the reference electrode.

An equation was found that described the polarization behavior of the oxygen or air electrodes. The equation is given by:

$$(1) \log \eta = \log a + \log i$$

η is the polarization in volts, i is the current density in amps per square centimeter, and a and b are constants of the equation. The equation was found to be valid

in the range of current densities from 5×10^{-4} to 10^{-1} A/cm². Its validity could be established for 19 out of 21 current voltage curves using various electrodes. The log-log plot of the polarization versus the current density was obtained by superimposing the measured potential values on the polarization ordinate (Figure 4) and assigning an arbitrary open circuit potential of 1.1 volts for oxygen and air electrodes vs the standard hydrogen electrode. We used an arbitrary open circuit potential since the experimental open circuit potentials are difficult to reproduce from one electrode to the next. The range of the experimental open circuit potentials observed was about 0.8 volts to 1.1 volts. This range is probably caused by mixed potentials whose value depend on various factors. The reversible open circuit potential of 1.229 V was not chosen because related investigations indicate the presence of another reaction mechanism.⁽⁴⁾

The equation (1) can also be expressed in the exponential form:

$$(2) \eta = a i^b$$

Dividing both sides of the equation by i results in:

$$(3) \frac{\eta}{i} = a i^{(b-1)}$$

Grouping $a i^{b-1}$ and setting it equal to the variable term R_1 , the equation is then arranged in the following form:

$$(4) \eta = R_1 i$$

R_1 is a variable term that is a function of the current density i . R_1 can be considered as an over all "Reaction Resistance".⁽⁵⁾

In Figure 5 a conventional Tafel plot is compared with a $\log \eta$ vs $\log i$ plot representing a typical set of data. It can be observed that there is no straight line portion in the Tafel plot. The $\log \eta$ vs $\log i$ plot shows that equation (1) is valid for practical ranges of current density. Deviations occur below current densities of 5×10^{-4} and above current densities of 10^{-1} A/cm². For low polarizations, small errors in experimental measurements are magnified due to the structure of the log-log plot. Above 10^{-1} A/cm², apparent effects of high concentration polarization are observed.

Determination of the constants a and b in equation (3) shows that low polarization is associated with low a values and high b values for b values less than one. No b values greater than one were observed. The high, low, and average values of a , b , and the limiting current density I_1 are tabulated in Figure 6 showing the differences arising from different preparation techniques. The table was compiled from nine trials of A, four trials of B and four trials of C. No significant deviations were observed in average a values for the three preparation techniques, although there was considerable variation in these values from one electrode to the next. Close agreement was found in all b values for techniques A and B, but C showed higher b values and more variation from one electrode to another. However, technique C was connected with strong effects of concentration polarization above current drains of 50 mA per sq cm.

The hydrogen electrodes tested showed low polarization in the order of 50 mV up to 100 mA/cm². No limiting current densities could be observed over the range of current density investigated.

Life tests were conducted on hydrogen and oxygen electrodes with paraffin and Teflon treated electrodes. The electrodes were operated for 8 hours per day. Figure 7 shows the results. Life tests of hydrogen electrodes showed nearly constant performance over all periods of operation.

With Teflon treated oxygen electrodes, over 850 hours of operation were obtained at 10 mA/cm^2 without loss in performance. Previously with paraffin treated electrodes, only 80 hours of operation at 10 mA/cm^2 were obtained before the oxygen cathode failed. It was observed that after 230 hours of operation, the Teflon treated electrodes showed a sharp rise in performance. This potential jump from 0.52 V to 0.76 V vs S.H.E. resulted from an increase of the oxygen gas pressure from 0.13 atm. to 0.35 atm. At the start of the test the bubble pressure for the oxygen electrode was 0.13 atm. This pressure was maintained for 230 hours of operation. It was then observed that the bubble pressure rose to 0.35 atm. The bubble pressure then remained stable from 296 to 850 hours of operation.

From these results it is evident that at relatively low drains of 10 mA/cm^2 , Teflon wetproofing does not impede the electrodes performance, but increases the life of the electrodes considerably over that of paraffin wetproofed electrodes.

In addition to the constant performance test, complete current-voltage curves were taken at 0, 296, and 800 hours. Figure 8 shows the curves for the oxygen electrodes in a $\log \eta$ vs $\log i$ plot. The curves show that a values decreased, b values increased, and I_1 values increased during the course of the life test. This means an increase in performance with aging of the electrode. This can be expected since the Teflon wetproofing initially prevents the electrolyte from making extended contact with the electrode surface. As the life test continues, the electrode surface becomes more wetted and the performance improves. This can be seen from the table in Figure 8. A decrease in the a value and a considerable increase in the b and I_1 values is observed from 0 to 296 hours. After that, little change in these values was observed.

Further, current voltage curves were taken for air cathodes and compared with curves obtained with pure oxygen cathodes. Paraffin and Teflon treated electrodes were used. First, a current-voltage curve was taken of the hydrogen-oxygen cell. Then, after thoroughly flushing the cathode with air for several hours, the second current-voltage curve was taken of the hydrogen-air cell. The results are shown in Figure 9. In both cases the oxygen electrode performed better than the air electrode. The performance of the Teflon treated electrode decreased only slightly when air was used instead of oxygen. In the case of the paraffin wetproofing, the air performance was poor.

In conclusion,

1. Paraffin wetproofed electrodes show high initial performance, but do not have long life.
2. Teflon wetproofed electrodes (by immersion) show excellent life characteristics without loss of electrochemical performance. This has been established so far for current densities up to 10 mA/cm^2 .
3. Teflon wetproofed electrodes (by electrodeposition) show high performance at low current densities, but have low limiting current densities. Life of the electrodes has not been established.
4. It was found that the polarization of oxygen electrodes can be described by the equation $\log \eta = \log a + b \log i$. The equation was found to be valid for the range of current densities investigated.

REFERENCES:

1. Taschek, W.G., Wynn, J.E., "H₂ and O₂ Electrodes for Acid Media" Proceedings of the 16th Annual Power Sources Conference (1962).

2. "Teflon", Inf. Bull. No. X-916, Polychemicals Dept., E. I. DuPont de Nemours & Co., (Inc), Wilmington, Delaware.
3. Kordesch, K., Marko, A., J. El. Chem. Soc., 107, 6, 480 (1960).
4. Wynn, J.E., "A Study of the Cathodic Reduction of Oxygen at Carbon Electrodes in Acid Electrolytes," presented at the Electrochemical Society Meeting, Detroit, Michigan, Oct 61, Extended Abstract No. 25 of Battery Division.
5. Hunger, H., Marko, A., Paper 275 K/11, 5th World Power Conference, Vienna, 1956.

Preparation Technique	a	a	b	b	I_1 (A/cm ²)	I_1 (A/cm ²)
		Average		Average		Average
A	0.72-1.10	0.90	0.12-0.145	0.13	0.07-0.3	0.19
B	0.87-1.05	0.96	0.13-0.14	0.13	0.08-0.2	0.12
C	0.59-1.15	0.89	0.13-0.22	0.18	0.05-0.1	0.08

Figure 6
Tabulation of a, b, and I_1 Values

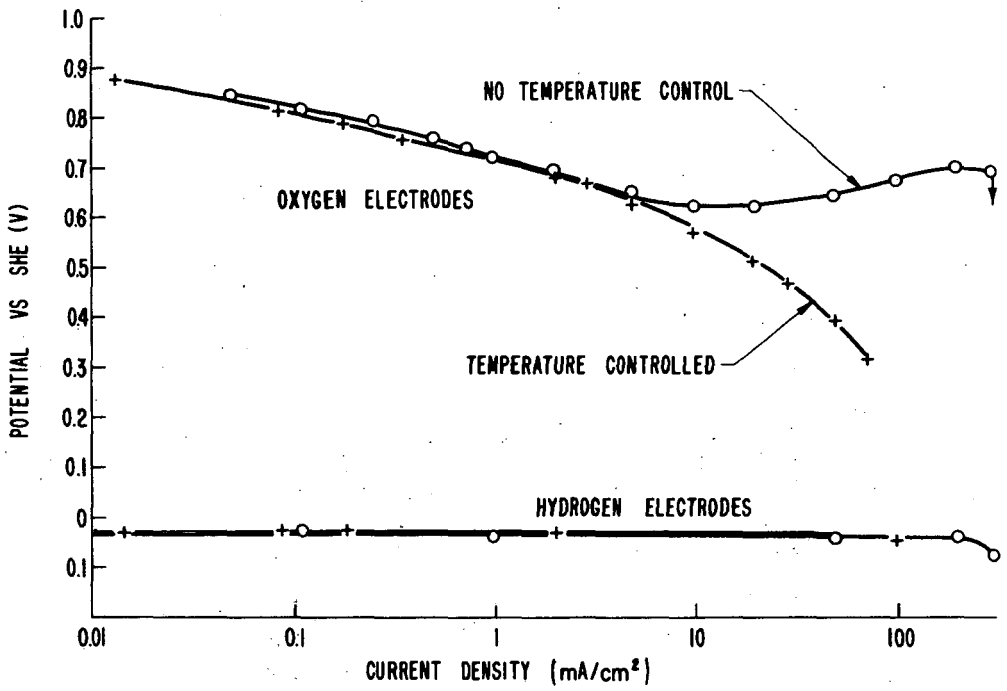


FIG. 1 HEAT EFFECT IN 6NH₂SO₄

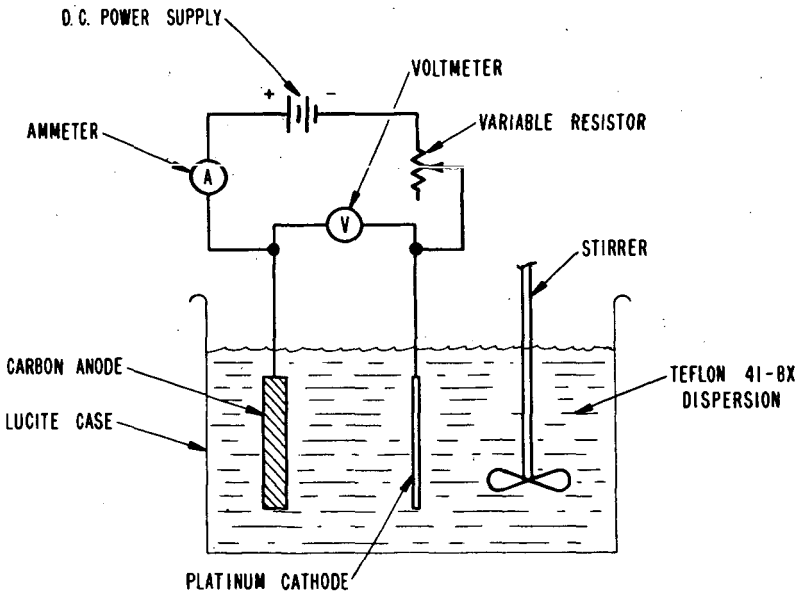


FIG. 2 SCHEMATIC OF ELECTRODEPOSITION APPARATUS

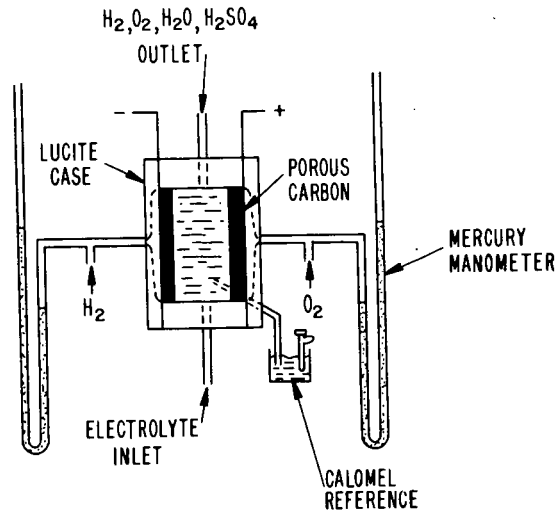


FIG. 3 SCHEMATIC OF EXPERIMENTAL CELL

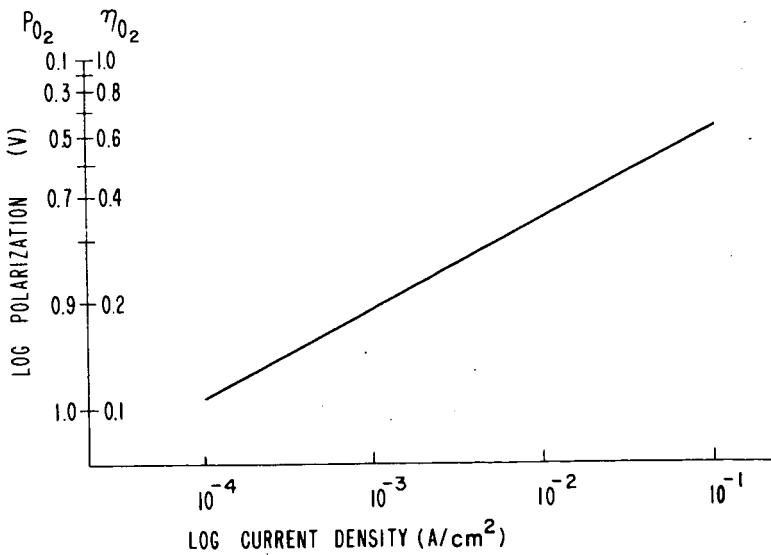


FIG. 4 CATHODE POTENTIAL SUPERIMPOSED ON POLARIZATION ORDINATE

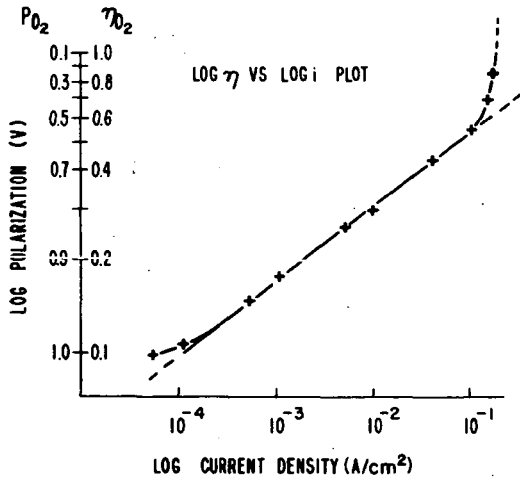
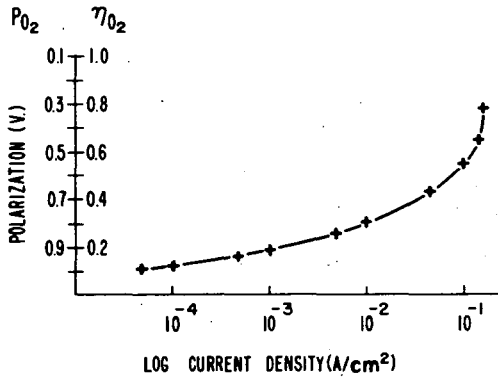


FIG. 5 TAFEL VS LOG η -LOG i PLOT

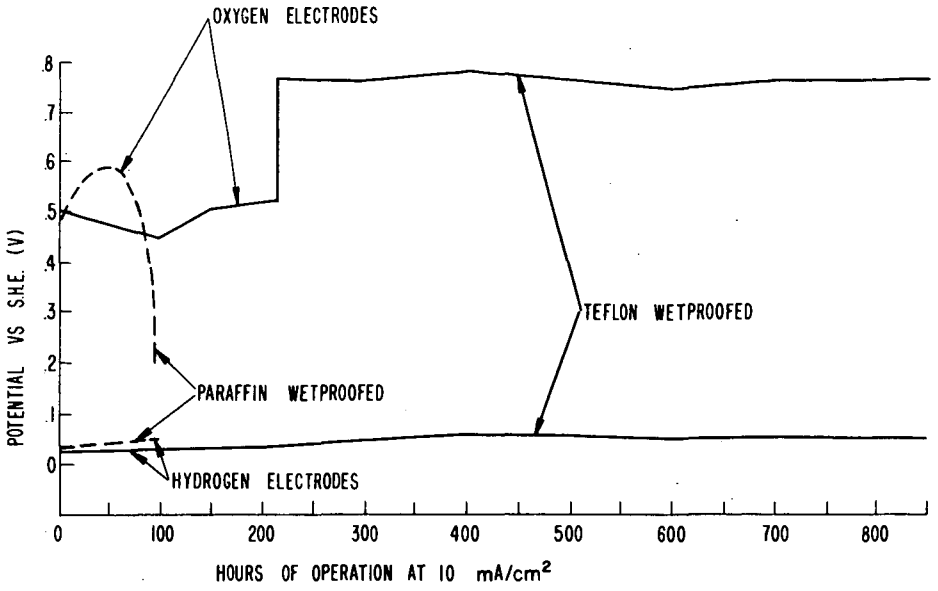


FIG. 7 LIFE TESTS

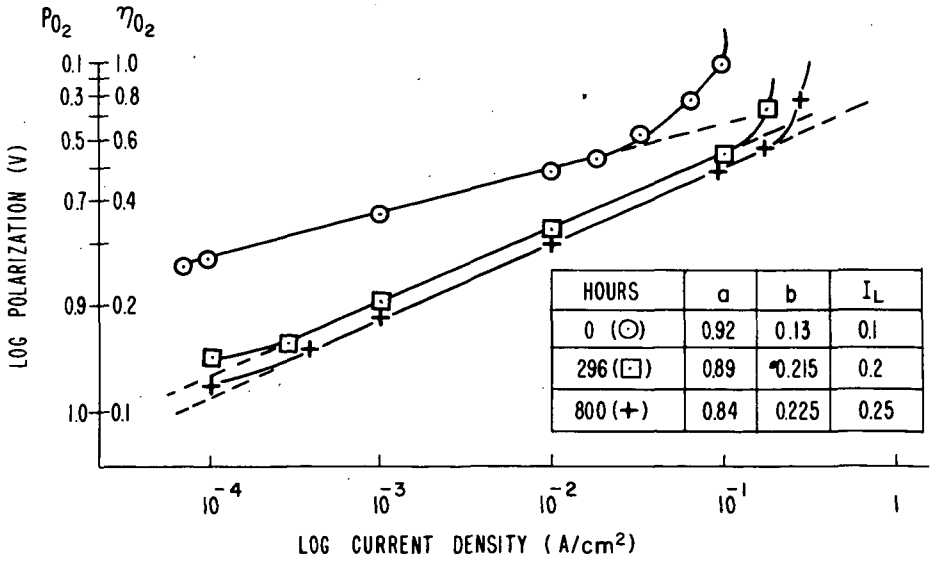


FIG. 8 LOG η - LOG i PLOT AS A FUNCTION OF TIME

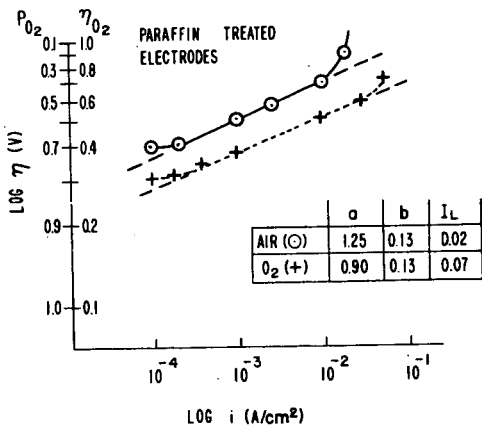
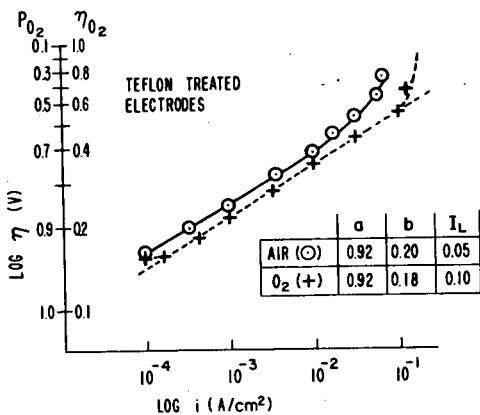


FIG. 9 AIR VS OXYGEN

ELECTROCHEMICAL CHARACTERISTICS OF GRADED POROSITY CARBON ELECTRODES*

Edward A. Heintz, Ronald W. Marek and William E. Parker

Research and Development Laboratories, Speer Carbon Company,
A Division of Air Reduction Co., Inc., Packard Rd. and 47th St.,
Niagara Falls, N. Y.

INTRODUCTION

For the past several years Speer has conducted a comprehensive investigation of porous carbon electrode materials for use in fuel cells. Much of the information obtained from this study has been presented in various reports and papers (1-9). One result of this prior work has been the development of techniques for fabricating, from given formulations, carbon materials in which permeability and macropore distribution can be consistently and predictably varied over wide ranges.

A logical extension of this finding was to prepare carbon electrode materials which exhibit a pore size gradient across their thickness. By further refinements of the techniques, bodies have been fabricated which contain a pre-chosen number of layers of selected pore size distributions. The evenness of these strata and their mutual compatibility during processing is remarkable. To avoid extraneous variation, all layers of each sample are taken from the same formulation and, indeed, from the same basic mix.

The physical properties of these carbon electrodes and their electrochemical characteristics in fuel cell operation are presented below.

EXPERIMENTAL

Electrode Preparation

A formulation of petroleum coke and coal tar pitch was selected for the initial fabrication of these novel materials. A lignon sulfate derivative marketed under the trade name Orzan was used as an additive. The latter is employed as a means of increasing the porosity of the baked carbon through exfoilation during the baking process. The materials were intimately mixed at 135°C. and then crushed to desired size when cooled. The sized materials were then placed in very even layers in a molding die in the chosen sequence and thickness. All samples were

* This work has been partially supported by USAELRDL, Power Sources Branch, Fort Monmouth, New Jersey.

then molded and baked under uniform conditions to yield electrodes of two of three zones of predictable permeability and macropore distribution. The physical properties of these samples are given in Table I.

Samples 1-Pt through 3-Pt were fabricated in similar fashion except that 2 mg of platinum black per square centimeter of geometrical surface were added to the zone marked with an asterisk. These materials were processed under conditions identical to the first set.

Samples 1-Ch through 3-Ch of Table I were identical to Samples 1 through 12 except for substitution of a hardwood charcoal for the petroleum coke used as the filler material in order to obtain very porous, hydrophillic materials. The contact angle with water, given in Table I, is a measure of the hydrophillic, i. e., wetting, character of the material; the lower the angle the more hydrophillic the material. It is readily seen that the charcoal materials are both quite porous and hydrophillic.

Electrochemical Evaluation

Polarization characteristics of carbon electrodes have been determined with the laboratory hydrogen-oxygen fuel cell previously described (10). The entire system was reduced to thermal equilibrium at $25.0 \pm 0.2^\circ\text{C}$. prior to measuring the electrode polarization in order to remove temperature dependent processes from consideration. Sulfuric acid (3.0 N) was employed as the electrolyte. The electrode preparation procedure was varied only in the application of wetproofing where desired. Some electrodes were wetproofed by treating with a solution of 2 g. paraffin per 100 ml petroleum ether (b. p. range $30-60^\circ\text{C}$.) and allowed to dry in air. This was normally followed by catalyzing with 2 mg. platinum black per square centimeter of geometrical surface area as recommended by Taschek (11). Where no wetproofing was applied, the pre-treatment proceeded directly to the catalyzing step. No activation of electrode materials was employed so that the possibility of masking the effects and interactions of electrode process variables, raw materials, etc., could be obviated. The electrodes were studied with a one-inch by one-inch surface in contact with the aqueous electrolyte.

A modified Kordesch-Marko bridge circuit (12) was constructed for interrupting the current during measurement of the electrode potential. This bridge circuit provides for the measurement of combined polarization due to activation and concentration by eliminating the influence of resistance polarization.

DISCUSSION OF RESULTS

Gas Pressure Studies

The pressures of hydrogen and oxygen were varied so that the electrical output could be determined as a function of gas pressure. The maximum pressure used was just less than that needed to cause rapid continuous gas bubbling from the surface of the electrode. The maximum pressure varied with the particular surface facing the electrolyte and the gas involved. In this work that quantity has been termed the "bubble pressure". The description of the porosity gradients for the materials studied is summarized in Table I which shows that a variety of two- and three-layered materials have been prepared. Some have a very coarse zone on one face which de-

TABLE I
Properties of Graded Porosity Electrode
Materials

Sample	Thickness (inches)			Permeability (darcys)			Probable Pore Diameter Range (in microns, μ)			Contact Angle ($^{\circ}$)			Surface Area (m^2/g)		
	of			of			of			of			of		
	Zone I	Zone II	Zone III	Zone I	Zone II	Zone III	Zone I	Zone II	Zone III	Zone I	Zone II	Zone III	Zone I	Zone II	Zone III
1	0.031	0.031	0.031	1.38	0.45	0.14	9->90	5-25	3-7	77.0	32.5	28.0	37.4	56.7	137.7
2	0.031	0.031	0.031	1.38	0.45	0.05	9->90	5-25	3-4	77.0	32.5	27.0	37.4	56.7	158.2
3	0.125	0.031	--	1.38	0.14	--	9->90	3-7	--	77.0	28.0	--	37.4	137.7	--
4	0.125	0.031	--	1.38	0.05	--	9->90	3-4	--	77.0	27.0	--	37.4	158.2	--
5	0.031	0.031	0.031	1.38	1.16	0.76	9->90	8-40	8-20	77.0	79.5	30.0	37.4	71.0	43.3
6	0.031	0.031	0.031	0.24	0.14	0.09	6-14	3-7	3-6	34.5	28.0	39.0	46.5	137.7	181.0
7	0.031	0.031	0.031	1.38	0.76	0.14	9->90	8-20	3-7	77.0	30.0	28.0	37.4	43.3	137.7
8	0.031	0.031	0.031	1.38	0.76	0.05	9->90	8-20	3-4	77.0	30.0	77.0	37.4	43.3	158.2
9	0.031	0.031	0.031	1.38	0.05	1.38	9->90	3-4	9->90	77.0	27.0	77.0	37.4	158.2	37.4
10	0.031	0.031	0.031	0.05	1.38	0.05	3-4	9->90	3-4	27.0	77.0	27.0	158.2	37.4	158.2
11	0.031	0.031	0.031	1.38	0.45	0.33	9->90	5-25	3-5	77.0	32.5	37.5	37.4	56.7	129.3
12	0.125	0.031	--	1.38	0.33	--	9->90	3-5	--	77.0	37.5	--	37.4	129.3	--
1-Pt	0.031*	0.031	0.031	1.38*	0.45	0.14	9->90*	5-25	3-7	77.0*	32.5	28.0	37.4*	56.7	137.7
2-Pt	0.031	0.031*	0.031	1.38	0.45*	0.14	9->90	5-25*	3-7	77.0	32.5*	28.0	37.4	56.7*	137.7
3-Pt	0.031	0.031	0.031*	1.38	0.45	0.14*	9->90	5-25	3-7*	77.0	32.5	28.0*	37.4	56.7	137.7*
1-Ch	0.031	0.031	0.031	0.26	0.35	0.24	1.5-20	1-7	0.9-6	41.5	11.0	16.0	--	--	--
2-Ch	0.031	0.031	0.031	0.24	0.27	0.26	0.9-6	0.9-6	0.9-6	16.0	35.0	27.0	--	--	--
3-Ch	0.031	0.031	0.031	0.26	0.23	0.35	0.9-6	0.9-5	1-6	27.0	26.0	25.0	--	--	--

creases to a finer zone on the opposite face; some are "uniformly coarse" or "uniformly fine"; and some have a coarse zone sandwiched between two fine zones or vice versa. Each material was evaluated with both the "fine" (F) and the "coarse" (C) side facing the electrolyte. The first six materials listed in Table I were also tested in the experimental fuel cell in both a wetproofed (WP) and non-wetproofed (NWP) condition. The next twelve materials were tested only in the non-wetproofed condition.

The observed current density at 0.3 volt polarization and the bubble pressure appear to vary with the surface facing the electrolyte and the application of wetproofing to the electrode material. These data are summarized in Table II for the samples 1 through 12. In a non-wetproofed condition, the graded electrodes usually yield a higher current density at a lower fuel gas pressure when the finer porosity zone faces the electrolyte. In all but one case (Sample 6), it is seen that better performance is attained when the materials are not wetproofed. Even in Sample 6 the non-wetproofed fine zone yields higher current densities on the fine side. This could be interpreted as evidence of increased available active carbon surface together with improved catalyst proximity to this active surface. Sample 6 is the most "uniformly fine" material (or perhaps most like a standard, non-graded electrode) and in this case wetproofing due to paraffin was found to be beneficial.

Another possibility is that the wetproofing treatment inhibits the total contact of catalyst with the electrode and electrolyte due to the fact that part of the catalyzing treatment involves a reheating of the electrode to a temperature well above the melting point of the hydrophobic agent (paraffin). During the heat treatment, while the paraffin is molten, it is probable that a fraction of the catalyst is also wetproofed. If this occurs, then the wetproofed, catalyzed electrode can be regarded as less active than a non-wetproofed, catalyzed electrode and may even result in a somewhat different electrochemical response. To test this hypothesis the following series of experiments were performed: A series of 5 mm carbon discs from the same bulk sample and prepared from identical materials as the graded porosity electrodes were sealed into the end of a glass tube. An electrical contact was made on the inside of the tube to the surface of the carbon. The tube was connected to a source of oxygen and placed into a 3 N sulfuric acid solution as part of a conventional polarographic system in which the carbon discs were the working electrodes. Oxygen pressure was then applied so that a bubble of oxygen was allowed to escape from the carbon disc into the solution at a rate no greater than once every 5 seconds. The potential was then scanned in a cathodic direction using a Sargent Model XXI Recording Polarograph over the range +0.3 to -1.2 v vs S.C.E. Four different electrodes were used: (1) an untreated carbon electrode, (2) a catalyzed but non-wetproofed electrode, (3) a catalyzed and wetproofed electrode and (4) an electrode which was only wetproofed. The first material gave $E_{1/2}$ values which corresponded to the reduction of oxygen to peroxide and the reduction of peroxide to hydroxide. The second material was so active that the size of the disc had to be cut down to 2 mm diameter in order to hold the current response on scale for the same two reductions. Electrode No. 3 gave only a poorly defined response for the second reduction, the first being entirely absent. The last material showed hydrogen evolution as the only electrode reaction. The presence of the wetproofing material inhibited the polarographic response, in probably the same manner in which the fuel cell process is retarded. Wetproofing is thus to be detrimental to optimum electrochemical performance. However, some exceptions to this behavior have been noted, as was seen for Sample 6, above, where the wetproofed sample showed a better electrochemical

TABLE II
 Current Density at 0.3 v Polarization and Bubble Pressure as
 a Function of Wetproofing and Porosity of Electrode Surface

Sample*	Wetproofed				Non-Wetproofed			
	Current Density (ma/cm ²)		Pressure †		Current Density (ma/cm ²)		Pressure †	
	H ₂	O ₂	H ₂	O ₂	H ₂	O ₂	H ₂	O ₂
1F	17.3	31.0	25.8	26.7	28.5	50	37.6	19.7
1C	12.8	13.5	2.1	7.3	23.0	29.5	1.6	1.4
2F	4.4	8.2	103.3	98.1	28.0	70	1.6	99.5
2C	7.3	3.9	101.1	95.7	12.2	18.9	16.3	1.7
3F	1.66	0.93	96.2	97.5	8.4	20	26.7	26.0
3C	15.5	10.00	1.9	48.2	11.8	9.5	1.4	1.1
4F	2.40	1.37	6.3	98.7	9.9	4.6	71.6	73.3
4C	2.75	0.61	3.1	1.7	3.8	1.0	52.4	47.0
5F	2.1	2.24	2.90	37.4	12.5	3.1	55.5	37.5
5C	2.9	0.76	30.0	1.1	5.4	1.3	33.6	32.6
6F	44.0	70	54.1	81.8	9.4	15	31.9	48.3
6C	29.8	1.11	1.6	35.1	15.4	3.35	47.0	2.4
7F					16.0	0.6	78.4	70.0
7C					9.2	2.9	67.0	53.5
8F					--	0.7	58.0	41.5
8C					15.0	1.0	68.8	50.8
9C					11.3	1.2	95.8	71.7
10F					22.0	21.0	31.2	30.9
11F					23.0	14.1	31.0	26.5
11C					17.0	5.8	80.3	84.5
12F					13.5	2.3	40.0	46.2
12C								

*F indicates fine side facing electrolyte, C coarse side; See Table I
 †in cm. of dibutyl phthalate

response. In all other samples wetproofing has a definite inhibiting effect on electrochemical performance. Because of this, it was decided to omit the wetproofing step from the evaluation of all remaining graded porosity electrode materials.

One interesting interpretation of these results can be made by utilizing the capillary transport theory proposed by Hunger (13). It is postulated that the force (i. e., pressure, p) needed to move the gas through a wetproofed capillary (i. e., pore) can be expressed as a function of the radius (r) of the pore, the surface tension (γ) of the electrolyte and the contact angle (Θ) of the meniscus formed between the electrolyte and the porous body. This relationship is expressed by a form of the Washburn equation (14)

$$p = \frac{2\gamma \cos \Theta}{r} \quad (1)$$

When "p" is the maximum pressure which can be applied to the porous body while still maintaining some electrolyte within the capillary, i. e., the bubble pressure, then a limiting value of the pore radius, r , can be calculated for a particular carbon electrode material. The results of such a series of calculations for the first twelve graded porosity materials listed in Table I are given in Table III. A comparison of these calculated pore radii with predicted pore diameter range presented in Table I leads to some interesting conclusions. It is apparent, from the comparison of the predicted and calculated pore sizes that the position of the reaction interface, i. e., the common point in the interior of the electrode material where the gas, electrolyte and electrode meet, varies from one electrode material to another. In some cases the electrolyte apparently diffuses well into the body of the electrode material as is shown by materials 1-WP, 2-WP, 3-WP, 6-WP and 1-NWP in which the calculated limiting pore radii appears not to be in the zone facing the electrolyte, but, rather into the middle or opposite outer zone. In most cases it is also apparent that the reaction interface is not on the apparent surface of electrode material but well within the body of the electrode. For the non-wetproofed materials it is interesting to note that the calculated limiting pore radii are smaller when the finer zone faces the electrolyte than when the coarser zone is in the reacting position. This is true for all the materials save Sample 1 which shows the opposite effect. When the materials are wetproofed, however, it would appear that the paraffin tends to close some of the smaller pores on the finer zone as most of the calculated limiting pore radii are larger than, or about the same magnitude as, the values obtained for the coarser zone. For those materials which have not been wetproofed the position of the reaction interface depends on the material. Referring to Table III, it is apparent that when the fine zone of Sample 1 is facing the electrolyte the limiting pore radius is 15.35 μ indicating that the reaction interface is at least in the middle zone or at the interface between the coarser and middle zone. When the coarser side faces the electrolyte the limiting pore radius decreases to an extent that the reaction interface must be in the fine zone. Thus the electrolyte appears to diffuse through two zones into the finer zone to react with the fuel gas. For Sample 1, when the coarse zone faces the electrolyte, the presence or absence of a hydrophobic paraffin coating makes little difference with respect to the position of the reaction interface. Apparently, the interface location is a function of the diffusability of both the fuel gas and the electrolyte, as well as the factors given in Equation 1. In the case of Sample 2 the untreated material is easily wet by the electrolyte as evidenced by the low contact angles ($F-28^\circ$, $C-77^\circ$). When the material possesses a hydrophobic film on the surface, however,

TABLE III
Electron Change (Δn) Values and Calculated Limiting Pore Radii
for the Oxygen Electrode

Sample*	Limiting	Bubble	E_0		O.C.V.		
	Pore Radius	Pressure,	at 1 atm	vs NHE	Δn^+	H_2	O_2
	μ	atm.					
1-F-WP	5.56	0.0730	--	NNB	-0.026	0.886	
1-C-WP	4.17	0.0975	0.797	3.38	-0.043	0.816	
2-F-WP	5.45	0.0745	0.810	2.27	-0.034	0.905	
2-C-WP	4.18	0.0970	--	--	-0.039	0.770	
3-F-WP	4.12	0.0985	--	NNB	-0.028	0.878	
3-C-WP	4.10	0.0900	--	NNB	-0.046	0.666	
4-F-WP	4.06	0.1000	0.785	0.83	-0.039	0.859	
4-C-WP	21.20	0.0191	0.782	3.48	-0.031	0.811	
5-F-WP	8.08	0.0502	0.808	2.27	-0.022	0.842	
5-C-WP	14.00	0.0290	--	NNB	-0.023	0.869	
6-F-WP	8.60	0.0471	0.832	0.75	-0.014	0.855	
6-C-WP	4.93	0.0825	0.786	2.82	-0.016	0.889	
1-F-NWP	15.35	0.0199	0.737	2.20	-0.017	0.857	
1-C-NWP	3.41	0.0972	0.843	4.18	-0.035	0.845	
2-F-NWP	1.30	0.1005	0.817	2.56	-0.020	0.929	
2-C-NWP	9.18	0.0360	0.765	1.42	-0.018	0.827	
3-F-NWP	2.76	0.0354	--	NNB	-0.017	0.944	
3-C-NWP	6.33	0.0523	--	NNB	-0.034	0.904	
4-F-NWP	1.76	0.0740	0.832	3.87	-0.027	0.928	
4-C-NWP	6.85	0.0480	--	NNB	-0.042	0.939	
5-F-NWP	3.32	0.0380	0.970	0.94	-0.040	0.879	
5-C-NWP	9.95	0.0333	1.025	0.89	-0.025	0.939	
6-F-NWP	1.77	0.0645	--	NNB	-0.016	0.897	
6-C-NWP	20.60	0.0248	0.730	1.42	-0.017	0.859	
7-F-NWP	5.50	0.0707	0.772	1.59	-0.019	0.934	
7-C-NWP							
8-F-NWP	2.40	0.0540	--	NNB	-0.021	0.976	
8-C-NWP	7.83	0.0420	0.793	2.60	-0.027	0.947	
9-C-NWP	6.40	0.0515	0.985	0.76	-0.020	0.900	
10-F-NWP	1.79	0.0725	0.887	0.92	-0.011	0.811	
11-F-NWP	3.72	0.0311	0.789	4.20	-0.019	0.769	
11-C-NWP	12.26	0.0268	--	NNB	-0.026	0.781	
12-F-NWP	1.36	0.0855	0.929	0.77	-0.008	0.848	
12-C-NWP	7.00	0.0468	--	NNB	-0.030	0.845	

*F signifies fine side facing electrolyte; C coarse side, See Table I

Average $E_0 = 0.832$ vs N. H. E.

†NNB = Non Nernstian behavior

there appears to be deeper penetration of the electrolyte from the fine side than when this film is absent. The small limiting pore radius of 1.30μ is well within the $3-4\mu$ diameter range expected for the unwetproofed fine zone of Sample 2. This low limiting pore radius indicates that the reaction interface is apparently at or just under the geometrical surface, in the fine zone. Apparently, the hydrophobic film present in wetproofed materials is not the only controlling factor influencing the diffusion of the electrolyte and the position of the reaction interface. Sample 6 gives a very unusual limiting pore radii for both its fine and coarse zones. When the fine zone faces the electrolyte it is quite apparent that the reaction interface can only be in the fine zone. When the coarse zone faces the electrolyte the calculated limiting pore radius is larger than the pores expected to be present in the material. Either the reaction is occurring at the "real surface" of the electrode or the material has developed unusually large and unexpected pores during fabrication. Samples 7 through 12 show limiting pore radii which are consistent with the pore size of the zone facing the electrolyte. Because Samples 9 and 10 are made up of a fine zone sandwiched between two identical coarse zones and a coarse zone sandwiched between two identical fine zones, respectively, it is impossible to determine which zone contains the reaction interface.

It has been suggested (15) that the concentration of the catalyst in a preferential location within the body of the material may influence the observed variation of the position of the limiting pore radius. To test this possibility, a series of materials duplicating Sample 1 were prepared in which 2 mg. of platinum black per square centimeter of geometrical surface area was added to one zone per sample. These materials were then examined in the fuel cell in the same manner as the other graded porosity materials. If the location of the catalyst exerts a preferential effect then the calculated limiting pore radius should be in the range of the zone which contains the catalyst. Sample 1 was chosen because its three zones represent a coarse, medium and fine porosity. The results of this study are summarized on Table IV in which Sample 1-Pt contains the catalyst in the coarse zone, Sample 2-Pt contains the catalyst in the middle zone and Sample 3-Pt has the catalyst in the fine zone. The results are, at best, inconclusive as to the relationship between limiting pore radius and catalyst position. Sample 1-Pt definitely shows that the limiting pore radius and thus the reaction interface is not in the fine zone, regardless of which side faces the electrolyte. However, the values obtained for the limiting radius leave considerable doubt as to whether the reaction interface is in the coarse (outside) or middle zone. For Samples 2-Pt and 3-Pt the location of the reaction interface appears to depend on which side of the electrode is facing the electrolyte. The values obtained for the limiting pore radius suggest that the reaction interface appears to be located in the zone facing the electrolyte. If diffusion into the bulk of the electrode material does occur, then these calculated radius values strongly suggest that the deepest electrolyte penetration is only into the middle zone. A similar conclusion can be obtained by inspection of the limiting pore radii given for the non-wetproofed samples in Table III.

The presence of a foreign hydrophobic material like paraffin apparently alters the physical as well as the electrochemical nature of the electrode material by filling up the smaller pores as well as covering the entire material with a fine film. In this respect, it is interesting to note that the bubble pressures are usually higher for a given material when it has been treated with paraffin. This can be explained if it is assumed that the wetproofing treatment tends to fill the smaller pores,

reduce the diameter of the larger pores and, perhaps, reduce the number of complete routes through the material in which a gas and/or electrolyte can flow.

Two standard, single-layered electrode materials made from the same raw materials as the graded porosity electrodes were also run at varying gas pressures. These results are given in Table V. Both these materials were wet-proofed before testing. It is seen that the finer material has the larger limiting pore radius, indicating that some of the smaller pores were filled with paraffin. These data are admittedly limited but it is interesting to note, as described in greater detail below, that the electron change values correspond to a peroxide or hydroperoxide mechanism at the reaction interface. This corresponds rather well with the assumed change using the layered, graded porosity materials described above.

TABLE IV
Electron Change (Δn) Values and Calculated Limiting Pore Radii for the
Oxygen Electrode at Platinum Loaded Materials

Sample	Limiting Pore Radius, μ	Bubble Pressure, atm.	E_0 at 1 atm vs N. H. E.	Δn	Open Circuit Voltage at Bubble Pressure	
					H ₂	O ₂
1-Pt-F	5.30	0.0242	0.857	3.50	-0.191	0.831
1-Pt-C	7.06	0.0465	1.042	1.26	-0.179	0.944
2-Pt-F	3.76	0.0345	1.015	3.75	-0.062	0.002
2-Pt-C	12.00	0.0273	1.000	2.15	-0.196	0.961
3-Pt-F	3.13	0.0413	0.962	2.73	-0.139	0.934
3-Pt-C	17.00	0.0193	1.070	2.64	-0.206	0.916

Average $E_0 = 0.991$ v vs N. H. E.

The open circuit voltages (O. C. V.) of the materials listed in Tables III, IV, and V provided some intriguing results. For the materials in Table III it is noted that generally the non-wetproofed materials have a higher O. C. V. than the wetproofed materials. Also, it is apparent that when the finer zone of a given electrode faces the electrolyte a higher O. C. V. is obtained regardless of the presence or absence of a hydrophobic agent. There are some exceptions to this, as for example Sample 5, but these occur in the materials in which the graded porosity is less extreme. The addition of platinum to the various layers during fabrication appears to enhance the values of the open circuit voltages. While the data in Table V is limited, the trend with respect to the fine-coarse-open circuit voltage relationship is consistent with that of the other materials.

Table VI lists the electrochemical performance of the charcoal materials. Unlike the former materials, charcoal based carbons are easily "wet" by aqueous solutions. Thus the limiting pore radius at the bubble pressure indicates a large amount of diffusion within the electrode by the electrolyte. The bubble pressures are all very low indicating the probable existence of a large number of continuous pores through the material.

TABLE V
Properties and Electrochemical Performance of Standard Electrodes

Sample	13	14*
Permeability (darcys)	0.285	0.366
Probable Pore Diameter (μ)	2-9	1.5-9
Calculated Limiting Pore Radius (μ)	3.60	2.22
Bubble Pressure (atm.)		
H ₂	0.0395	0.0520
O ₂	0.0350	0.0550
E ₀ at 1 atm. (vs N.H.E.)	0.840	0.892
Δn	1.8	2.5
Open Circuit Voltage		
H ₂	-0.017	-0.016
O ₂	0.859	0.782

- Basal planes of crystallites in this sample orientated perpendicular to surface of material; other sample orientation is parallel.

TABLE VI
Electron Change (Δn) Values and Calculated Limiting Pore Radii for the Oxygen Electrode at Charcoal Materials

Sample	Limiting Pore Radius, (μ)	Bubble Pressure atm.	E ₀ at 1 atm vs N.H.E.	Δn^{\dagger}	Open Circuit Voltage at Bubble Pressure	
					H ₂	O ₂
1-Ch-C	4.92	0.0222	0.740	1.65	-0.022	0.799
1-Ch-F	10.01	0.0141	0.595	1.45	0.043	0.699
2-Ch-C	3.81	0.0370	0.727	3.87	-0.019	0.749
2-Ch-F	7.65	0.0170	0.820	5.80	-0.016	0.839
3-Ch-C	7.52	0.0173	0.675	3.92	-0.022	0.699
3-Ch-F	7.07	0.0187	--	NNB	-0.022	0.739

[†]NNB = NonNernstian Behavior

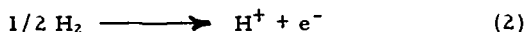
Average E₀ = 0.771 v vs NHE

Current Density (ma/cm²) at 0.3 v Polarization and Bubble Pressure

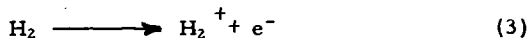
	H ₂	O ₂
1-Ch-C	4.6	17.5
1-Ch-F	5.2	4.5
2-Ch-C	4.5	6.0
2-Ch-F	6.2	--
3-Ch-C	5.2	4.8
3-Ch-F	4.7	6.8

It will be noted that the finer materials (increasing sample number corresponds to increasing fineness) give higher oxygen electrode current densities at lower polarization in the non-wetproofed condition. The hydrogen electrode showed little correlation with respect to electrochemical performance and fineness of the electrode material. Generally, higher current densities at lower polarizations are obtained for non-wetproofed materials for both the hydrogen and oxygen electrodes. This indicates that there is an inhibiting effect caused by the wetproofing agent on charcoal materials similar to the effect described for electrodes made from other fillers. The effect would be expected to be greater for the charcoal filler materials than for the standard filler materials in that the untreated materials are very hydrophilic. When these easily wet materials are treated with the paraffin in the wetproofing process it would be expected that great changes would be produced in electrochemical performance. However, the open circuit voltages of these charcoal based materials give a reverse response to wetproofing compared to the other materials in this study. Usually, non-wetproofed materials have higher open circuit voltages than wetproofed materials. In the case of charcoal based electrodes, wetproofed samples gave superior performance for both the hydrogen and oxygen electrodes.

While both the hydrogen (anode) and oxygen (cathode) electrodes showed definite bubble pressures which varied with the particular electrode material, only the oxygen electrode showed a large variation in open circuit potential with gas pressure. The variation in O. C. V. of the hydrogen electrode was in the order of 5 millivolts or less for hundred fold changes in pressure. This is probably because the reaction at the hydrogen electrode is a simple one electron change given by

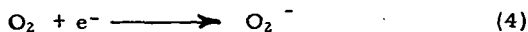


or if the molecule is considered to react in a step wise fashion then

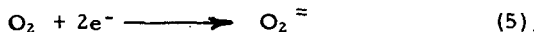


The existence of H_2^+ is considered to be very transitory (16, 17) so that the possibility of a long half-life can be discounted. Gaseous hydrogen also has a rate of diffusion some four times greater than oxygen and is considerably more soluble in an aqueous electrolyte of low pH than is oxygen.

Oxygen, on the other hand, has the possibility of undergoing several reactions at the cathode, all of which vary in the electron change per mole of oxygen. Under the proper conditions one mole of oxygen can add one electron to form the perhydroxyl ion as shown by



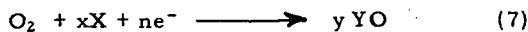
Oxygen can also add two electrons to form the doubly charged peroxide ion



And, finally, oxygen can add four electrons to form the oxide ion



A general reaction can be written to cover all three cases which takes the form



in which n is the electron change, X is a species such as C , Pt or H^+ present in the system and YO is either a surface carbon-oxygen complex or some compound with Pt (i. e., PtO , PtO_2) or H^+ (i. e., HO_2 , H_2O_2 , HO_2^- , or H_2O). Substituting the factors of equation (7) into the Nernst equation one obtains

$$E = E'_O + \frac{RT}{nF} \ln \left[\frac{a_X^x P_{O_2}}{a_Y^y O} \right] \quad (8)$$

in which "a" signifies the activity of the various reactants and products, P_{O_2} is the pressure in atmospheres of gaseous oxygen and the other symbols have their usual electrochemical significance. If only the pressure of oxygen (P_{O_2}) is varied then a_X^x and a_Y^y become constant and E'_O will equal E_O , the standard electrode potential. Substituting the numerical values for the constants in equation (8) and reducing to \log_{10} the equation becomes

$$E = E_O + \frac{0.059}{n} \log P_{O_2} \quad (9)$$

at 298.16°K. A plot of the observed potential versus the \log of P_{O_2} should yield a straight line with a slope equal to $n/0.059$. Further, at P_{O_2} equal to 1 atmosphere it is seen that E equals E_O . Such a plot for a typical electrode is shown in Figure 1. Thus, it should be possible to obtain an indication as to which of the reactions given in equations (4), (5) and (6) may be occurring at the cathodic reaction interface. Such an approach has been used recently in a study of the rest potentials of the oxygen-platinum-acid system (18).

A tabulation of the Δn values calculated using the above technique is given in Tables III, IV, V, VI along with other electrochemical observations. Some of the carbons tested gave a non-Nernstian behavior pattern (i. e., $\log P_{O_2}$ versus E observed lines not linear) and these materials are marked "NNB" under the Δn heading. For those samples that have been wetproofed (Table III), it is noted that when the coarser side of the carbon body is facing the aqueous electrolyte the Δn value is predominantly in the 3 to 4 electron region. This is an indication that the reaction occurring at the gas-electrode-aqueous interface (i. e., the reaction interface) is due to the reduction of oxygen directly to the dinegative state (i. e., an oxide ion). On the finer side, however, the electron change is in the 1 to 2 region indicating formation of perhydroxyl (O_2^-), peroxide (O_2^{2-}) or hydroperoxide (HO_2^-) at the reaction interface. For the non-wetproofed materials it is apparent that the predominant electron change is in the 1 to 2 range indicating the formation of perhydroxyl or more probably hydroperoxide intermediates at the pH values employed in this study. There appears to be no rigorous relationship between limiting pore radii, or bubble pressure, and the Δn values in the materials under study. The average E_O value is 0.832 ± 0.059 vs the N. H. E. Using data from a standard source of electrode potentials (19) it is seen that this value does not correspond to the formation of HO_2 , H_2O_2 , or H_2O . The average E_O , as well as the individual values, do, however, fall well within the range of the listed values for the formation of some substituted quinones. The formation of such a species on the surface of a carbon body is quite possible as their presence has been determined on certain carbons by polarographic (20) and spectrophotometric (21) techniques. The fact that the E_O values have a wide variation indicates the influence of various functional groups, in different positions relative to the quinone groups, on the standard potential.

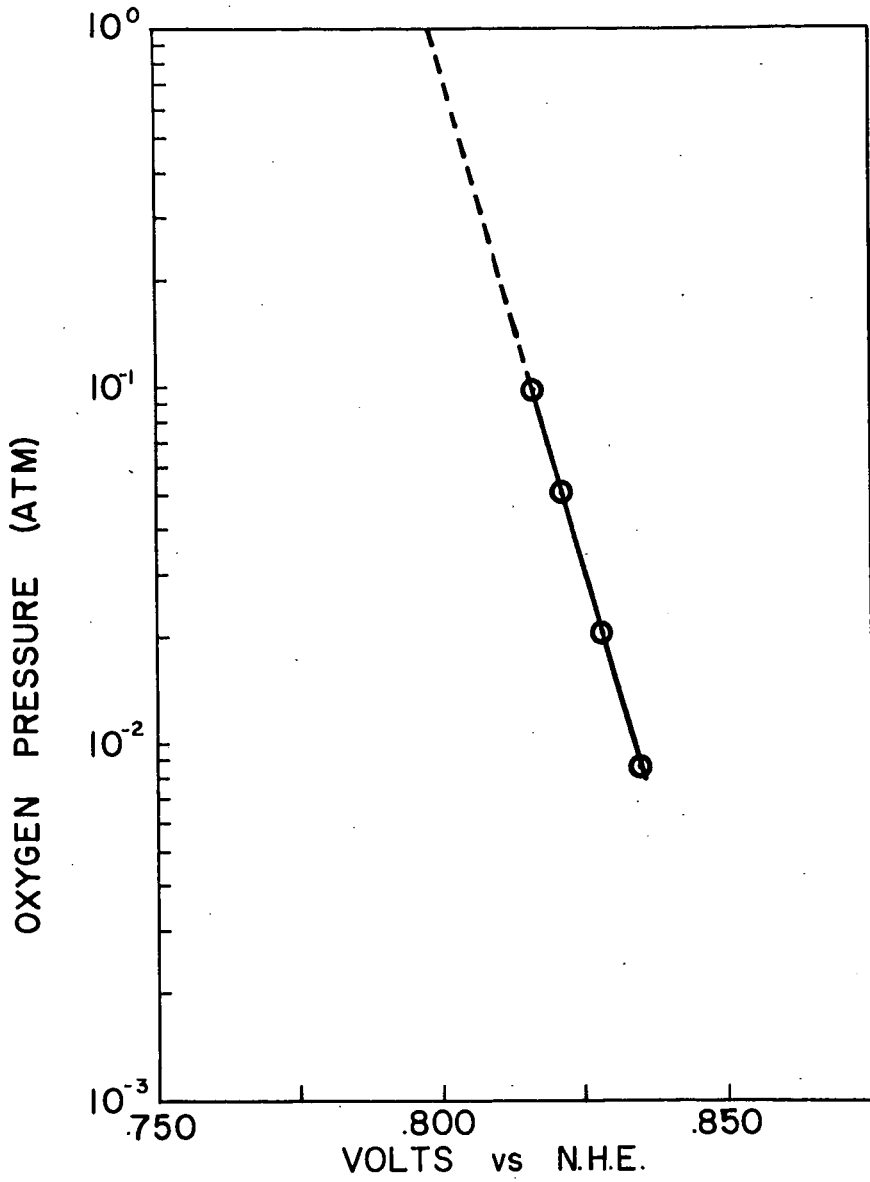


FIGURE I
LOG O_2 PRESSURE VS. OBSERVED POTENTIAL
SAMPLE I-C-WP (536-29-1)

When platinum black is incorporated into the electrode materials during the fabricating process the electron change values appear to be radically different. In these materials the reaction at the interface seems to proceed directly to the oxide ion rather than through the intermediate, less negative, perradical as shown in Table IV. The E_0 value for electrodes containing platinum black is 0.991 ± 0.054 v vs the N. H. E., a good indication that a different reaction is occurring since the value is quite different from that found for similar materials catalyzed in the standard manner. For the quinone-hydroquinone system, higher E_0 values indicate more highly substituted aromatic structures similar to those which could be expected on a carbon surface.

The use of charcoal as a filler material results in electron change values which depend, to a degree, on the pore size of the electrode. The data for samples with coarser pores indicates reduction of the oxygen to a peroxide or hydroperoxide stage. The average E_0 obtained for these materials is 0.711 ± 0.063 v vs the N. H. E. indicating the presence of less complicated aromatic ring structures (19) on the surface. The calculated limiting pore radii of these materials vary only slightly from one material to another, even though the expected change is a twenty-fold variation. This effect could be caused by the fact that these materials are readily wet by the electrolyte as shown by their extremely low contact angles.

The wide range in E_0 values obtained could well be due to the nature of the porous electrode material. In comparison with solid, impermeable electrode materials, porous electrodes possess a larger (by orders of magnitude) contact area per unit volume of electrolyte, reactant and electrode. Because of this there can be a range of reactions, occurring at different reaction rates, within the pores. The distribution of these reactions and the predominance of one or more of these will be a function of the physical structure of the electrode matrix as well as the environment in which the electrode material is placed (22, 23). Also, because of the porous nature of the electrode material, concentrations of reacting species are constant only at the instant the circuit is closed (i. e., commencement of current flow) so that reaction distributions can be quite non-uniform within the electrode matrix. Thus linear polarization may occur only at very low overpotentials where the electrode reaction is initiated. As the reaction interface proceeds further into the matrix of the electrode, the predominating electrode reaction becomes less uniform in its distribution and more complex in its nature. The wide variation in electron change values, Δn , can be considered as evidence for the complexity of the reactions at the reaction interface on a "carbon surface". The Δn and E_0 values listed in Tables III, IV, V and VI are most probably those for the rate controlling step at the reaction interface so that it is quite probable that some carbons have surface properties which enhance the formation of one quinone intermediate over another. On a given carbon the formation of a simple quinone group,

$O = \overset{\text{C}}{\text{C}} = \overset{\text{C}}{\text{C}} = O$, may occur. On a second carbon, or at another reaction site

on the same carbon, the formation of a degenerate quinone grouping such as $\overset{\text{C}}{\text{C}} = \overset{\text{C}}{\text{C}} - O - O - \overset{\text{C}}{\text{C}} = \overset{\text{C}}{\text{C}}$ could be favored prior to a rearrangement to the quinone grouping. Considerably more experimental work is needed before a firmly supported mechanism can be postulated.

No attempt was made to interpret the electrochemical data in terms of Tafel slopes (17) derived from activation polarization data since linear polarizations were obtained only at very low overpotentials, at the initiation of the electrode reaction, due to the heterogeneous nature of a porous electrode. In addition, other investigators have also reported (24) that fuel cell systems do not yield linear polarization curves.

CONCLUSIONS

The electroreduction of oxygen at a porous carbon cathode in 3.0 N sulfuric acid in a fuel cell system appears to proceed through a quinone-hydroquinone reaction based on the comparison of measured potentials with standard potentials. The initial step in the reduction of oxygen may proceed via a one electron change to hydroperoxyl (HO_2), a two electron change to peroxide (H_2O_2) or hydroperoxide (HO_2^-) or a four electron change to water (H_2O) depending on the particular carbon material serving as the electrode. When the electrode material has been wetproofed the reduction is directly to the oxide ($\Delta n \sim 4$) state when the coarser side faces the electrolyte and to either the perhydroxyl or hydroperoxide ($\Delta n \sim 1$ or 2) when the finer zone is facing the electrolyte.

For non-wetproofed materials the electron change is apparently a function of the particular electrode surface facing the aqueous electrolyte, perhaps indicating the relative ease of formation of one substituted quinone-hydroquinone group versus another. No direct correlation between pore size distribution and electron change values is apparent. Generally, however, zones of finer porosity tend to give higher Δn values than coarser zones when a platinum black catalyst has been fabricated into the electrode material. This could be due, in part, to the increased resistance offered by the electrode matrix to diffusion resulting in more complete oxygen reaction.

The limiting pore radii of the graded porosity electrodes were calculated in order to define the position of the reaction interface within the electrode matrix. When the materials had been wetproofed by the addition of paraffin it was shown that the reaction interface was probably in the same location regardless which porosity zone faces the electrolyte. This could be explained on the basis that the wetproofing process plugged the smaller pores in the electrode, producing an electrode material without a porosity gradient. For non-wetproofed materials, the limiting pore radii showed that the reaction interface was located closer to the zone facing the electrolyte. This is an indication that the aqueous electrolyte does not penetrate the electrode matrix as deeply as the gas in the graded porosity materials. There was no correlation of electron change and/or extrapolated standard potential with the calculated limiting pore radii. When hardwood charcoal was substituted for petroleum coke as a filler material, the extrapolated standard potential indicates that a less substituted quinone-hydroquinone system may be present at the surface. Since the limiting pore radii for these materials were not appreciably different from the petroleum coke materials, it appears that material differences are the principle contributory factors to this effect.

BIBLIOGRAPHY

- 1) W. E. Parker, R. W. Marek and E. A. Heintz, "Fuel Cell Electrode Materials", U. S. A. E. L. R. D. L., Contract No. DA 36-039 SC-88954, Report No. 1, 1 March 1962 - 31 May 1962.
- 2) ibid., Report No. 2, 1 June 1962 - 31 August 1962.
- 3) ibid., Report No. 3, 1 September 1962 - 30 November 1962.
- 4) ibid., Report No. 4, 1 December 1962 - 28 February 1963.
- 5) W. E. Parker and F. Rusinko, Jr., "Development of Electrode Materials for Fuel Cells", U. S. A. S. R. D. L., Contract No. DA 36-039 SC-85356, Report No. 1, 1 July 1960 - 30 September 1960.
- 6) W. E. Parker, F. Rusinko, Jr. and R. W. Marek, "Development of Electrode Materials for Fuel Cells", U. S. A. S. R. D. L., Contract No. DA 36-039 SC-85356, Report No. 2, 1 October 1960 - 31 December 1960.
- 7) ibid., Report No. 3, 1 January 1961 - 31 March 1961.
- 8) ibid., Report No. 4, 1 April 1961 - 30 June 1961.
- 9) ibid., Report No. 5, 1 July 1961 - 30 September 1961.
- 10) F. Rusinko, Jr., R. W. Marek, W. E. Parker, and J. E. Wynn, Proc. 15th Annual Power Sources Conf., p 9, 1961.
- 11) W. Taschek, U. S. A. E. L. R. D. L., private communication.
- 12) K. Kordesch and A. Marko, J. Electrochem. Soc., 107, 480 (1960).
- 13) H. Hunger, "Investigation of the Hydrogen-Oxygen Fuel Cell", U. S. A. S. R. D. L., Technical Report No. 2001, 15 December 1958.
- 14) H. L. Ritter and L. C. Drake, Ind. Eng. Chem., 17, 782 (1945).
- 15) H. Hunger, U. S. A. E. L. R. D. L., private communication.
- 16) M. Stern and A. L. Geary, J. Electrochem. Soc., 104, 56 (1957).
- 17) G. Kortum and J. O'M. Bockris, "Textbook of Electrochemistry", pages 418-60, Elsevier Publishing Co., New York, 1951.
- 18) J. P. Hoare, J. Electrochem. Soc., 109, 858 (1962).
- 19) W. L. Latimer, "The Oxidation States of the Elements and Their Potentials in Aqueous Solution", Prentice-Hall, Inc., New York, 1952.
- 20) J. Hallum and H. V. Drushel, J. Phys. Chem., 62, 110 (1958)
- 21) R. E. Test and R. S. Hansen, "Acid Base Properties of Carbon Black Surfaces", AEC Report No. IS-341, May 1961.
- 22) J. Euler and W. Nonnenmacher, Electrochim., Acta., 2, 268 (1960).
- 23) J. S. Newman and G. W. Tobias, J. Electrochem. Soc., 109, 1183 (1962)
- 24) J. VanWinkle and W. N. Carson, Electrochem. Tech., 1, 18 (1963)

A MODEL FOR ANALYSIS OF POROUS GAS ELECTRODES

E. A. Grens II,* R. M. Turner, and T. Katan

Materials Sciences Laboratory
 Lockheed Missiles & Space Company
 Sunnyvale, California

The porous gas electrode, usually with oxygen or hydrogen as the reactant gas, has found wide application in fuel cell systems. The charge transfer reactions for such electrodes occur under conditions quite different from those at a plane electrode surface; the transport of current and reacting species to and from the reaction sites and the location of these sites must be considered in establishing overpotential-current density curves for these half cells. Several investigators have considered this problem, and from several separate points of view (1 - 5). Various models have been used, corresponding to different liquid configurations in the pores, to different methods of reactant transport, and to different local electrode overpotential relationships at the reaction site. The results have varied as widely as the models. Some may correspond to one type of electrode, electrolyte, and operation; some to another. The present treatment analyzes porous gas electrodes in which the electrolyte wets the pore walls. This situation commonly occurs, except where pore walls have been purposefully rendered lyophobic to prevent flooding, a practice necessary only where the electrolyte gas interface is not fixed by pore geometry.

The ability of the electrolyte to wet the pore walls generates a liquid film covering the walls of part of the gas-filled portion of the pore. The electrode reaction takes place beneath some portion of this film, where the gaseous reactant can reach the reactant site. Will (4) has shown that the reactant must be supplied by diffusion of dissolved gas through the film. However, in Will's analysis of his model, assumptions are made which restrict consideration to those cases where dissolved gas diffusion is the only rate-determining process. This can be the case only where reaction exchange current densities are large compared with the limiting diffusion currents through the film. Since the latter must be on the order of 0.02 amp/cm² in pores of micron order,** exchange current densities larger than usually accepted for many gas reactions (e. g. , O₂) would be necessary for diffusion control. The influence on electrode performance of dissolved gas diffusion, local overpotential, and transport of current and ionic products are all considered in the analysis presented in this paper.

ELECTRODE MODEL

A porous electrode consists of a very complex arrangement of interconnected voids or pores in a conducting solid matrix. For simplicity of description, however, an idealized pore structure consisting of parallel, straight tubes of circular cross section may be adopted. Each such pore is in part filled with electrolyte, the remainder being occupied by the gas phase.

*Department of Chemical Engineering, University of California, Berkeley

**For a diffusion coefficient, D_g , of 10^{-5} cm²/sec, a gas solubility of 2×10^{-7} gmol/cm³, and a film thickness of 0.1μ , the diffusion current is

$$\frac{D_g c_g^0}{\delta} F = \frac{(10^{-5})(2 \times 10^{-7})(10^5)}{10^{-5}} = 2 \times 10^{-2} \text{ amp/cm}^2$$

The diameter of such pores may be taken as slowly varying compared with the diameter itself. A changing diameter is necessary for a stable liquid meniscus at constant differential pressure. Thus, one of the many pores present in the electrode may be represented as in Fig. 1. The transport of reactant and product species, and of current, may be considered for three basic regions of the pore: first, transport of ionic species in the electrolyte in the pore up to the meniscus; second, phenomena in the reaction zone; and third, transport of gas reactant in the gas-filled part of the pore. The first of these effects may be important in many cases but is easily treated by standard electrolytic mass transport techniques (6); it should be kept small in well-designed electrodes. The third effect is absent for pure gas reactants and is readily treated otherwise (6). The treatment here is concerned with the reaction zone, the most critical area in electrode performance.

The meniscus and the associated electrolyte film which wets the pore wall for a very long distance into the gas region may be simplified to the representation shown in Fig. 2, so long as the reaction occurs over a length of film that is long compared with the meniscus dimensions. This will later be shown to be the case under most operating conditions. Here the meniscus is assumed to be flat, dropping directly to the constant film thickness, δ , which covers the wall for a distance equivalent to many times its thickness. The reaction is assumed to occur entirely at the pore wall beneath this film. This implies a negligible portion of reaction occurring at the walls of the liquid-filled portion of the pore, a condition verified by the data of Will (4). Moreover, it is shown in the Appendix that current which can be generated by reactions in this region are small compared with most current drains that would be encountered in operating fuel cell systems. The film thickness is taken as sufficiently small, compared with pore diameter, that the wall curvature may be disregarded and a unit width of film on an essentially plane surface investigated.

The electrode reaction for this model is the general gas reaction



where G represents the chemical symbol for some reactant gas and S_1 that for an ionic species of charge Z_1 which participates in the reaction; μ and ν are stoichiometric coefficients. For this reaction, a realistic overpotential expression of the redox or Erdey-Gruz type is used [see Vetter (7)], giving a transfer current density

$$j^s = j_0 \left\{ \frac{c_g}{c_g^0} \exp \left[\frac{\alpha m F}{RT} (\phi - \phi_e) \right] - \frac{c_1}{c_1^0} \exp \left[\frac{(\alpha - 1) m F}{RT} (\phi - \phi_e) \right] \right\} \quad (2)$$

This expression is characterized by the exchange current density, j_0 , and the equilibrium potential, ϕ_e , at bulk electrolyte concentration, c_1^0 , and gas saturation, c_g^0 . It should be noted that the electron transfer in the rate-determining step m is not necessarily the overall electron transfer n .

In treating the electrode model, the following assumptions are invoked:

1. Isopotential electrode matrix
2. Uniform gas phase composition
3. Constant transport parameters
4. Electrolyte saturated with reactant gas at gas liquid interface
5. Isothermal operation

The examination is restricted to cases in which only one significant nonreacting ionic species, S_2 , is present.

The transport of chemical species and current in the film are governed by the fundamental flux equations for electrolytes. For a species i , the flux, \underline{N}_i , in the absence of hydrodynamic flow, is

$$\underline{N}_i = - D_i \nabla c_i - z_i u_i \epsilon \nabla \phi \quad (3)$$

The current density, i , in the film is then

$$\underline{i} = F \sum_{\text{SPECIES}} z_i \underline{N}_i \quad (4)$$

For electrolyte systems (at points outside the electric double layer) the electroneutrality condition may be used in place of the potential (Poisson) equation. This condition is

$$\sum_{\text{SPECIES}} z_i c_i = 0 \quad (5)$$

Using the assumptions enumerated above, along with the Nernst-Einstein relation, $u_i = D_i/kT$, which is of the same order of approximation as assumption (3), the steady-state transport equations for the model may be derived. For the ionic species, fluxes must be almost entirely in the x direction because of the thinness of the film.

$$N_1 = - D_1 \frac{dc_1}{dx} - D_1 \frac{Fz_1}{RT} c_1 \frac{d\phi}{dx} \quad (6)$$

$$N_2 = - D_2 \frac{dc_2}{dx} - D_2 \frac{Fz_2}{RT} c_2 \frac{d\phi}{dx} = 0 \quad (7)$$

The flux of the nonreacting species is, of course, zero at steady state, as shown. The dissolved gas diffuses through the film, having a significant flux only in the y direction.

$$N_g = - D_g \frac{dc_g}{dy} \quad (8)$$

The current in the film is carried only by species 1 and is thus

$$i = z_1 F N_1 \quad (9)$$

These equations have the following boundary conditions:

$$\text{at } x = 0: c_1 = c_1^0; c_2 = c_2^0; \phi = \phi^0$$

$$x = \infty: \frac{dc_1}{dx} = \frac{dc_2}{dx} = \frac{d\phi}{dx} = 0 \quad (10)$$

$$y = \delta: c_g = c_g^0$$

Since a change in current per unit width of film, $i\delta$, can occur only by a transfer to the pore wall, i can be related to j^S of Eq. (2) by

$$\frac{di}{dx} = - \frac{j^S}{\delta} \quad (11)$$

Similarly, the flux of dissolved gas must correspond to the reaction rate at the pore wall at the same value of x , giving

$$N_g = - \frac{j^S}{nF} = \frac{\delta}{nF} \frac{di}{dx} \quad (12)$$

If now the electroneutrality condition (5) is substituted into Eq. (7); Eq. (6) is inserted into Eq. (9); Eq. (12) is combined with Eq. (8); and the transformation to dimensionless form,

$$\begin{aligned} C &= \frac{c_1}{c_1^0} & ; & \quad Y = \frac{y}{\delta} \\ G^* &= \frac{c_g}{c_g^0} & ; & \quad X = \frac{x}{\delta} \\ \Phi &= \frac{F}{RT} (\phi - \phi_e) & ; & \quad I = \frac{-i\delta}{z_1 F D_1 c_1^0} \end{aligned} \quad (13)$$

is introduced, the equation system describing the film model becomes

$$\frac{dC}{dX} = - z_2 C \frac{d\Phi}{dX} \quad (14)$$

$$I = \frac{dC}{dX} + z_1 C \frac{d\Phi}{dX} \quad (15)$$

$$\frac{dG^*}{dY} = - \Omega \frac{dI}{dX} \quad (16)$$

and the overpotential expression (2) takes on the form

$$\frac{dI}{dX} = - \gamma \left\{ G \exp [\alpha m \Phi] - C \exp [(\alpha - 1) m \Phi] \right\} \quad (17)$$

where G is the value of G^* at $Y = 0$ and the dimensionless parameters Ω and γ are

$$\begin{aligned} \Omega &= \frac{-z_1 D_1 c_1^0}{n D_g c_g^0} \\ \gamma &= \frac{-j_0 \delta}{z_1 F D_1 c_1^0} \end{aligned} \quad (18)$$

The boundary conditions (10) are:

$$\begin{aligned} \text{at } X = 0 : C &= 1, \quad \Phi = \Phi^0 = \frac{F}{RT} (\phi^0 - \phi_e) \\ X = \infty : \frac{dC}{dX} &= \frac{d\Phi}{dX} = 0 \\ Y = 1 : G^* &= 1 \end{aligned} \quad (19)$$

Integrating Eq. (14) and substituting in Eq. (15) gives

$$\frac{d\Phi}{dX} = \frac{I}{z_1 - z_2} e^{z_2(\Phi - \Phi^0)} \quad (20)$$

Also integrating Eq. (16) and substituting this and the previous integrated result for C in Eq. (17) yields

$$\frac{dI}{dX} = \frac{1}{\Omega + \frac{1}{\gamma} e^{-\alpha m \Phi}} \left\{ e^{z_2 \Phi^0} e^{-(z_2 + m)\Phi} - 1 \right\} \quad (21)$$

Equations (20) and (21), taken together with the conditions

$$\text{at } X = 0 : \Phi = \Phi^0 ; \text{ at } X \rightarrow \infty ; I = \frac{dI}{dX} = 0 \quad (22)$$

are amenable to analog computer solution. Such a solution, applied to the oxygen electrode in 5M KOH, is discussed in a following section.

APPROXIMATE ANALYSIS FOR LOW ELECTRODE OVERPOTENTIALS

To obtain analytic solutions for the model, it is necessary to restrict consideration to cases where the overpotential is small. Then perturbation of a basic condition in which no current flows can describe behavior of the model.

The variables of the system may be broken down into those representing the nonperturbed condition, G_0 , C_0 , Φ_0 , I_0 , and small perturbations G' , C' , Φ' , I' . For the unperturbed state characterized by no current flow,

$$G_0 = 1 ; C_0 = 1 ; \Phi_0 = \Phi^0 ; I_0 = 0 \quad (23)$$

and the variables with perturbations are

$$\begin{aligned} G &= G_0 + G' = 1 + G' \\ C &= C_0 + C' = 1 + C' \\ \Phi &= \Phi_0 + \Phi' = \Phi^0 + \Phi' \\ I &= I' \end{aligned} \quad (24)$$

Then Eqs. (14) and (15) and the integrated form of Eq. (16) become

$$\frac{dC'}{dX} = -z_2 (1 + C') \frac{d\Phi'}{dX} \quad (25)$$

$$I' = \frac{dC'}{dX} + z_1 (1 + C') \frac{d\Phi'}{dX} \quad (26)$$

$$G' = \Omega \frac{dI'}{dX} \quad (27)$$

and the overpotential relation (17) appears as

$$\frac{dI'}{dX} = -\gamma \left\{ (1 + G') \exp [\alpha m (\Phi^0 + \Phi')] - (1 + C') \exp [(\alpha - 1) m (\Phi^0 + \Phi')] \right\} \quad (28)$$

Neglecting second-order terms and expanding the exponentials in Eq. (28), these equations take the linear forms

$$\frac{dC'}{dX} = -z_2 \frac{d\Phi'}{dX} \quad (29)$$

$$I' = \frac{dC'}{dX} + z_1 \frac{d\Phi'}{dX} \quad (30)$$

$$\frac{dI'}{dX} = -\gamma e^{\alpha m \Phi^0} \left\{ 1 + G' + \alpha m \Phi' - [1 + C' + (\alpha - 1) m \Phi'] e^{-m \Phi^0} \right\} \quad (31)$$

Combining Eqs. (29) and (30) yields

$$\frac{dC'}{dX} = \frac{z_2}{z_2 - z_1} I' ; \quad \frac{d\Phi'}{dX} = \frac{-1}{z_2 - z_1} I' \quad (32)$$

Then differentiating Eq. (31) with respect to X and substituting for $\frac{dC'}{dX}$, $\frac{d\Phi'}{dX}$, and $\frac{dG'}{dX}$ from Eqs. (32) and (27) gives

$$\frac{d^2 I'}{dX^2} = -\gamma e^{\alpha m \Phi^0} \left\{ \Omega \frac{d^2 I'}{dX^2} - (\alpha m + [z_2 - (\alpha - 1) m] e^{-m \Phi^0}) \left(\frac{I'}{z_2 - z_1} \right) \right\} \quad (33)$$

But, since I' is I , this rearranges to just

$$\frac{d^2 I}{dX^2} = \frac{I}{L^2} \quad (34)$$

where

$$L^2 = \frac{\Omega + \frac{1}{\gamma} e^{-\alpha m \Phi^0}}{\alpha m + (z_2 + m - \alpha m) e^{-m \Phi^0}}$$

Equation (34) is easily solved with the condition of Eq. (19) at $X \rightarrow \infty$ to yield the expression

$$I = I^0 e^{-\frac{X}{L}} \quad (35)$$

The equivalent expressions for C and Φ are easily determined from Eqs. (32) and (24).

$$C = 1 + \frac{z_2}{z_2 - z_1} LI^0 \left(1 - e^{-\frac{X}{L}} \right) \quad (36)$$

$$\Phi = \Phi^0 + \frac{1}{z_2 - z_1} LI^0 \left(e^{-\frac{X}{L}} - 1 \right) \quad (37)$$

In all these solutions, the constant I^0 , representing current in the film at the meniscus ($X = 0$), appears. This quantity is determined by substituting dI/dX obtained from Eq. (35) into Eq. (17) evaluated at $X = 0$. This gives the result

$$I^0 = L \frac{1 - e^{-m\Phi^0}}{\Omega + \frac{1}{\gamma} e^{-\alpha m\Phi^0}} = \frac{1 - e^{-m\Phi^0}}{\sqrt{\left(\Omega + \frac{1}{\gamma} e^{-\alpha m\Phi^0} \right) \left(\alpha m + (z_2 + m - \alpha m) e^{-m\Phi^0} \right)}} \quad (38)$$

These approximate solutions are valid only for small values of Φ^0 . By comparison with analog computer solutions developed in the next section, it appears that they can be used for values of $\Phi^0 \leq 0.5$ with good accuracy. (See Fig. 5.) This includes single electrode overpotentials (at 25°C) less than 12 mv, a considerable restriction. However, at $\Phi^0 = 1$ the approximate solutions deviate by only about 25 percent; thus, they may be used over a wider range of operation for qualitative predictions.

The quantity L is characteristic of the length of the film over which reaction takes place. Its magnitude in commonly encountered situations (e. g., $10^3 - 10^4$ for the O_2 electrode in 5 M KOH) indicates that the original conditions assumed in simplifying meniscus shape are well justified.

ANALOG COMPUTER SOLUTIONS

Equations (20) and (21) have been analyzed on an Electronic Associates Type 131-R analog computer, mechanized as shown in Fig. 3. The solution is carried out by assuming I^0 and checking the approach of I and (dI/dX) to 0 as X becomes very large. Behavior at large X is used to correct I^0 for given Φ^0 until all boundary conditions are satisfied.

The analog solution has been carried out for the case of the oxygen electrode in 5 M KOH. For this system, the following values were utilized (at 25°C):

$$z_1 = -1 ; z_2 = +1$$

$$c_1^0 = 5 \times 10^{-3} \text{ gmol/cm}^3 ; c_g^0 = 2 \times 10^{-7} \text{ gmol/cm}^3$$

$$D_1 = 4 \times 10^{-5} \text{ cm}^2/\text{sec} ; D_g = 1 \times 10^{-5} \text{ cm}^2/\text{sec}$$

$$n = 4 ; m = 3 ; \alpha = 0.5$$

The exchange current density was assumed at 10^{-4} amp/cm² (there being no well established values for this reaction), and values of film thickness of 10^{-4} , 10^{-5} , and 10^{-6} cm were investigated. This gave values of the parameters of the model as

$$\Omega = 2.5 \times 10^4.$$

$$\gamma = 5 \times 10^{-7}, \quad 5 \times 10^{-8}, \quad \text{and} \quad 5 \times 10^{-9}.$$

The analog computer produced curves of I and $-(dI/dx)$ (reaction rate) versus X as shown in Fig. 4 for one case studied ($\Phi^0 = 1.0$, $\gamma = 5 \times 10^{-8}$). Comparison of solutions over a range of values of overpotential, Φ^0 , results in curves of inlet film current, I^0 , and characteristic active length, L , versus electrode overpotential, Φ^0 , as shown in Figs. 5 and 6. It must be remembered that the graphs are of the dimensionless variables, conversion to single electrode overpotential, $\Phi^0 - \phi_e$, in volts, and superficial current density, j , in amp/cm², being according to

$$\Phi^0 - \phi_e = \frac{RT}{F} \Phi^0 \quad \text{volts} \quad (39)$$

$$j = - \frac{2pz_1 FD_1 c_1^0}{r} I^0 \quad \text{amp/cm}^2 \quad (40)$$

or for this example with a 50 percent porosity and 1μ pore, $\Phi^0 - \phi_e \approx 0.025 \Phi^0$ volts ;
 $j = 400 I^0$ amp/cm².

The results of the approximate solution for this example are plotted in Figs. 5 and 6. The close agreement for values of Φ^0 less than 0.5 is apparent.

CONCLUSIONS

This investigation of porous gas electrodes with wetting electrolytes has established two significant points about the behavior of such systems. First, except for reactions of very high exchange current densities at the conditions in the pores ($> 10^{-2}$ amp/cm² referred to elemental surface area), the diffusion of reactant gas through the film on the pore wall is not a controlling effect for the majority of the area over which reaction occurs. Second, significant reaction rates exist at the wall under the electrolyte film at distances from the "intrinsic" meniscus equal to thousands of film thicknesses.

The extent of dissolved gas diffusion control can be seen by examination of Eq. (21). The effect of this diffusion manifests itself only when the term Ω is large compared with the term $\exp(-\alpha m \Phi / \gamma)$ (both terms in the denominator on the right-hand side). This condition can exist, for values of Ω and γ possible for gas electrodes, only if Φ is quite large (say ≥ 5) - that is, only if the electrode overpotential, Φ^0 , is large. Even then, gas diffusion controls only at positions near the meniscus. For diffusion control throughout the entire reaction zone, Φ^0 must exceed perhaps 20 or 25. This corresponds to few cases of electrode operation.

The prediction of significant reaction rates under the film at distances of $10^3 - 10^4$ film thickness from the meniscus involves a considerably longer reaction zone than the ~ 200 film thicknesses proposed by Will (4) for a similar model (for H_2 in acid). This difference is due principally to Will's assumption of no local overpotential except that due to dissolved gas concentration. This condition would give considerably higher local reaction rates, and thus a narrower reaction zone. It is equivalent to setting γ to ∞ in Eq. (21) (with perhaps some adjustment in the coefficients of Φ) and corresponds to the physical case of infinite exchange current density. The assumption is not realistic for most electrode reactions.

In addition to the general conclusions mentioned above, this analysis has yielded approximate expressions for overpotential-current density behavior and for current distribution in gas electrodes at low to moderate overpotentials, and a method of analog computation to determine these relationships under any reasonable conditions.

NOTATION

English Letters

c_i	concentration of species i in electrolyte (gmol/cm^3)
c_i^0	reference concentration of species i (gmol/cm^3)
D_i	diffusion coefficient of species i (cm^2/sec)
F	Faraday's constant (96,500 coul/equiv.)
i	current density in electrolyte film (amp/cm^2)
j	superficial current density for electrode (amp/cm^2)
j_0	exchange current density of electrode reaction (amp/cm^2)
j^s	local transfer current density due to reaction (amp/cm^2)
k	Boltzmann constant
m	number of electrons transferred in rate-determining reaction step
N_i	flux of species i in electrolyte ($\text{gmol/cm}^2\text{-sec}$)
n	number of electrons transferred in overall electrode reaction
p	electrode porosity
R	gas constant
r	pore radius (cm)
S_i	chemical symbol of species i
T	absolute temperature ($^{\circ}\text{K}$)
u_i	mobility of species i (cm/sec-dyne)
x	distance coordinate along film (cm)
y	distance coordinate across film (cm)
z_i	charge number of species i

Greek Letters

α	transfer coefficient
δ	film thickness (cm)
ϵ	electronic charge
μ, ν	stoichiometric coefficients
ϕ	potential in electrolyte film (volts)
ϕ_e	equilibrium electrode potential at c_i^0 (volts)

Subscripts

g	refers to dissolved reactant gas
1	refers to ionic species involved in electrode reaction
2	refers to nonreacting ionic species

ACKNOWLEDGMENT

The authors wish to acknowledge the financial support of this research by the U. S. Navy, Bureau of Weapons, under research contract NOW 60-0738-d.

LITERATURE CITED

1. Justi, E., Pilkuhn, M., Scheibe, W., and Winsel, A., "High-Drain Hydrogen Electrodes Operating at Ambient Temperature and Low Pressure," Verlag d. Akademie d. Wissenschaften u. d. Literatur, 1959.
2. Urbach, H. B., "Theory of Polarization of Gaseous-Diffusion Electrodes," in Fuel Cells, G. J. Young, ed., Reinhold, New York, 1963, p. 77.
3. Austin, L. G., "Polarization at Diffusion Electrodes," in Fuel Cells, op. cit., p. 95.
4. Will, F. G., J. Electrochem. Soc., **110**, 152 (1963).
5. Meissner, H. P., and Reti, A. R., "Predicted Performance of an Air Electrode," paper presented at 50th National A. I. Ch. E. meeting, Buffalo, N. Y., 1963.
6. Winsel, A. W., "Improved Calculation of Polarization of Porous Electrodes," paper presented at Symposium on Porous Electrodes of The Electrochemical Society, Boston, 1962; also in Advanced Energy Conversion (in press).
7. Vetter, K. J., Elektrochemische Kinetik, Springer Verlag, Berlin, 1961, Sec. 49.

Appendix

ESTIMATE OF CONTRIBUTION OF ELECTRODE REACTION IN FLOODED PORTIONS OF THE PORES

To establish an estimate of the maximum contribution to electrode current arising in electrode reaction at the walls of the flooded portions of a pore (see Fig. 1), consider a one-dimensional analysis under conditions most favorable to such a reaction. If the coordinate system of Fig. 2 is utilized, the potential locus of such reaction is $-\infty < x < 0$. In this region, reactant gas supply is by diffusion essentially in the x direction.

$$N_g = -D_g \frac{dc_g}{dx} \quad (\text{A. 1})$$

For conservation of dissolved gas at steady state,

$$0 = -\nabla \cdot N_g + \text{source term} = D_g \frac{d^2c_g}{dx^2} - \frac{j^s a}{nF} \quad (\text{A. 2})$$

where a is specific area of electrode based on pore volume ($= 2/r$ for cylindrical pores). The overpotential expression (A. 2) may be simplified, for high electrolyte conductivity and constant ionic concentrations, to the approximation

$$j^s = A c_g - B \quad (\text{A. 3})$$

where

$$A \approx j_o \exp \left[\frac{\alpha n F}{RT} (\phi^o - \phi_e) \right] ; B \approx j_o \exp \left[\frac{(\alpha - 1) n F}{RT} (\phi^o - \phi_e) \right]$$

This corresponds to pure gas diffusion control, which is to be expected for any reaction in this region. Substitution of Eq. (A.3) into Eq. (A.2) gives

$$\frac{d^2 c_g}{dx^2} = \frac{Aa}{nFc_g^0} c_g - B \quad (\text{A.4})$$

which has the following boundary conditions:

$$\begin{aligned} \text{at } x = 0 : c_g &= c_g^0 \\ x \rightarrow -\infty : \frac{dc_g}{dx} &= c_g = 0 \end{aligned} \quad (\text{A.5})$$

This equation has the solution, for the concentration gradient,

$$\frac{dc_g}{dx} = + \sqrt{\frac{Aa}{nFc_g^0} c_g^2 - \frac{Ba}{nF} c_g} \quad (\text{A.6})$$

which corresponds to a flux of dissolved gas at the meniscus of

$$N_{g_{x=0}} = \left(- D_g \sqrt{\frac{a}{nF} c_g} \sqrt{\frac{A}{c_g^0} c_g - B} \right)_{x=0} = - D_g \sqrt{\frac{a}{nF} c_g^0} \cdot \sqrt{j_{x=0}^s} \quad (\text{A.7})$$

or to a total superficial current density resulting from reaction in the flooded portion of the pores, j^f , of

$$j^f = - nFN_g = D_g \sqrt{anFc_g^0} j_{x=0}^s \quad (\text{A.8})$$

Since $j_{x=0}^s$ cannot be much greater than j_o for the reaction, this contribution is very small indeed. For the oxygen electrode treated in the text, with $a = 10^5 \text{ cm}^2/\text{cm}^3$,

$$j^f \leq (10^{-5}) \left[(10^5)(4)(10^5)(2 \times 10^{-7})(10^{-4}) \right]^{1/2} \approx 10^{-5} \text{ amp/cm}^2$$

which is negligible. Even if the exchange current density were as high as 1 amp/cm^2 , this contribution to superficial current density would be less than 10^{-3} amp/cm^2 .

Thus, reaction in the flooded portion of the pores can be ignored if a film is present.

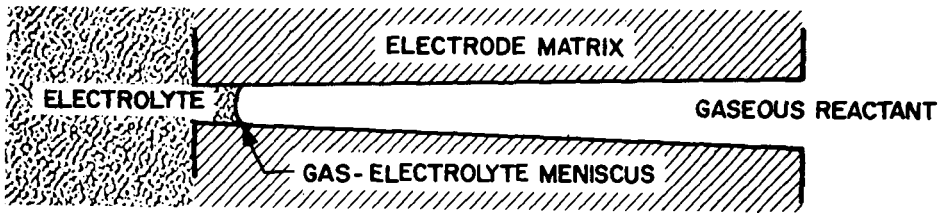


Fig. 1 Idealized Pore of Gas Electrode

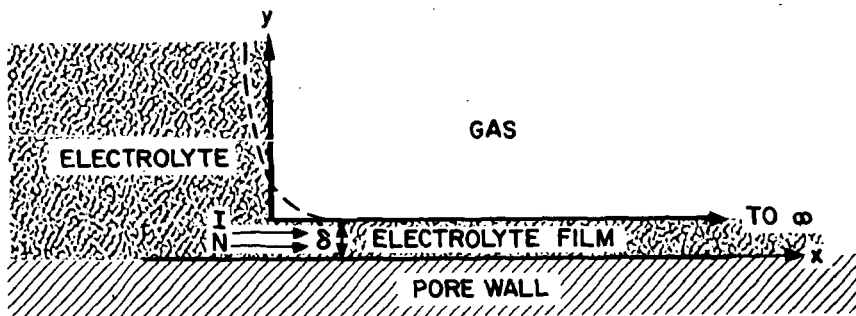


Fig. 2 Model for Reaction Zone of Porous Gas Electrode

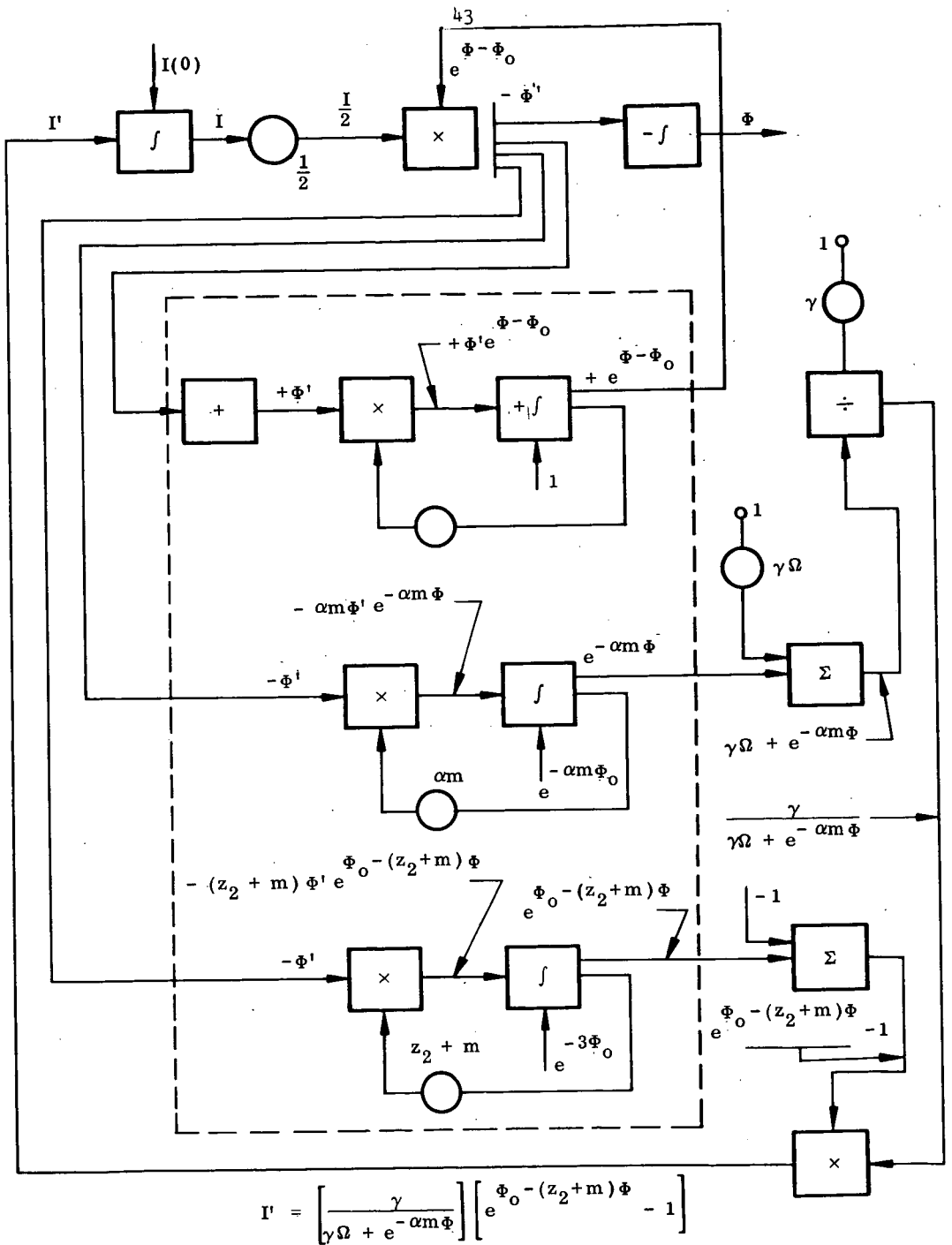


Fig. 3 Block Diagram of Analog Computer Mechanization

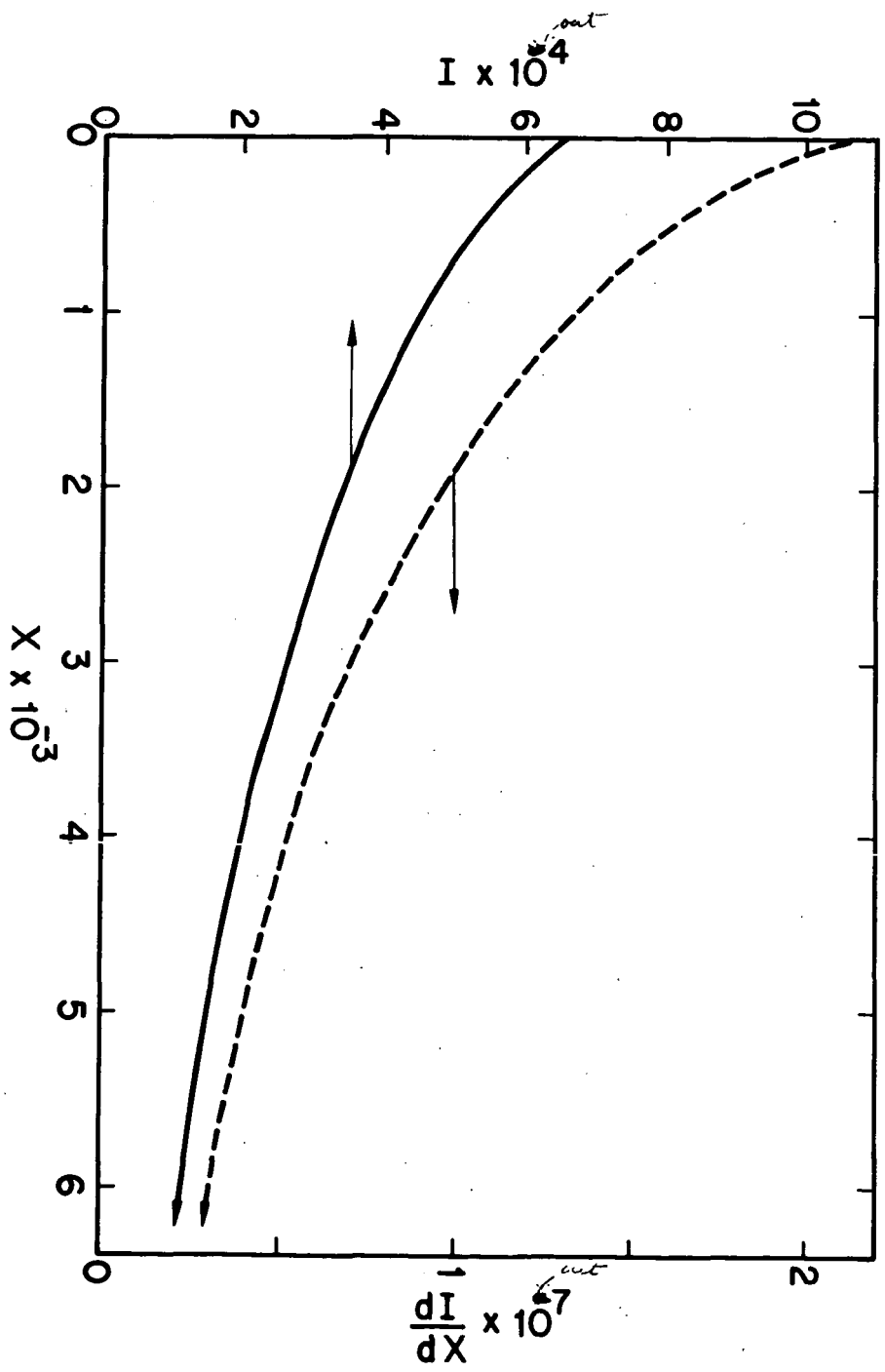


Fig. 4 Analog Computer Output Curves (Partial) for I and dI/dX Versus X for O_2 Electrode (KOH) ($\Omega = 2.5 \times 10^{-4}$, $\gamma = 5 \times 10^{-8}$, $\phi^0 = 1.0$)

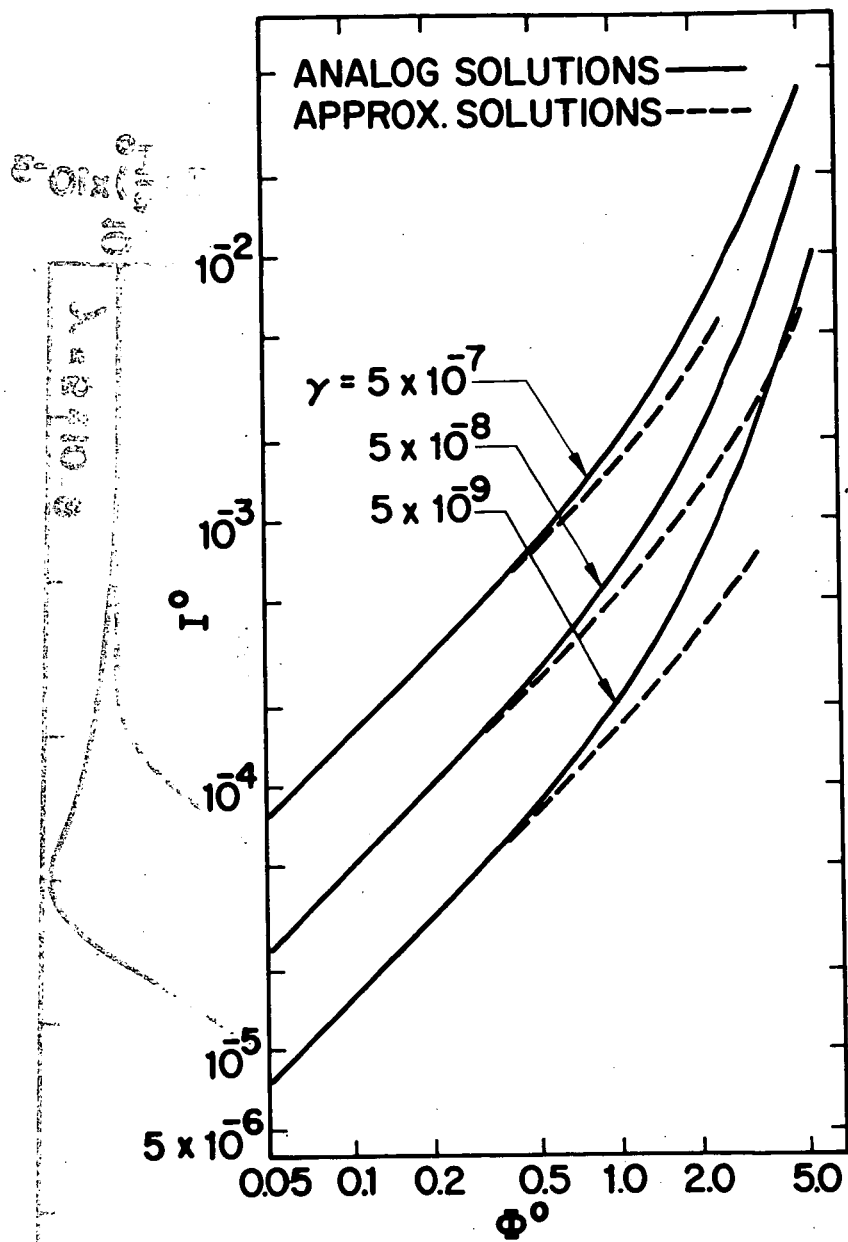


Fig. 5 Current-Overpotential Relations in Dimensionless Form for O_2 Electrode (KOH) ($\Omega = 2.5 \times 10^4$, γ as Shown)

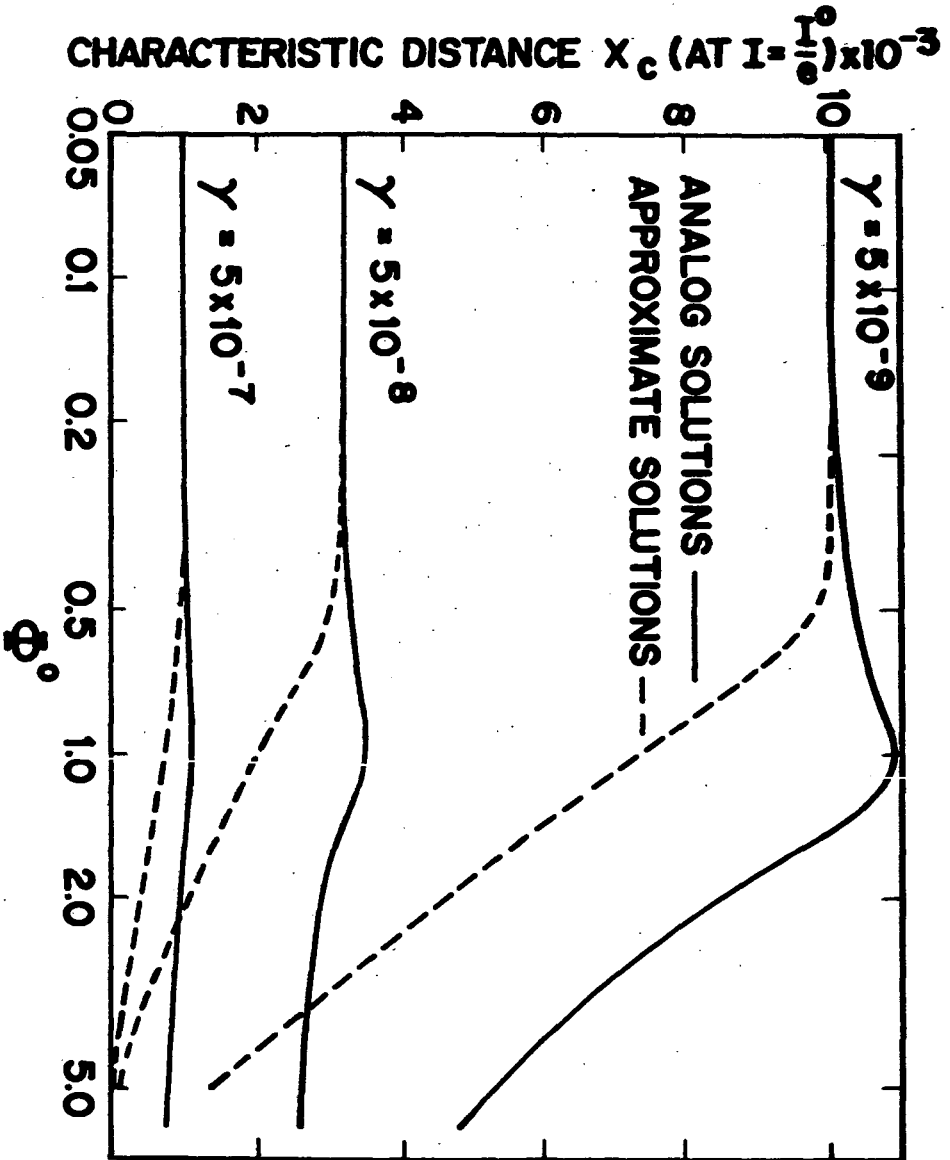


Fig. 6 Characteristic Distances for Active Length of Film Versus Overpotential for O_2 Electrode (KOH) ($\Omega = 2.5 \times 10^4$, γ as Shown)

THE OPERATION MECHANISM OF POROUS GAS ELECTRODE

R. Burshtein

Institute for Electrochemistry
Academy of Sciences, USSRAbstract*

In order to study the operation mechanism of porous gas diffusion electrodes the pore radii distribution and the surface area of nickel electrodes having different structures were determined.

On the basis of data on the electrode structure and of measurements of the rate of the electrochemical reaction at various gas/electrolyte pressure differences, a model for the operation of a porous gas electrode has been proposed.

The electrochemical reaction is assumed to occur at the surface of macropores from which the electrolyte has been expelled by the gas near the orifice of micropores filled with electrolyte, the latter ensuring the transport of current. It is further assumed that the sites at which the current is generated are uniformly distributed over the whole electrode surface.

According to this model the electrochemical activity of a porous gas electrode depends on the ratio of the surface area of pores free from electrolyte to the total cross section of pores filled with electrolyte.

The maximum electrochemical activity corresponds to definite relations between the experimentally determined structural parameters. A theoretical treatment of several porous electrode models has been carried out, the results obtained being in good agreement with the experimental data.

* Complete manuscript not received in time for inclusion in the Divisional Preprints.

POLARIZATION AT POROUS FLOW-THROUGH ELECTRODES

L. G. Austin, P. Palasi and R. R. Klimpel
 Fuel Technology Department, Pennsylvania State University,
 University Park, Pa.

INTRODUCTION

The flow-through electrode is an electrochemical system which has received little attention. It is of primary interest in redox fuel cells (1, 2, 3) where a dissolved ionic fuel (or oxidant) is to be reacted at an electrode. In such a system, where liquid is circulated through the cell, it is clearly much better to force the fresh liquid through the electrode and take spent liquid from the exit side. The electrode then acts as a separator between fresh and spent liquid and, more important, the mass transport of reactant to the electrode can be easily controlled. By forcing electrolyte through the electrode, we no longer have to rely on diffusion of fuel to the electrode and, consequently, the mass transport problems of non flow-through electrodes can be considerably diminished. Similarly, for fuels or oxidants such as methanol, hydrazine, nitric acid, etc., which can be dissolved in high concentrations in the electrolyte, it may be desirable to use flow-through electrodes (4, 5, 6).

When the processes occurring in flow-through electrodes are considered, it readily becomes apparent that several parameters are of first importance. The concentration of reactant and rate of flow determine the maximum current which can be drawn, since we cannot draw more current than the corresponding amount of reactant put in per second. The speed of the electrochemical reaction, in the form of the exchange current for the reaction (7), is of importance in determining the polarization at a given current. In addition, the ohmic voltage gradient in the electrolyte in the pores of the electrode also affects the polarization.

Perskaya and Zaideman (8) gave the basic mathematical form of the process. However, they solved the equation only for low current density, low polarization conditions, where the approximation $\exp(\alpha n F \eta / RT) = 1 + \alpha n F \eta / RT$ applies. In our analysis we have found that this can only rarely be applied. The treatment we give explains reasonably well the whole current-voltage range of their experimental results and also explains the experimental results of Bond and Singman (9). However, the assumptions made in the theory are not generally valid and the breakdown of the theory is demonstrated and discussed.

PHYSICAL SYSTEM TREATED AND ASSUMPTIONSINVOLVED.

The physical system studied consists of a uniform, porous, plane electrode with reactant dissolved in electrolyte flowing into the left hand face; unreacted reactant and dissolved product flow out of the right hand face (see Figure 1). The reaction could be a simple redox reaction such as $Fe^{2+} \rightleftharpoons Fe^{3+} + e$ in acid solution. In a redox cell employing a separator the circuit is completed within the cell by (H^+) flowing from the anode to the cathode. The following assumptions are made. (i) The flow is uniform through the electrode. This is very nearly true for a small experimental electrode, but it may not be so for a large electrode. (ii) Ohmic loss in the material of the electrode is negligible. This will be a good approximation for properly constructed electrodes of metal or carbon. (iii) The reaction at the external faces of the electrode is small compared to the total reaction. The external faces can be considered as extensions of the internal area and the assumption would only be false in the limit where the internal area became

small. (iv) The pores of the electrode are small in radius compared to their length, so that negligible concentration gradients exist across the radius of the pore. In other words, the pore radius is so small that radial diffusion is rapid enough to maintain uniform concentration across the pore radius; the only concentration changes will be linear along the axis of the pore. With this assumption, the variation of laminar flow rate across the pore radius is of no consequence. This assumption is discussed later in more detail. (v) The porous electrode has its pores so well interlinked that it can be considered to act as a homogenous system, with variation of conditions at a given penetration applying only over small regions. Electrodes must be constructed so that no major cracks or pinholes exist. (vi) The flow rate is great enough that axial mass transfer of reactant and product by diffusion and ionic migration is negligible compared to mass transfer by the bulk flow. It should be noted that the current must be supported by ionic migration and, therefore, this assumption may not always be valid. It will be a good approximation, however, when the concentration of supporting electrolyte is high, e.g. a strongly acid solution is used. In this case we can also assume that the specific conductivity of the electrolyte remains constant. (vii) The streaming potential is small compared to other effects, which will be true when strong electrolytes are used.

A less easily justified assumption is that the electrochemical reaction at the pore surface is a simple reaction with the rate form (7)

$$i = i_0 \left[(R/R_i) e^{\eta/b} - (P/P_i) e^{-\eta/b} \right] \quad (1)$$

R_i , P_i are the entering concentrations (assumed equivalent to activities) of the reactant and product; i , i_0 refer to unit area of the pore surface, (see list of nomenclature). Equation 1 may apply to simple redox reactions, but one would expect, for example, dissolved methyl alcohol fuel to have a more complex form. At open circuit conditions, with no current flow, R and P are constant though the electrode and equal to R_i and P_i , and they determine the theoretical potential. However, if the basic exchange current is small then impurities in the feed may give rise to leakage current and a mixed potential may be obtained. A sufficient rate of flow will prevent diffusion of a disturbing material from the other electrode, but any impurities in the feed are being constantly replaced. Thus, very low current density measurements and open circuit potentials may not correspond to ideal values.

THEORY

Consider unit face area of the electrode. Let the velocity of flow through the electrode be v , cm^3 per sq cm of face per second. Consider element dx in Figure 1. The amount of reactant flowing in per second is Rv and the amount flowing out is $[R + (dR/dx)dx]v$. The amount of R reacted to P in the element, per second, is given by

$$di/nF = i_0 \left[(R/R_i) e^{\eta/b} - (P/P_i) e^{-\eta/b} \right] (S/nF) dx \quad (2)$$

n is the total number of electrons involved for each complete reaction; S is the reacting area per unit volume of electrode. At steady state, therefore,

$$Rv - [R + (dR/dx)dx]v = (i_0 S/nF) \left[(R/R_i) e^{\eta/b} - (P/P_i) e^{-\eta/b} \right] dx$$

or

$$-dR/dx = (i_0 S/vnF) \left[(R/R_i) e^{\eta/b} - (P/P_i) e^{-\eta/b} \right] \quad (3)$$

Also, at steady state, $R_i + P_i = R + P$, therefore

$$-dR/dx = (i_0 S/vnF) \left[R \left(\frac{e^{\eta/b}}{R_i} + \frac{e^{-\eta/b}}{P_i} \right) - \frac{(R_i + P_i)}{P_i} e^{-\eta/b} \right] \quad (4)$$

If the specific resistance of the electrolyte is ρ' , the porosity of the electrode

ϵ and the tortuosity factor q (10) then, by Ohm's law,

$$(\rho'q/\epsilon)i = d\eta/dx$$

or

$$i = (1/\rho) d\eta/dx \quad (5)$$

where ρ is understood to include the porosity and tortuosity factors.

The complete solution to the problem is given by the solution of equations 4 and 5. We could not, however, obtain an analytical solution. Computed results are presented later, but it is informative to consider a limiting condition which has an analytical solution. The limiting condition is that the ohmic drop within the electrolyte in the pores is negligible. The effect of ohmic drop can be considered as a disturbance of this limiting condition.

CASE 1. Ohmic Effects Neglected

Neglecting ohmic drop and working with equation 4 only, we can separate and integrate from $x = 0$, $R = R_i$ to $x = x$, $R = R$,

$$(i_o S/vnF)x = \frac{1}{((e^{\eta/b}/R_i) + (e^{-\eta/b}/P_i))} \ln \left[\frac{(e^{\eta/b} - e^{-\eta/b})}{(R/R_i)e^{\eta/b} - ((R_i + P_i - R)/P_i)e^{-\eta/b}} \right] \quad (6)$$

When $x = L$, the thickness of the electrode, $R = R_f$, the final concentration of reactant issuing from the right hand face of the electrode. The current per sq cm of electrode is

$$i = nFv(R_i - R_f) \quad (7)$$

The limiting current density is clearly given by

$$i_L = nFvR_i \quad (7a)$$

Thus

$$i/i_L = 1 - R_f/R_i = \text{degree of conversion} \quad (8)$$

To get the relation between current and polarization we have to substitute for R_f in equation 6 using equation 8, as follows

$$\begin{aligned} (Li_o S/vnF)((e^{\eta/b}/R_i) + (e^{-\eta/b}/P_i)) \\ = \ln(e^{\eta/b} - e^{-\eta/b}) - \ln[(R_f/R_i)e^{\eta/b} - (R_i/P_i)e^{-\eta/b} + (R_f/P_i)e^{-\eta/b}] \end{aligned}$$

For algebraic convenience let $\gamma = R_i/P_i$, $Q = e^{\eta/b} - e^{-\eta/b}$, then

$$\begin{aligned} (Li_o S/vnFR_i)(e^{\eta/b} + \gamma e^{-\eta/b}) \\ = \ln Q - \ln[(R_f/R_i)(e^{\eta/b} + e^{-\eta/b}) - (1 + \gamma)e^{-\eta/b}] \end{aligned}$$

Again, for algebraic convenience let $e^{\eta/b} + \gamma e^{-\eta/b} = f$, then

$$e^{-(Li_o S/i_L)f} Q = (R_f/R_i)f - (1 + \gamma)e^{-\eta/b}$$

$$\begin{aligned} \text{or } i/i_L = 1 - R_f/R_i &= (f - Qe^{-(LSi_o/i_L)f} - (1 + \gamma)e^{\eta/b})/f \\ &= (e^{\eta/b} + \gamma e^{-\eta/b} - e^{-\eta/b} - \gamma e^{-\eta/b} - Qe^{-(LSi_o/i_L)f})/f \end{aligned}$$

$$\text{or } i/i_L = Q(1 - e^{-(LSi_o/i_L)f})/f \quad (9)$$

This is the equation relating current to polarization and it includes the parameters of i_o , S , L , v , R_i , P_i .

Two limiting cases can be considered. Firstly, let us consider the low current case where $\eta \rightarrow 0$.

Using $e^{\eta/b} = 1 + \eta/b$ when η/b is small,

$$i/i_L = \frac{2(\eta/b)}{1 + \frac{\eta}{b} + \gamma \left(1 - \frac{\eta}{b}\right)} \left(1 - e^{-(LSi_o/i_L)[1 + \frac{\eta}{b} + \gamma(1 - \frac{\eta}{b})]}\right)$$

When LSi_o/i_L is small, that is, it is a reaction with a relatively low exchange current,

$$i/i_L = 2(LSi_o/i_L)(\eta/b) \quad (10)$$

This is the required logical result since, as $b = RT/\alpha n_1 F$, $\alpha \sim 1/2$ (n_1 is the electron transfer in the rate controlling step),

$$i = (LSi_o)n_1 F \eta / RT .$$

On the other hand, if LSi_o/i_L is large, then

$$\begin{aligned} i/i_L &= Q/f \\ &= (e^{\eta/b} - e^{-\eta/b}) / (e^{\eta/b} + \gamma e^{-\eta/b}). \end{aligned}$$

Rearranging

$$\eta = (2.3RT/nF) \log \left[\frac{(1 + \gamma i/i_L)}{(1 - i/i_L)} \right] \quad (11)$$

This is again the expected result: it corresponds to pure concentration polarization (see reference 7, p. 15, where the above result can be obtained from equation 26a by setting $i/I = 0$).

At large values of η (the larger is γ the larger η must be for the following approximation to hold) $e^{-\eta/b}$ can be neglected compared to $e^{\eta/b}$ and

$$i/i_L = 1 - e^{-(SLi_o/i_L) e^{\eta/b}} \quad (12)$$

As necessary, as η/b becomes large, $i/i_L \rightarrow 1$. Figure 2 shows the form of i versus η for various values of exchange current. To make the curves as general as possible it is convenient to plot in the form i/i_L versus η/b , with \bar{I}_o/i_L as the variable parameter. \bar{I}_o is defined by

$$\bar{I}_o = i_o SL . \quad (13)$$

For small values of \bar{I}_o/i_L , the electrode is highly polarized and the factor $\gamma (=R_i/P_i)$ does not affect the result. A Tafel region is observed at current densities well below the limiting current. This can be predicted from equation 12, since when i/i_L is less than 0.1, the exponential term is near 1 and

$$\begin{aligned} i/i_L &\simeq (\bar{I}_o/i_L) e^{\eta/b} \\ \eta &\simeq (2.3RT/\alpha n_1 F) \log(i/\bar{I}_o) \end{aligned} \quad (12a)$$

CASE 2. Ohmic Effects Included

From equation 5 we have

$$di/dx = (1/\rho) d^2\eta/dx^2 .$$

From equation 7 we have

$$di/dx = -vnF dR/dx .$$

We can also combine equations 5, 7 and 7a to give

$$R/R_i = (1 - (1/i_L \rho) d\eta/dx) .$$

Combining these equations with equation 4 gives

$$d^2\eta/dx^2 = \rho i_o S \left[R_i \left(\frac{1-1}{i_L \rho} \frac{d\eta}{dx} \right) \left(\frac{e^{-\eta/b}}{R_i} + \frac{e^{-\eta/b}}{P_i} \right) - \left(\frac{R_i + P_i}{P_i} \right) e^{-\eta/b} \right] . \quad (14)$$

Equation 14 is the basic equation relating polarization to distance into the electrode. We were not able to find a general analytical solution to the equation,

therefore, the equation was put into a form suitable for numerical integration.

For computational convenience it is helpful to define reduced values of η , x by

$$\bar{\eta} = \eta/b \quad (15)$$

$$(15f) \quad \bar{x} = x/L \quad (15a)$$

It is also convenient to define a maximum ohmic polarization Δ by

$$\Delta = i_L \rho_L \quad (16)$$

Δ is the maximum possible ohmic loss through the electrode and is obtained under conditions where the reaction is completed in a differential element at $x = 0$, so that all the ions supporting i_L have to be transported from L to $x = 0$ (or $x = 0$ to L). This can only occur at very large total polarizations. Replacing R_i/P_i by γ , η/b by $\bar{\eta}$, and x/L by \bar{x} , equation 14 goes to

$$d^2 \bar{\eta} / d\bar{x}^2 = (\bar{i}_0 / i_L) (\Delta / b) \left[\left(\frac{1-b}{\Delta} \frac{d\bar{\eta}}{d\bar{x}} \right) (e^{\bar{\eta}} + \gamma e^{-\bar{\eta}}) - (1 + \gamma) e^{-\bar{\eta}} \right].$$

Again, it is convenient to define a reduced Δ by

$$\bar{\Delta} = \Delta / b \quad (16a)$$

Then dropping the bar but remembering that i_0 , η and Δ are reduced quantities,

$$d^2 \eta / dx^2 = (i_0 / i_L) \Delta \left[(1 - (1/\Delta) d\eta/dx) (e^{\eta} + \gamma e^{-\eta}) - (1 + \gamma) e^{-\eta} \right].$$

The boundary conditions are $\eta = \eta_0$ at $x = 0$ and $\eta = \eta_L$ at $x = 1$, where η_L is the polarization at the right hand face of the electrode in multiples of b . Integrating equation 17 once,

$$\begin{aligned} \Delta \int_{\eta_0}^{\eta} (e^{\eta} + \gamma e^{-\eta} - e^{-\eta} - \gamma e^{-\eta}) dx - \int_{\eta_0}^{\eta} (e^{\eta} + \gamma e^{-\eta}) d\eta \\ = (i_0 / i_L) \Delta \left[\int_{\eta_0}^{\eta} (e^{\eta} - e^{-\eta}) dx - ((e^{\eta} - \gamma e^{-\eta}) - (e^{\eta_0} - \gamma e^{-\eta_0})) \right] \end{aligned}$$

If x is divided into M small increments of Δx such that over any Δx , η is proportional to x and $\Delta \eta / \Delta x$ is a constant we get, at the N 'th increment,

$$\Delta \sum_{1}^N (\Delta x / \Delta \eta_N) \left[(e^{\eta_N} + e^{-\eta_N}) - (e^{\eta_{N-1}} + e^{-\eta_{N-1}}) \right] - [(e^{\eta_N} - \gamma e^{-\eta_N}) - (e^{\eta_0} - \gamma e^{-\eta_0})] \quad (18) *$$

$\Delta \eta_N$ is the increase in polarization over the $N-1$ to N 'th increment. Also, from equation 5,

$$(18f) \quad i / i_L = (1 / \rho_L) d\eta / dx$$

where η , x are actual values. Replacing, as before, η/b with $\bar{\eta}$, x/L with \bar{x}

$$i / i_L = (b / \rho_L) d\bar{\eta} / d\bar{x} = (1 / \bar{\Delta}) d\bar{\eta} / d\bar{x}.$$

Dropping the bars,

$$i / i_L = (1 / \Delta) d\eta / dx.$$

Thus the total current density from the electrode is

$$i / i_L = (1 / \Delta) (d\eta / dx)_{x=1} \quad (19)$$

To calculate η and i / i_L , equation 18 is progressively solved using a suitable value of Δx and the value of η plotted versus x . The value of $d\eta / dx$ at $x = 1$ is obtained graphically. Equation 18 is solved by assigning a value of η_0 and guessing at a value of $\Delta \eta_1$. This is substituted into the R.H.S. of equation 18, with $\eta_1 = \eta_0 + \Delta \eta_1$. $\Delta \eta_1$ is calculated. When it agrees with the substituted value of $\Delta \eta_1$ within a specified error, the calculation is correct and may proceed to the

* The program for computation of equation 18 is available from the authors.

next step. The final polarization is at $x = 1$, $N = M$, and the total current is obtained from equation 19. This is repeated for another value of η_0 (which is the polarization at the left hand face of the electrode) and other values of η (at the right hand face) and i/i_L are obtained. By this means, the complete range of η_0 , η and i/i_L , from i/i_L small to $i/i_L \rightarrow 1$ can be obtained. For $\gamma \leq 1$, terms in $e^{-\eta}$ can be neglected when η_0 is greater than 1, and equation 18 goes to

$$\Delta\eta_N \simeq (i_0/i_L)\Delta x e^{\eta_0} [\sum \Delta(\Delta x/\Delta\eta_N) (e^{\eta^1_N} - e^{\eta^1_{N-1}}) - (e^{\eta^1_N} - 1)] \quad (20)$$

where η^1 is measured from η_0 , that is, $\eta = \eta^1 + \eta_0$. This form can be fairly rapidly computed. When $(i_0/i_L)(\Delta x)e^{\eta_0\Delta}$ is small, the final value of η^1 is small and

$$\begin{aligned} d\eta/dx &= (i_0/i_L) e^{\eta_0\Delta} \frac{\Delta x}{\Delta\eta} (1 + \eta_N - 1 - \eta_{N-1}) \\ &= (i_0/i_L) e^{\eta_0\Delta} \Delta x \\ &= (i_0/i_L) \Delta e^{\eta_0 x} \end{aligned}$$

Therefore,

$$\begin{aligned} \eta^1_x &= (i_0/i_L) e^{\eta_0\Delta} \int^x dx \\ &= (i_0/i_L) \Delta e^{\eta_0 x^2/2} \end{aligned} \quad (21)$$

For this low current condition

$$\begin{aligned} i/i_L &= (1/\Delta)(d\eta/dx)_{x=1} = (1/\Delta)(i_0/i_L) e^{\eta_0\Delta} \\ &= (i_0/i_L) e^{\eta_0} \end{aligned} \quad (22)$$

This, of course, is a Tafel form. The equations tell us that, for an irreversible reaction at low current, the additional polarization η^1 caused by ohmic loss is one-half that expected if all of the current flowed completely through the porous system, since, from equation 21

$$\begin{aligned} \eta^1_{x=1} &= (i_0/i_L) e^{\eta_0\Delta/2} \\ &= (i/i_L) \Delta/2 \end{aligned}$$

This is reasonable, since, under these conditions, the electrode is reacting uniformly throughout its thickness and the mean distance the ions have to penetrate is half the thickness.

Equation 20 predicts that, for irreversible conditions, the shape of the η versus i/i_L curves will be the same for any i_0/i_L value (for a given Δ value, of course) but shifted to higher or lower polarizations. This is because $(i_0/i_L)e^{\eta_0}$ is the controlling parameter and we therefore know that η^1 is the same for a given value of $(i_0/i_L)e^{\eta_0}$. Thus for a given set of η^1 values

$$(i_0/i_L)_1 e^{\eta_0} = (i_0/i_L)_2 e^{(\eta_0 + \Delta\eta_{12})}$$

where $\Delta\eta_{12}$ represents the bodily shift. Then

$$\Delta\eta_{12} = 2.3 \log[(i_0/i_L)_1 / (i_0/i_L)_2]$$

or

$$\Delta\eta_{12} \text{volts} = (2.3b) \log[(i_o/i_L)_1 / (i_o/i_L)_2]$$

Let us now consider the limiting case where activation polarization is negligible and only concentration and ohmic effects are present. From equation 17, when $(i_o/i_L)\Delta$ is large, $d^2\eta/dx^2/(i_o/i_L)\Delta$ tends to zero and we get equation 11. Equation 11 thus represents the limiting case whether an internal ohmic voltage gradient is present or not. For a given η_o , a larger ohmic effect will give a higher i/i_L since the concentration of reactant and product will change to keep match with the voltage: but since η_o is essentially zero at all currents up to near the limiting current, η is determined solely by i/i_L , according to equation 11. The position of reaction in the interior will change with Δ , but the final result will not.

At intermediate conditions where neither equation 20 nor equation 11 apply, equation 18 is tedious to compute. However, if $\gamma = 1$ the equation goes to

$$\Delta\eta_N = (2i_o/i_L)\Delta x \left[\sum_1^N \Delta \frac{\Delta x}{\Delta\eta} (\cosh \eta_N - \cosh \eta_{N-1}) - (\sinh \eta_N - \sinh \eta_o) \right] \quad (18a)$$

Tables of hyperbolic functions can then be used.

RESULTS OF COMPUTATIONS

In a previous report (11), the equations were solved by hand computation. They have since been solved more accurately on an IBM 7074 digital computer. The later results show a slight change in the values of η_o as compared to the former. Figure 3, 4 and 5 show the results of computations of the full equation, allowing for ohmic resistance. (A value of $\Delta x = 1/20$ was found to be satisfactory over most of the current range.) To avoid confusion, the η calculated for the case of no ohmic effect is termed η_s , the polarization at the entering face is termed η_o and the polarization of practical importance, at the exit face, is termed η .

The physical picture of the effect of ohmic voltage gradient which emerges from the solution of the equations is as follows. The flowing electrolyte, with a high concentration of fuel, enters at one face and, with a suitable polarization, it starts to react. The ionic transfer through the electrolyte, which maintains charge balance, gives rise to an ohmic voltage gradient. This ohmic effect increases the polarization at further penetration into the electrode and the reaction rate is increased. Therefore, as the fuel flows through the electrode, it is consumed more and more rapidly, which increases the cumulative ion transfer, which causes increased ohmic effect, which increases the rate of consumption and so on. Thus for a large value of Δ (the index of ohmic effect) the reaction is concentrated towards the exit face of the electrode. This is shown in Figure 6 for $\Delta = 100$ and currents of 0.84 and 0.23 of the limiting current. For the larger value, most of the reaction occurs in the final one-tenth of the electrode. For the lower value, most of the reaction occurs in the final three-tenths. An important effect of this concentration of the reaction in a zone towards the exit face is that radial mass transfer limitations across the pore may come into play sooner than would be expected if reaction were more uniformly distributed through the pore.

The curves in Figure 3 are calculated for a Δ/b value of 10. Examining the curves for $I_o/i_L = 10^{-2}$ it is seen that η_o and η lie on either side of the η_s curve. This is as expected, because the ohmic voltage gradient in the electrode speeds up the reaction toward the exit face, therefore, the initial activation polarization η_o , has to be less to give a certain i/i_L value. As predicted by equations 22 and 12a, the η_o value at low current density (but reaction still irreversible) approaches η_s , both being given by a Tafel form. At $i/i_L = 0.1$, $\eta - \eta_o \approx 1/2b$. If this current flowed completely from the left hand face of the electrode, the ohmic drop would be $(i/i_L)\rho L i_L = (i/i_L)\Delta = (0.1)(10b)$. Thus the actual $\eta - \eta_o$ is one-half the maximum possible $\eta - \eta_o$, as predicted previously by equation 21. Over most of the current

density range of importance, i/i_L , from 0.2 to 0.95 for example, the difference between η and η_s is less than $1/5$ of the maximum possible ohmic effect. Again, this is reasonable, because the increase in polarization from entrance to exit in the electrode causes the reaction to proceed faster towards the exit. Therefore, the mean distance which the current carrying ions have to traverse is strongly weighted to be near the exit face, giving a relatively small ohmic drop. Of course, as the limiting current is approached very closely, all of the reaction occurs towards the entrance face giving the complete ohmic drop. This condition is only reached as the polarization becomes very large.

We can see, therefore, that the simpler analytical equations leading to Figure 2 are of value since they predict the main features of the process. The ohmic effect is a secondary effect. Both Figures 2 and 3 show that a decrease in the basic parameter \bar{I}_0/i_L causes a bodily shift of the curves, with no difference in shape. Considering Figure 2, it can be seen that, as expected, decrease of \bar{I}_0/i_L by a factor of 10 bodily shifts the polarization curve down by 2.3b volts. (The 2.3 arises because b is $RT/\alpha n_1 F$, whereas the normal Tafel coefficient is $2.3RT/\alpha n_1 F$.) For a one electron process at room temperature the shift would be about 0.12 volts, and for a two electron process, 0.06 volts.

In Figure 2, the uppermost curve represents equation 11 with $\gamma = 1$. This is a pure concentration polarization curve and applies for all values of \bar{I}_0/i_L above about 1 or 2. The reaction is essentially reversible at all fractional current densities*. For the more polarized, irreversible curves, γ has no significance, but it has a large effect for the reversible case.

The effect of change of Δ is shown in Figure 4. The results were computed for $\Delta/b = 0, 10, 20, 50$ and 100. This covers most of the range likely to be encountered for electrodes of reasonable porosity and strongly conducting electrolytes. Figure 5 shows the polarization for a one electron rate controlling step at room temperature where the normal Tafel coefficient would be 0.12 volts. For a given limiting current (given by the flow rate and concentration of reactant), the important parameters are the effective exchange current \bar{I}_0 , the effective ohmic resistance of the electrolyte in the pores and αn_1 , determined principally by the number of electrons transferred in the rate controlling step. The ohmic effect, represented by Δ , does not give a linear effect on the polarization. For example, in going from $\Delta/b = 10$ to $\Delta/b = 50$, the difference between η and η_s over the practical range is not increased 5 times, but less than 5 times. Again, this is to be expected since the higher ohmic voltage gradient forces the reaction to occur at nearer the exit face.

Figure 7 shows the results plotted for limiting currents in the ratios 1:2:5, but with the same \bar{I}_0 . This would correspond to a given electrode and fuel at different flow rates. Note that Δ/b will vary in the same ratio, while \bar{I}_0/i_L will vary as the inverse of the ratio. Figure 7 shows that the initial portions of the curves are almost identical. The figure may be compared with the experimental results given later.

DATA FROM THE LITERATURE

The theory discussed above was first tested on two sets of experimental results taken from the literature. The first set (9) is shown in Table 1. The results for $i_L = 80$ m amps/cm² are plotted in Figure 8. Comparing with Figure 5 it can be seen that $i_0/i_L = 10^{-2}$, $\Delta/b = 20$, $\alpha n_1 = 1/2$, is one set of conditions that approximately fit the experimental results. The test of these values is whether they will accurately predict the polarization at the other limiting current

* It should be noted, however, that $\exp(\eta/b)$ cannot be set equal to $1 + \eta/b$ over all the range, because, although reversible, strong concentration polarization exists.

TABLE I

Polarization versus current for anodic reaction of $\text{Sn}^{2+}/\text{Sn}^{4+}$
in a flow-through electrode of porous carbon (9)

Thickness of electrode	=	0.4cm
Feed concentration of Sn^{2+}	=	0.26 N
Feed concentration of Sn^{4+}	=	0.30 N
Electrolyte	=	6 N HCl
Temperature	=	23°C
Area of electrode	=	5 cm ²

i mA/cm	Expt A		B		C	
	i_L mA/cm ²	η volts	i_L	η	i_L	η
10	80	0.17	150		400	
20		0.23				
30		0.27		0.265		
40	Flow 0.96 ml/min	0.31	Flow 1.80 ml/min	0.29	Flow 4.92 ml/min	0.30
50		0.34		0.315		
60		0.38		0.34		0.34
70		0.42		0.37		0.375
80				0.39		0.41
90				0.41		0.41
100				0.43		0.435
110				0.46		0.465
120				0.50		0.485
140				0.65		0.51
160			0.53			
180						
200						

densities. Thus, for $i_L = 150$ m amps/cm² i_0/i_L must be $(80/150) 10^{-2} = (5.3) 10^{-3}$, and $\Delta/b = (150/80) 20 = 38$. For $i_L = 400$ m amps/cm², $i_0/i_L = (2) 10^{-3}$, $\Delta/b = 100$. Figures 8a, 8b, 8c compare the predicted with the experimental values. Bearing in mind that the values of $i_0/i_L = 10^{-2}$, $\Delta/b = 20$, $\alpha n_1 = 1/2$ were obtained by visual comparison and are thus only estimations, the agreement between predicted and experimental results is good. Figure 8c also shows the predicted values of η_s , the activation-concentration polarization without ohmic effects.

If the value of Δ/b is 20 at $i_L = 80$ m amps/sq cm then the effective specific resistance ρ is given by

$$\Delta = i_L L \rho = 20b, \rho = (20)(0.052)/(0.08)(0.4) \text{ ohm cm} = 32.5 \text{ ohm cm.}$$

The concentrated solutions used (6N HCl) should have a resistivity of about 2 therefore

$$\rho' = \rho(\epsilon/q) \simeq 2 \text{ or } \epsilon/q = 2/(32.5) = 1/16.$$

This value appears to be lower than the optimum, since we would expect ϵ/q to be about 1/5 for normal porosities and tortuosity coefficients. However, a tortuosity factor of 5 and a porosity of about 30% would give the required ϵ/q value, and tortuosity factors up to 5 or even much higher are often found in compacted bodies (10). Such high tortuosity factors can sometimes be lowered to more normal values of about $\sqrt{2}$ by burning out the carbon to remove constrictions and blockages in the structure.

The interesting question now arises as to why $\alpha n_1 = 1/2$ gives reasonable values, when the over-all process is a two electron process. If αn_1 is set equal to 1, b is 0.026. This means that the predicted polarization due to activation-concentration effects at any given i/i_L is very much reduced and more of the actual polarization must be ascribed to ohmic loss. The values of Δ/b (and hence q/ϵ) become much greater; the values of i_0 and Δ obtained using one set of experimental results do not give predictions which fit the other two sets of experiment results. There is strong evidence, therefore, that the $\text{Sn}^{2+} \rightarrow \text{Sn}^{4+}$ reaction has a one electron rate controlling step. An explanation for this has been given by Vetter (12).

I_0/i_L for a limiting current of 80 m amps/sq cm is 10^{-2} , therefore, the exchange current for the carbon electrode is 0.80 m amps/sq cm. Since the thickness of electrode is 0.4 cms, the exchange current per cubic cm of electrode is 2 m amps. As the internal area of the carbon electrode is now known it is not possible to convert this figure to a true exchange current per unit area. It must be recognized that the absence of data on η_0 values makes the treatment somewhat conjectural.

The second set of experimental results obtained from the literature are those of Perskaya and Zaideman (8). These authors give essentially the same equation as equation 14, but they solved it (analytically) only for a short range of current density, for low polarization conditions. The analytical form is too complex to be of much use. In one experiment, however, they measured η_0 and η . They used a 1 mm thick disc of porous platinum prepared from platinum powder and the reaction studied was $\text{Fe}^{2+} \rightarrow \text{Fe}^{3+}$, at equal inlet concentrations of 0.005 N in 1 N H_2SO_4 . Figure 9 shows their results in terms of η versus i/i_L , for a limiting current of about 180 m amps/sq cm. These results may be compared to the shape of the η , η_0 curves computed for $i_0/i_L = 0.5$ and $\Delta/b = 5$, also shown in Figure 9 (if αn_1 is 1/2, the scales of the two figures are identical). The two curves have a strong resemblance and adjustment of αn_1 , i_0/i_L and Δ/b could no doubt be made to bring the η values into better correspondence. The η_0 values, however, appear to be too different to correct by such an adjustment, since the experimental values approach the limiting current more gradually than predicted. This may be due to assumption

iv being false near the limiting current, (see section on Second Limiting Current).

Assuming the values of \bar{I}_O/i_L to be about 0.5 for the experimental results, the exchange current per unit volume of electrode is about 0.9 amps/cm³. Parsons (13) gives the exchange current for this reaction as 6 m amps/sq cm (with a cathodic α_{n_1} value of 0.58, which suggests an anodic α_{n_1} of 0.42) on platinum, at 0.015 N in 2N H₂SO₄. Assuming the same exchange current applies here and correcting for the difference in concentration, the effective specific area of the electrode would be (0.9/2)(1000) = 450 sq cm per cm³, which is a reasonable figure. Assuming Δ/b to be about 5, b about 0.052 volts, then for $i_L = 185$ m amps/sq cm, ρ is equal to 14 ohm. cm. The specific resistance of 1 N H₂SO₄ is about 2.6 ohm. cm, therefore

$$q/\epsilon = \rho/\rho^1 \approx 5.3$$

5.3 is a very reasonable value since an electrode of, for example, 30% porosity with a tortuosity factor of $\sqrt{2}$ would give $q/\epsilon = 4.7$.

EXPERIMENTAL RESULTS

The results reported here have been only recently obtained and insufficient work has been done to present a complete picture. However, some interesting results on half cells can be reported which show the limits of the range of application of the theory presented above. The data has been obtained using a galvanostatic technique, with a porous electrode mounted in a lucite holder (the circuit and apparatus will be described in a later report).

To test whether the theory could explain, in a qualitative manner, results for dissolved fuels such as methanol, a porous electrode made of platinum black was used. The use of this catalytic material made it possible to reach the limiting currents at voltages before the oxygen evolution potential. A known weight of platinum black was compressed between two 80 mesh screens of bright platinum. For the thicker electrodes made with a greater weight of platinum black, a third screen was used in the centre of the electrode. The electrode was clamped in a lucite holder to give compression of the powder. The ohmic resistance through the electrode material was found to be negligible. A fritted glass disc was used at the entrance face of the electrode to provide a rigid backing and to ensure even flow distribution. A counter electrode of platinum screen was mounted in the lucite tube, in line with the porous electrode. The cell was run vertically, with the reactant dissolved in the electrolyte entering at the bottom, flowing through the fritted disc and the platinum black electrode, up past the counter-electrode (at which hydrogen was evolved) and out to a collector for flow rate measurement. Evolved gases were taken off from the top of the cell. The voltage between the electrode and the entering electrolyte was measured versus a saturated calomel electrode. The electrode-electrolyte voltage at the exit face was also measured, versus the saturated calomel electrode, by extrapolation to the electrode face of measurements at two known positions downstream.

Blank measurements made without a dissolved reactant showed negligible current densities between hydrogen evolution potentials and oxygen evolution potentials. Some typical results using dissolved fuel are shown in Figures 10 to 13. All tests were made at room temperature. The broken lines represent the inlet voltage and the solid lines the exit voltage, where the latter is the curve which shows the full voltage loss at the electrode (see later discussion of Figure 15). In general the curves were very stable and providing the voltage was not taken too near to oxygen evolution, it was usually possible to go up and down the curve with negligible hysteresis.

It is obvious that the results for this type of electrode cannot be completely explained by the simple theory developed previously. In general, the limiting currents obtained at the larger flow rates were less than those expected from the amount of reactant being forced through the electrode. A discussion of the reasons

for this apparent anomaly is given in the next section.

SECOND LIMITING CURRENT

A study of the results in Figures 10 and 11 show that at low rates of flow, the limiting current obtained was higher than the expected value. This is partly due to external back diffusion of unreacted fuel present in the exit volume of the cell. In time, the flow of fuel-depleted electrolyte will flush out the exit compartment, but at low rates of flow this is a slow process. In later tests on a slow flow rate we kept an electrode near the limiting current for over an hour and a slow drift of the limiting current to the expected value was observed. (This was a tedious process since it required constant adjustment of the current to prevent the potential going to oxygen evolution.) Diffusion from the entrance volume was negligible due to the sintered glass disc at the entrance, and back diffusion could have been greatly decreased by using another disc at the electrode exit. However, this could have prevented the use of a simple extrapolation method to obtain the exit face polarization. At higher flow rates and limiting currents, the back diffusion is proportionately less and the flushing of the exit dead space proportionately faster. It was found that at a flow rate of about 0.4 cm/min the back diffusion effect was almost negligible.

Figures 10 and 11 also show that at high flow rates the limiting current is less than that expected. There are at least three possible reasons for this. Firstly, radial mass transport hindrance across the pores of the electrode might be significant. Secondly, the rate of chemisorption of the fuel might be rate limiting, in which case a chemisorption limiting current is obtained when the fractional surface coverage θ tends to zero all over the electrode (7). Thirdly, the electrochemical discharge may be preceded by a dissociation in the bulk of the pore electrolyte and the limiting current would then be determined by a limiting rate of the predissociation.

Considering the first possibility, that of radial mass transport, the problem can be solved with sufficient accuracy by considering the mass transfer analogy to radial heat transfer in laminar flow systems. The solution for laminar flow, for a fixed concentration at the wall and for fully developed velocity and concentration profiles, is given by (14)

$$Nu = hD/k = 3.66$$

$$\text{rate per unit area} = h(R_m - R_w) \quad (23)$$

D is the pore diameter; k is the mass transfer coefficient, which is the diffusion coefficient of the reactant in this case; R_m is the mass flow mean concentration of reactant and R_w is the concentration at the wall of the pore. The assumption of negligible entrance effects, and fully developed flow, is probably reasonably good because of the very low Reynold's numbers of flow in fine pores. A limiting current is clearly reached when $R_w = 0$ at all points along the wall of the pore. Let A be the specific geometric area of the walls of pores, in cm^2 of area per cm^3 of electrode (note that A does not necessarily equal S). Then the differential current density in an element dx at the condition where $R_w = 0$ is

$$di = nF \cdot 3.66(k/D)AR_m dx \quad (24)$$

At the same time

$$\begin{aligned} di &= nFv \, dR \\ i &= nFv(R_i - R_m) \\ i_{L1} &= nFvR_i \end{aligned}$$

Therefore,

$$R_m = (i_{L1} - i)/nFv$$

and
$$\int_0^{i_{L2}} (1/(i_{L1} - i)) di = 3.66(Ak/Dv) \int_0^L dx$$

or
$$i_{L2}/i_{L1} = 1 - e^{-3.66(AkL/vD)} \quad (25)$$

Thus the ratio of the observed limiting current i_{L2} to that of the expected limiting current i_{L1} is given by equation 25, where A/D is an unknown factor. An estimate of the ratio of limiting currents can be made by taking L as 0.1 cm, k as 10^{-5} cm²/sec, v as 1 cm/sec, A as 500 cm²/cm³ and D as 10 microns. The exponent of the exponential term is then approximately -20 and the radial mass transport effect would be negligible. However, a 10 fold decrease in the magnitude of exponent, given for example by $A = 250$ cm²/cm³ and $D = 50$ microns, would give a significant effect.

The second possibility, that of a chemisorption rate limitation can be analyzed by assuming that the limiting rate of chemisorption is given by,

$$\text{rate per unit area} = k_1 R, \text{ gm moles/cm}^2\text{sec.} \quad (26)$$

This follows from a chemisorption rate equation when $\theta \rightarrow 0$, $1 - \theta \rightarrow 1$. k_1 is the rate constant. Equation 24 is now replaced by

$$di = nFk_1 SR dx.$$

The treatment then follows as before giving

$$i_{L2}/i_{L1} = 1 - e^{-(Sk_1L/v)}$$

The third possibility, of a dissociation before discharge, is similarly handled by assuming a dissociation rate of

$$\text{rate per unit volume} = k_2 R$$

A limiting rate is obtained when the reaction is irreversible and the product of reaction is removed, by electrochemical reaction, as fast as it is formed. Then the differential current density is given by

$$di = nFk_2 RE dx$$

and, as before,

$$i_{L2}/i_{L1} = 1 - e^{-(k_2 CL/v)} \quad (29)$$

Thus the three possibilities all give rise to a form

$$i_{L2}/i_{L1} = 1 - e^{-(JL/v)} \quad (30)$$

where the exponent includes L/v in all cases, but J has a different physical meaning for the different cases.

If equation 27 or 29 applied it might be expected that different fuels would give different values of J , whereas if equation 25, that for radial mass transport, applied then J would be nearly constant for different fuels.

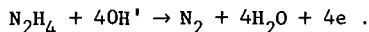
DISCUSSION OF RESULTS

Table 2 shows the value of J calculated for a number of different tests. L was determined from the weight of platinum black used in constructing the electrode, from the relation 100 mg per cm² \approx 1 mm of thickness. For methanol and potassium formate the value of J was approximately constant, with a mean value of 4.8. When it is considered that the electrodes are pressed powder and can vary between one pressing and another, it must be concluded that J is constant within the reproducibility of the system. No significant difference was present between methanol in acid or methanol in alkali, or between these and potassium formate in alkali. This

TABLE 2. Values of J for Various Systems

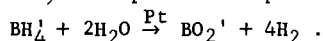
Fuel	n, Electrons Used to Calculate $\frac{I}{L}$	Molar Concentration of Fuel	Electrolyte	mg/cm ² of pt. Black	L cm	v cm/min	J
Methanol	6	0.05	4MKOH	230	0.23	1.0	4.3
		0.1	4MKOH	200	0.20	0.57	6.8
		0.1	3MH ₂ SO ₄	80	0.08	0.4	4.3
		0.1	3MH ₂ SO ₄	80	0.08	1.0	5.1
Potassium Formate	2	0.04	4MKOH	230	0.23	1.0	3.9
		0.05	4MKOH	230	0.23	2.03	4.3
		0.2	4MKOH	230	0.23	0.37	5.4
		0.2	4MKOH	230	0.23	1.0	4.0
					Mean	4.8	
Potassium Borohydride	8	0.02	4MKOH	80	0.08	2.5	28
		0.02	4MKOH	80	0.08	4.0	33
Hydrazine	4	0.02	4MKOH	80	0.08	1.37	33
		0.02	4MKOH	80	0.08	2.0	37
		0.1	4MKOH	80	0.08	1.0	43
					Mean	35	

is evidence that the effect is one of radial mass transfer. However, the results from hydrazine (see below) suggest that if radial mass hindrance is present then gas evolution reduces this effect. Gas evolution was observed with methanol in acid electrolyte. For potassium borohydride and hydrazine, on the other hand, J was again reasonably constant but with a mean value of 35. Bigger J means less departure from the expected limiting current and would be due to an increased mass transport factor, increased rate of chemisorption or increased rate of predissociation. The hydrazine reaction is;

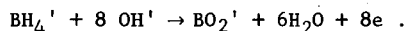


Vigorous gas evolution from the test electrode was observed. Thus for this type of electrode, the nitrogen evolved within the electrode may increase the effective radial mass transport factor; it does not appear to block the electrode. A blockage of the electrode by trapped gas bubbles would be expected to reduce the effective internal area of the electrode, leading to higher polarization and a reduction in J . Blockage does not seem to occur and the reason may be that since reaction is concentrated towards the exit face, the small bubbles produced by the reaction may reach the exit face, by vertical travel, before they grow very large.

Decomposition of the borohydride to produce H_2 was noted at open circuit conditions. Therefore, some prior decomposition reaction may be postulated,



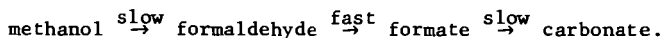
However, the released hydrogen was readily used when appreciable currents were drawn, giving an over-all reaction,



Certainly, some of the hydrogen released to the surface from the borohydride will never be released as gas under load, since surface hydrogen will be discharged electrochemically. However, it is possible that enough is released and later reused to cause increased radial mass transport, comparable to that observed by hydrazine.

The analysis of J factors given above show that, at least for the platinum powder electrode, the assumption of a negligible radial mass transfer effect may not be valid. Alternatively, a slow chemisorption or dissociation may be present. Although we have not completed the inclusion of these effects in a more comprehensive treatment, it is reasonable to suppose that the voltage-current curves will fit into three categories. Case 1 would be where JL/v is large, the interfering effect is small and the curves correspond to the basic theory. For a one electron rate controlling step at room temperature, the voltage change between $i/i_L = 0.1$ and $i/i_L = 0.9$, for the center of the η_0, η band, is about 0.15 volts. Case 2 would be for a moderate value of JL/v , such that $i_{L2} \approx i_{L1}$, but a considerable effect on the shape of the curve is present. The effect will be to increase the general slope of the voltage-current curves, especially near the limiting current. Case 3 is for a small value of JL/v , which gives a greatly reduced limiting current. At low currents the curves will be nearly the same, but the greater the effect of JL/v then the more gradually will the curves approach the limiting current, the slopes will be greater, and the sharp bend-over near the limiting current for the η_0 line will be replaced by a gradual approach. Case 2 behaviour can be seen in Figure 11, the results for potassium formate, where the general slope of the curves is greater than expected, even when the limiting current is close to the theoretical value. Figure 10, the results for methanol in basic solution, also shows this general behaviour but the increase in slope is greater than for the formate case. This is almost certainly due to two steps of comparable rate being involved. Other results we have obtained show that formaldehyde is more rapidly oxidized than methanol or formate, therefore the over-all methanol curve is composed

of,



If the formate oxidation were much slower than the methanol, two waves in the voltage-current plot would be observed. However, since they are of comparable rate, methanol is reacted to give appreciable concentrations of formate in the electrode, which then further reacts as the voltage increases. The two waves fuse into one long curve.

The analysis of J factors given above indicate that the hydrazine and borohydride reactions are less influenced by the effect. Therefore, it is possible that results for a high value of L/v for these systems may approach the expected values for the simple theory. (It is not possible to use too low flow rates, since back diffusion then becomes appreciable.) Figure 14 shows a comparison of experimental results with computed results for hydrazine, assuming a value of Δ/b of 10, $\alpha_n = 1/2$, and a value of \bar{I}_0/i_L of 10^{-3} , based on a theoretical open circuit potential of 1.40 volts (v. saturated calomel). The values were selected from the difference in entrance and exit polarizations and from the position of the curves along the voltage scale. It can be seen that the shapes of the experimental curves are in fair agreement with theory up to values of i/i_L of about 0.7, after which they show steeper slopes and a less abrupt change to the limiting current. Thus, the J factor effect comes into play at the higher current densities, in the expected manner. The observed open circuit potential is considerably more positive than theoretical but this is to be expected since, as the voltage is past the hydrogen evolution potential, a mixed potential will result. Calculation of ϵ/q in the same manner as before gives a value of about 1/9, which is reasonable.

The results shown in Figures 10 to 13 were deliberately taken at low concentrations and flow rates, so that the limiting currents could be reached without heating effects. At concentrations of several moles/litre, and high flow rates, the limiting current densities became so great that heating occurred on the passage of the electrolyte through the electrode. Under these conditions it was possible to obtain current densities of two or three amps/cm² at voltages well below the point of oxygen evolution but, in the design of cell used, the ohmic heating at this high current caused instability due to boiling of the electrolyte.

The voltage in a fuel cell consisting of two flow-through electrodes using fuel and oxidant is illustrated in Figure 15. Line ab represents the voltage change between the electrode potential at a and the electrolyte at b, at ideal zero current conditions. cd is the voltage change from the electrolyte to the cathode under these conditions. Under load, eb is the loss of voltage, η_{o1} , due to initial activation polarization on the fuel electrode, while η_1 is the total polarization through the electrode. The line fghi represents the ohmic voltage gradients through the free electrolyte, gh being that across a separator. ijk is the equivalent cathode voltage curve to gef for the anode. The terminal voltage is now V, where $V = E_0 - (\eta_1 + \eta_r + \eta_2)$. The results presented in Figures 10 to 13 show only η_1 values versus current density for the given fuels.

CONCLUSIONS

The theory developed for the combined effects of activation, concentration and ohmic polarization at porous flow-through electrodes is likely to apply for simple redox systems and electrodes of small pore diameter. In studies of this kind of electrode it is essential to make measurements of entering and exit voltage in order to obtain a complete picture of the process. Results using methanol, formaldehyde, potassium formate, hydrazine and sodium hydroboride at non-consolidated electrodes of platinum black show that further factors are involved. These factors may include more complex forms of the electrochemical discharge equation, involving a bulk predissociation or chemisorption step, or a radial mass transfer hindrance.

Further work is planned on the theory of such systems. It is also planned to test the basic equation for simple redox systems and fine-pore consolidated electrodes.

Using platinum black flow-through electrodes at room temperature it was found that, at appropriate flow rates, methanol could be completely oxidized to carbonate in alkaline solution or CO_2 in acid solution. Tests on formaldehyde and potassium formate in basic solution showed that the formaldehyde is relatively rapidly oxidized compared to methanol, while formate is only slightly more readily oxidized. It was not possible to tell whether the chemisorption of methanol or the initial breakdown of methanol to formaldehyde was the first slow step. On the same type of electrode, potassium borohydride could be completely utilized giving eight electrons per molecule and hydrazine could be utilized to N_2 , giving four electrons per molecule. The evolution of gas did not hinder the performance of the electrode.

REFERENCES

- (1) Posner, A. M., *Fuel* 34, 330 (1955).
- (2) General Electric Company, Aircraft Accessory Turbine Dept., "Research on Low Temperature Fuel Cell Systems", Progress Report No. 8, Contract No. DA-44-009-ENG-4771, U. S. Army E.R.D.L., Ft. Belvoir, Virginia. ASTIA No. AD 243 474; (1960).
- (3) Austin, L. G., "Fuel Cells" in "New Techniques for Energy Conversion", Ed. S. N. Levine, Dover Pub. Inc.
- (4) Guillou, M., "Repartitions couplees du potential et des concentrations dans les cellules electrochimique." Thesis presented to Faculte des Science de p'Universite de Paris, 1963. Also private communications from R. Buvet, Electricite de France.
- (5) Lockheed Missiles and Space Company, "Basic Studies on Fuel Cell Systems", Quarterly Reports No. III and IV, Contract NOW60-0738-d, Bureau of Naval Weapons. ASTIA Nos. AD 273 702, AD 278 353; (Nov. 1961 to May 1962).
- (6) Monsanto Research Corporation, "Compact Power Fuel Cell", Report ASD-TDR-62-42, Contract AF33(616)-7735, Flight Accessories Lab., Wright Patterson Air Force Base. ASTIA No. AD 282 862; (June 1962).
- (7) Austin, L. G., "A Discussion of Some Aspects of Electrode Kinetics Relevant to Fuel Cell Studies", Report No. 1, Contract DA49-186-502-ORD-917, Diamond Fuze Laboratories, Washington, D. C. (June 1962).
"Electrode Kinetics and Fuel Cells", Proc. Inst. Elec. and Electronic Engineers, 51, 820 (1963).
- (8) Perskaya, R. M. and Zaidenman, I. A., Proc. Acad. Science U.S.S.R., Physical Chemistry Section, 115, 513 (1957).
- (9) Bond, A. P. and Singman, D., "Electrode Kinetics of Oxidation - Reduction Couples", Diamond Ordnance Fuze Laboratories, Washington 25, D.C. (1960).
- (10) Carman, P. C., "Flow of Gases Through Porous Media", Academic Press, Inc., New York, 1956.
- (11) Austin, L. G., "Polarization of Porous Flow-Through Electrodes, Report No. 2, Contract DA49-186-502-ORD-917, Diamond Ordnance Fuze Laboratories, Washington 25, D. C. (Sept. 1962).
- (12) Vetter, K. J., "Elektrochemische Kinetik", Springer-Verlag, Berlin, p. 380, 1961.

- (13) Parsons, R., "Handbook of Electrochemical Constants", Academic Press, Inc., New York, 1959.
- (14) Rohsenow, W. M. and Choi, H. Y., "Heat, Mass and Momentum Transfer", Prentice Hall, Inc., New Jersey, p. 141, 1961.

LIST OF NOMENCLATURE

A,	specific geometric area of pore walls.
b	= RT/cm_1F
D,	pore diameter
f	= $\exp(\eta/b) + \gamma \exp(-\eta/b)$
F,	Faraday
i,	current density
i_o ,	true exchange current density
i_o ,	= i_oSL , apparent exchange current density for the electrode
i_L ,	limiting current density
i_{L1}	= $nFvR_i$, expected limiting current density
i_{L2}	obtained limiting current density
J,	defined by equations 28, 30, 32, 33
k,	mass transfer coefficient of reactant, cm^2/sec
k_1 ,	specific rate constant for chemisorption
k_2 ,	rate constant for dissociation
L,	thickness of electrode, cm
M,	number of increments into which L is divided
n,	number of electrons involved in the reaction
n_1 ,	number of electrons involved in the rate controlling step
N	N'th increment between 0 and M
Nu	Nusselt number
P,	concentration (activity) of product at distance x in the electrode
P_i ,	initial value of P, at $x = 0$
q,	tortuosity factor for conduction in electrolyte in the pores of the electrode
Q	= $\exp(\eta/b) - \exp(-\eta/b)$
R,	concentration (activity) of reactant at distance x in the electrode
R_i ,	initial value R, at $x = 0$
RT,	gas constant times absolute temperature
S,	effective specific area of electrode interior, cm^2/cm^3
v,	velocity of flow of feed, cm/sec
x,	distance into electrode from entrance face
\bar{x}	= x/b
α ,	transfer coefficient in the direction of reaction
Δ	= $i_L \rho L$, maximum ohmic polarization
$\bar{\Delta}$	= Δ/b
ϵ ,	porosity of the electrode
η ,	polarization
$\bar{\eta}$	= η/b
η^L	= $\eta - \eta_o$
η_o ,	polarization at entrance face
η_s ,	Polarization with negligible internal ohmic effect
γ ,	ratio of inlet reactant concentration to inlet product concentration
ρ_i	effective specific resistance of electrolyte in the pores, ohm.cm
ρ^L ,	true specific resistance of the electrolyte

ACKNOWLEDGEMENTS

The work reported here has been performed for the Harry Diamond Laboratories, Washington, D.C. under contract DA49-186-502-ORD-917. Grateful acknowledgement is made to the United States Army Materiel Command for permission to publish the work.

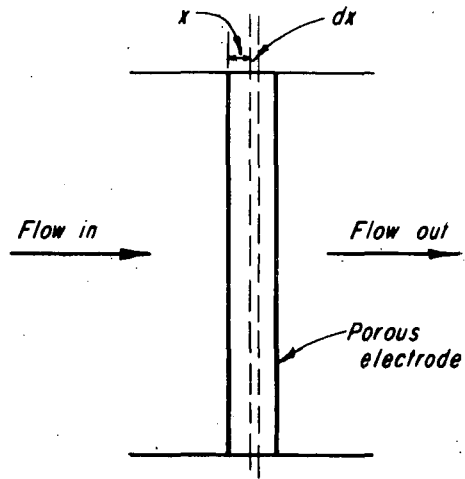


FIGURE 1. Illustration of System Studied.

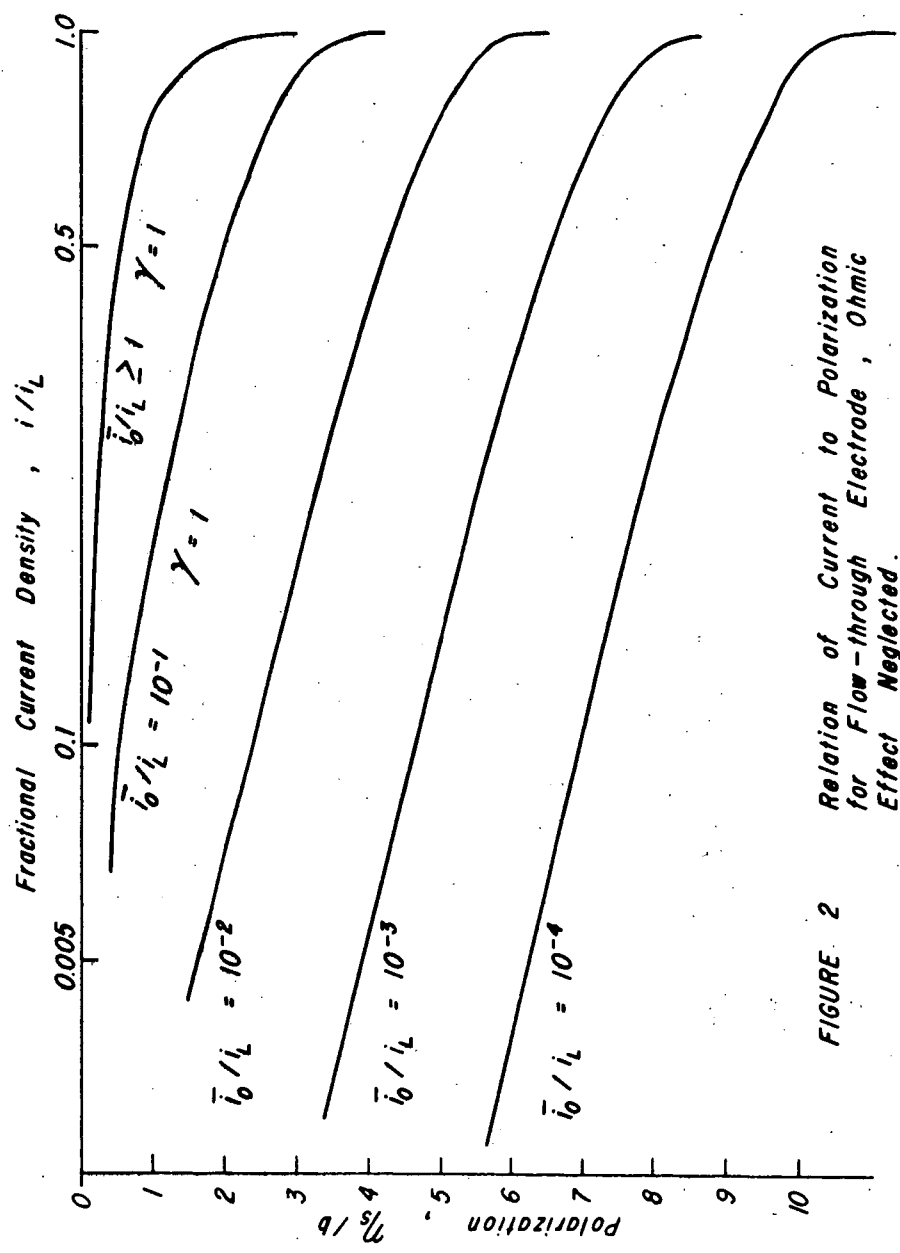


FIGURE 2 Relation of Current to Polarization for Flow-through Electrode, Ohmic Effect Neglected.

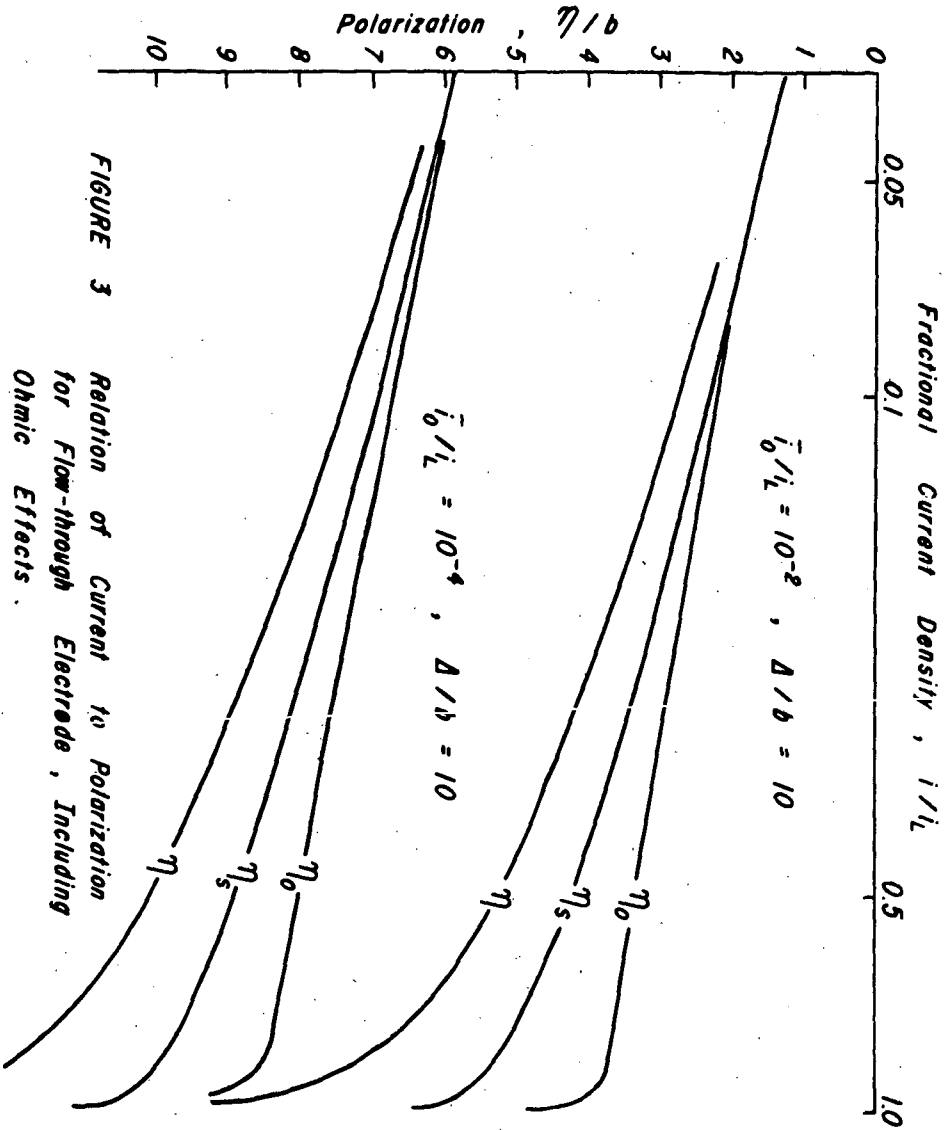


FIGURE 3 Relation of Current to Polarization for Flow-through Electrode, Including Ohmic Effects.

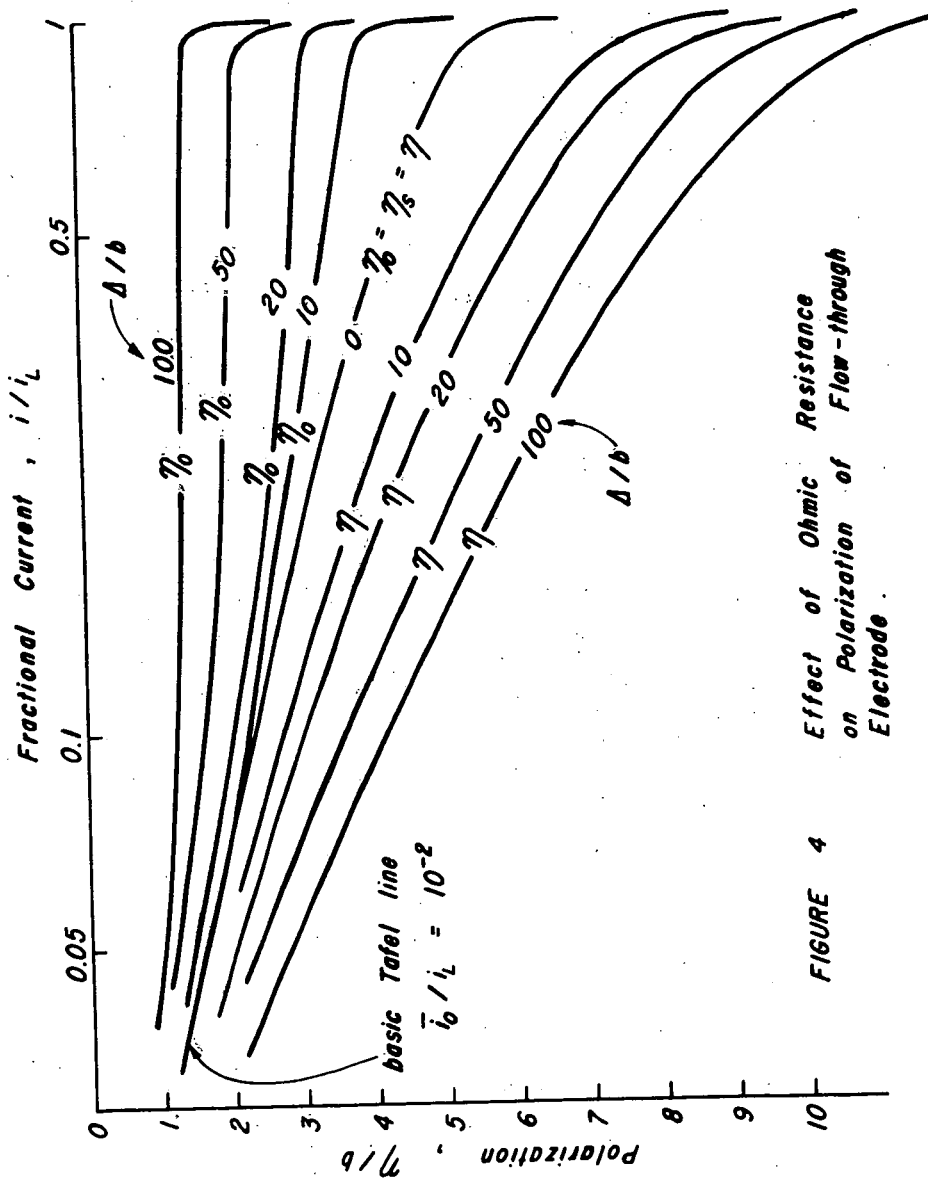


FIGURE 4 Effect of Ohmic Resistance on Polarization of Flow-through Electrode.

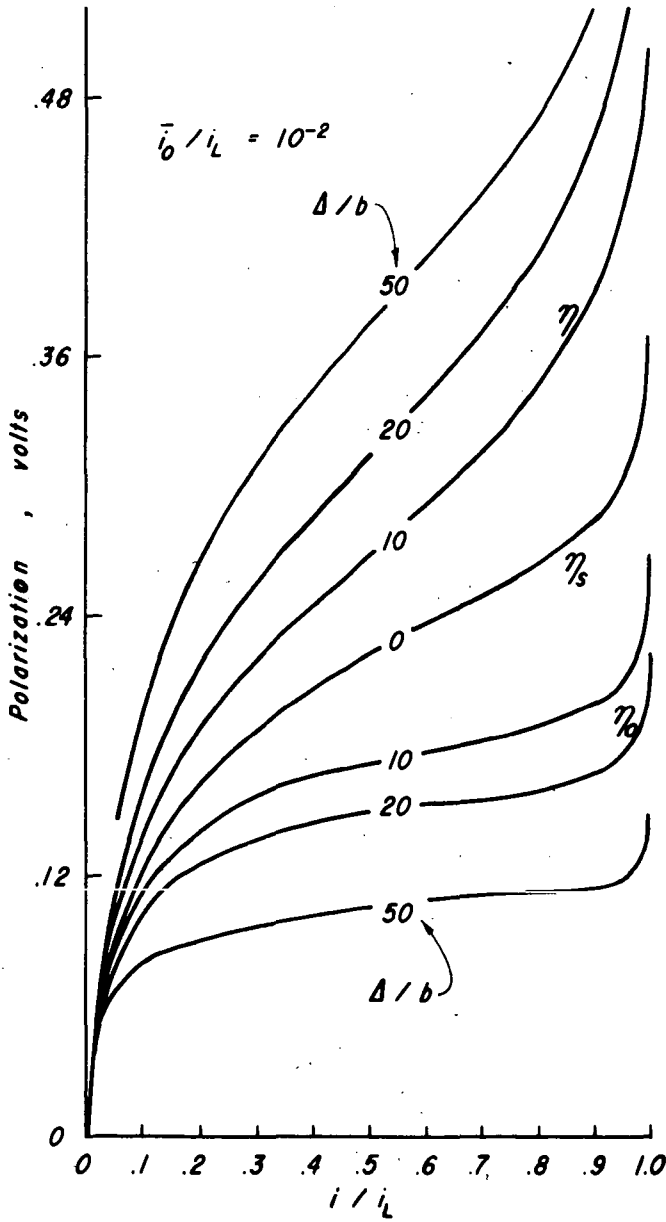


FIGURE 5 Results of Figure 4 for a One Electron Rate Controlling Step, Tafel Coefficient Equal to 0.12volts.

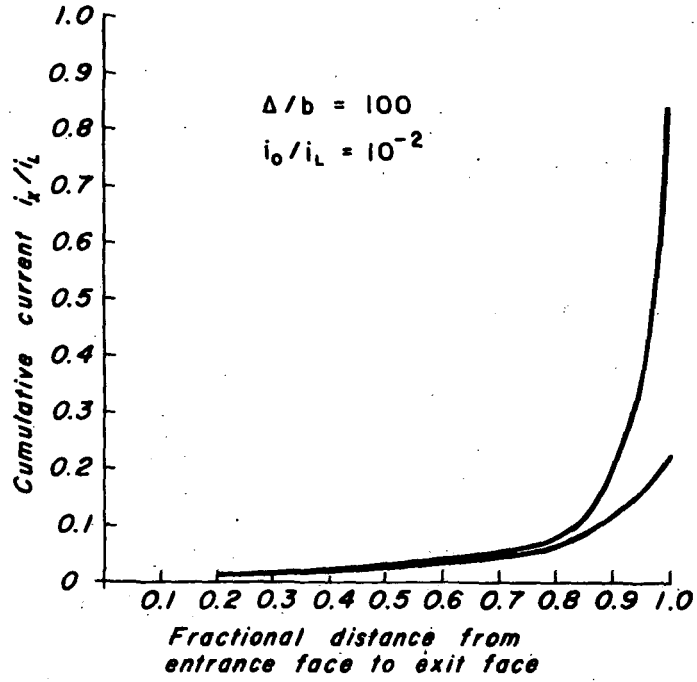


FIGURE 6 Cumulative reaction through a flow-through electrode.

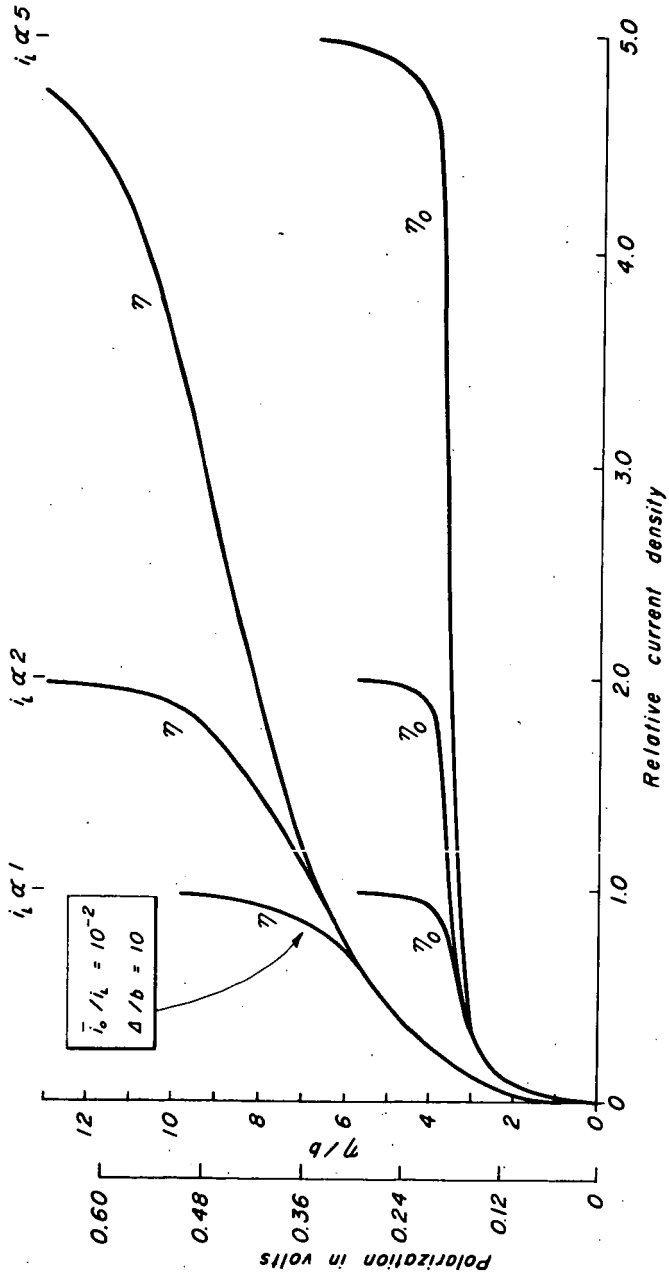


FIGURE 7 Computed Effect of Increasing Flow Rate.

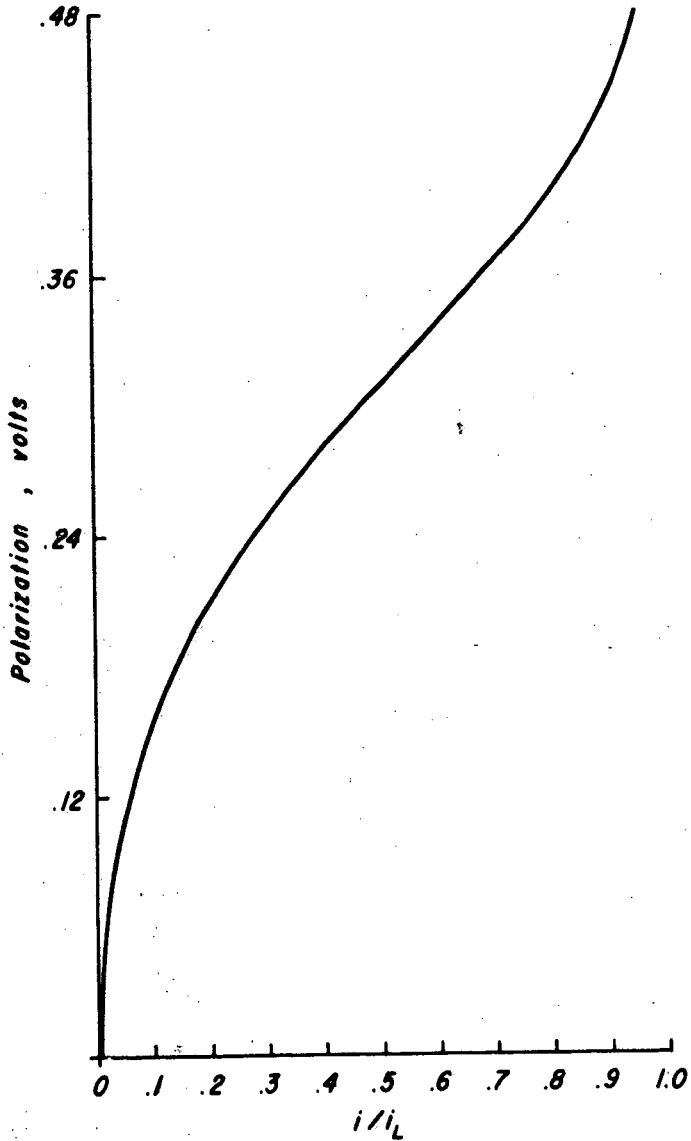


FIGURE 8 . Polarization Curve for $\text{Sn}^{2+} \rightarrow \text{Sn}^{4+}$,
 $i_L = 80 \text{ mamps/cm}^2$. (see table 1)

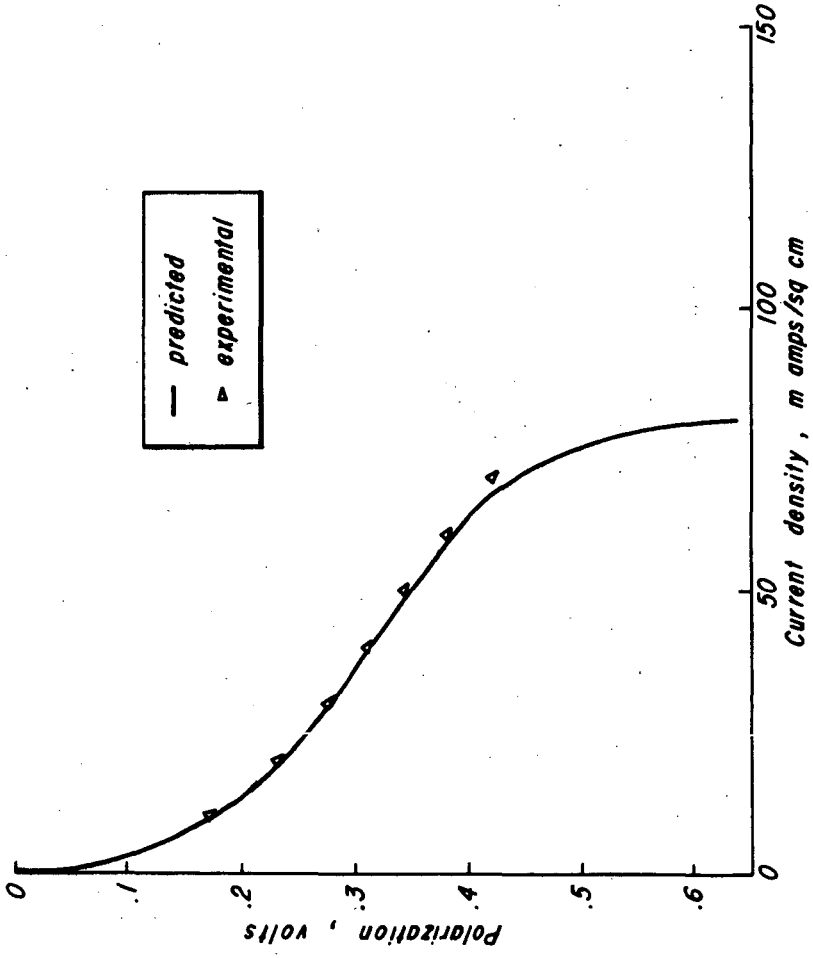


FIGURE 8a Comparison of Computed with Experimental Polarization.
(Sn-Zn couple)

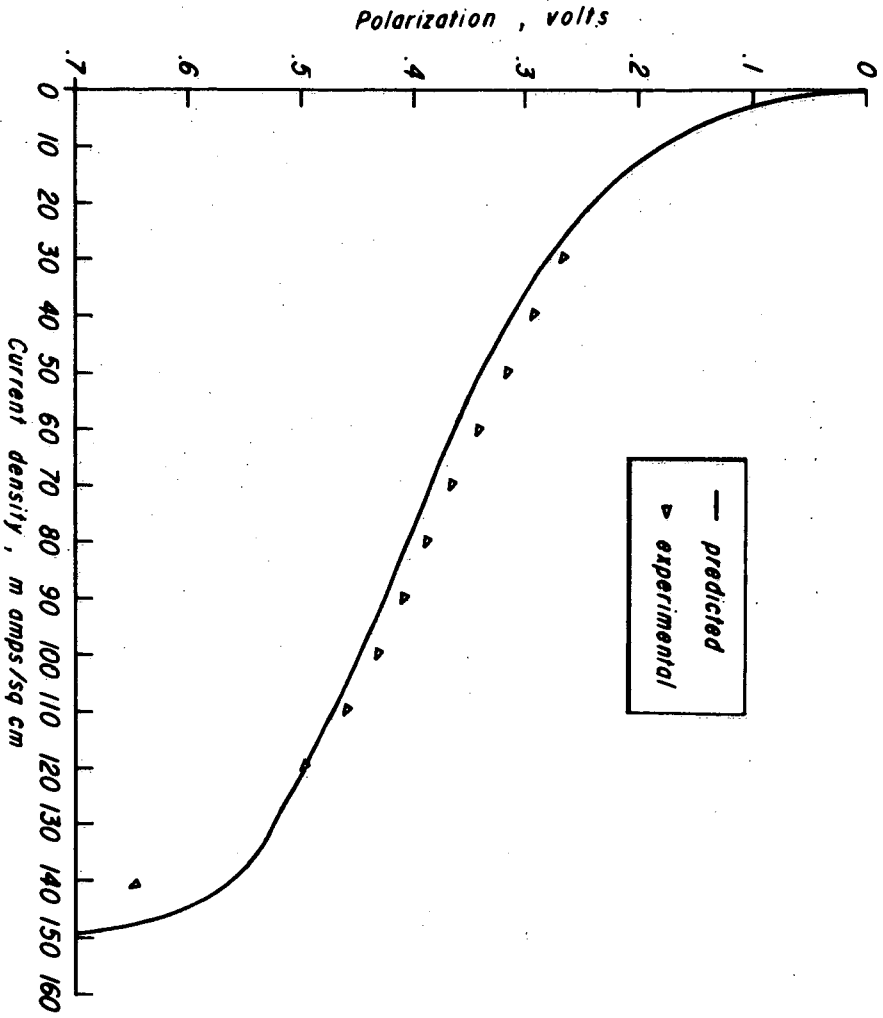


FIGURE 8b Comparison of Computed with Experimental Polarization.
($\text{Sn}^{2+}/\text{Sn}^{4+}$ couple)

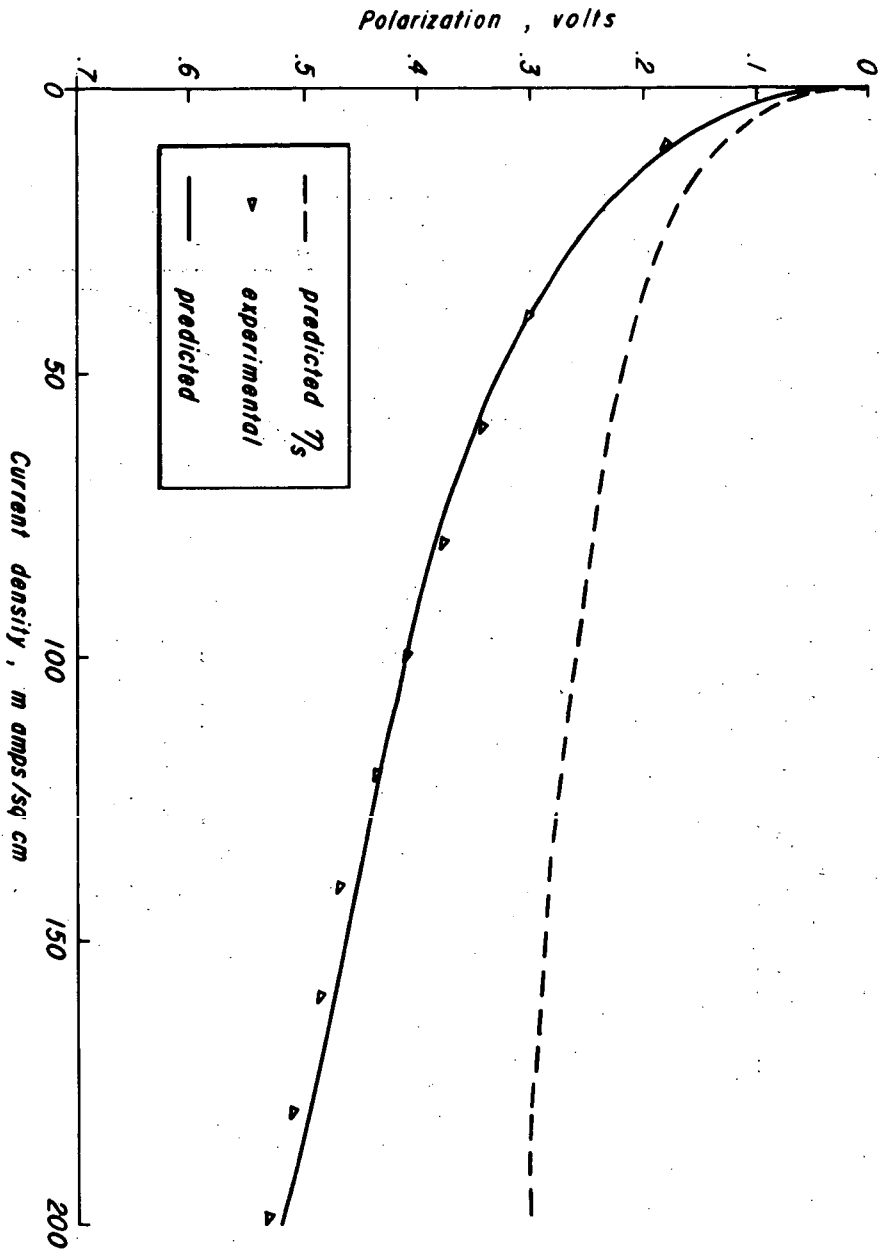


FIGURE 8c Comparison of Computed with Experimental Polarization.
($\text{Sn}^{2+}/\text{Sn}^{4+}$ couple)

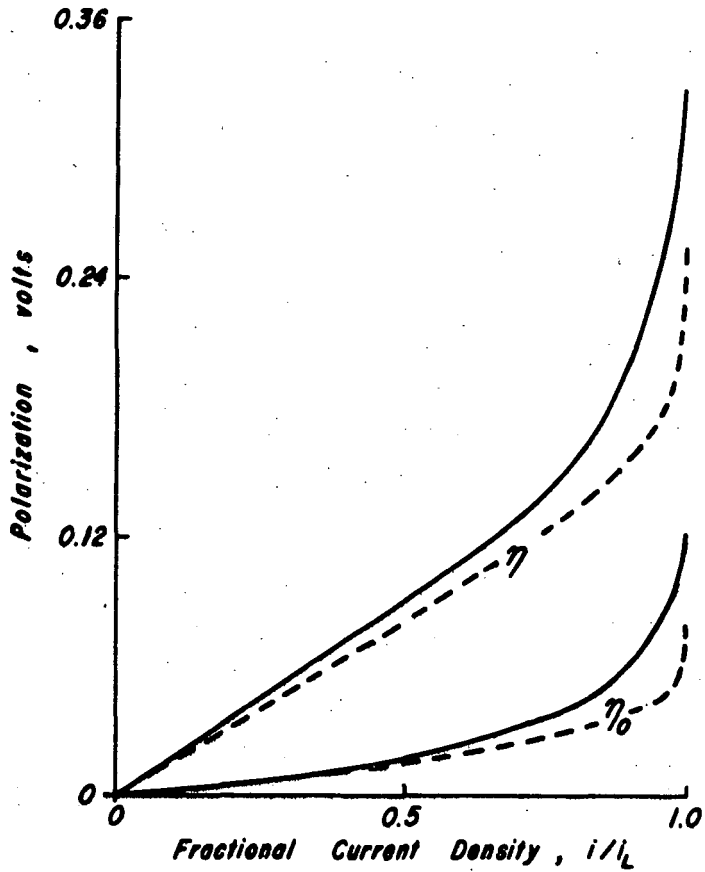


FIGURE 9 — Polarization Curve for $Fe^{2+} \rightarrow Fe^{3+}$,
 $i_L = 185$ m amps/cm².
 -- Computed Polarization for Flow-
 through Electrode; $i_0/i_L = 0.5$,
 $\Delta/b = 5$.

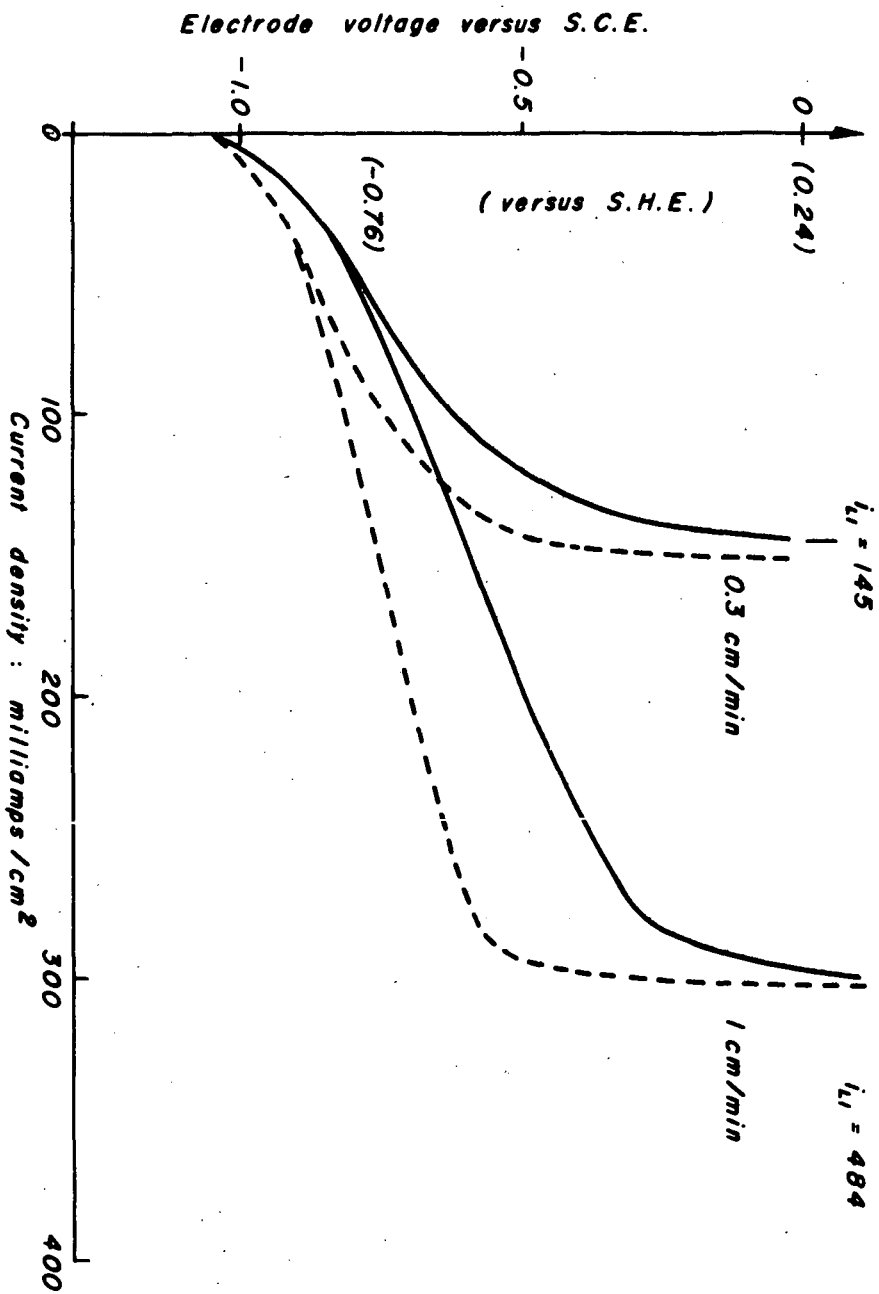


FIGURE 10 Fuel, Methanol 0.05M; Electrolyte, 4M KOH; Electrode, 230 mg/cm² Pt Black.

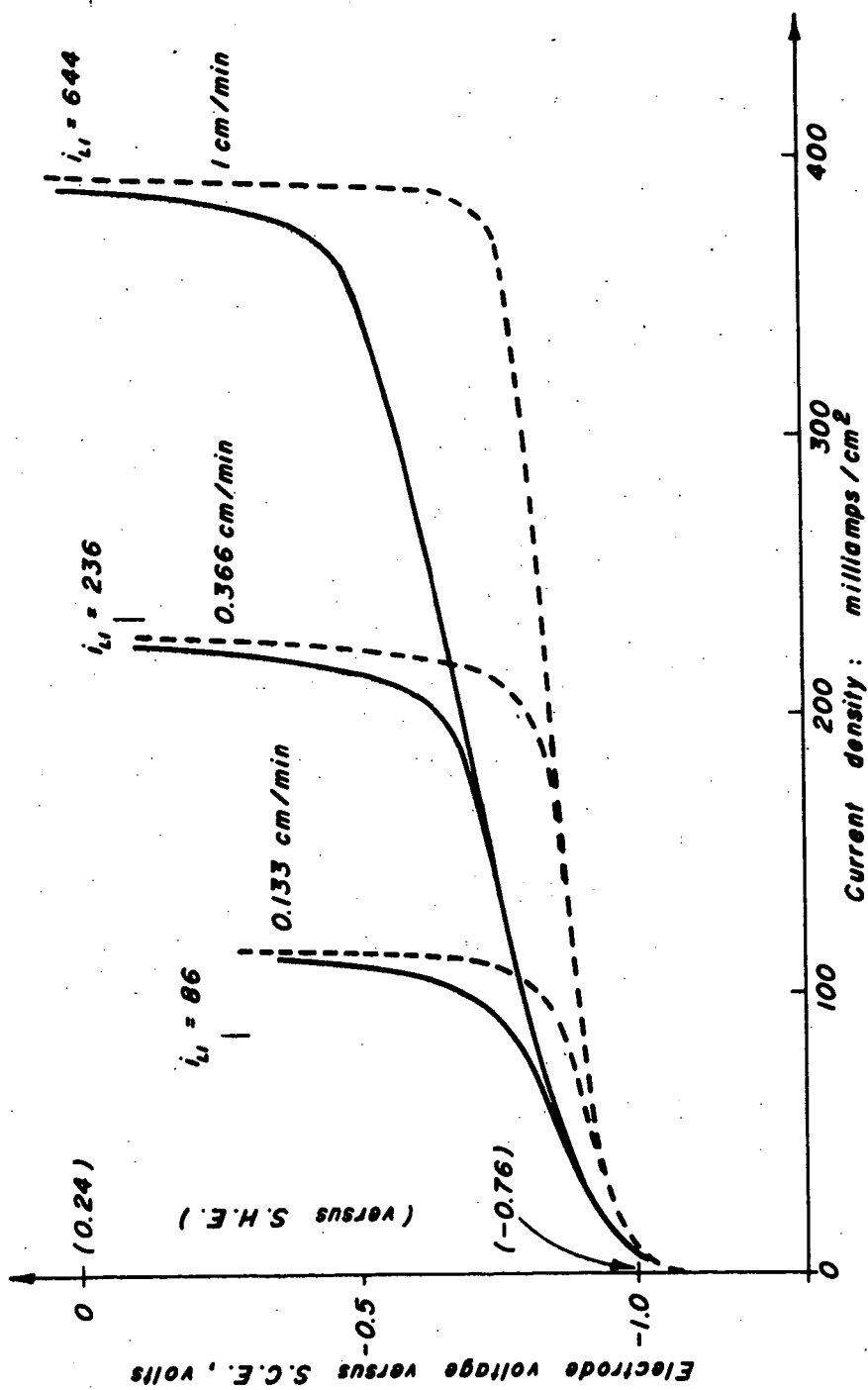


FIGURE 11 Fuel, Potassium Formate 0.2M; Electrolyte, 4M KOH; Electrode, 230 mg/cm² Pt Black.

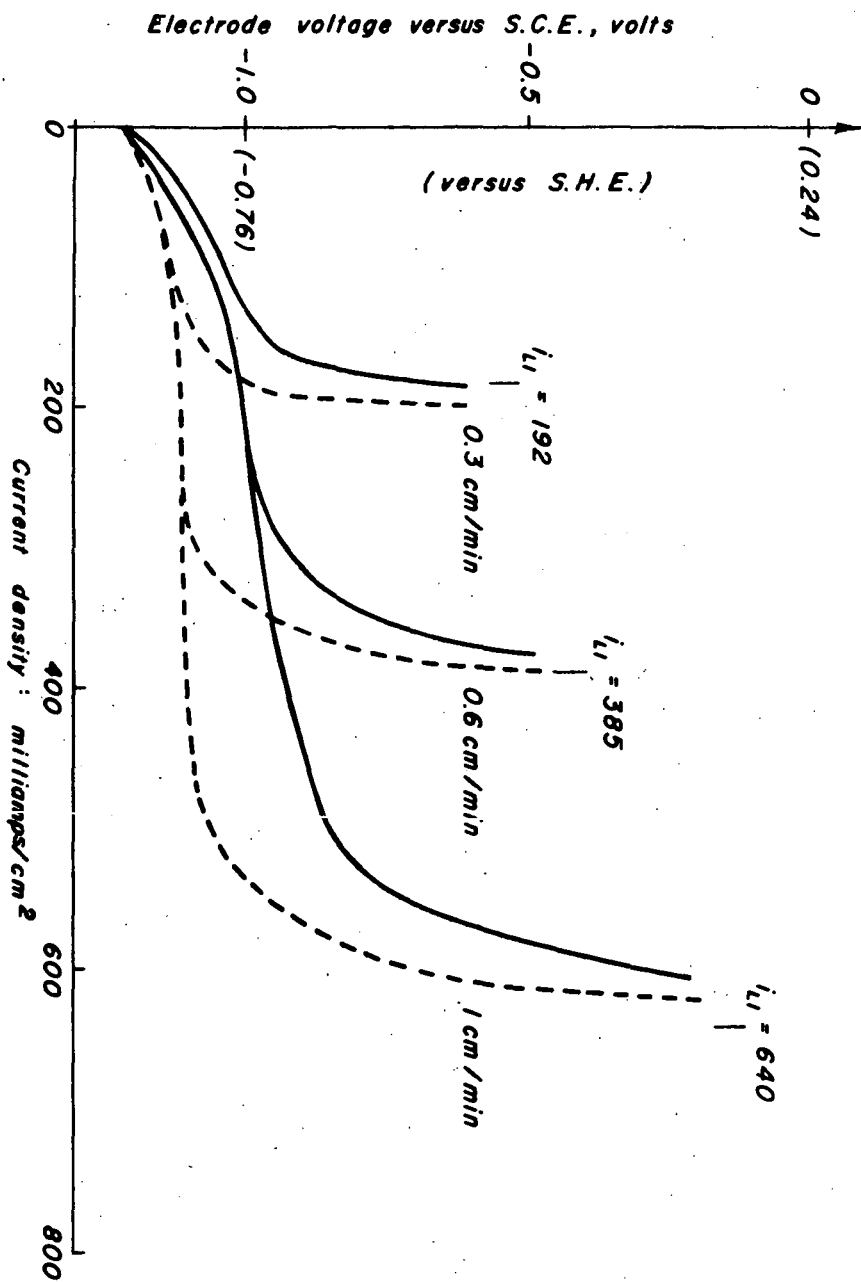


FIGURE 12 Fuel, 0.1M N_2H_4 ; Electrolyte, 4M KOH; Electrode, 80mg/cm² Pt block.

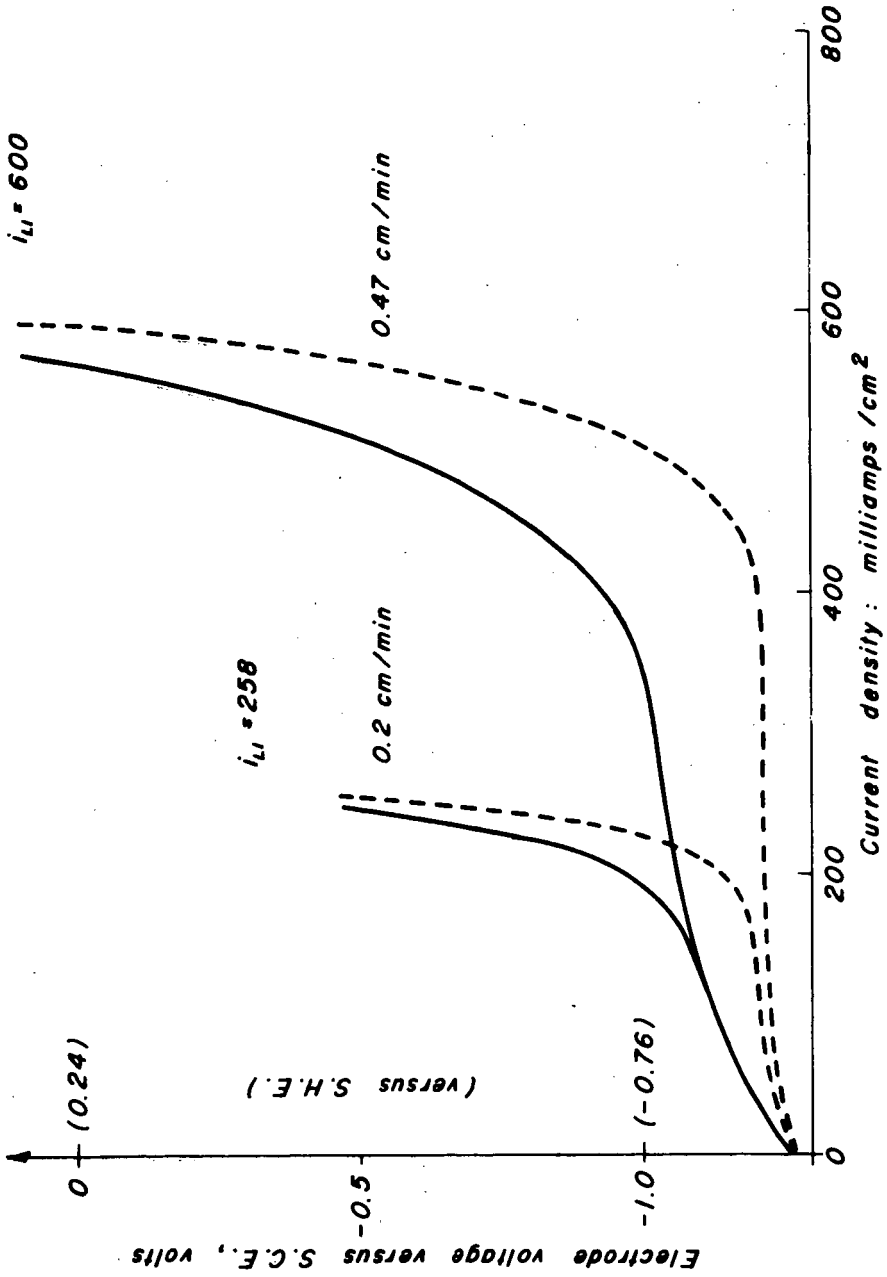


FIGURE 13 Fuel, 0.1M KBH₄; Electrolyte, 4M KOH; Electrode, 80 mg/cm² Pt Black.

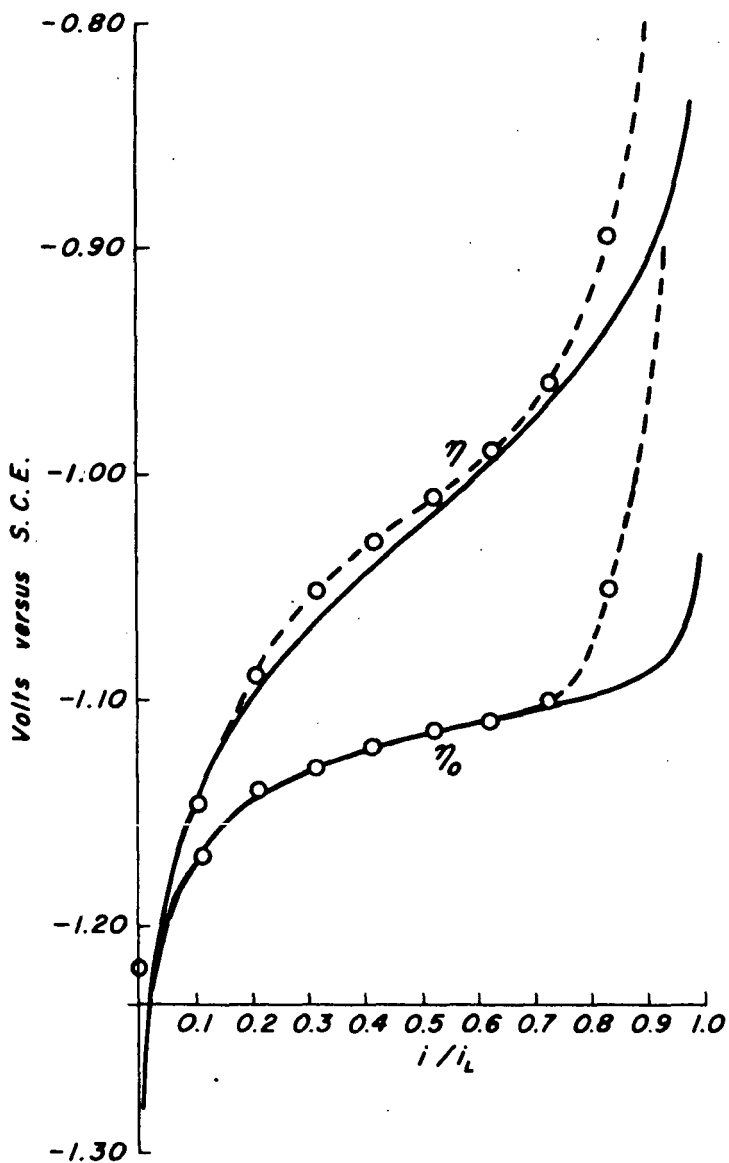


FIGURE 14

- Experimental values for 0.1M N_2H_4 in 4M KOH, 0.6 cm/min, 80mg/cm² Pt black.
- Computed curve for $\Delta/b = 10$, $i_0/i_L = 10^{-3}$

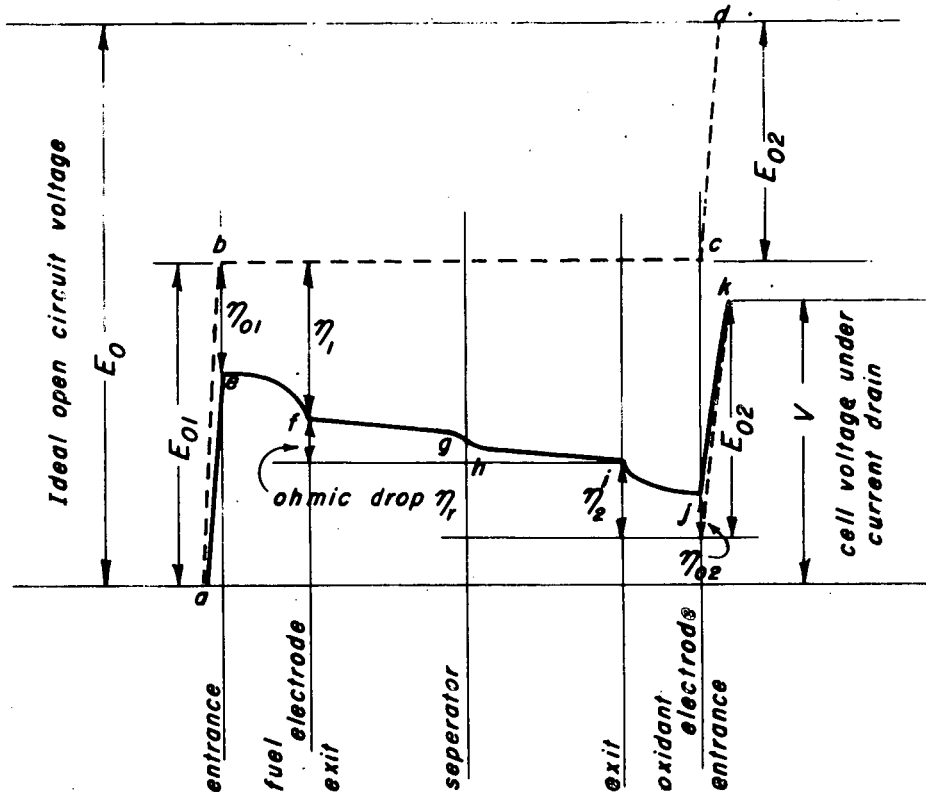


FIGURE 15 Illustration of Voltage Gradients within Cell.

THE DEVELOPMENT OF A HIGH EFFICIENCY NON-POROUS HYDROGEN
DEPOLARIZED ANODE FOR FUEL CELLS

H. G. Oswin and S. M. Chodosh

Leesona Moos Laboratories, A Division Of Leesona Corporation
Great Neck, New York

During investigations of many types of anodes we have found that all conventional porous anodes suffer from the disadvantage that physical control of the three phase interface is necessary in order to stabilize the system and maintain an acceptable level of polarization. There are presently three ways of achieving this control over the meniscus:

1. The interface can be maintained by controlling the porosity of the electrode in the manner developed by F. T. Bacon¹, and generally known as the biporous electrode structure. Essentially this consists of two porous structures, the one facing the electrolyte having a mean pore size smaller than that of the coarse pore structure facing the gas phase. Thus by careful control of the differential pressure applied across the electrode, a stable interface is maintained somewhere within the electrode. If a certain differential pressure is exceeded, bubbling will commence at the largest pore in the fine pore layer.

2. Many other investigators have used the homoporous electrode structures, such as those described by Justi², which are used in a bubbling condition. This again necessitates a certain differential pressure at which an acceptable rate of bubbling occurs through some of the larger pores while a stable interface is maintained in pores of smaller diameter.

3. The third commonly used technique is to waterproof the electrode structure. This consists of applying a waterproofing layer to the surface of the porous structure, which apparently prevents gross flooding of the larger pores. Whether or not the smaller pores of the structure are flooded is not obvious. Likewise, electrodes can be constructed by incorporating waterproofing agents such as Teflon or Kel-F into a finely dispersed metal powder which is then fabricated into a porous layer.

All these three types of electrode have certain disadvantages such as the difficulty of controlling bubbling on waterproofed or homoporous structures with the consequent loss of fuel and its attendant dangers, or in the case of biporous structures quality control during manufacture is essential to achieve reproducible porous structures.

The case of true, solid electrolytes is, of course, unique, and it is more difficult to define interphase structures in the case of such systems as Pt/ion exchange membranes and Pt/ZrO₂-CaO.

However, it was evident that if a solid diffusion anode could be made by simple procedures, it would possess some unique advantages. With this object in view, we chose to investigate the palladium alloy systems as a possible way of making solid non-porous diffusion anodes.

PHYSICAL AND ELECTROCHEMICAL MECHANISMS INVOLVED

The processes occurring in the solid non-porous diffusion type electrode are shown in Figure 1. The first stage involves chemisorption and dissociation of the hydrogen accompanied by the formation of metal hydrogen bonds at the surface. The hydrogen then diffuses as a proton interstitially through the bulk metal; the nature of the diffusion mechanism at grain boundaries is not defined. On reaching the electrolyte surface of the membrane the protons emerge into specific bound surface states from which they are removed by the potential difference across the double layer. Thus the total process involves three distinct activation energies: activation energy of dissociation, activation energy of the bulk diffusion process, and the activation energy for the transfer of protons at the electrolyte interface. There exists a concentration gradient of protons across the membrane which provides the driving force for the diffusion process. Part of the investigation has been to determine the role of these various processes and the rate-controlling mass-transfer mechanisms.

EXPERIMENTAL PROCEDURES

During the development of this electrode both electrochemical studies and gaseous diffusion studies were carried out simultaneously. The diffusion studies will, however, be reported separately, but it will be noted that they have confirmed the findings of the electrochemical studies.

The electrochemical studies were carried out under controlled conditions of temperature and pressure using in most cases half cells, that is, the cathode of the cell consisted of a platinum gauze from which hydrogen was evolved. Certain of the early feasibility studies and the scale-up studies were conducted on cells containing oxygen depolarized cathodes. During the feasibility stage some of the electrodes investigated consisted of tubular structures of the type used for gaseous diffusion and separation of hydrogen. It had been hoped that these could be incorporated into concentric type cells giving high power density per unit volume, but the many problems associated with fabricating, sealing, and gasketing biporous tubular cathodes resulted in the use of more suitable designs. It was also found extremely difficult to calculate current-density distributions in cells using circular cross-section electrodes, i. e., tubes, unless the surrounding cathode was exactly concentric.

Polarization measurements were made in all cases against a hydrogen electrode which consisted of a palladium-silver tube containing hydrogen under pressure which acted as a non-polarizable reference. Thus, all potentials quoted are measured against the reversible hydrogen electrode in the same electrolyte under the same conditions (sometimes referred to as the E^* scale).

Electrode dimensions were in most cases one-inch diameter flat membranes; in scale-up studies three-inch, five-inch and six-inch square electrodes were used. Except where stated, 75% Pd-25% Ag was the alloy used.

Electrolytes used during the studies consisted of USP grades of potassium hydroxide, sulfuric acid, and phosphoric acid over the temperature range from room temperature to 250°C.

Luggin capillaries were used to measure the potential at the electrode surface. All of the data presented here (except Figure 6) are steady state polarization data and do not include any data derived from galvanostatic transients. Thus all electrode IR drops are included in the measurements: i. e., those caused by conductor resistances.

FEASIBILITY STUDIES

Initial feasibility studies were conducted on 25% silver 75% palladium alloy membranes at temperatures up to 250°C. These early results were somewhat variable, but very encouraging. Limiting currents up to several amps/cm² were observed and polarizations of the order of 150 mV were obtained over the current density range of 200 to 400 amps/ft². However, at lower temperatures occasional irreproducibility and varying rates of surface poisoning prompted a study of surface treatment and preparation.

THE EFFECTS OF SURFACE PRE-TREATMENT

The effects of surface preparation are shown in Figure 2, which clearly indicates the effect of treating of gas and electrolyte surfaces separately and in combination. In order to demonstrate the effects clearly, polarization values are shown for various membranes at 150°C. Pre-treatment of the electrolyte surface has a significant effect on the activation polarization and has obviously resulted in a much more active surface, either by lowering the activation energy of the process or by increasing the number of sites available. Limiting currents are not affected however. Activation of the gas surface demonstrates a marked effect on the limiting current density obtainable from the membranes, confirming as we had suspected that the surface absorption and dissociation processes were a rate controlling mechanism. It is of interest to note also that pre-treatment of the gas-side surface has an effect on the "activation-polarization" region as well as limiting currents. This is in fact accounted for by the increased diffusion of hydrogen to the electrolyte surface resulting in a greater concentration of hydrogen in the double layer. This increases the pre-exponential factor in the rate equation, resulting in higher currents at a given polarization value. The combination of gas and electrolyte side pre-treatment results in an electrode having both high limiting currents and low polarization.

Diffusion studies conducted concurrently confirmed the results of the electrochemical investigation, namely, that at lower temperatures the surface processes were rate controlling. However limiting currents are always somewhat larger than those predicted from diffusion experiments. The probable explanation of this anomaly is that on polarizing the electrode a very low pressure of hydrogen

exists at the electrolyte interface. Taking a very simple view, the electrochemical process eliminates the recombination step: $H + H \rightarrow H_2$. The removal of H from the surface under conditions of polarization can be far more rapid than desorption of H_2 .

The investigation of surface treatment indicates clearly that the "electrolyte-surface" is potential-controlling while the "gas-surface" is rate-controlling.

From a practical point of view, this phase of the investigation resulted in methods of preparing the diffusion electrodes with extremely good reproducibility and with a minimum need for quality control procedures.

Having easily reproducible electrodes available, a series of parametric investigations were conducted.

TEMPERATURE DEPENDENCE

The effects of temperature on polarization and limiting currents are shown in Figure 3 over the range from room temperature to 200°C. Although at room temperature polarization is considerably increased, limiting currents of the order of 300 to 400 mA/cm² are still obtainable and the electrode can provide adequate starting power from ambient. Above 100°C the measurement of limiting current becomes extremely difficult due to the very high current values involved. For example, measurements at 200°C have indicated limiting currents in the region of 3,500 to 4,000 amps/ft²; it is virtually impossible to measure such high limiting currents with accuracy.

DURABILITY OF THE ANODES

Many anodes of various sizes have been investigated for periods up to 500 hours under varying load conditions. Corrosion appears to be the only factor controlling electrode durability. However, since the corrosion potential of palladium silver is some 800 mV positive to hydrogen, only complete poisoning of the electrode surface can result in such excessive polarization and subsequent corrosion. It has been our experience using the electrolytes described and gases of commercial purity that this situation does not, in fact, arise and there appears to be no theoretical limit to the lifetime of the electrodes.

THE EFFECT OF ELECTROLYTE COMPOSITION

The effect of electrolyte concentration has been studied and there appears to be no particular effect on polarization or limiting current over the composition ranges of interest. Naturally the specific resistivity of the electrolyte varies and this can, of course, affect the over-all polarization of the cell. The lack of invariance with electrolyte concentration indicates the minimum importance of concentration polarization at the surface due to electrolyte species.

Polarization in acidic or basic electrolytes is similar.

THE LIMITING EFFECTS OF HYDROGEN PARTIAL PRESSURE

A study of the partial pressure effects of hydrogen indicated that partial pressure has little or no effect on polarization until limiting current density regions are approached. The effects of partial pressure of hydrogen on limiting current density is demonstrated in Figure 4. It will be noted that significant current densities can be sustained at partial pressures of hydrogen as low as 1 psia.

In connection with our original concept for a solid, diffusion-anode capable of operating with impure hydrogen streams, this is an extremely important finding since it determines the degree of utilization of the fuel. For example, if the limiting current density acceptable is 150 mA/cm^2 , then the partial pressure of hydrogen in the purge gas, i. e., the gas being discarded from behind the electrode, would be approximately 1 psia. If the in-going partial pressure of hydrogen is atmospheric, i. e., 15 psia, this would represent about 93% utilization of the hydrogen. An in-going partial hydrogen pressure of 25 psia would result in 96% fuel utilization.

THE EFFECTS OF MEMBRANE THICKNESS

The effects of membrane thickness on the polarization and limiting current are shown in Figure 5. The effects on polarization at current densities below the limiting current density region are negligible. Limiting current density, however, is an inverse function of thickness for a given partial pressure of hydrogen, thus indicating that performance, as well as economics, can be improved by the use of extremely thin membranes.

STUDY OF POISONING EFFECTS

A comprehensive study of poisoning has been conducted. Poisoning of the electrode/electrolyte interface is of course effected (as are all metal surfaces) by excessive amounts of heavy metal ions and chloride ions but in all cases using USP grades of electrolyte and distilled water no deterioration in performance has been observed under working conditions.

A comprehensive study of poisoning of the gas surface has been made including in the hydrogen-containing streams hydrocarbons, methanol, formaldehyde, formic acid, CO, CO₂, ammonia, nitrogen, and water. By control of flow rates and conditions on the gas side of the membrane, none of the above-mentioned materials have been observed to cause significant polarization effects.

The studies of sulfur impurities and trace metals such as vanadium have not been completed. It is difficult at this time to predict in what form and in what quantity these particular elements might occur in reformed streams. Also if a reformer stream is used for the fuel cell we do not expect the membrane to be any more susceptible to poisoning than the reforming catalyst, which may, in fact, remove selectively some of the undesirable materials such as sulfur and vanadium. Generally speaking, we can expect sulfur poisoning to become more important at lower temperatures. Carbon deposition on the gas surface has never been observed.

An interesting effect, which is a form of poisoning has been studied. The effect was reported by Darling³ in the course of hydrogen diffusion studies through palladium. He observed that even when using electrolytic hydrogen of high purity, that a constant diffusion rate could only be maintained by "purging" the high pressure side of the membrane. We observed the same phenomenon with "pure" hydrogen using the Pd-Ag anode. If the gas-vents were closed, a steady increase in polarization ensued. An experiment in which the "pure" (electrolytic) hydrogen was first diffused through Pd-Ag and then supplied to the Pd-Ag anode resulted in the disappearance of the phenomenon. It can only be concluded that an impurity is present in small quantities and since the "Darling effect" is observed over a range of temperature from ambient to 600°C, it is likely that the impurity does not chemisorb or physically adsorb. Most probably it accumulates in surface micro-pores restricting hydrogen diffusion to active sites on the metal surface of such pores and cracks.

ELECTROCHEMICAL CHARACTERISTICS OF THE SOLID DIFFUSION ELECTRODE

Polarization values for the electrode at 200°C derived by transient techniques are shown in Figure 6 plotted on a semi-log basis. It would appear, as might have been predicted, that the electrode exhibits Tafel behaviour. Unfortunately because of the large currents involved it has not been possible to study the electrode polarization far into the linear Tafel region; IR contributions become excessively large. Essentially, at practical current densities the electrode polarization is in the non-linear Tafel region.

THE EFFECT OF MEMBRANE COMPOSITION

The effects of various alloy compositions were studied and results are shown in Figure 7. The 25% silver 75% palladium alloy demonstrates superior polarization and higher limiting currents than all other compositions studied and there appears to be little economic advantage at this stage to increasing the amount of silver in the alloy.

SCALE-UP STUDIES

Scale-up studies have been conducted on electrodes from one inch diameter to six inch square size. Results are shown in Figure 8 for electrodes of one, and five inch diameter. The differences in polarization behaviour are not significant.

FUTURE APPLICATIONS OF THE ELECTRODES

This non-porous diffusion anode has been developed to the stage where reproducibility and simplicity of manufacture have been amply demonstrated. Its extreme thinness and ability to handle high current densities make it intrinsically suitable for very high power density systems.

Further, its ability to handle impure streams of hydrogen and its low susceptibility to poisoning show it to be an electrode which is extremely suitable for use with reformer streams using cheap hydrocarbons, methanol or ammonia, as fuel. Its ability to operate in alkaline or acid electrolyte make it a versatile anode, as does the fact that it can operate at negative, zero, or positive differential pressures.

The authors acknowledge the technical contributions and experimental studies of Mr. F. Malaspina and the results of the diffusion studies conducted by Mr. N. I. Palmer.

LITERATURE CITED

- (1) British Patent 667, 298
- (2) United States Patent 2, 860, 175
- (3) Darling, A. S., Plat. Met. Rev., 2, 16, (1958)

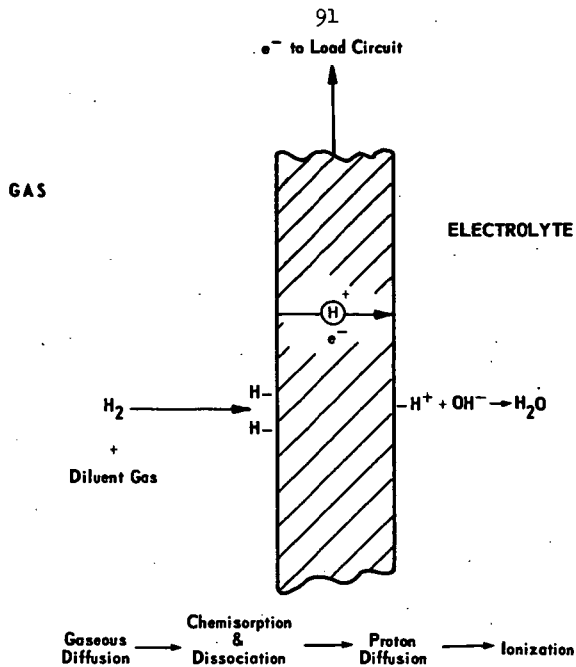


Figure 1 - Sequence of Mechanisms Involved at Non-Porous Anode

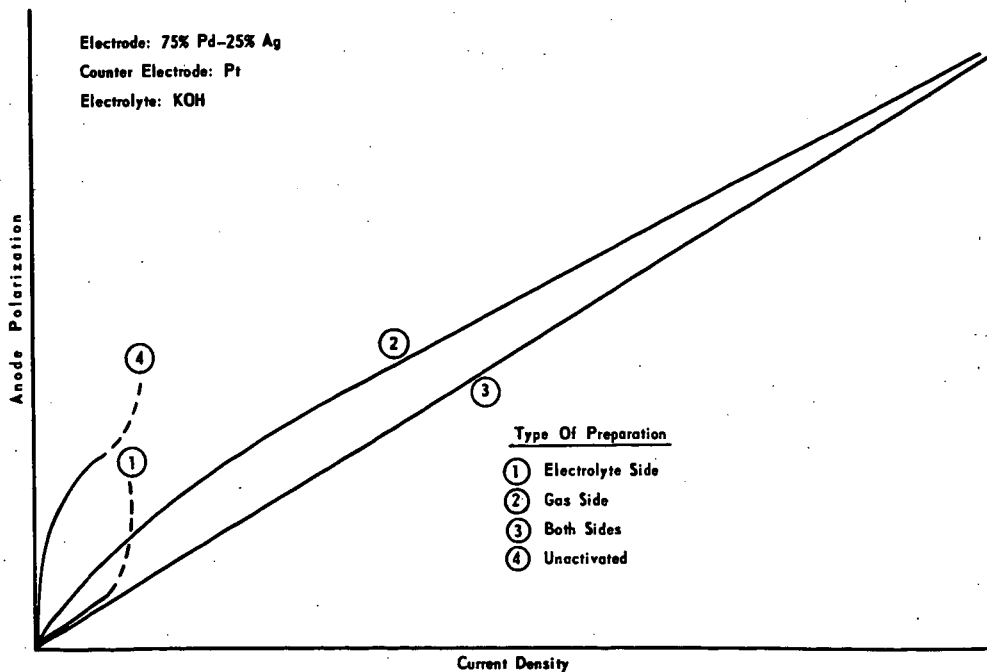


Figure 2 - Effect of Surface Preparation on Polarization of Membrane Anode

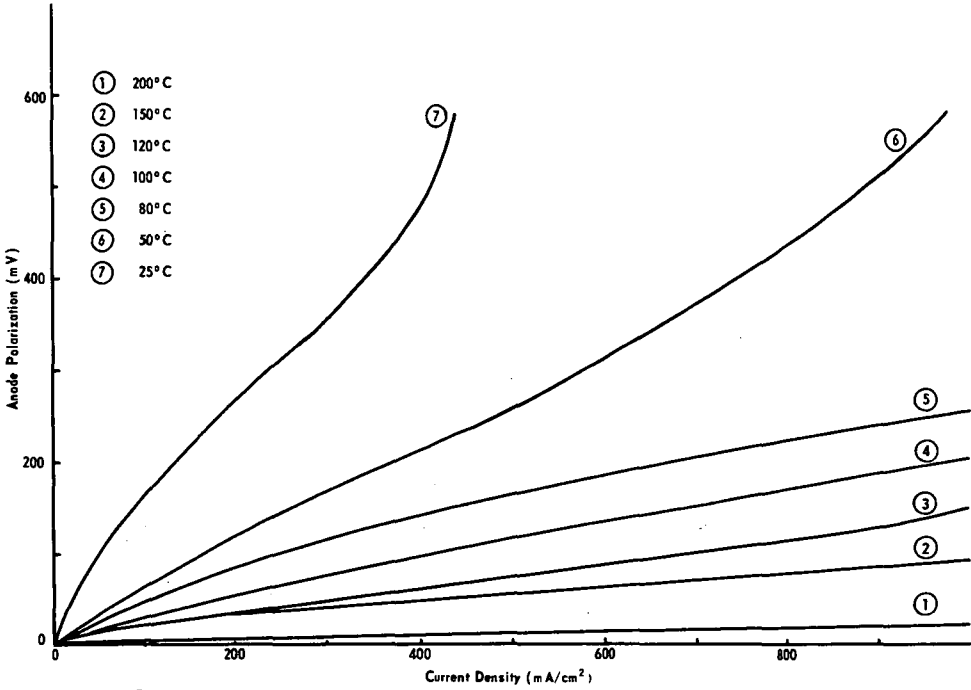


Figure 3 - Polarization of Pd-Ag/H₂ Anode as a Function of Temperature

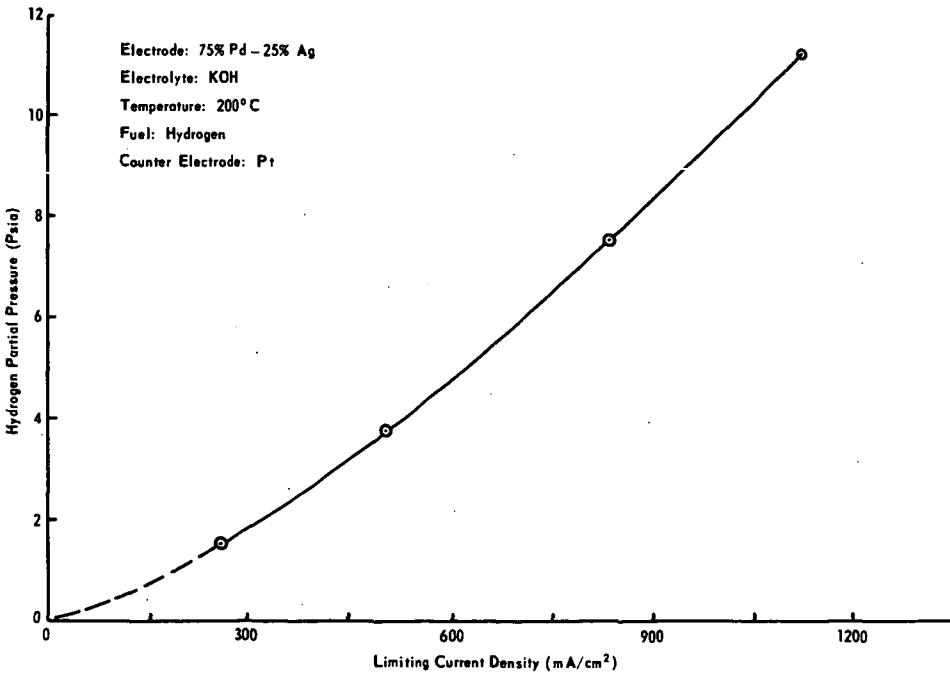


Figure 4 - Limiting Current Density of Pd-Ag/H₂ Anode as a Function of Hydrogen Partial Pressure.

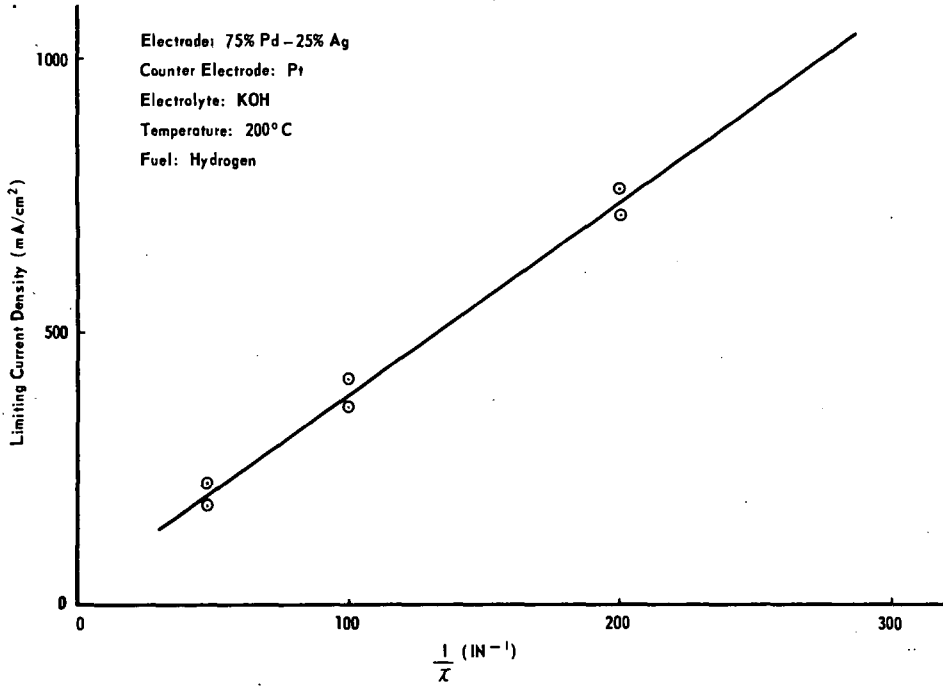


Figure 5 - Limiting Current Density as a Function of Anode Thickness.

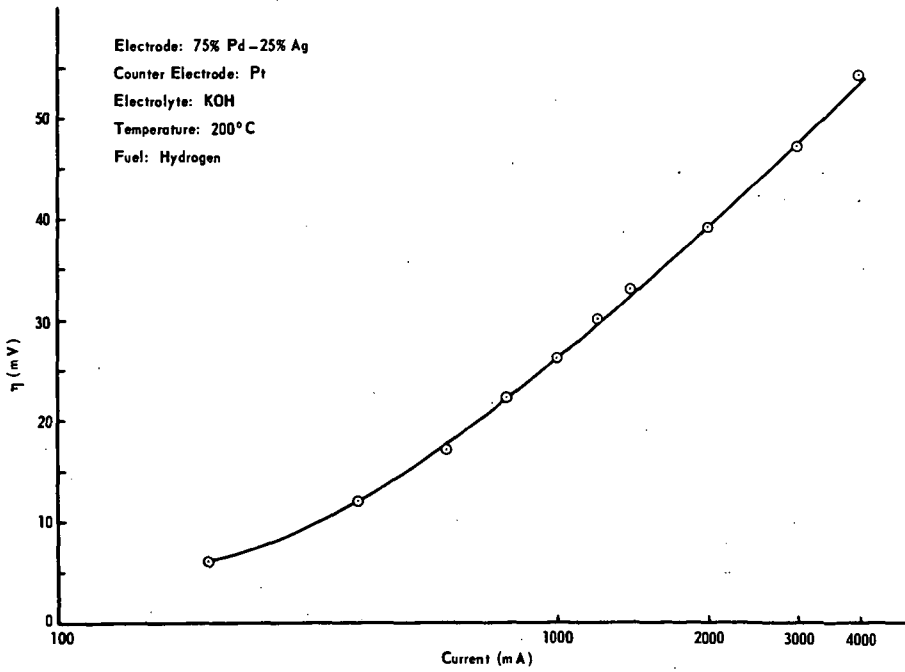


Figure 6 - Tafel Plot of Pd-Ag/H₂ Anode

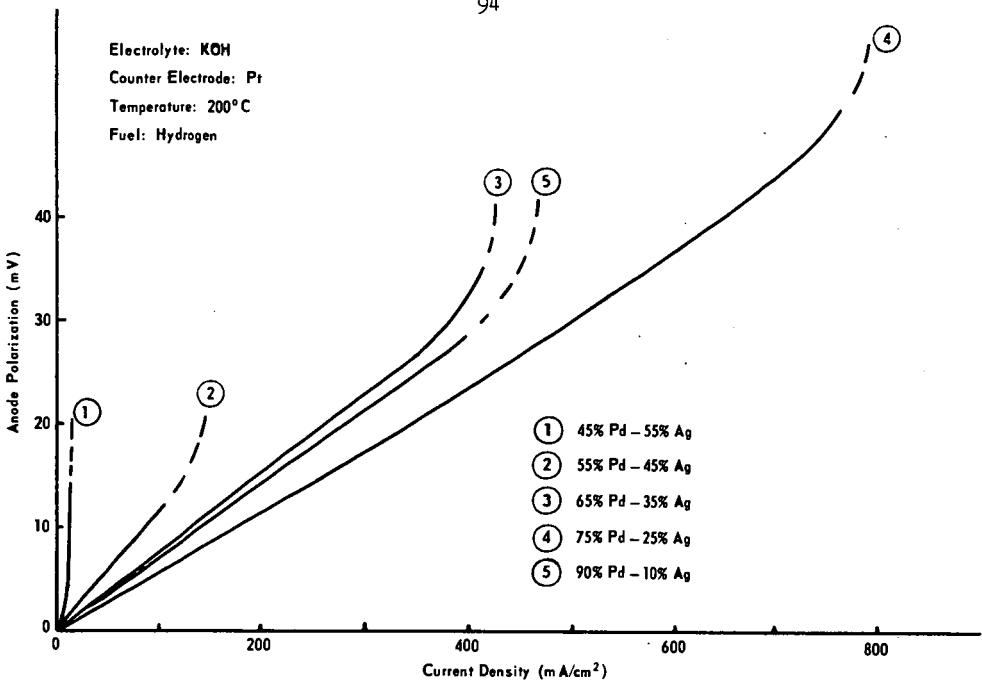


Figure 7 - Anode Polarization as a Function of Membrane Composition.

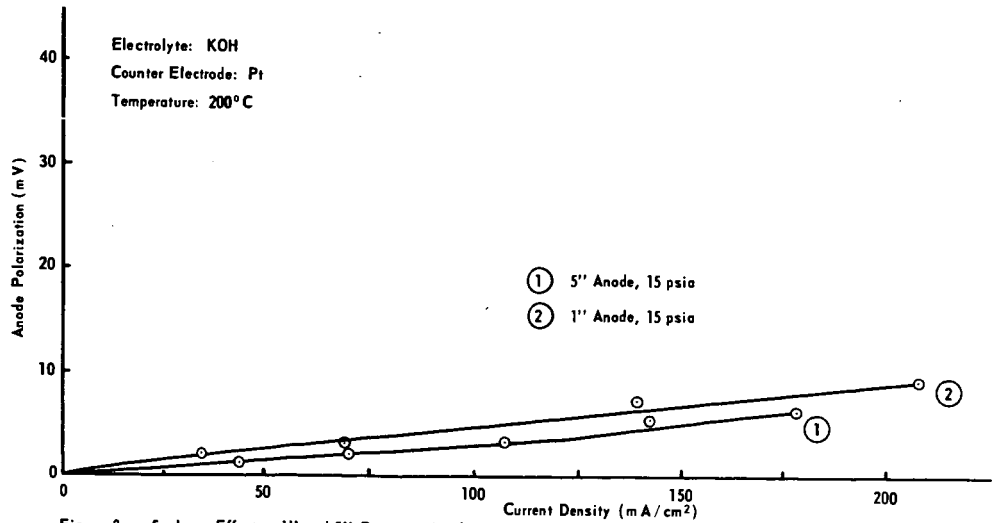


Figure 8 - Scale-up Effects: 1" and 5" Diameter Anodes

95 - 108

(Paper withdrawn as final copy was being sent to the printer for preprinting.)

A New Fuel Cell Anode Catalyst
Raymond Jasinski
Research Division, Allis-Chalmers Manufacturing Company
Milwaukee 1, Wisconsin

Introduction

The operating cost of a fuel cell power plant is determined primarily by the cost of the fuel. Although hydrogen is generally more expensive than methanol or propane, there are a number of situations in which fuel cells operating on hydrogen could be economical. An example of this is the on-the-site fuel cell oxidation of by-product hydrogen obtained from commercial processes such as the electrolytic production of chlorine. Air would be used as the oxidant.

One of the principal items which affects the capital cost of the fuel cell power plant itself is the cost of the anode and cathode catalysts. The majority of the ambient temperature H_2/O_2 fuel cells described in the literature have employed noble metals such as platinum and palladium. These metals are expensive, and some question has been raised regarding an adequate natural abundance of the elements (1).

There are two alternatives to developing inexpensive catalyst-anodes, either reduce the amounts of the noble metal catalyst on the electrode to about 1 mg/in² of electrode, or employ less expensive non-noble metal catalysts.

The latter approach has been followed for example, by E. Justi (2), who successfully constructed hydrogen anodes starting with the Raney alloy (Ni_2Al_3). It would appear, however, that the economic advantage of employing relatively inexpensive metals, nickel and aluminum, is more than balanced by the relatively involved, and hence costly, procedure of electrode preparation. Furthermore, the problems in adapting these procedures to the preparation of large electrodes for the construction of fuel cell power plants may limit the applications of this catalyst.

These problems are not significant with the use of a new, non-noble metal, hydrogen anode catalyst, nickel boride, (3). This material is relatively inexpensive and is easily synthesized in the form of an electrode.

The properties of nickel boride as an anode in the hydrazine/ O_2 cell and the KBH_4/O_2 cell have been discussed elsewhere (4,5). It was shown that for these cells, the nickel boride catalyst-anodes were approximately 0.1 volt more effective for the direct fuel cell oxidation of N_2H_4 and KBH_4 than a palladium catalyst.

The chemical hydrogenation properties of this catalyst have been discussed only briefly in the literature. Nickel boride has been reported to be superior in catalyst activity to Raney nickel, and more resistant to fatigue in the hydrogenation of saffrole, furfural and benzonitrile (6). Some of the properties of this material have also been described in the Russian literature (7). More recently, H. Brown has discussed the hydrogenation of olefins by nickel boride (8).

Nickel boride can be formed by heating nickel oxide to 700-1000°C in a stream of BCl_3 and H_2 (9). Another method of preparation involves electrolysis of nickel oxide "dissolved in variable quantities of alkali tetraborates" (10). The compound can also be formed directly from the elements by diffusing powdered boron into the reduced nickel (11). However, the most convenient method has been that developed by H. Schlesinger (12) in which Ni_2B is formed by combining solutions of potassium borohydride and a nickel salt.

Chemisorption Properties

Nickel boride, prepared by the Schlesinger method, is formed in an atmosphere of hydrogen, produced by the decomposition of the excess KBH_4 on the catalyst surface. As a result, there is a considerable quantity of H_2 chemisorbed on the material so that in some cases it may be pyrophoric. However no difficulty was experienced in handling the electrodes.

The chemisorption of hydrogen on nickel boride was studied as a function of temperature. (The sample employed in these experiments had a surface area of $15 \text{ m}^2/\text{gm}$, as determined from the physical adsorption of nitrogen at -196°C .) Adsorbed hydrogen was removed by evacuating the sample at 200°C to a pressure of less than one micron. As will be shown below, heating at this temperature has only a minor effect on surface area. The results are summarized in Table I for the adsorption of hydrogen at a pressure of one atmosphere.

TABLE I

Adsorption of H_2 on Ni_2B

<u>Temperature</u>	<u>Volume Adsorbed (STP)</u> <u>(cc/gram)</u>
-196°C	0.6
0°	3.5
25°	3.4
150°	3.2
275°	2.3

The volume of nitrogen required to form a physically adsorbed monolayer on this sample was 3.5 cc/gram. Thus the adsorption of H_2 at room temperature corresponds very closely to a monolayer.

The variation of the quantity of hydrogen adsorbed with temperature, as shown in Table I, is characteristic of activated adsorption. At -196°C , the hydrogen has insufficient energy to overcome the energy barrier for adsorption. At the higher temperatures, (275°) there is sufficient energy to break the chemical bonds holding the hydrogen to the surface of the solid and the quantity of gas adsorbed decreases.

A brief study was also made of the physical structure of the catalyst as a function of sintering temperature. A sample of Ni_2B was heated under vacuum to a range of successively higher temperatures. The surface area of the sample was determined between heat treatments from the N_2 adsorption isotherm.

The sample was first degassed at ambient temperature until a constant pressure of less than one micron was reached. A nitrogen adsorption isotherm, measured at -195°C , indicated a surface area of $22.5 \text{ m}^2/\text{gm}$. The boride was then heated under vacuum to 200°C and held at a pressure of less than one micron for four hours. A second nitrogen isotherm indicated a surface area of $21.3 \text{ m}^2/\text{gm}$. The decrease is small, indicating little, if any, sintering of the nickel boride. Next, the sample was heated to 350°C for 17-1/2 hours at a pressure of less than one micron. The surface area dropped to $13.3 \text{ m}^2/\text{gm}$. Finally the sample was heated to 475°C for 2-1/2 hours. The final surface area was $6.38 \text{ m}^2/\text{gm}$. This data is plotted in Figure 1.

Very little chemisorption of hydrogen was noted on the Ni_2B sample after sintering at 350°C . The sample was cooled to 25°C and the hydrogen isotherm measured. After evacuating to a pressure of $<1\mu$ at this temperature to remove only physically adsorbed hydrogen, another hydrogen isotherm was measured. The two isotherms were identical, indicating at most, weakly adsorbed hydrogen. This loss of active adsorption sites on sintering is confirmed by electrochemical data. Fuel cells containing Ni_2B anodes which had been sintered at 500°C did not attain a voltage greater than 0.4V, while the samples sintered at 400°C attained a cell voltage of one volt but only very slowly.

Apparently, the activity of the electrocatalyst was more sensitive to heat treatments than would be expected simply from changes in surface area. A 3" x 3" anode, generating approximately $10 \text{ ma}/\text{cm}^2$ must have at least 10^{19} hydrogen atoms chemisorbing and reacting per second. The minimum current involved in the voltmeter reading of 1 volt was approximately 10^{-6} amps, i.e., 10^{13} hydrogen atoms reacting per second. A catalyst-anode sintered at 500°C achieved an open circuit voltage of only 0.4 volt. Assuming a proportionality between the rate of reaction and the number of active sites, there must have been a decrease by a factor of 10^6 in the number of active sites upon sintering at 500°C . The surface area, however, was decreased only by a factor of four.

This conclusion is also apparent from a comparison of the hydrogen chemisorption after sintering at 350°C with the loss of surface area. The chemisorption of H_2 was reduced to a negligible value while the surface area had decreased by a factor of four.

Anode Oxidation of H_2

Nickel boride was studied as a H_2 anode catalyst in two forms, first as the powder and then supported on a porous nickel plaque. The powder was prepared by combining a basic solution of 5% KBH_4 with a dilute aqueous solution of a nickel salt, e.g., nickel acetate. A voluminous black precipitate formed immediately, and was accompanied by a rapid evolution of hydrogen gas. The details of the procedure are all well documented (6) and Ni_2B is the sole, insoluble, reaction product. As a check on the procedure, a sample of this material was analyzed and shown to have a Ni/B atom ratio of 2.05. The plaque-electrode was formed by depositing Ni_2B in the voids of a porous sintered nickel plaque. The substrate, commercially available, measured 3" x 3" x 0.03".

Since the nickel boride is an electrical conductor, it was possible to study the catalyst directly, i.e., it was not necessary to first

support the catalyst on a conducting substrate. The catalyst was formed into a plug and placed in the catalyst test electrode shown in Figure 2. The fuel gas was passed down the metal tube, through the catalyst plug and into the "free" electrolyte. Studying the catalyst in this form alleviated many of the problems involved in operating H_2/O_2 fuel cells, such as maintaining the proper moisture balance in the cell. The two electrodes were "driven" with the commutator (13), hence the voltages measured were IR free. In such a system, H_2 was consumed at the anode and water was electrolyzed at the auxiliary electrode. A saturated calomel electrode, connected to the cell by a salt bridge, was used as the reference electrode. The entire cell was mounted in a constant temperature bath maintained at $80^\circ C$. A typical voltage-current curve obtained for a Ni_2B "plug" hydrogen anode is shown in Figure 3. A curve recorded under similar conditions for 1:1 palladium black-graphite mixture is included for comparison purposes. It is apparent that the nickel boride anode is sufficiently active to support high current densities, e.g., 260 ma/cm^2 . The palladium-graphite anode is only 0.04 volt more negative than the more economical nickel boride electrode at current densities of 65 to 260 ma/cm^2 .

A test electrode was then operated at a constant load of 65 ma/cm^2 and the anode voltage recorded as a function of time. This data is summarized in Figure 4. There is apparently a small fall-off in performance over the first 200 hours, i.e., from $-0.87V$ to $-0.83V$. The voltage then remained constant for the next 700 hours, at which time the test was terminated. It is quite apparent from this data that Ni_2B is capable of extended performance as a hydrogen anode catalyst.

The Ni_2B catalyst was then evaluated in complete fuel cells of the conventional Allis-Chalmers design, shown in Figure 5. It was possible to apply the active powder directly to the surface of the capillary membrane, and a number of cells of this type were built. Since this procedure is inefficient in the use of catalyst, it was desirable to employ a catalyst support to more efficiently disperse the catalyst across the electrode. As mentioned above, a porous, sintered nickel plaque ($3" \times 3" \times 0.03"$) was used for this purpose with the Ni_2B catalyst deposited in the pores of the substrate. A voltage-current curve obtained for a fuel cell employing such an anode is shown in Figure 6. The cell temperature in this case was $78^\circ C$. It was possible to support a load of approximately 70 ma/cm^2 at a cell voltage of $0.7V$. Recent improvements in cell and electrode design have increased this performance to $100 \text{ ma/cm}^2 @ 0.7V$.

Extended Performance Tests

The fuel cell data shown in Figure 6 described the initial performance of the catalyst electrodes, i.e., the voltage-current characteristics obtained during the first day or two of operation. However, fuel cell electrodes generally do show some loss in activity with time as shown in Figure 4. This effect was also studied with a fuel cell of the type shown in Figure 5 employing an anode of Ni_2B deposited onto a porous nickel substrate. The initial performance was essentially that described by the voltage-current curve of Figure 6.

Before discussing the extended performance data, it is necessary to briefly mention the subject of fuel cell "controls". The principal problem, common to all H_2/O_2 fuel cells, centers about maintaining

the proper water balance in the cell. It is desirable to withdraw from the operating fuel cell only that amount of water produced by the fuel cell reaction. If an excess is removed, the cell will dry out; if insufficient water is removed, the electrode will flood and/or the electrolyte will be diluted. In both cases, the extended performance of the H_2/O_2 fuel cell would be adversely affected.

A high operating current density provides for a high rate of water production and the problem of maintaining the proper amount of water in the cell becomes more severe. The life test on the Ni_2B hydrogen anode was carried out at a relatively low current density, i.e., 32 ma/cm². At this level, the rate of water production was determined to be sufficiently low so as not to require an involved water monitoring system. The moisture in the cell was controlled empirically by adjusting the hydrogen flow rate to establishing either a wetting or a desiccating condition as needed. The variation in cell voltage with time is shown in Figure 7 for a cell operated in this manner for 1200 hours. There does appear to be a small, gradual fall-off in cell performance with time. Comparing this data with that of Figure 4, most of the fall-off after the first 200 hours must be ascribed to problems of cell control. Nevertheless, this data is sufficient to establish the point that it is possible to construct large nickel boride catalyst-electrodes which are capable of extended operation as hydrogen anodes.

The data presented was taken with 3" x 3" electrodes. No difficulty has been experienced in adapting the preparative procedures to 6" x 4" nickel boride catalyst-anodes. The use of electrodes of this size in the hydrazine/oxygen fuel cell has already been described (4).

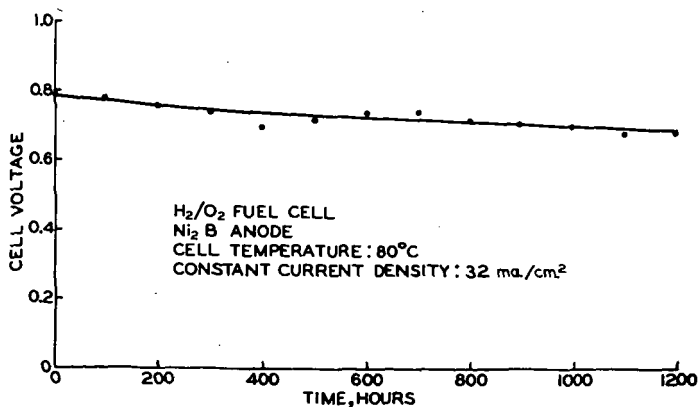
Acknowledgements

The author wishes to acknowledge the efforts of James Huff in obtaining the gas adsorption data and the efforts of David Cary in carrying out the extended performance tests. The catalyst test electrode was developed with assistance of Phil Horwitz and Larry Swette.

BIBLIOGRAPHY

1. Slaughter, J., paper presented at 121st Meeting Electroch. Soc., Los Angeles, Calif., May, 1962.
2. Justi, E., Pilkuhn, M., Schiebe, W., and Winsel, A.: "High Drain Diffusion-Electrodes Operating at Ambient Temperature and Low Pressure", Abh. d. Math. - Nat. K. I. d. Akad. d. Wiss, u.d. Lit Mainz No. 8, Komm Verlag Steiner, Wiesbaden 1959.
3. Jasinski, R., patent applied for.
4. Jasinski, R., paper presented at 123rd Meeting Electroch. Soc., Pittsburgh, Pa., April 15, 1963.
5. Jasinski, R., *ibid.*
6. Paul, R., Buisson, P., Joseph, N., Ind. Eng. Chem. 44, 100 (1952).
7. Iverdovskii, I. P., Tupitsyn, I. F., Problemy Kinetiki i Kataliza, Akad. Nauk, S.S.S.R. Inst. Fiz. Khim. Soveshchanie, Moscow 9, 86-70 (1956).
8. Brown, C. A., Brown, H. C., J. Am. Chem. Soc. 85, 1003 (1963).
9. Deiss, W. J., Blum, P. Compt. rend 244, 464 (1957).
10. Marion, S., Bull Soc. Chim. France 1957, 522.
11. Fruchant, R., Michel, A., Bull. Soc. Chim. France 1959, 422-3.
12. Schlesinger, H. I., U.S. Patent 2,461,611 (Jan. 9, 1945).
13. Pollnow, G., Kay, R., J. Electroch. Soc. 109, 648 (1962).

Figure 7 - Extended operation of a H_2/O_2 fuel cell employing a nickel boride anode.



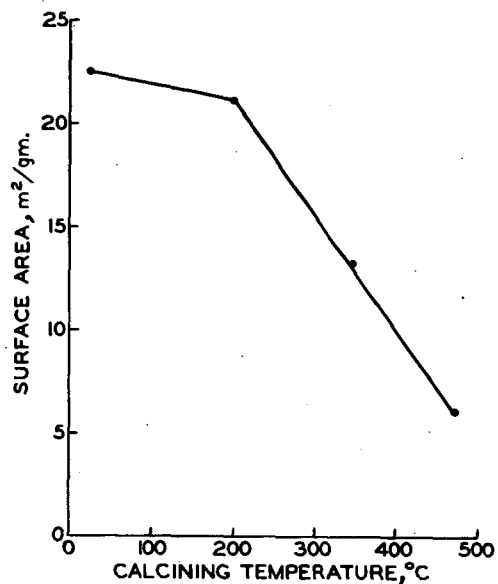


Figure 1 - The variation in surface area with temperature of sintering.

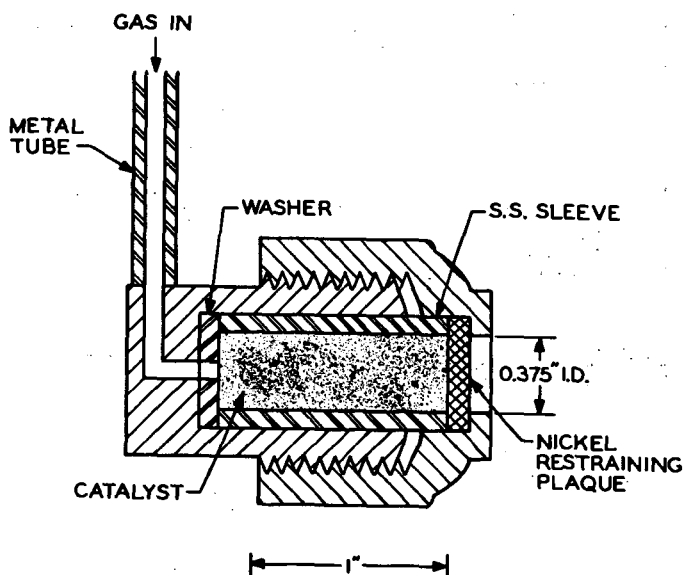


Figure 2 - Catalyst test electrode.

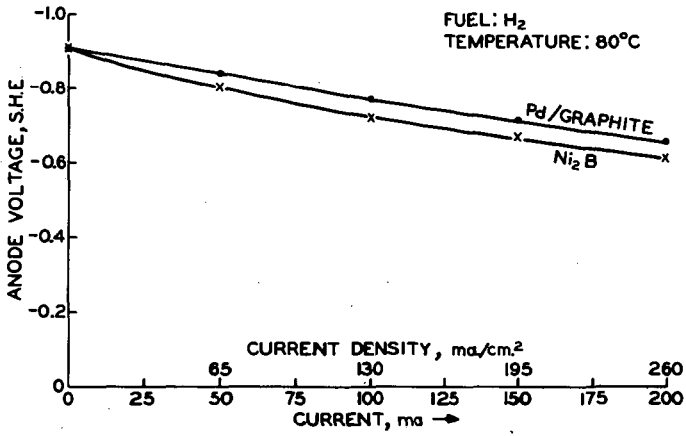


Figure 3 - The anodic oxidation of hydrogen by nickel boride and by palladium black.

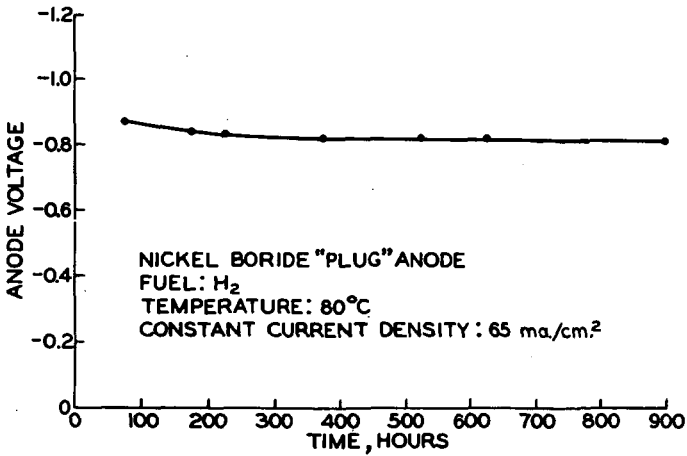


Figure 4 - Extended operation of a nickel boride hydrogen electrode.

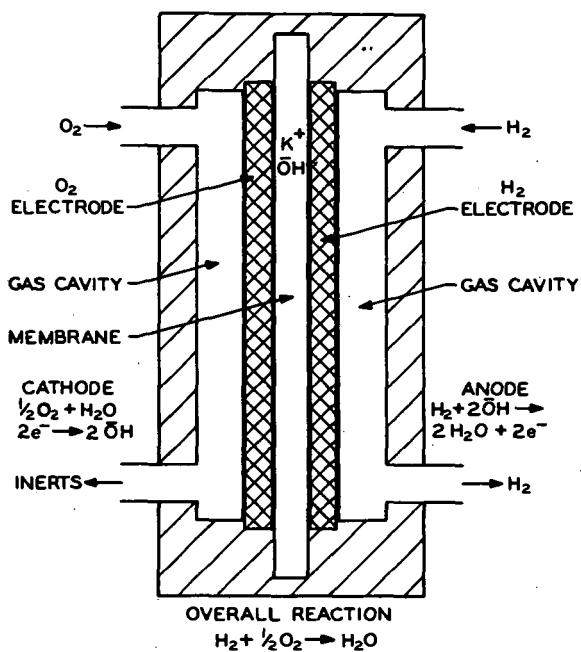


Figure 5 - Allis-Chalmers H_2/O_2 capillary membrane fuel cell.

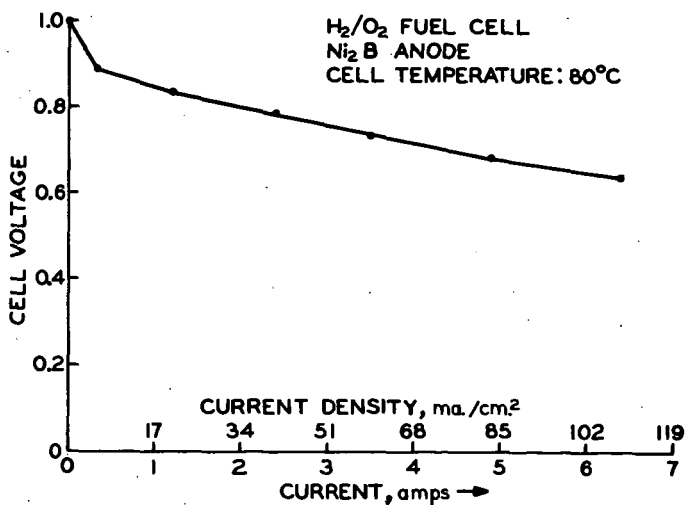


Figure 6 - Voltage - Current characteristics of a H_2/O_2 fuel cell employing a Ni_2B anode.

Thin Fuel Cell Electrodes

R. G. Haldeman, W. P. Colman, S. H. Langer, and W. A. Barber

Central Research Division, American Cyanamid Company
Stamford, Connecticut

I. Introduction

There is considerable current interest in low temperature, light-weight, high-performance H_2-O_2 fuel cell components. This company has had for several years a research program directed toward development of thin electrode structures for the "equilibrated matrix" hydrogen-oxygen or hydrogen-air cells. Electrodes developed for this system should be useful also in the ion exchange membrane fuel cell, and with some modification in the free electrolyte fuel cell.

As a short range objective, we have required that such electrodes, when assembled into an H_2-O_2 cell, should sustain currents of at least 200 ma/cm^2 , developing a potential corrected for internal resistance of 0.8-0.9 volts. They should be useful with suitable modification of support material in either strong acid or base and should be capable of sustained operation at temperatures from ambient to 100°C . They should be capable of manufacture in large sizes, e.g., one foot square, and have good uniformity and reproducibility. Further, material costs/kw of power should be minimum.

II. Experimental

A. Procedures

Much of the initial evaluation work has been carried out in one inch diameter (5 cm^2) matrix cells. We have found that scale up to 2" x 2" cells (25 cm^2 active area) can be readily achieved, and the larger cell is preferred for life testing.

For the alkaline system, asbestos is a suitable matrix material, while glass-fiber paper performs well in the acid system. Several types of organic matrix may also be used.

In life testing, in order to obtain stable operation, it is necessary to remove water from the system as fast as it is formed by the electrochemical reaction. In our work this has been accomplished by using just sufficient gas flow to permit evaporation of the proper amount of water.

B. Electrodes

For the equilibrated matrix system electrodes have been developed consisting of a porous layer of platinum black and a waterproofing agent with or without extenders, spread uniformly on and supported by a wire mesh screen. The thickness of the electrode and platinum loading can be varied by using screens of differing mesh and wire diameter, and also by varying the amount of extender used. Two major variations are under study.

In Type A no extender is used. Thus, with screens in the range 50-100 mesh and .002-.004 inch wire diameter, platinum loadings are typically in the range 7-10 mg/cm² and electrode thickness 0.004-0.008 inch. Resistivity is nearly that of the support screens. In Type B electrodes, platinum is supported on a carbon or graphite extender. Electrodes of this type may contain 0.5 to 4 mg Pt/cm² electrode area and have the same thickness and resistivity characteristics as Type A electrodes.

C. Studies of Type A Electrodes

Comprehensive studies have been made with platinum black-metal screen electrodes, since these are capable of sustaining very high currents at low polarization.

1. Acid System

In Figure 1, we show typical polarization curves for 50 mesh tantalum screen electrodes containing 7-9 mg Pt/cm² as used on both sides of H₂-O₂ and H₂-air cells. Temperature was ambient and the electrolyte 2N H₂SO₄ in a glass fiber paper matrix. The polarization curve for H₂-O₂ uncorrected for internal resistance indicates a potential of about 0.72 volts at 200 ma/cm². Indeed, similar curves have been found to be approximately linear to 600 ma/cm² and 0.55 volts. The H₂-O₂ curve corrected for internal resistance (based on open current measurements with a Universal AC bridge) indicates an essentially constant IR free potential of about 0.82-0.87 volts.

The performance of this type of electrode in a hydrogen-air cell is shown in the lower curve of Figure 1. It will be seen that the increase of polarization is only 50 mv at 50 ma/cm² and 60 mv at 200 ma/cm² and apparently indicates that at these current densities performance is not limited by inadequate diffusion of oxygen into or nitrogen out of the electrode structure.

Performance of these electrodes seems to be substantially independent of temperature as indicated in Figure 2. Somewhat higher performance might be expected at elevated temperature; however, these cells have not yet been optimized for performance at higher temperature.

Some indication of life performance has been obtained with the tantalum screen electrodes in the H₂-O₂ system at ambient temperature. These electrodes have been operated for over 1000 hours at currents up to 150 ma/cm² without evidence of deterioration.

2. Base System

Extensive studies have been made of platinum black spread on 100 mesh nickel screens. In Figure 3 we show initial polarization for H₂-O₂ and H₂-air of the system consisting of these electrodes with 5N KOH in a matrix cell. The uncorrected H₂-O₂ curve indicates a cell potential of 0.76 volts at 200 ma/cm². This curve has also been extended to 600 ma/cm², a potential of 0.6 volts being obtained. Thus, the electrodes are capable of sustaining very high electrochemical rates in the alkaline system.

When the H₂-O₂ polarization curve is corrected for internal resistance a steady potential of 0.85-0.90 is obtained over most of the range of current density. This is roughly 20-30 mv higher than was observed for the acid system. Individual electrode polarization studies have been made which indicate that at these platinum levels the major part of the initial 0.3-0.4 volt polarization occurs at the oxygen electrode in both acid and base systems.

The H₂-air performance is plotted in the lower curve of Figure 3. Additional polarization on air is 40 mv at 50 ma/cm² and 100 mv at 150 ma/cm². These electrodes have not been optimized for operation on air.

Performance at higher temperatures has been examined at 70° and 95°C and, again essentially no change from ambient is found. The data indicate maintenance of a high level of performance of the electrodes at higher temperatures, at which operation is probably desirable to facilitate removal of product water.

Life tests for over 1000 hours at ambient temperature and several hundred hours at 80°C at currents up to 125 ma/cm² indicate excellent performance stability.

D. Studies of Type B Electrodes

Type B electrodes represent an approach to more effective utilization of catalytic materials. Carbons added to the formulation act as extenders and substrates for the spreading of platinum or other activating ingredient. Excellent control of distribution of catalyst and waterproofing agent is achieved.

1. Choice of Carbons

As the result of a survey of over seventy-five carbons, half a dozen promising carbons have been discovered with good chemical stability and high catalytic activity when platinized, ranging in structure from graphitic to amorphous, and in surface area from 8 to 800 m²/g. One of these is Cyanamid 99% graphite, which is a byproduct of the manufacture of calcium cyanamide from calcium carbide. Some properties of this material are listed in Table I.

This material can be compacted into a rather uniform porous structure having a conductivity characteristic of graphite. Its surface area and pore structure are such that no appreciable amount of catalytic material need be buried in tiny inaccessible pores.

2. Base System

Electrodes were prepared from platinized Cyanamid 99% graphite by methods similar to those described for electrodes of Type A. Waterproofing level was held constant. Platinum loadings of 1 and 2.5 mg/cm² on appropriate screens were obtained. Electrode thickness was approximately 0.007 inches. In Figure 4 is shown the performance of these electrodes in the base type matrix cell. Platinum loadings on each side are indicated in the table in the lower part of the graph. It is evident that reduction of platinum loading at either electrode produces some loss in performance. However, even at a total loading of 3.5 mg/cm² for both sides, the additional polarization is only about 100 mv at 200 ma/cm². It is believed that substantial improvement in performance by improved methods of platinization can be achieved. Additional polarization when these electrodes are operated on air is similar to that obtained at high platinum loadings. Life studies conducted for over 1000 hours, including substantial periods at 150 ma/cm², indicate no significant change in electrode properties when operated as either anode or cathode.

Similar studies have been made of Type B electrodes in acid systems.

III. Discussion

Based on the above performance and physical characteristics, we can project that cells constructed with these electrodes will have very desirable weight and volume characteristics. A typical electrolyte matrix with two thin electrodes would have a total thickness of about 0.030 inches and a weight of about 0.3 lbs/ft². For a fuel cell operating at 75 watts/ft² total electrode-electrolyte weight would be about 4 lbs/kw.

If it is assumed that individual cells could be stacked at 4 to the inch and operate at 100 amps/ft² with the potential indicated in the above polarization curves, power levels of 65-85 watts/ft² could be achieved on either oxygen or air, and power densities in excess of 3 kw/ft³ of battery exclusive of auxiliaries should be feasible.

It is believed a power density of 75 watt/ft² can be achieved in the near future with a platinum usage of about 2 g/ft² of cell area (including both electrodes). This represents an investment in platinum of about \$80/kw. Moreover, it is believed that major part of this platinum value can be recovered when the useful life of the battery has ended.

TABLE I

PROPERTIES OF CYANAMID 99% GRAPHITE

Purity	99.0 Wt. %
Impurities	SiO ₂ , CaO, Fe ₂ O ₃ , Al ₂ O ₃
Particle Size	Approximately 0.25 to 2.0 Microns
Surface Area	11.4 m ² /gram
Conductivity*	50 mho/cm
Bulk Density*	1.28 g/cc
% Porosity*	40
X-ray	Graphitic

* Measured at 2000 psi.

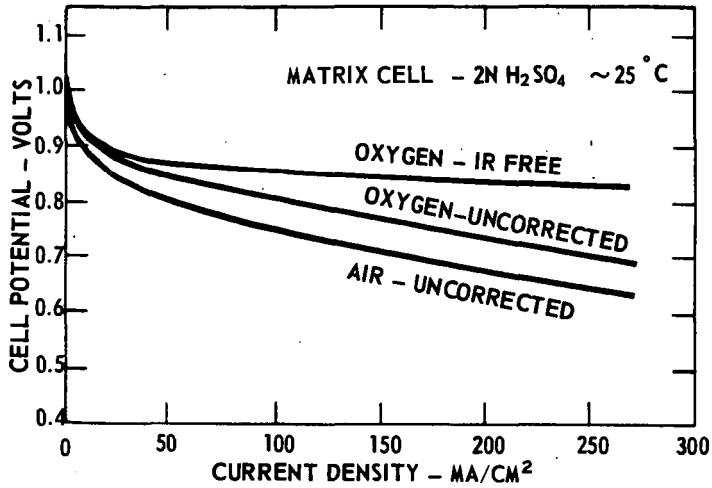


FIG. 1 TYPE A ELECTRODES - ACID SYSTEM

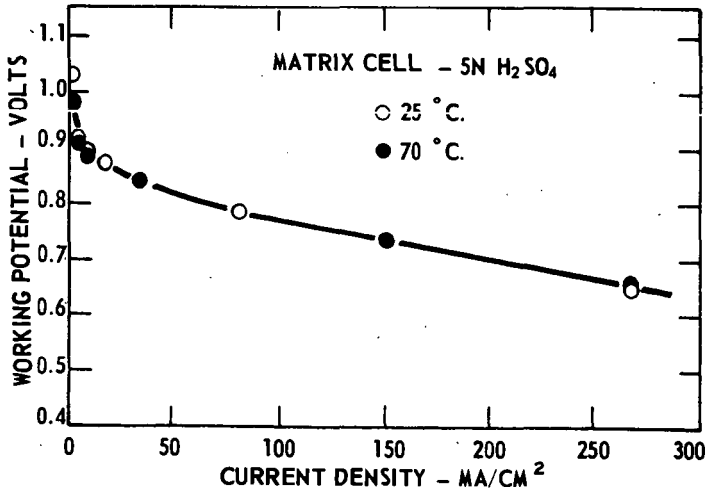
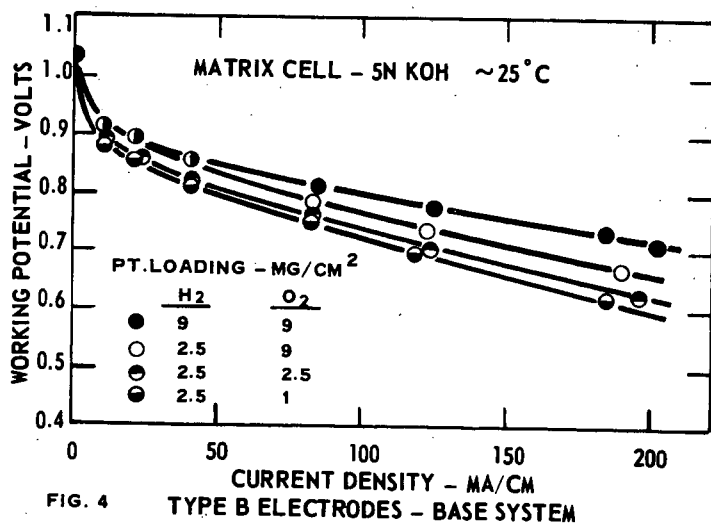
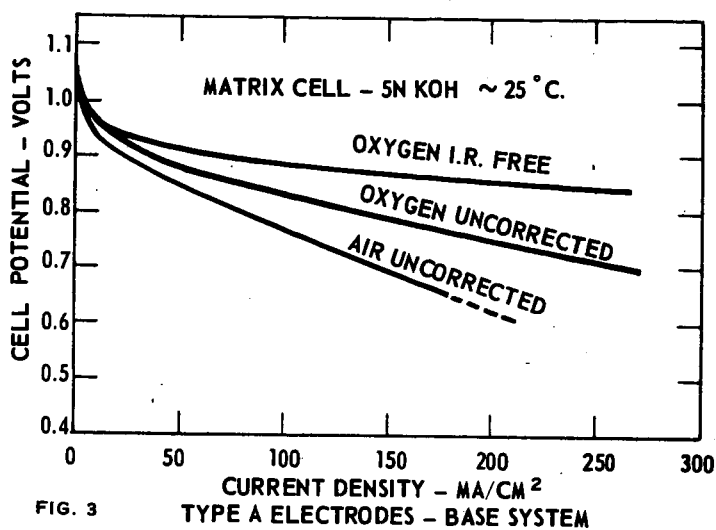


FIG. 2 TYPE A ELECTRODES, EFFECT OF TEMPERATURE



Current Density and Electrode Structure
A Qualitative Survey

H. A. Liebhafsky,
E. J. Cairns
W. T. Grubb, and
L. W. Niedrach

General Electric Research Laboratory
Schenectady, N. Y.

Abstract*

The effect of electrode structure on the current density obtainable in a fuel cell is second only to that of the electrocatalysts. The structure and the functioning of such electrodes are so complex that the quantitative treatment of simple models can scarcely be expected to do more than suggest further experiments. In this situation, a qualitative appraisal of the relationship between electrode structure and current density seems in order.

The qualitative appraisal we have made leads to these conclusions, most of which are based on work by others:

1. A working fuel cell electrode owes much of its effectiveness to thin electrolyte films through which the reacting gases diffuse.

2. These films are so thin that they can change rapidly in thickness and extent: a working fuel cell electrode is a dynamic system.

3. The oversimplified idea that electrode reaction occurs mainly at the 3-phase boundary should be abandoned.

4. The increased importance of gas diffusion through thin electrolyte films makes the name "gas diffusion electrode" even more ambiguous. Redefinition is in order.

5. Under the simplest conditions (e.g. pure hydrogen at an anode), thin electrodes are likely to perform in fuel cells at least as well as thick; and they seem preferable when conditions are more complex.

6. A good electrode structure should give almost as good performance on air as on oxygen over a large range of current densities.

* Complete manuscript not received in time for inclusion in Divisional Preprints.

A Contribution to the Theory of Polarization of Porous Electrodes

Karel Micka

Polarographic Institute, Czechoslovak Academy of Science, Prague

Introduction

The problem of polarization of porous electrodes with relation to the resistance of the electrode material was solved first by Coleman (1) in the case of cylindrical cathodes of Leclanché elements. In his differential equation, a supposition is implicitly included that the faradayic current, i , is directly proportional to the polarization of manganese dioxide particles, although he considered the "electromotive force of the manganese dioxide particle" as constant. Therefore, Coleman's expression for the faradayic current as a function of the distance from electrode surface is substantially in accord with that of Euler and Nonnenmacher (2) who assumed a linear polarization curve of manganese dioxide electrode. Daniel-Bek (3) was the first to deduce fundamental differential equations in the form which is used nowadays. He gave the solution for two limiting cases, viz., that the faradayic current is an exponential or a linear function of polarization. Finally, Newman and Tobias (4) solved the differential equations under the supposition that the faradayic current is an exponential function of polarization and their results are substantially in accord with those of Daniel-Bek.

None of the mentioned authors' solutions is valid for the whole polarization region, but only for limiting cases of either small or large overvoltage. However, it is possible to deduce a generally valid solution, as follows.

Mathematical solution

For exactness, let us consider an electrode of rectangular shape with pores in form of linear channels parallel to one edge of the electrode, although it is possible to abandon any assumption concerning

the geometry of the pores (4). The x-axis runs parallel to the pores, on the electrolyte side being $x = 0$. A metallic conductor as current collector is placed on the end of the pores, at $x = L$. For potential, φ_1 , in the electrode material, Ohm's law holds:

$$\frac{d\varphi_1}{dx} = -\rho_1 i_1, \quad /1/$$

where ρ_1 is the resistance of a cubic centimeter of the porous electrode material in the direction of x-axis, and i_1 is the electronic current density corresponding to 1 sq. cm. of the electrode section perpendicular to the x-axis.

When the electrode consists of a depolarizer and an excess supporting electrolyte, and when the concentration polarization can be neglected with respect to the activation and resistance polarization, then an analogous equation holds for the potential, φ_2 , in the electrolyte:

$$\frac{d\varphi_2}{dx} = -\rho_2 i_2, \quad /2/$$

where ρ_2 is the resistance of the electrolyte contained in one cubic centimeter of the electrode, and i_2 is the ionic current density corresponding again to 1 sq. cm. of the electrode section. Finally, according to Daniel-Bek (3), we may write the following equation for the density of faradayic current, D , on the inner pore surface:

$$\frac{di_2}{dx} = -SD, \quad /3/$$

where S is the inner surface of a cubic centimeter of the electrode. Let us choose for D the following function of polarization /overvoltage/, E :

$$D = 2i_0 \sinh \beta E, \quad /4/$$

where $E = \varphi_2 - \varphi_1$ fulfills the condition that $E = 0$ when $D = 0$, i_0 is the exchange current density, and $\beta = F/2RT$; it is possible, however, to substitute for β an empirical value obtained by measurement of polarization curves with a planar electrode. For anodic and cathodic polarization, the values of β can be different. Therefore, it would be more correct to use the well known general relation between current and overvoltage from the theory of absolute reaction rates, rather than equation /4/. In that case, however, the mathematical solution would become too complicated, without yielding any substantial improvement.

The boundary conditions for equations /1/-/3/ are:

$$x = 0: \quad i_1 = 0, \quad \varphi_2 = 0, \quad /5/$$

$$x = L: i_1 = I, \quad /6/$$

and the conservation law of current:

$$i_1 + i_2 = I. \quad /7/$$

For a cathodic current, $I > 0$, $E > 0$, and $D > 0$; for an anodic current, $I < 0$, $E < 0$, and $D < 0$. The problem defined by equations /1/-/7/ can be reduced to the following differential equation:

$$\lambda^2 \frac{d^2 u}{dx^2} = \sinh u \quad /8/$$

with boundary conditions:

$$x = 0: \frac{du}{dx} = -\beta \rho_2 I, \quad /9/$$

$$x = L: \frac{du}{dx} = \beta \rho_1 I, \quad /10/$$

with $u = \beta E$, and $\lambda = 1/\sqrt{2\epsilon_0 S}(\rho_1 + \rho_2)$.

The solution of equations /8/-/10/ is:

$$|x - x_m| = k\lambda F(k, \psi), \quad /11/$$

where $F(k, \psi)$ stands for the elliptic integral of the first kind with the modulus

$$k = \frac{1}{\cosh \frac{1}{2} u_m}, \quad /12/$$

and amplitude

$$\psi = \arccos \frac{\sinh \frac{1}{2} u}{\sinh \frac{1}{2} u_m}. \quad /13/$$

Further x_m is the value of x at which $|u|$ has the minimum value $|u_m|$. Formally, the solution /11/ is analogous to that which Winsel (5) derived for the case of $\rho_1 = 0$.

The expression for faradayic current takes the form:

$$D = \frac{D_m}{\cos^2 \psi} \sqrt{1 - k^2 \sin^2 \psi} \quad /14/$$

ψ being defined by equation /11/ as

$$\sin \psi = \operatorname{sn} \left(\frac{|x - x_m|}{k\lambda}, k \right), \quad /15/$$

where sn denotes Jacobi's elliptic function. Further D_m stands for $2i_0 \sinh u_m$, so that $|D_m|$ represents the minimum value of $|D|$.

An important measurable quantity is the potential, φ_{1L} , of the metallic conductor at the end of the pores /vs. the electrolyte potential at $x = 0$ /. For this we obtain:

$$\varphi_{1L} = -\frac{\rho_2}{\rho_1 + \rho_2} (E_0 + I L \rho_1) - \frac{\rho_1}{\rho_1 + \rho_2} E_L, \quad /16/$$

where E_0 and E_L are the values of E for $x = 0$ and $x = L$, which fulfill the following relationship:

$$\cosh \beta E_0 - \cosh \beta E_L = \frac{1}{2} \beta^2 \lambda^2 I^2 (\rho_2^2 - \rho_1^2). \quad /17/$$

The value of E_0 can be computed from the equation

$$\sinh \frac{1}{2} \beta E_0 = \frac{I}{I_0 \sin \psi_0}, \quad /18/$$

where $I_0 = 2/\beta \lambda \rho_2$, and ψ_0 is the solution of the equation

$$\frac{L}{k\lambda} = F(k, \psi_0) + F(k, \psi_L) \quad /19/$$

with $\psi_L = \arctg[(\rho_1/\rho_2) \tg \psi_0]$, and $k = 1/\sqrt{1 + I^2/I_0^2 \tg^2 \psi_0}$.

Some limiting cases

When the pores are short so that $L < \frac{1}{2} \pi k \lambda$ and the current is large, then $k \ll 1$ and the expression for faradaic current becomes:

$$D = D_m \sec^2 \frac{x - x_m}{k\lambda}. \quad /20/$$

In this case, the polarization of the electrode is large, so that the hyperbolic sine in equation /4/ may be substituted by an exponential function. Equation /20/ can be shown to correspond exactly to the solution given by Newman and Tobias (4).

When, on the contrary, the pores are long and the current small, so that $|I| \ll I_0 \sinh(L/2\lambda)$, equation /14/ becomes

$$D = D_m \cosh \frac{x - x_m}{\lambda} \sqrt{k^2 + (1-k^2) \cosh^2 \frac{x - x_m}{\lambda}}. \quad /21/$$

When, in addition, the polarization of the electrode is small, so that the hyperbolic sine in equation /4/ may be substituted by a linear function, we can set $k = 1$ in equation /21/ to obtain a simple formula which /after suitable rearrangement/ can be shown to correspond exactly to the solution given by Euler and Nonnenmacher (2).

When the specific resistances of both phases, electrode and electrolyte, are equal, then equation /17/ yields simply $E_0 = E_L$, so that the polarization at one end of the pores is equal to that at the other.

Further $x_m = \frac{1}{2}L$, that is, the minimum of the absolute value of polarization is in the middle of the electrode. Hence, the faradayic current distribution in the electrode is symmetrical. Equation /16/ becomes

$$\varphi_{1L} = -E_0 - \frac{1}{2} IL\rho_1. \quad /22/$$

When the specific resistance of the electrode is negligible, so that $\rho_1/\rho_2 \rightarrow 0$, we have the case already discussed by Winsel (5); then $\varphi_{1L} = -E_0$, $x_m = L$. On the contrary, when the specific resistance of the electrode is very great, so that $\rho_1/\rho_2 \rightarrow \infty$, we have $\varphi_{1L} = -E_1$, $x_m = 0$. The results of Winsel (5) can be applied in this case, if we introduce a new independent variable $x' = L - x$. In other words, we consider the end of the pores as the beginning and vice versa.

An interesting and very simple case is when the specific resistances of both phases are equal and, simultaneously, the pores are long and/or the current is small. Then we can express φ_{1L} simply as a function of the current, I :

$$\varphi_{1L} = -\frac{2}{\beta} \operatorname{arsinh} \left(\frac{I}{I_0} \coth \frac{L}{2\lambda} \right) - \frac{1}{2} IL\rho_1, \quad /23/$$

from which it can be seen that the electrode polarization, φ_{1L} , is directly proportional to the total current when $|I| \ll I_0$. Further, we can define the initial polarization resistance as

$$R = -\left(\frac{\partial \varphi_{1L}}{\partial I} \right)_{I=0} = \frac{2}{I_0\beta} \coth \frac{L}{2\lambda} + \frac{1}{2} L\rho_1. \quad /24/$$

The symmetrical form of faradayic current distribution can be readily seen from equation /21/, if we set $x_m = L/2$.

Other cases are more complicated and we have to compute the polarization curves, $\varphi_{1L} = f(I)$, numerically for a given set of parameters I_0 , L , λ , ρ_1 and ρ_2 . This will be the purpose of further work.

References

1. J.J. Coleman: Trans. Electrochem. Soc. 90, 545 /1946/.
2. J. Euler and W. Nonnenmacher: Electrochim. Acta 2, 268 /1960/.
3. V.S. Daniel-Bek: Zhur. Fiz. Khim. 22, 697 /1948/.
4. J.S. Newman, Ch.W. Tobias: J. Electrochem.Soc. 109, 1183/1962/.
5. A. Winsel: Z. Elektrochem. 66, 287 /1962/.

EFFECTS OF OXYGEN PARTIAL PRESSURE ON FUEL CELL CATHODES

A. J. Hartner, M. A. Vertes, V. E. Medina and H. G. Oswin

Leesona Moos Laboratories, A Division Of
Leesona Corporation
Great Neck, New York

INTRODUCTION

The study of transport and electrochemical processes occurring at the oxygen cathode is of fundamental importance in fuel cell development. The oxygen depolarized cathode is the major determining factor for cell efficiency in H_2 /Air fuel cells. It becomes important then to investigate this factor since the oxygen depolarized cathode is common to all fuel/air cells. Additional value may be derived from this study since the investigation of the transport processes occurring at the oxygen cathode would afford an insight into the processes occurring at anodes using insoluble fuels and exhibiting activation polarization.

In order to obtain larger practical current densities, it is necessary to provide a large reaction zone for apparent electrode area. This is usually accomplished by employing porous electrodes having a high ratio of reaction area to apparent electrode area. The liquid electrolyte would then partially permeate the pores of the electrode and the balancing gas pressure on the reverse side of the cathode establishes a liquid meniscus of a three-phase (electrode/oxidant/electrode) interface.

During this study, the three-phase interface was produced by partly immersing a flat-plate cathode into the electrolyte. This arrangement was preferred because of two inherent difficulties associated with porous matrices, namely; poor reproducibility, and the difficulty in accurately defining the reaction zone. The effects of p_{O_2} up to 10 atm on the current-voltage characteristics of these complex porous structures compared favorably with results obtained with flat-plate electrodes. The materials used for the flat-plate electrodes were Pt, Au, Ag and Pd.

Experimental. The experimental arrangement used is shown in Figure 1. Standard potential-current measurements were made in the p_{O_2} range 0.10 to 10 atm. A Wenking potentiostat was used for the series of experiments when the potential was maintained constant. In order to eliminate any slight current contributions that would arise from the electrode portion immersed in the electrolyte, the data reported herein were obtained with the electrode entering at the surface of the electrolyte. The results indicate that the bulk of the current is generated in a zone near the meniscus or three-phase interface as also reported by Sama et al ¹ and Will ².

The difficulty in defining the three-phase interface is complicated by the presence of oxides and uneven surfaces. For this reason we obtain reproducible current densities by expressing them in μA per linear centimeter of the interface. In order to prevent disturbance of the interface, the electrolyte was not stirred while measurements were taken.

EFFECT OF p_{O_2} ON OCV AND POLARIZATION

Results and Discussion. As shown in Figure 2, the partial pressure of oxygen affects both the OCV and potential at constant current. Although changes in OCV are anticipated in accordance with the Nernst equation, the changes in the potential at constant current merit closer examination. It can be readily seen from Figure 2 that potentials at constant current become more anodic with increasing p_{O_2} and that polarization decreases as the p_{O_2} increases. However, this polarization decrease becomes less rapid as p_{O_2} rises.

A better understanding of the diminishing effect of p_{O_2} on polarization can be derived when p_{O_2} or $\log p_{O_2}$ values are plotted vs. polarization at constant current density (see Figures 3 and 4).

According to Weber, Meissner and Sama¹ the rate limiting step for a partially immersed depolarized oxygen cathode is mass transport of oxygen through the liquid meniscus zone. Since p_{O_2} is a major mass transport parameter our studies were extended to partial pressures of oxygen ≤ 10 atm to study its effect.

It is evident from our studies that p_{O_2} has a decided effect on the polarization of the electrodes and that the p_{O_2} polarization relationship is not linear. The current (i) obtainable from the transport of oxygen through an electrolyte layer can be expressed by the following equation,³

$$i_C = DZF(C_1 - C_2) / \delta \quad (1)$$

where: D = the diffusion coefficient
 C_1 = concentration of O_2 at the gas/liquid interface
 C_2 = concentration of O_2 at the electrode surface
 δ = thickness of the diffusion layer
 Z = no. of electrons transferred during the reaction
 F = the Faraday constant

For a limiting current (i_1), $C_2 = 0$ and $i_1 = DZF(C) / \delta$ (2)

The relationship for concentration polarization (η_C) is:³

$$\eta_C = (2.303 RT / ZF) \log i_1 \left(\frac{i_1}{i_1 - i_C} \right) \quad (3)$$

where: R = the Ideal Gas Constant
 T = Temperature, °K
 i_C = the current obtained at η_C

According to equation 3, a drop in concentration polarization may be obtained by increasing limiting current. Equation 2 implies that this can be accomplished by:

- a. Increasing D (i. e., increasing temperature).
- b. Decreasing δ (through agitation).
- c. Increasing C_1

D and δ were kept constant in our experiments by maintaining constant temperature and preventing agitation of the electrolyte.

By substituting equations 1 and 2 in 3

$$\eta_C = (2.303 RT/ZF) \log \left(\frac{DZFC_1/\delta}{DZFC_1/\delta - DZF(C_1 - C_2/\delta)} \right)$$

At constant current, $(C_1 - C_2)$ will be constant, i. e., equal to K_1 . Then

$$\eta_C = (2.303 RT/ZF) \log \left(\frac{C_1}{C_1 - K_1} \right)$$

The concentration of oxygen at the gas/liquid interface C_1 is a function of p_{O_2} . Therefore,

$$\eta_C = \frac{2.303 RT}{ZF} \log \left[\frac{f(p_{O_2})}{f(p_{O_2}) - K_1} \right]$$

where $\lim p_{O_2} = \infty$

$f(p_{O_2}) \rightarrow \infty$. According to this relationship, for a given current:

- a. $\lim \eta_C = 0$
 $f(p_{O_2}) \rightarrow \infty$
- b. $\lim \eta_C = \infty$
 $f(p_{O_2}) \rightarrow K_1$.

This has been confirmed by experimental data.

Our experimental results show that highly active porous structures having a three-phase interface exhibit the same sensitivity to p_{O_2} as the flat-plate cathodes (see Figures 5 and 6).

These results also illustrate the limitation imposed by oxygen mass transport through an electrolyte layer. This is significant because although the flat-plate cathode may be considered as an idealized model of a porous structure, the same limiting process (oxygen mass transfer through the electrolyte meniscus) occurs for both electrode types. Therefore, the flat-plate "model" electrode system is directly applicable to a porous electrode for purposes of comparison of p_{O_2} effects.

Equipotential Current. It has been observed that at -0.8 volt from OCV, the four catalysts tested (Pt, Pd, Ag, and Au) yielded identical currents on flat-plate electrodes. This reference potential (-0.8 V) was chosen because a true limiting current could not be obtained before reaching the H_2 -deposition region. The maximum obtainable current (i_E) refers to the current produced per cm length of meniscus at -0.8 volt polarization vs. OCV.

EFFECT OF p_{O_2} ON "MAXIMUM CURRENT"

In the initial experiments, p_{O_2} was varied and the corresponding i_E values were observed. The $i_E - p_{O_2}$ data obtained were plotted using log coordinates (see Figure 5, curve 2). It can be seen from this curve that i_E is independent of the catalytic material and varies with $(p_{O_2})^{1/2}$, i. e., $i_E = A \log p_{O_2} + B$, where the constant A is 0.5 (calculated) and the constant B approximately equals $740 \mu A$ per cm length of meniscus on the flat-plate cathodes. This relationship enables prediction of i_E at any p_{O_2} within the range studied

by the equation:

$$\frac{i_{E, 1}}{i_{E, 2}} = \left(\frac{p_{O_2, 1}}{p_{O_2, 2}} \right)^{1/2} \quad (4)$$

where $i_{E, 1}$ and $i_{E, 2}$ are the maximum currents obtainable for a flat-plate cathode in the same electrolyte concentration at $p_{O_2, 1}$ and $p_{O_2, 2}$, respectively. From the above data it could be safely concluded that either the four metals tested have identical catalytic activity, which is unlikely, or that under the experimental conditions (800 mV polarization from the rest potential), the catalytic activity no longer has a significant effect on the current. This is explainable since at potentials 800 mV from the rest potential, the electrochemical reaction is no longer rate controlling, and its effect is masked. Figure 5, line 1 is a log plot of the results obtained using a porous structure with negligible activation polarization. It can be seen that with this structure, the currents obtained at equal polarization also vary with $(p_{O_2})^{1/2}$.

Oxygen Transport. When it was established that the catalytic activity of the electrode was not a current controlling factor, attention was then focused on other possible factors such as mass transport of oxygen to the catalytic sites. Sama, et al.¹ reported, that the bulk of the current obtained from a half immersed flat-plate electrode, was generated near the immediate vicinity of the triple interface. It was also established that oxygen is transported to the catalytic sites through the electrolyte.

There are two possible rate-controlling steps in such a case. One is liquid phase diffusion of dissolved oxygen, the other is interphase mass transfer of oxygen from the gas into the liquid phase. Should ordinary diffusion in the liquid phase be the rate controlling step, and the liquid surface in contact with the gas is saturated with oxygen, then a linear variation of current with p_{O_2} would occur.

Investigating the case where liquid phase diffusion could be the only possible rate controlling factor, Reti⁵ performed an experiment, in the course of which he pre-saturated electrolytes with O_2 at various partial pressures. He then pumped the electrolytes through silver or platinum screen electrodes. Under constant hydrodynamic conditions, (flow rate and temperature), he found a linear relationship between equipotential currents and the partial pressure of oxygen in the pre-saturating gas. Higher currents therefore can be obtained for a given p_{O_2} if pre-saturated electrolyte is used.

If ordinary linear diffusion was the mass transfer controlling step under the experimental conditions of our study then p_{O_2} would exhibit a linear relationship with current. Our experimental data show that $i_E \propto (p_{O_2})^{1/2}$, which would appear to eliminate the possibility of ordinary diffusion being a mass transfer controlling step.

Effect of O_2 Solubility on i_E . The curves in Figure 8 were plotted from i_E vs. electrolyte molar concentration data which were obtained to determine the effects of O_2 solubility on i_E . If equation 4 is valid at all concentrations then the maximum current obtainable at any p_{O_2} can be predicted from the actual data measured at any other p_{O_2} at the same KOH concentration. For example (refer to Figure 8), if the calculations are based on data at $p_{O_2} = 1$ atm, the predicted (dotted line) and experimental (solid line) values at $p_{O_2} = 0.6$ atm and 0.21 atm are in close agreement.

Studies were made of the currents obtained at various electrolyte concentrations in which the equilibrium concentration of O_2 in the electrolyte was kept constant (by adjusting p_{O_2}).

As seen in Table 1 (similar plot as Figure 8), at equal equilibrium concentrations of O_2 in KOH at a given p_{O_2} (C^*), the currents obtained are approximately equal. Because data for solubility of O_2 in KOH is very limited in the literature, extrapolations had to be made at several points to obtain the solubility value. Thus, because of the lack of solubility data, the actual KOH molar concentrations at which C^* values are equal at different p_{O_2} values cannot be accurately predicted. According to the data shown in Figure 7, i_E varied with $(p_{O_2})^{1/2}$. It is well known that in the case of transport of a slightly soluble gas into a liquid, the bulk of the resistance is in the liquid phase. Due to this limitation the bulk liquid near the transfer zone is not reaching the equilibrium saturation as predicted using Henry's law. If we plot i_E vs. the equilibrium solubility of oxygen (C^*) at various electrolyte concentrations we obtain a relationship similar to the one previously shown, that is $i_E = A' \log C^* + B$ where the experimentally obtained A' value is 0.48, which compares well with the previously obtained 0.5 value (see Figure 9). Use of extrapolated C^* values due to the scarcity of actual solubility data in the literature may be used to account for this deviation.

TABLE 1
 i_E OBTAINED FOR VARIOUS C^* VALUES
IN KOH ELECTROLYTE

$C_{KOH} = 1M$			$p_{O_2} = 1 \text{ atm}$		
p_{O_2} (atm)	C^* (ml/l)	i_E ($\mu A/cm^\ddagger$)	C_{KOH} (M)	C^* (ml/l)	i_E ($\mu A/cm^\ddagger$)
1	22.2	1320	-	-	-
0.6	13.32	1008	2.18	13.32	1130
0.21	4.66	685	5.5	4.66	700

\ddagger Length of meniscus

Note- Electrode: Polished Flat Gold-Plate Cathode
Temperature: 25°C

The current-partial pressure relationship developed earlier in this paper (see equation 4), can be used to predict electrode polarization when E-i curves are linear. This is the case, for example, for the highly active complex porous electrode structures shown in curve 1 of figure 7.

If the slope of the linear E-i curve is b then at a given polarization, :

$$b_1 = \eta/i_1$$

and similarly

$$b_2 = \eta/i_2$$

Thus

$$b_1/b_2 = i_2/i_1$$

If η is a linear function of i, then

$$\eta = J i (p_{O_2})^{-1/2}$$

or

$$\log \eta = \log i - \frac{1}{2} \log p_{O_2} + \log J$$

Data illustrating this equation are shown in figure 10.

CONCLUSIONS

Data have been presented to show the effect of oxygen partial pressure on the polarization and maximum current of partially immersed flat-plate cathodes. It has been proven that polarization - oxygen partial pressure dependence for the flat-plate electrodes is valid for complex porous structures as well. A marked decrease in electrode polarization was observed at the lower range of p_{O_2} studied (0.1 to 1.0 atm). Beyond this range the polarization decrease is not as marked. Therefore extremely high p_{O_2} values are ineffective in obtaining minimum cathode polarization for practical fuel cell operation.

The following equations are very useful for predicting cathode currents under different operating conditions if the cathode current is known for one condition, and there are no other experimental data available.

$$\left(\frac{i_{E,1}}{i_{E,2}} \right) = \left(\frac{C^*_{1}}{C^*_{2}} \right)^{1/2}$$

$$\left(\frac{i_{E,1}}{i_{E,2}} \right) = \left(\frac{p_{O_2,1}}{p_{O_2,2}} \right)^{1/2 \dagger}$$

These equations are valid for complex porous structures only when:

1. The activation polarization is small.
2. Diffusion (both ionic and gaseous) limitations and electrical resistance of the structure are negligible.

The difficulty in defining the three-phase interface is complicated by the presence of oxides and uneven surfaces. For this reason we obtain reproducible current densities by expressing them in μA per linear centimeter of the interface. In order to prevent disturbance of the interface, the electrolyte was not stirred while measurements were taken.

Since the relationship $i_E \propto (p_{O_2})^{1/2}$ exists at all electrodes involving interphase transport of O_2 (gas/liquid), it seems likely that interphase transport is the mass transfer rate controlling mechanism.

† Used when the same KOH concentration is used

APPENDIX

P_{O_2}	=	partial pressure of O_2 (atm)
i_E	=	maximum obtainable current on a half-immersed flat-plate electrode that results from the electro-reduction of O_2 (μ A/cm meniscus length)
N	=	number of moles of O_2 diffusing per unit area - unit time
D	=	diffusivity coefficient (unit area/unit time)
δ	=	mean length diffusion path in the meniscus
ΔC	=	difference in O_2 concentrations between that at the gas/liquid and liquid/solid interfaces in the meniscus (moles of O_2 /unit volume of electrolyte)
μ	=	viscosity
C^*	=	equilibrium concentration of O_2 in KOH electrolyte at a given P_{O_2} (ml stp of O_2 /liter of electrolyte)
A	=	proportionality constant
J	=	proportionality constant
b	=	slope of linear E-i curve
η	=	polarization (volts)

LITERATURE CITED

- (1) D. A. Sama, H. C. Weber, and H. P. Meissner, J.E.S., 109, No. 10, 884-9 (1962).
- (2) F. G. Will, J.E.S., 110, No. 2, 145-160 (1963)
- (3) G. Charlot, J. Badoz-Lambling, B. Tremillon, "Electrochemical Reactions", Elsevier Pub. Co., New York, N. Y., 1962.
- (4) E. C. Potter, "Electrochemistry, Principles and Applications", Macmillan Co., New York, N. Y., 1956.
- (5) A. R. Reti, "Rate Limiting Step on Fuel Cell Electrodes", Doctorate Thesis, M. I. T. (June 1962).

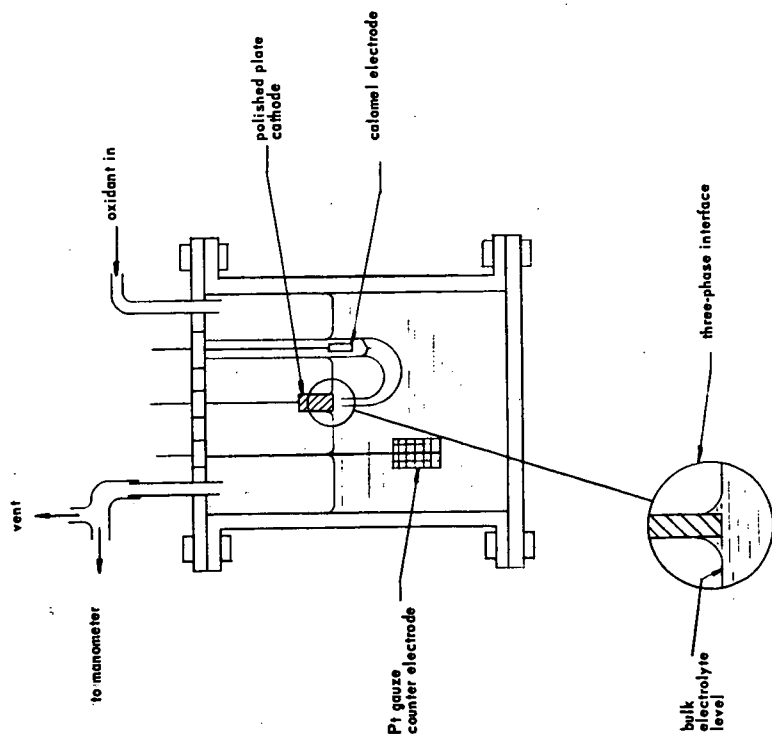


Figure 1 - Experimental Arrangement

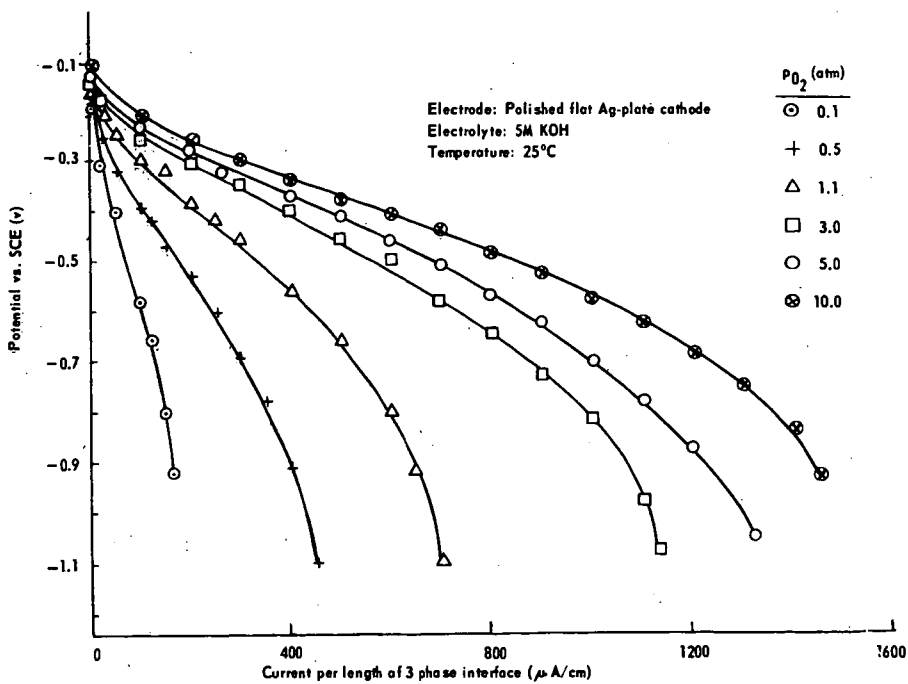


Figure 2 - Polarization of Flat-Plate Electrode Partially Immersed in KOH Electrolyte

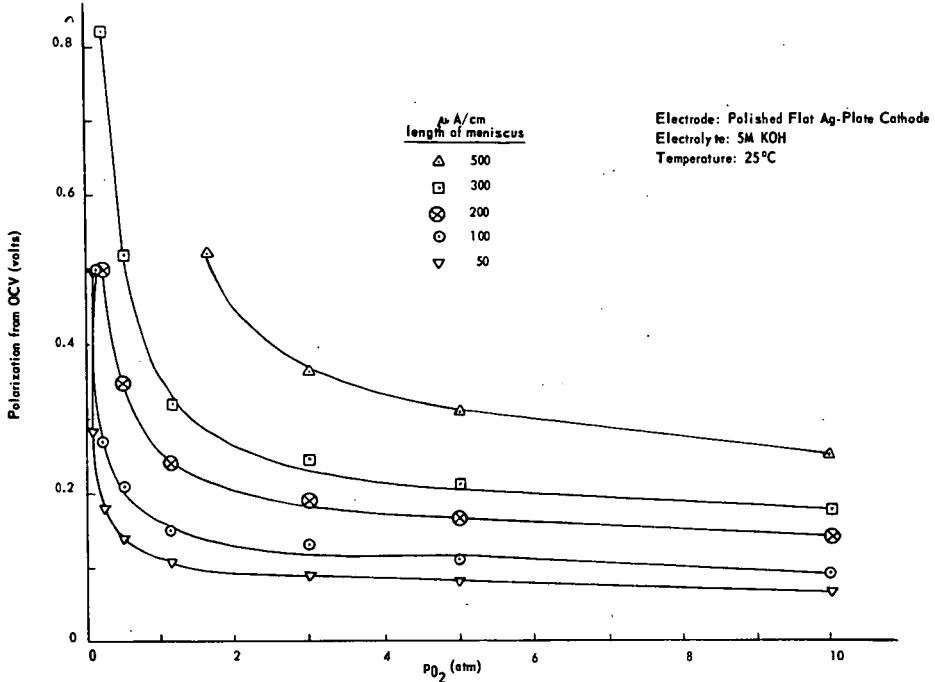


Figure 3 - Polarization from OCY vs. p_{O_2} for a Flat-Plate Electrode Partially Immersed in KOH Electrolyte

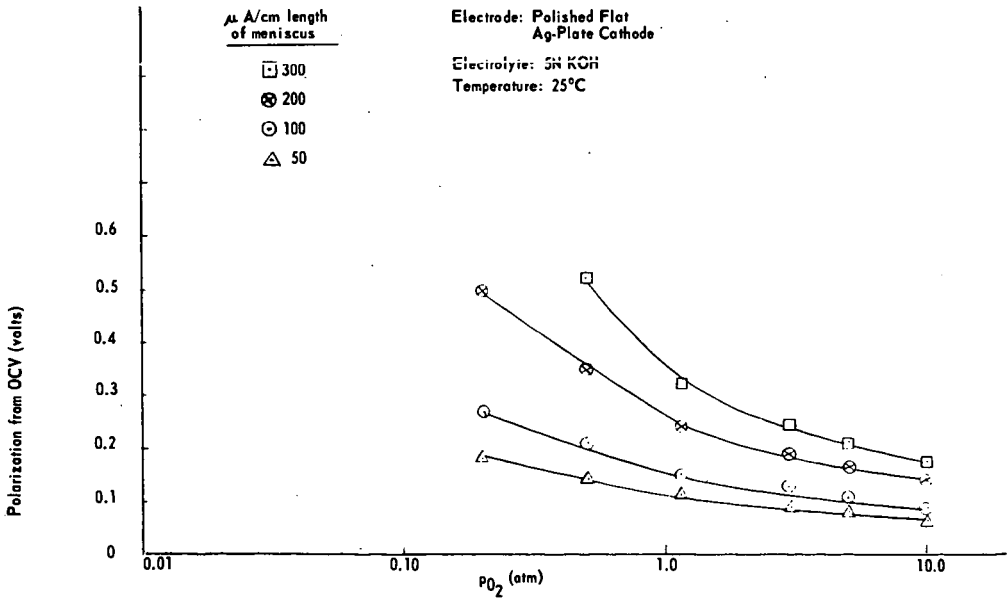
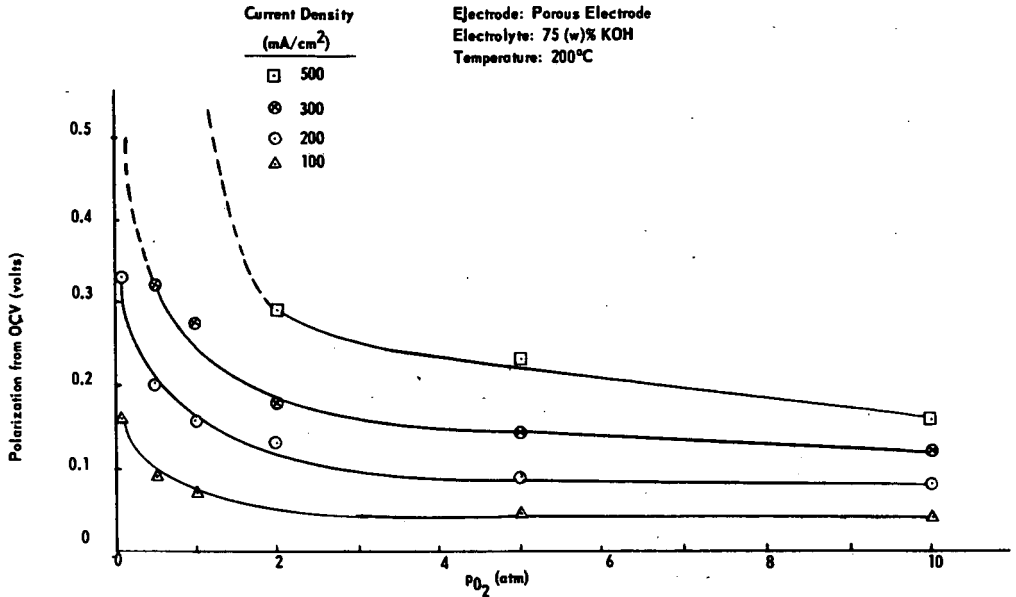


Figure 4 - Polarization from OCY vs. p_{O_2} for a Flat-Plate Electrode Partially Immersed in KOH Electrolyte



• Figure 5 - Polarization vs. p_{O_2} for Complex Porous Structures

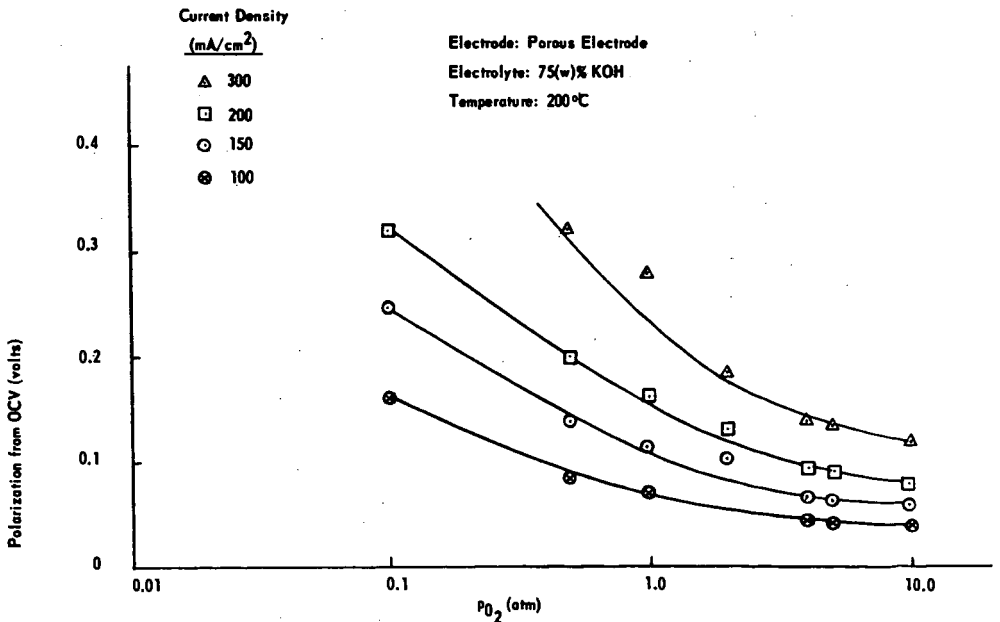


Figure 6 - Polarization vs. p_{O_2} for Complex Porous Structures

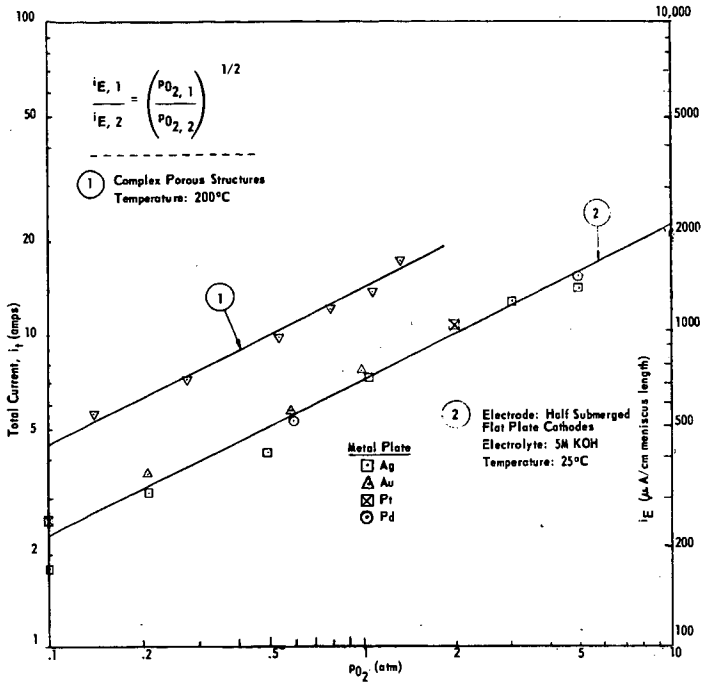


Figure 7 - i_E vs. p_{O_2} for Various Electrodes

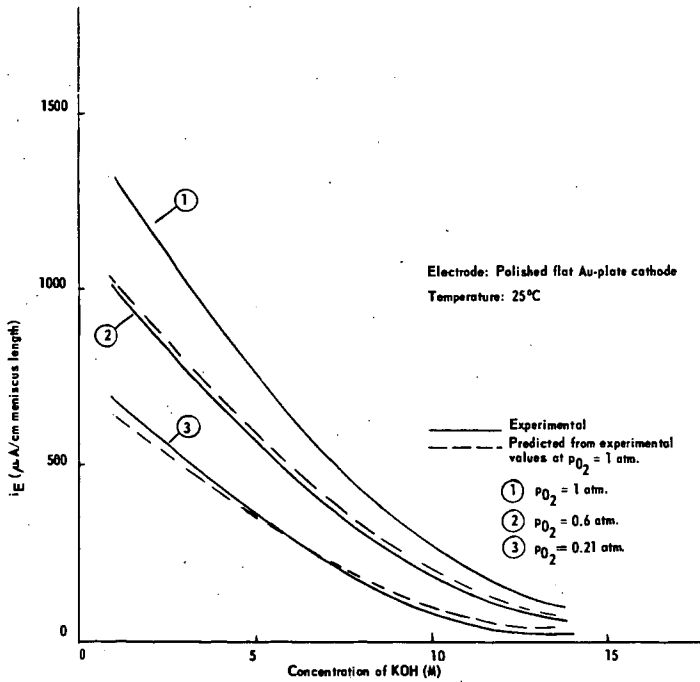


Figure 8 - i_E vs. Concentration of KOH for a Flat-Plate Electrode

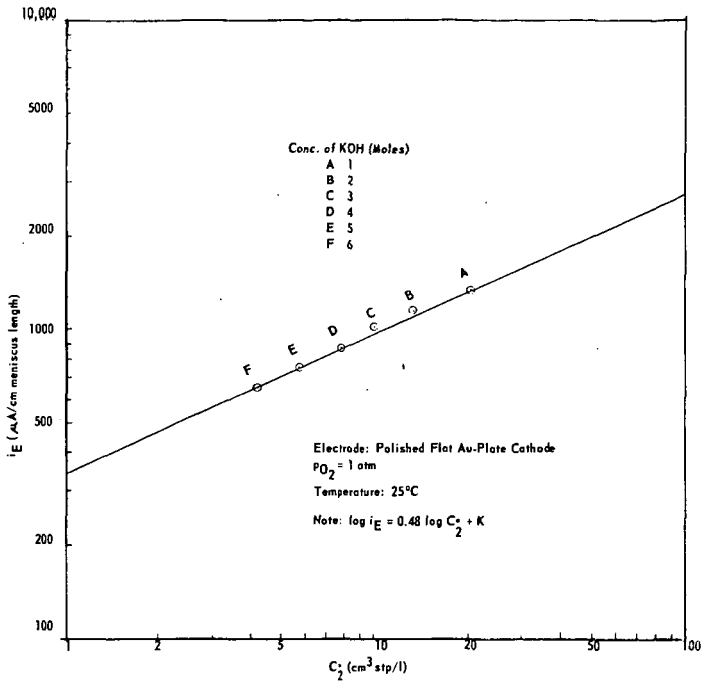


Figure 9 - i_E vs. C_2 for Flat-Plate Electrode

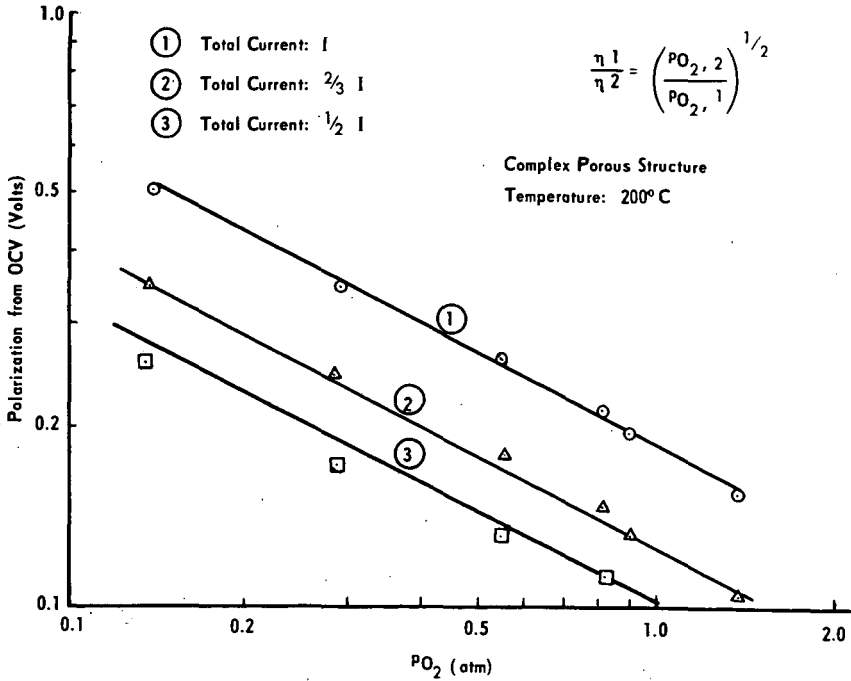


Figure 10 - Polarization vs PO_2

Diffusion Polarization in Air Channels

Henri J. R. Maget and Eugene A. Oster

General Electric Company, Direct Energy Conversion Operation
Fuel Cell Laboratory, West Lynn 3, Mass.

Introduction

Rates of cathodic oxygen reduction, that is, cell currents are dependent on partial pressures of the oxidant if rate-controlling steps involve the concentration or partial pressure of oxygen. This is likely to be observed since reaction rates will be either liquid film or gas diffusion controlled. However, cases can arise where removal of the reaction product may be hindered by slow transport processes, thus resulting in, possibly, appreciable lower rates. This could be the case of water removal from the catalyst surface of an oxygen electrode. If local current densities are either dependent on partial pressures of oxygen or water, it will become necessary to establish relationship predicting such local current densities and to design electrode geometries favorable to uniform current distribution, and as a result uniform distribution of the main influential variables affecting oxygen electrode performance. Such considerations, however, would imply knowledge of limiting current densities.

In reestablishing over-all oxygen electrode capabilities for fuel cell application, one of the important variables is the limiting current density. Although these limiting currents are not simply dependent on some limited parameters, i. e. electrode activity, electrode structure, electrolyte properties, local temperatures, anisotropic current density distributions, etc. . . , actual measurements are valuable if some reproducible characteristics can be controlled, i. e. catalytic activity, electrode structure, electrolyte properties. Thus, measurements are valuable for a specifically designed system, as related to limiting current densities, and very generally applicable to any air electrode current collector design, if the geometry is influential on, and descriptive of, the limiting currents.

The ultimate goal, that is quantitative description of current-voltage relationships as a function of main variables, can be, in principle, attained from experimental studies, involving the determination of limiting current densities at discrete positions in the channels, the establishment of the rate-controlling process for known channel geometries in the high current density range (corresponding to 0.85 - 0.5 volts), the derivation of relationships describing the current-voltage behavior over practical operational ranges, the transport phenomena explaining polarization potentials at these practical currents and the experimental values of open circuit potentials. If all these equilibrium conditions, rates and processes are known, a reasonable analytical description of local as well as over-all currents and potentials, can be expected.

It is possible then, that limiting currents can be associated with channel geometry and that diffusional processes in restricted channels become small enough i. e., rate-controlling.

The purpose of the present work was to obtain experimental results and interpretation to explain polarization in channels of defined geometry and to establish influential parameters which would affect electrode performance. In order to establish applicability of a self-breathing air electrode, viz. without forced convective air-flow, for low current densities, experimental investigations were started on straight air channels. Furthermore, since such a self-breathing electrode had to operate away from limiting currents, in order to minimize diffusion polarization, additional work for forced flow (at various air flow rates) was conducted in straight air channels. This work will be reported elsewhere. (2)

Experimental Equipment

The system chosen for experimental investigation was based on platinum black electrodes associated with a solid-matrix electrolyte (cation exchange membranes). Such a system offered multiple advantages in preparing discretely separated small electrodes, displaying good and uniform contact with the electrolyte. The individual electrodes included metallic screens in order to increase surface conductivity.

Reference potential measurements were based on a Luggin-type capillary-SCE system, specially developed for application to ion exchange membrane electrolytes (1). A low-leakage capillary was placed against the membrane and sulfuric acid used to establish the bridge with the calomel electrode. In all cases, the ion exchange membrane extended outside of the apparatus for potential measurements. Effects of capillary positions were investigated by placing the tip against and within the membrane. No appreciable differences were observed.

The ten segmented electrodes allowed the determination of limiting currents as a function of position and represented values for discrete electrode sizes. In many instances, the presented data will represent smooth interpolation of position-dependent limiting currents.

Investigations were conducted under galvanostatic operating conditions. The equipment is represented in Figure 1. All experimental work was conducted on air channels 2-1/2" long and 1/2" wide. Channel height could be varied by changing a removable Lucite bar placed on the channel top. Thus, channel heights could be 1/16, 1/8, 1/4 and 1/2". The channel was mounted on an air electrode and placed in a large Lucite box in order to avoid small air flow sweeps over the air electrode. Both channel ends were open to allow for oxygen diffusion.

In order to determine local current densities, the air electrode was manufactured by placing ten parallel electrode/screen strips on an Ion Exchange Membrane. Gaps of 1/16" between electrodes allowed for electrical insulation of the various electrodes. Electrode dimensions were 1/2" x 3/16" with an actual area of $0.60 \pm 0.05 \text{ cm}^2$. The Ion Exchange Membrane extended out of the channel for reference potential measurements and stainless rods contacted the screens for current pick-up.

The counter electrode (H_2 -electrode) was prepared in a similar manner. Catalytic electrodes faced each other across the electrolyte (membrane).

The two ends of the self-breathing channel were open, thus displaying planar symmetry on either side of the channel center cross-section. Closing one channel end actually corresponded to doubling the channel length. Single electrode failure would not affect results too appreciably since experimental results could be obtained from mirror-image electrode.

Experimental Results

Representative single electrode polarization characteristics are presented in figure 2 for a channel height of 1/16". These polarization curves represent the largest changes from the edge to center electrodes for the smallest channel height investigated.

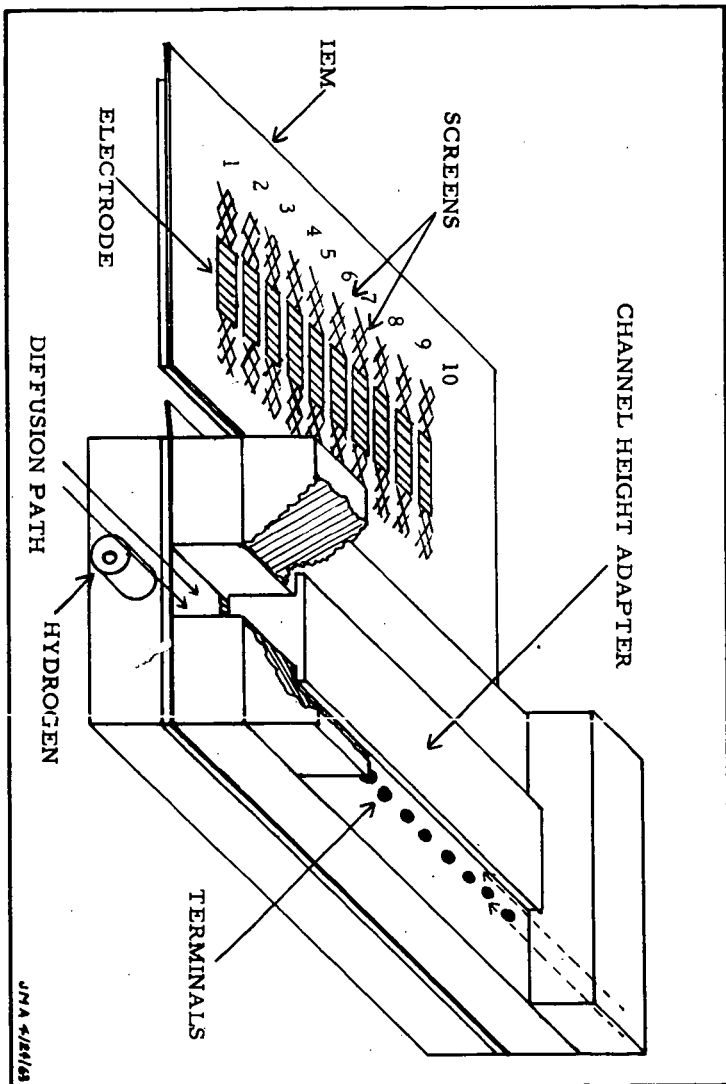


FIGURE 1

EXPERIMENTAL DEVICE FOR MEASUREMENTS OF LOCAL CURRENTS IN AIR CHANNELS OF VARIABLE GEOMETRY

POLARIZATION CHARACTERISTICS OF INDIVIDUAL ELECTRODES FOR TEN PARALLEL ELECTRODES - CHANNEL HEIGHT: 1/8" ELECTRODE SURFACE: 0.6cm²

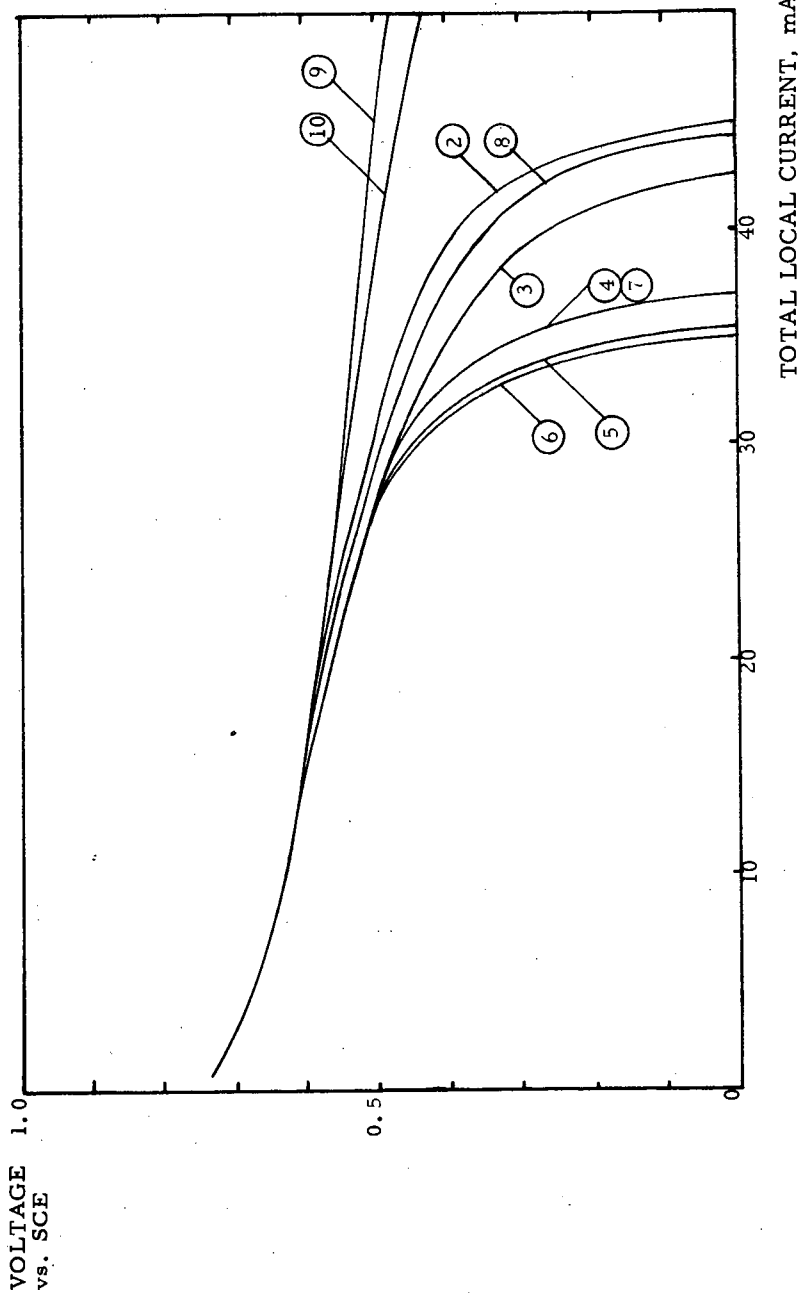


FIGURE 2

CURRENT DISTRIBUTION FOR INDIVIDUAL ELECTRODES IN THE SELF-BREATHING
LOCAL CURRENT CHANNEL - ELECTRODE SURFACE: 0.6 cm^2 . CHANNEL HEIGHT: $1/8''$
mA

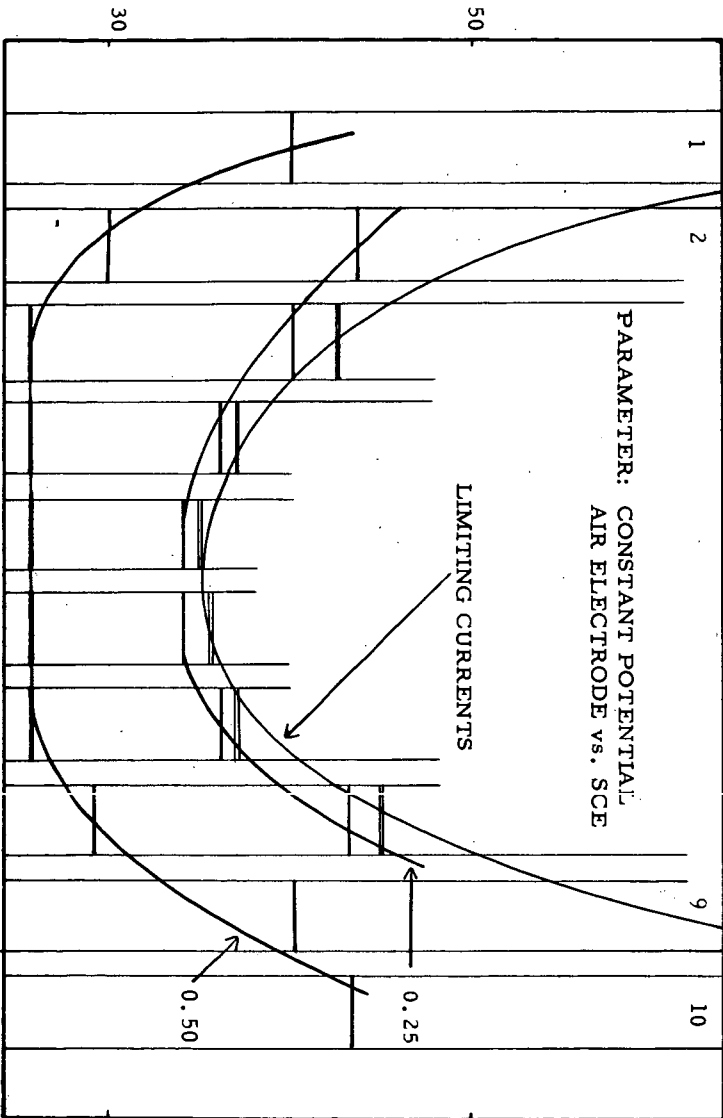


FIGURE 3

CURRENT DISTRIBUTION FOR INDIVIDUAL ELECTRODES IN THE SELF BREATHING/CHANNEL-ELECTRODE SURFACE: 0.6 cm². CHANNEL HEIGHT: 1/16"

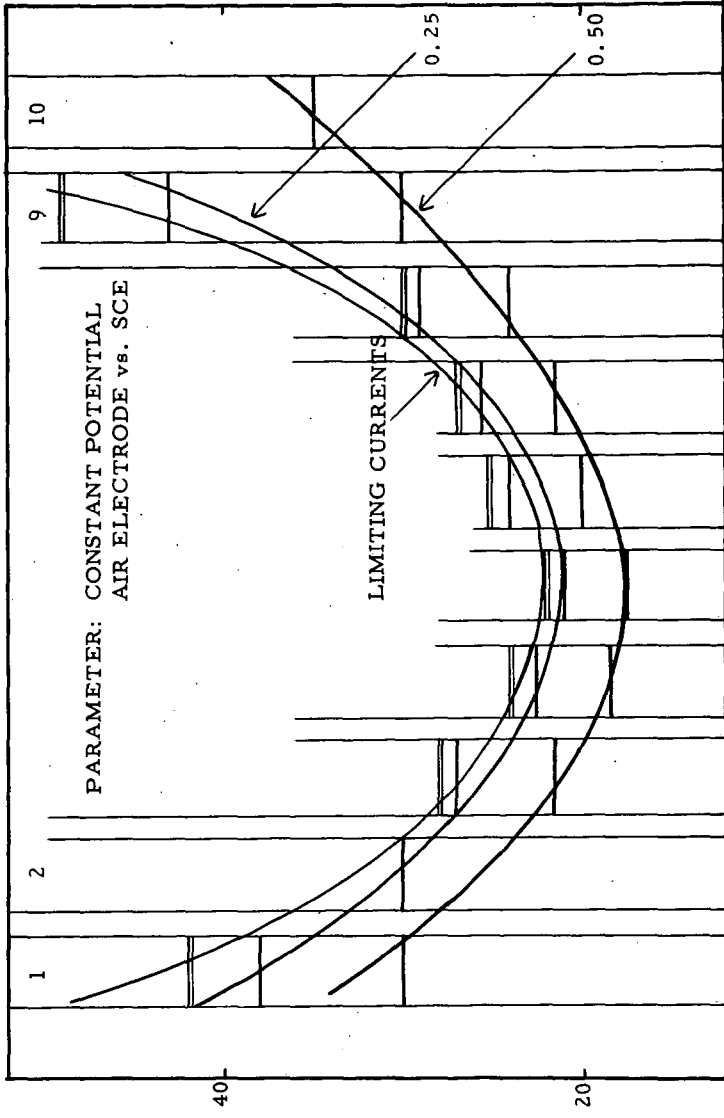


FIGURE 4

Limiting current densities for edge electrodes # 1 and 10 should be about 130-140 ma/cm^2 (as determined independently for electrodes exposed to semi-infinite air space). Figure 2 already indicates that appreciable polarization is encountered as soon as measurements are conducted slightly away from the channel edge. Larger currents are observable for all electrodes for increasing channel height. For $1/2''$ channels, very little polarization is observable even at current densities near limiting values, i.e. 130-140 ma/cm^2 . Polarization is less severe for all electrodes at small local currents, as expected.

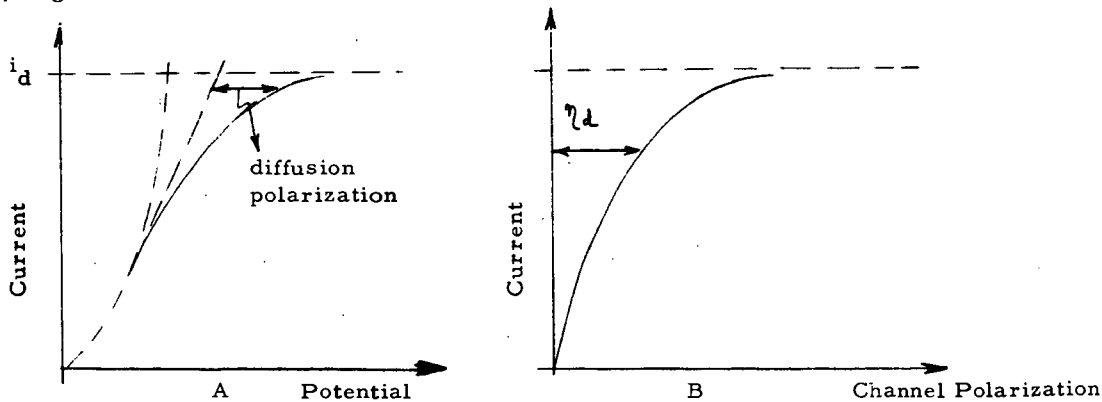
Channel heights affect polarization characteristics to a large degree, i.e. limiting currents for center electrodes are 22 and 35 ma , for $1/16''$ and $1/8''$ channels, respectively. These current densities correspond to oxygen partial pressures of 0.07 to 0.1 respectively, as determined independently from exposed electrode measurements.

For identical polarization potentials (as determined for polarization curves) current density distributions display minima for inner electrodes and can be extrapolated to edge values of limiting currents as determined from previous measurements. Strictly speaking these current densities can not be described from figure.2. However, the partial pressure of oxygen in the channel would not be too greatly affected at higher current corresponding to limit currents of the edge electrodes. Results would be affected greatly at the edge electrodes, let's say electrodes 1 and 2 and their corresponding symmetrical position.

Current density distributions for channel heights of $1/8$ and $1/16''$ for various applied potentials are represented in figures 3 and 4. Edge currents (about 80 mA) can become 2 to 4 times larger than center channel currents, but display much more uniform distribution for lower electrode polarization, i.e. 0.5 volt vs. SCE for $1/8''$ channel.

Interpretation of Individual Polarization Curves

Current potential behavior for the investigated systems can be represented by Figure 5.



i_d = diffusion-limited current
 channel polarization $\eta_d = E_a - E_{wce}$ = Actual Voltage-voltage in absence of channel effects.

SINGLE ELECTRODE DIFFUSION POLARIZATION

Figure 5

Figure 5A represents polarization characteristics as observed in absence and presence of diffusion polarization (including activation polarization, in absence of ohmic contribution, which are generally eliminated). Figure 5B represents strictly diffusion polarization terms in absence of other possible polarization.

Polarization characteristics can be represented by the equation:

$$\left(1 - \frac{i}{i_L}\right) = e^{\alpha(E^\circ - E)} \quad (1)$$

where i and i_L represent actual and limiting currents, respectively; $\alpha = \beta F/RT$, $E^\circ =$ reference potential in absence of channel polarization, $E^\circ - E = \eta_d$

$$\ln\left(1 - i/i_L\right) = \alpha(E^\circ - E) = \alpha \eta_d \quad (2)$$

By differentiation:
$$\frac{dE}{di} = \frac{1}{\alpha i_L (1 - i/i_L)} \quad (3)$$

with
$$\left(\frac{dE}{di}\right) \rightarrow \infty \text{ as } i \rightarrow i_L$$

and
$$R_d = \left(\frac{dE}{di}\right)_{i=0} = \frac{1}{\alpha i_L} \quad (4)$$

Since $i_L(x)$ displays a monotonous decrease up to channel center, equation 4 is expected to display an increase from channel edge to center. Figure 6 represents smoothed experimental results for 1/4, 1/8 and 1/16" channel heights. Since no additional position-dependent polarization was observed for 1/4" channels, the value $R_d = 4$ was chosen as reference systems resistance to obtain a relationship between channel-induced diffusion resistance $R_d(x)$ and $i_L(x)$. Now, in equation (4), the slope (dE/di) defined as diffusional resistance becomes dependent on α and i_L . (If i_L can be determined analytically and since α represents defined constants, (dE/di) is defined). Equation 4, if represented by $\left(\frac{1}{i_L}\right) / \left(\frac{\Delta V}{\Delta i}\right)$ should yield a constant value, determining α . $\left(\frac{\Delta V}{\Delta i}\right)$ representing the diffusional resistance should display:

- no diffusional resistance at the edges, at least as related to electrode geometry
- maximum diffusional resistance for center electrodes
- increased resistance for reduced channel cross-section

Experimental results regarding these observations are represented in Table I for channel heights of 1/8 and 1/16", and different electrode positions.

$$\frac{\Delta V}{\Delta I}$$

SLOPES ($\Delta V/\Delta I$) FOR VARIOUS ELECTRODES IN THE SELF-BREATHING AIR ELECTRODE CHANNEL

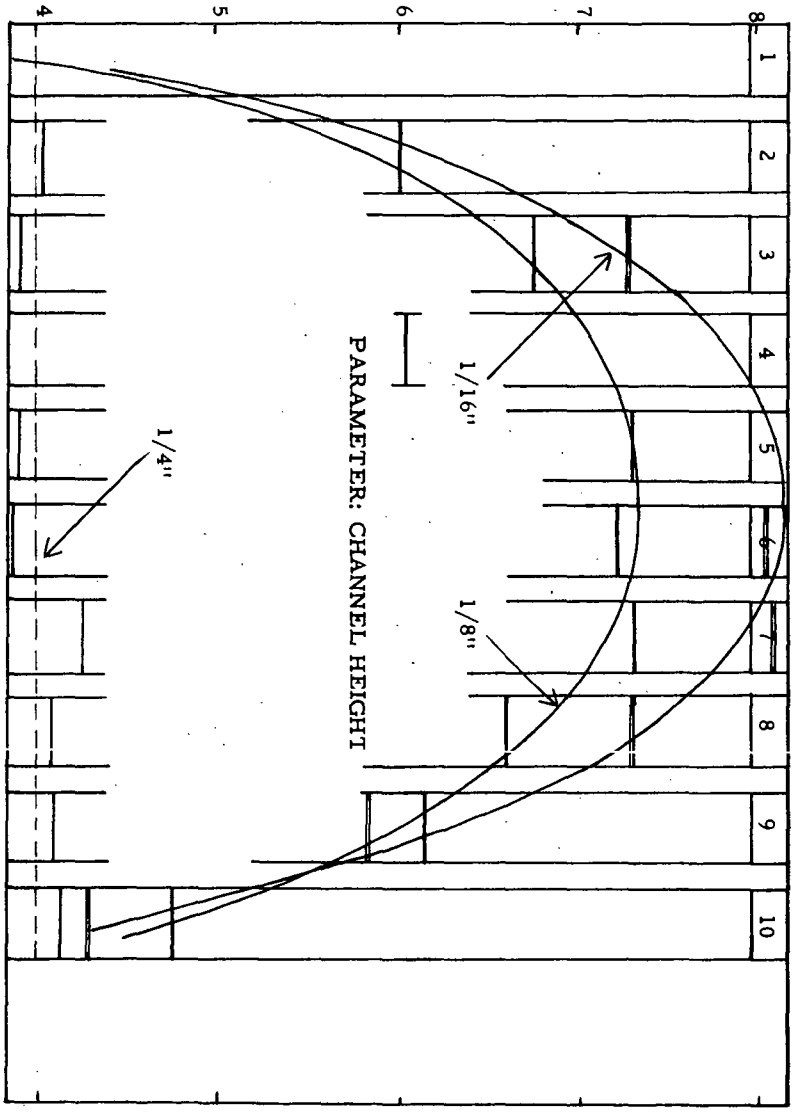


FIGURE 6

TABLE I

Determination of α from experimental data

Electrode Position	Limiting Current, i_L Amps.	$1/i_L$ (Amps) ⁻¹	$\left(\frac{\Delta V}{\Delta I}\right)^{\text{exp.}}$ (ohm)	$\left(\frac{\Delta V - R}{\Delta I}\right)$ (ohm)	$\frac{1}{\left(\frac{\Delta V}{\Delta I} - R\right)}$ (ohm) ⁻¹
<u>Channel Height 1/16"</u>					
1	0.041	-	-	-	-
2	-	-	-	-	-
3	0.028	35.8	7.3	3.3	10.8
4	0.024	41.7	7.8	3.8	11.0
5	0.022	45.5	8.2	4.2	10.8
6	0.025	40.0	8.1	4.1	9.8
7	0.027	38.0	7.9	3.9	9.7
8	0.030	33.3	7.3	3.3	10.1
9	~ 0.050	~ 20.0	6.1	2.1	9.6
					Average $\alpha = 10.4$
<u>Channel Height 1/8"</u>					
1	-	-	-	-	-
2	0.045	22.2	6.0	2.0	11.1
3	0.043	23.2	6.7	2.7	8.6
4	0.037	27.0	7.1	3.1	9.0
5	0.035	28.6	7.3	3.3	8.7
6	0.035	28.6	7.3	3.3	8.7
7	0.037	27.0	7.1	3.1	9.0
8	0.044	22.7	6.8	2.8	8.2
					Average $\alpha = 9.0$

Since the coefficient α represents actually $\beta\mathcal{F}/RT$ in equation 1, average values of β as determined from Table I would be 0.24-0.27.

Now, since α has been obtained experimentally and represents values near theoretical, a complete description of the polarization curves will be available, providing $i_L(x)$ can be established.

Evaluation of the limiting current $i_L(x)$

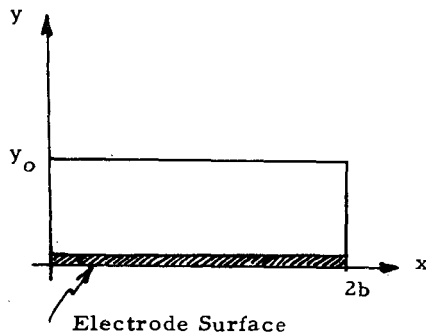
The analytical evaluation of $i_L(x)$ will allow the description of the polarization curves by means of equation 4. Local limiting currents can be evaluated by solving Laplace's equation, providing transport by convection is considered to be negligible.

A. Determination of concentration distribution in channels

$$\nabla^2 c_i = 0 \quad (5)$$

$$\sum_i c_i = 1 \quad (6)$$

c_i represents partial pressures in the three component systems. Boundary conditions are:



$$\left. \begin{aligned} c_i(0, y) &= c_i^i \\ c_i(2b, y) &= c_i^i \end{aligned} \right\} \text{B.C. 1}$$

$$\left. \begin{aligned} c_{O_2}(x, 0) &= 0 \\ c_{N_2}(x, 0) &= 1 - f(\tau) \\ c_w(x, 0) &= f(\tau) \end{aligned} \right\} \text{B.C. 2}$$

$$\left. \frac{dc_{O_2}}{dy} = \frac{dc_{N_2}}{dy} \right|_{y=y_0} = 0 \quad \text{B.C. 3}$$

$$c_{O_2} + c_{N_2} \Big|_{y=y_0} = 1 - g(\tau) \quad \text{B.C. 4}$$

The concentration of component (i) is related to the partial pressure by:

$$c_i = \frac{n_i}{V} = \frac{p_i}{RT} \quad (7)$$

Solutions of equation 5 are, for the different components:

$$c_{O_2} = c^0 \left[1 - \sum_{n=1} A_n \sin \alpha_n x (\cosh \alpha_n y - \tanh \alpha_n y_0 \operatorname{sh} \alpha_n y) \right] \quad (8)$$

$$c_w = \sum_{n=1} A_n \sin \alpha_n x \left[\frac{g(\tau) - f(\tau) \cosh \alpha_n y_0}{\operatorname{sh} \alpha_n y_0} \operatorname{sh} \alpha_n y + f(\tau) \cosh \alpha_n y \right] \quad (9)$$

with

$$A_n = \frac{(-1)^n - 1}{b \alpha_n} \quad \text{and} \quad \alpha_n = \frac{n\pi}{2b}$$

where $g(T)$ and $f(T)$ represent partial pressures of water under equilibrium conditions at $y = y_0$ and $y = 0$, respectively.

Local current densities can now be obtained from:

$$j(x) = -n'FD \left. \frac{dC_{O_2}}{dy} \right|_{y=0} \quad (10)$$

and are, (for O_2 diffusion):

$$j(x)_{O_2} = -n'FDc^0 \sum_{n=1} \alpha_n A_n \sin \alpha_n x \operatorname{th} \alpha_n y_0 \quad (11)$$

and for H_2O diffusion:

$$j(x)_w = -n'FD \sum_{n=1} \alpha_n A_n \sin \alpha_n x \left[\frac{g(T) - f(T) \cosh \alpha_n y_0}{\operatorname{sh} \alpha_n y_0} \right] \quad (12)$$

Average channel current densities are:

$$J_{\text{Ave. } O_2} = \frac{n'FDc^0}{b\pi} \sum_{n=1} \frac{[(-1)^n - 1]^2}{n} \operatorname{th} \left(n\pi \frac{y_0}{2b} \right) \quad (13)$$

and

$$J_{\text{Ave. } H_2O} = \frac{n'FD}{b\pi} \sum_{n=1} \frac{[(-1)^n - 1]^2}{n} \left[\frac{g(T) - f(T) \cosh \alpha_n y_0}{\operatorname{sh} \alpha_n y_0} \right] \quad (14)$$

B. Application to specific environmental conditions

For operation with air, equations 11 and 12 become:

$$j(x)_{O_2} = 0.235 \sum_{n=1,3..} \sin \left(n\pi \frac{x}{2b} \right) \operatorname{th} \left(n\pi \frac{y_0}{2b} \right) \quad (15)$$

$$j(x)_w = 0.031 \sum_{n=1,3..} \sin \left(n\pi \frac{x}{2b} \right) \left[\frac{1 - \cosh \alpha_n y_0}{\operatorname{sh} \alpha_n y_0} \right] \quad (16)$$

Equation 15 and 16 are based on:

$$D_{O_2} = 0.21 \text{ cm}^2/\text{sec}$$

$$D_w = 0.29 \text{ cm}^2/\text{sec}$$

$$g(T) = h(T) = 30 \text{ mmHg (vapor pressure of water at } 30^\circ \text{C)}$$

- n' = number of equivalent/mole
 F = Faraday constant = 96,500
 $2b$ = channel length = 6.35 cm
 y_o = channel height = 0.32 and 0.16 cm

Some calculated data are presented in Table II for a channel height of 1/16".

Table II
Local Current Density for 1/16" channel height

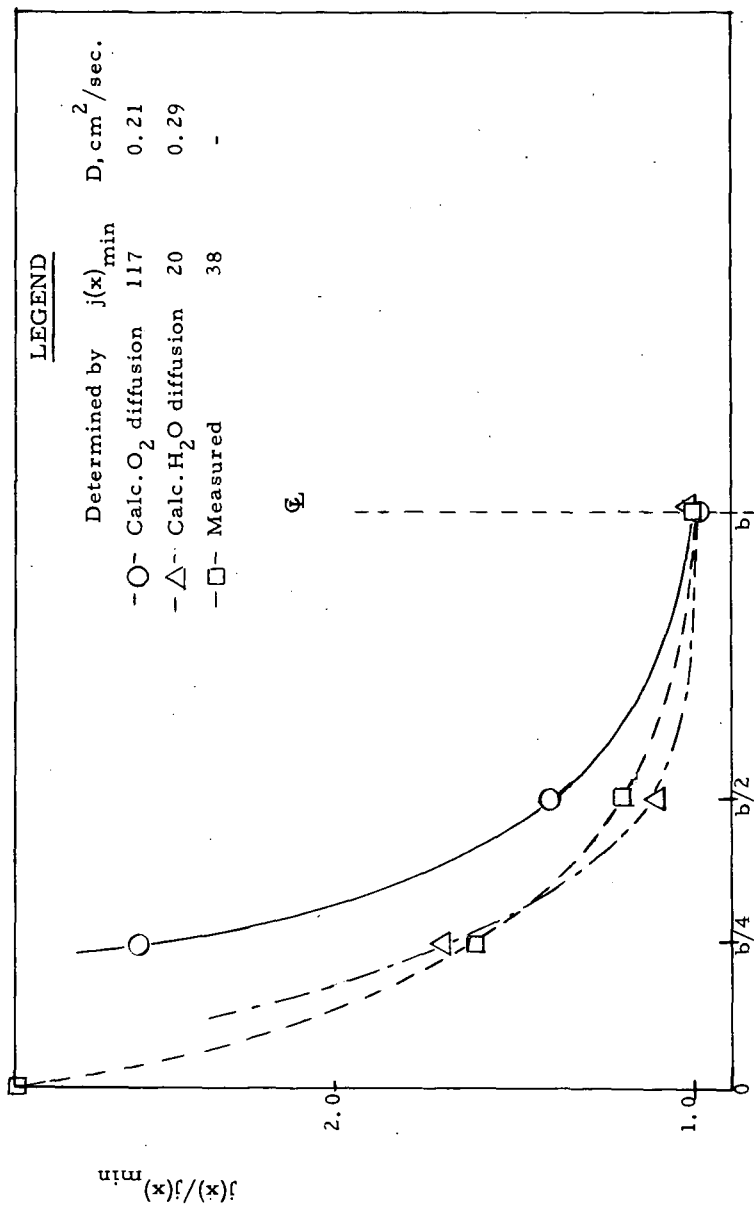
	Position	Local current density $j(x)$ in mA/cm ²	$j(x)/j(x)$ min.	Minimum Current density $j(x)$ min.
Oxygen Diffusion	b	117	1.0	
	b/2	163	1.41	117
	b/4	298	2.55	
Water Diffusion	b	20	1.0	
	b/2	22	1.1	20
	b/4	35	1.7	
Measured	b	38	1.0	
	b/2	44	1.2	38
	b/4	61	1.6	
	0	110	2.9	

Calculated and experimental results are presented in figure 7 for the 1/16" channel and for fixed diffusion coefficients. Data can be represented fairly well by assuming a water diffusion-controlled process.

Discussion

Restriction of channel cross-section, i.e. of y_o , may result in appreciable reduction in gas-phase transport rates. In fact these rates may be calculated from purely gas-diffusion controlled processes. In channel where forced air-flow rates may be small, unfavorable current density distribution may also be encountered. The results also suggest reduction of channel length (for defined y_o) in an attempt to maintain quasi-uniform oxygen partial pressure and surface temperature. The results indicate applicability of self-breathing electrodes up to about 25 mA/cm² (at ambient temp.) in a design where air-electrodes would be disposed face-to-face and separated by air-channels such that $y_o \gg 1/4"$. Better current distribution may also be expected for disc-shaped electrodes, by careful selection of the channel-gap/electrode-radius ratio.

CURRENT DISTRIBUTION IN 1/16" CHANNEL



CHANNEL LENGTH

FIGURE 7

Application

This section will include application of previous results to a system where channel length has been reduced, that is results on perforated sheets as cathodic current collector. (3)

One figure will be added as reported at the Power Sources Conference. (4)

References:

1. "Ion Exchange Membrane Fuel Cell - #3". U.S. Army Signal Corps Res. and Dev. Lab., Ft. Monmouth, N. J. Sept. 1962. ARPA No. 80.
2. Ibid. - Report #2, June 1963. "Current Distribution in Air-Breathing Electrode Channels Under Forced Flow Conditions."
3. Ibid. - Report #2, June 1963 - J. Dankese: "Heat and Mass Transfer Investigations of the Air-Breathing IEM Fuel Cell."
4. P.S.C. 17th Annual Meeting, May 1963. "Progress with Air-Breathing Solid Electrolyte Fuel Cells."

THE INVESTIGATION OF OXYGEN ADSORPTION AND OF ITS
IONIZATION BY THE TRIANGULAR VOLTAGE METHOD

N. A. Shumilova

Institute for Electrochemistry
Academy of Sciences, USSRAbstract*

Anodic and cathodic $i - \phi$ curves on a rotating silver electrode were obtained using periodic and single triangular voltage pulses. The experiments were carried out in alkaline solutions in argon and oxygen atmospheres.

The range of the electrode potentials was determined in which adsorption and desorption of oxygen and hydrogen take place as well as formation and destruction of the silver oxides Ag_2O , AgO , Ag_2O_3 .

When the rate of voltage change is increased a decrease of the oxygen adsorption on anodic polarization as well as a decrease of oxygen desorption on cathodic polarization are observed. In the range 0,05-0,85 v the change in the formation ratio of hydroxyl and hydrogen peroxide ions is connected with a change in the strength of the bond between oxygen and electrode surface. The presence of a large amount of oxygen on the silver surface and the increase of the bond strength result in a decrease of the oxygen reduction rate.

* Complete manuscript not received in time for inclusion in the Divisional Preprints.

The Nitric Acid-Air Redox Electrode

Joseph A. Shropshire and Barry L. Tarmy

Process Research Division
Esso Research and Engineering Company
Linden, New Jersey

One approach to the development of a satisfactory oxygen or air electrode for a fuel cell operating in an acid electrolyte is the use of a so-called redox electrode. Such a system utilizes the more favorable electrochemical activity of a secondary oxidant with the electrochemical reduction products regenerated chemically by oxygen or air. In this manner it is possible to obtain higher electrical performance than is attainable by direct electrochemical reduction of oxygen. This increased performance is of particular significance in the operation of air electrodes, where high concentrations of nitrogen seriously affect electrode efficiency. Recent reports have cited the use of $\text{Br}^- - \text{Br}_2$ and $\text{Ce}^{+4} - \text{Ce}^{+3}$ for this purpose (1,2). However, these systems have shown serious limitations in practical operation.

This paper describes the performance and mechanism of operation of another redox cathode, one based on the reduction of nitric acid in sulfuric acid. Previous investigators have studied the cathode reaction on platinum in $\text{HNO}_3/\text{HNO}_2$ systems under various conditions (3,4,5,6). However, none of these considered the possibility of using this system as a redox oxygen electrode. Furthermore, with the acid concentrations used, the presence of HNO_3 could seriously impair the performance of a fuel electrode. With the intent of avoiding this difficulty, a study has been made of the redox behavior of low concentrations of HNO_3 in sulfuric acid electrolyte. The results of that study are presented here.

EXPERIMENTAL

All electrochemical measurements described here were carried out in conventional glass cells with either parallel or coaxial electrode arrangements. Anode and cathode compartments were separated by either glass frits or cationic exchange membranes. Noble metal and carbon electrodes were employed and performance in most cases was obtained during operation against a "driven" counterelectrode, power being supplied by 6-12 volt regulated D.C. sources. All solutions were prepared using C.P. grade sulfuric (96.5%) and nitric (70%) acids diluted with deionized water of conductivity 10^{-6} mho/cm. Electrode voltages were measured against commercial saturated calomel electrodes equipped with Luggin capillary probes. Voltages and current measurements were obtained with Keithley electrometers of 10^{14} ohms input impedance.

More specific details, when necessary, will be found in the text. All electrode potentials reported herein are referred to the standard hydrogen electrode (N.H.E.), and sign conventions conform to the adopted standards. No attempt has been made to correct the voltage measurements for liquid junction and thermal potentials, the magnitude of which may be significant in strong acids, about 50 to 100 mv.

PERFORMANCE OF THE HNO₃ REDOX ELECTRODE

The initial performance tests using platinized-carbon oxygen electrodes in 3.7 M H₂SO₄ at 80-82°C., indicated that the addition of 0.2 M HNO₃ to the H₂SO₄ electrolyte resulted in large improvements in performance as measured by conventional voltage-log current plots. Further tests indicated that these improvements were not limited to carbon based electrodes alone, but were also attainable with noble metal electrodes. The performance, an example of which is shown in Figure 1, was found to be independent of the supply of primary oxidant, i.e., oxygen or air, but did depend on both HNO₃ and H₂SO₄ concentrations.

Typical E-log I plots showed little evidence of a well defined Tafel slope. At temperatures above 50°C. open circuit potentials as high as 0.92 volts vs the calomel reference were obtained. Neglecting liquid junction and thermal potentials, this is equivalent to 1.16 volts vs N.H.E. High performance in a fresh electrolyte was shown to occur only at temperatures in excess of 50°C., but accumulation of reduction products with continued operation enabled the return of the system to 25°C. with retention of relatively high performance levels.

Furthermore, coulometric determinations in the experiments with oxygen showed that the number of coulombs involved was far greater than that needed to account for reduction of all HNO₃ in the system. Thus a redox cycle exists, consisting of an electrochemical reduction of some species in the HNO₃ system and the reoxidation of the products by oxygen.

Concentration Variables

A concentration variable study was carried out in which performance (E vs log I) and limiting currents were determined for a series of electrolyte compositions covering the range of 0.2-1.0 M HNO₃ at a H₂SO₄ concentration of 3.7 M, and 0.5-3.7 M H₂SO₄ at a HNO₃ concentration of 0.2 M. The results of this study showed that limiting currents were not only linearly dependent on HNO₃ concentration (Figure 2), but were also linearly dependent on the proton activity in the system neglecting the contribution from the HNO₃ (Figure 3). It was also observed that for these systems limiting currents decreased with increasing agitation of the electrolyte. The data, therefore, are reported with respect to a fixed rate of gas flow agitation or at quiescent conditions. Similar observations of decreasing limiting currents with increasing agitation were made by previous investigators in HNO₃/HNO₂ systems (4,6).

Effects Of Temperature

Variation of the HNO₃ electrode activity with temperature was studied in the range of 50-106°C. Limiting currents were measured with the electrolyte solution presaturated with either O₂, N₂ or NO. The data provided a straight-line plot of log limiting current vs reciprocal absolute temperature (Figure 4) with a slope corresponding to an activation energy of about 10 kcal/mol for all three gases. An activation energy of this magnitude indicates a chemical rate-limited rather than diffusion limited current. The absolute level of the limiting currents varied, however, among the three gases used. This effect will be discussed in a later section.

MECHANISM STUDIES

These data suggest a relatively complex reaction mechanism. Furthermore, it was felt that the practical development of this redox system for fuel cell use would require a complete knowledge of the reduction and regeneration reactions. Consequently, studies were directed toward establishing the reduction mechanism and determining the reaction products.

Cathodic Transients

A system was assembled to investigate the response of an electrode to constant current pulses during the HNO_3 reduction reaction. Current pulses were applied to the electrode in a 3.7 M H_2SO_4 —0.2 M HNO_3 electrolyte at 82°C. Constancy of current (< 1%) was obtained using a high voltage (175 V.) D.C. regulated power supply and a high series resistance. Voltage transients, measured against a saturated calomel electrode-Luggin capillary arrangement, were displayed on a Tektronix 545A oscilloscope (Type D—D.C. Preamp.) and photographed. Input impedance of this oscilloscope (10^6 ohms) represented an insignificant load in the voltage measuring circuit.

Voltage-time variations at constant current can be analyzed in terms of the transition time, τ . This transition time is a function of concentrations, diffusion coefficients and current density for reactions under diffusion control (7). It is measured from the inception of the reaction wave to its inflection (see Figure 8) and can be used analytically as a measure of concentration of a reacting species. Thus,

$$i \tau^{\frac{1}{2}} = \frac{\pi^{\frac{1}{2}} n F C^{\circ} D^{\frac{1}{2}}}{2}$$

where C° is the bulk concentration of the reacting species and all other symbols have their usual significance.

Initial experiments with this technique confirmed that HNO_3 itself was not directly reduced. Under conditions where diffusion controlled transition times for HNO_3 reduction would be expected to begin at about +0.95 volts vs N.H.E. and to exceed 10 seconds duration, observed transition times at this level were less than 0.1 second. Transients at currents slightly less than that required for complete polarization showed autocatalytic behavior. Typically the electrode polarized several tenths of a volt and rapidly recovered to more positive voltages all at constant current load. (Figure 5) The reaction wave at more negative potentials in Figure 5-A disappeared upon degassing with N_2 .

The extreme autocatalytic nature of the electrode reaction was further emphasized by transients observed following extended periods of cathodization and under conditions of repetitive current pulses. An electrode placed in a fresh electrolyte solution extensively sparged with O_2 polarized completely to H_2 evolution potentials upon application of a 1 ma/cm² current pulse. Upon slowly increasing the current from zero, however, a level of 5 ma/cm² was easily obtained. After five minutes cathodization at this level followed by several seconds at open circuit, the electrode withstood a current pulse of 66 ma/cm² with equilibrium polarization of only 0.1 volts (Figure 6). A gradually improving response could be observed with repetitive current pulses in a fresh solution as shown in Figure 7.

Based on the high temperature dependence of the limiting currents, and absence of a well defined tafel slope, a reduction reaction with chemical rate-limitation is indicated. The dependence of limiting currents on HNO_3 concentration, in conjunction with the autocatalytic behavior, suggests that this rate limiting step involves reaction of a product species with the HNO_3 itself to produce the electrochemical reactant.

Product Identification

To clarify the mechanism and assess the possibilities of this system as an efficient redox electrode, experiments were run to establish the identity of the reaction products. A cell with 3.7 M H_2SO_4 - 0.2 M HNO_3 electrolyte containing a

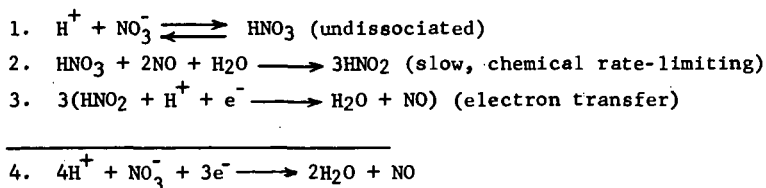
large auxiliary cathode was used for reacting the nitric acid. Another electrode (0.27 cm² in area) was placed in close proximity and used as a product detection device. At desired intervals this electrode was supplied with an anodic current pulse to reoxidize the product material present. The potential transient produced was recorded photographically from the oscilloscope trace. A typical transient found for product reoxidation is shown in Figure 8. Using this technique, it was possible to follow the build-up of product and its rate of disappearance under conditions of O₂ or N₂ sparging. It was found that the product was removed during both N₂ and O₂ sparging but that removal occurred more rapidly with O₂ sparge, suggesting reaction with O₂. The data obtained are shown in Figure 9, where $1/i \cdot \tau^{1/2}$ is recorded versus sparge time. This quantity, as previously described, is proportional to reciprocal concentration ($1/C_R$) of the reacting species.

This evidence strongly indicated NO as the electrochemical reaction product. This conclusion was confirmed by observations on transients obtained in an air-free 3.7 M H₂SO₄ solution saturated with NO gas. Transients obtained in this system were identical to those of Figure 8. Furthermore, saturation of the H₂SO₄-HNO₃ electrolyte with NO caused the complete absence of all autocatalytic effects previously observed.

The effect of temperature on limiting current in this latter system was previously shown in Figure 4. The increase in limiting currents in this NO equilibrated solution over those obtained with O₂ and N₂ also affirms the role of NO as the electrochemical product which participates in the chemical rate limiting step. Limiting currents with NO are not disproportionately high, however, since electrochemical NO evolution at the limiting current is sufficient to essentially saturate the solution in the vicinity of the electrode.

Proposed Mechanism

Based on the observed behavior, the over-all mechanism of the cathodic reaction in the 3.7 M H₂SO₄ - 0.2 HNO₃ electrolyte would seem best suited by the following scheme:



As previously indicated, the rate limiting step is the slow chemical production of HNO₂, the electrochemical reactant. Reaction 3 is assumed to operate reasonably reversibly, with the potential at any given current density being fixed by the local ratio of HNO₂ and NO activities. At the limit of the chemical reaction rate, the concentration of HNO₂ at the electrode surface falls to zero and the potential increases until another reaction potential is reached. This scheme takes full account of the observed dependence of limiting current on stirring, since excess agitation tends to remove the product NO, making it unavailable for reaction 2 near the surface. The dependence of limiting current on both HNO₃ and H₂SO₄ concentration probably indicate that HNO₃ is undissociated in reaction 2.

Minc (3) has studied polarization curves for platinum electrodes in HNO_3 . He found that the high positive potential cathode process takes place only in solutions of HNO_3 at concentrations sufficient to contain appreciable amounts of the nonionized form of nitric acid. His work indicates a linear relation between the log of the concentration of the nonionized form and electrode voltage at constant current values in the Tafel region. In our high proton activity solutions, it is expected that significant quantities of nonionized HNO_3 also exist. Thus, equilibrium of reaction 2 at low current densities would result in a similar dependence on acid concentration.

The mechanism proposed here differs from the one advanced by Vetter (6) to account for similar effects in the system $\text{HNO}_3/\text{HNO}_2$ at 25°C . That investigator, following the earlier work of Beinert et al. (8), measured anodic and cathodic polarization curves in various $\text{HNO}_3/\text{HNO}_2$ systems. He concluded that the reduced species of the reactive electrochemical couple was HNO_2 or a species in rapid equilibrium with HNO_2 (e.g., NO , NO_2^- , etc.). Vetter derived a mechanism involving the reduction of NO_2 to HNO_2 and entrance of the product HNO_2 into a rate limiting chemical step analogous to reaction (2). The distinction between these mechanisms rests on two observations:

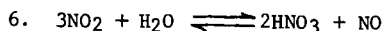
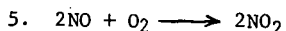
(1) Since there is little likelihood of further reduction beyond NO (the observed product) the reaction wave in Figure 5-A which is removed by degassing must represent NO_2 reduction. This is reinforced by the fact that spontaneous reversion to the low polarization level of activity ($\sim + 0.97$ volt vs N.H.E.) occurs upon reaching this reaction plateau. Such behavior would occur if this reaction level represented another source of HNO_2 , i.e., by a one-electron electrochemical reduction of NO_2 . Thus, if insufficient HNO_2 is available to support the reaction at the low polarization level, the system has a built-in "safety" for electrochemical HNO_2 production at the higher polarization, if sufficient NO_2 is present in solution.

(2) As was indicated earlier, saturation of degassed 30% H_2SO_4 with NO gas alone produced an anodic transient identical to that observed for the product of the cathodic reaction. Moreover, this oxidation wave of NO , and the observed cathodic reaction wave are symmetrical about the observed rest potential of the system. It would then appear that NO , rather than HNO_2 , is the reduced component of the reversible couple operating at this potential. The reduction wave in Figure 5-A, presumed to be NO_2 , occurs at much less positive potentials.

Vetter's work was carried out at 25°C . and in general much higher HNO_3 concentrations than were employed in this study. Thus there need be no direct relationship between the behavior observed in these systems. At low nitric acid concentrations Ellingham (5) points out the importance of reaction 2 in determining the equilibrium between NO and HNO_3 .

REGENERATION

With no regard to the mechanism involved, it has been definitely established that the net product of the cathode reaction is gaseous NO . Thus the problem of completing the redox cycle by conversion of NO to HNO_3 then becomes a process well known in the nitric acid production industry (9). The reaction goes by the scheme:



Reaction 5 is a classical termolecular reaction with negative energy of activation, favored by low temperature and high pressure. Reaction 6 at normal pressures is not limiting but suffers the drawback that NO is produced, thus requiring infinite reaction space for completion of reactions 5 and 6. On a practical basis, however, sufficient NO conversion is obtained by maximizing gas contact times before and during hydrolysis.

Using standard methods of contacting the NO produced at the electrode with O₂ and the electrolyte, it is possible to regenerate HNO₃ to the extent that the electrochemical cathode process of HNO₃ reduction may be carried out for periods of time equal to several times the coulombic equivalent of HNO₃ added. However, under carefully optimized O₂ regeneration conditions, it has been possible in our laboratories to pass currents at low polarization equal to 225 times the coulombic equivalent of the HNO₃ lost from the system. Under comparable conditions, this number with air is about 30. Operation at this regeneration efficiency reduces the amount of HNO₃ make-up to a small quantity, about 0.1 lb/kwh.

COMPATIBILITY

Although it is not the purpose of this paper to deal with the operation of entire fuel cell systems, a few words concerning compatibility seem appropriate. Due to the highly active oxidizing nature of the cathode reactant, it is necessary to carry out the cathode reaction at the lowest possible nitric acid concentration consistent with the current required. A nitric acid concentration of 0.2 M is sufficient to obtain currents of 75-100 ma/cm².

The effect of HNO₃ on the opposing electrode generally will be less with highly electroactive anode fuels. Thus, a fuel such as H₂ will suffer least. Deleterious effects seem to arise primarily from accumulation of intermediate species in the HNO₃ systems, e.g. HNO₂, NO₂, and thus efficient regeneration on the cathode side increases compatibility. For instance, addition of HNO₃ at concentrations below 0.6 M directly to a separated anolyte compartment causes no deleterious effects at an operating methanol electrode. Effects were evident, however, at 0.25 M when an operating HNO₃ cathode was not separated from the anode compartment and reduction products were allowed to accumulate.

SUMMARY

The use of HNO₃ in a fuel cell cathode redox cycle has been shown to provide improved cathode performance over that generally achieved with direct electrochemical reduction of O₂. The system provides equal electrical performance using either O₂ or air. The product of cathode reaction in this system is gaseous NO and efficiency of the redox cycle depends on its reconversion to HNO₃. While both oxygen and air provide high levels of regeneration, oxygen, as would be expected, shows superiority. A consistent mechanism has been advanced to account for all aspects of the cathode reaction in this system. Basic rate limitation in the electrochemical reduction reaction appears to be a chemical step involving the reaction of NO and HNO₃.

The redox concept, as applied here, can of course be extended in principle to improvement of any electrode reaction where reactants exhibit low electroactivity. The requirements naturally necessitate that the redox intermediate be less easily reduced (or more difficultly oxidized) in theory than the oxidant (or fuel) species to be replaced. Thus while actually exhibiting more electrochemical activity than the oxidant or fuel to be replaced, the chemical regeneration of the intermediate is still feasible. For most practical fuel cell systems, the redox intermediate would thus be restricted to those couples exhibiting reversible potentials not more than about 0.2 volts less positive (or 0.2 volts more positive) than the oxidants (or fuels) to be replaced.

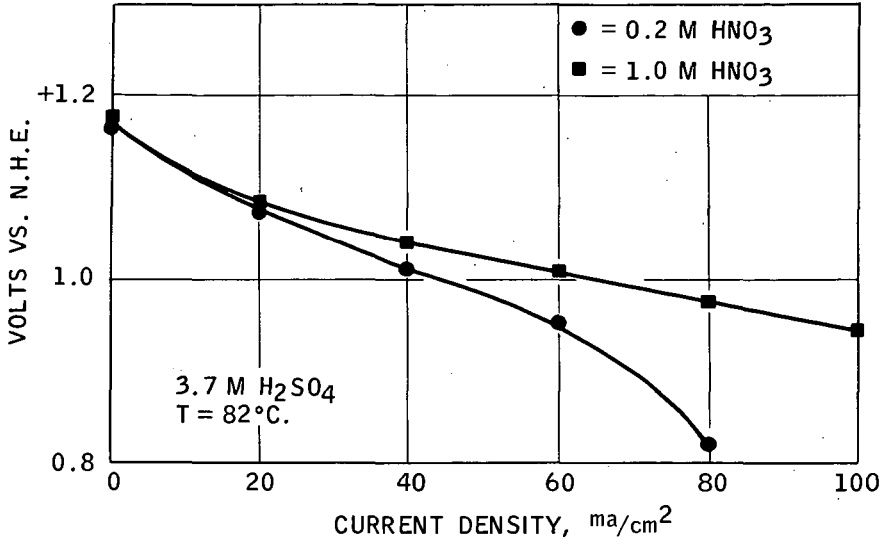
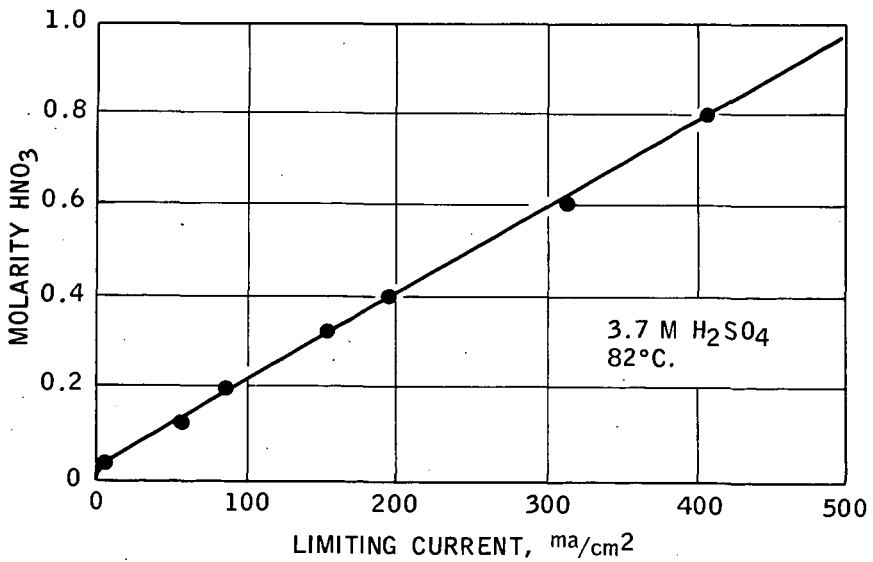
ACKNOWLEDGEMENT

This research is part of the Energy Conversion Project sponsored by the Advanced Research Projects Agency, Department of Defense. The contract, DA 36-039 SC-89156, was administered by the United States Army Electronics Research and Development Laboratory.

Some of the data presented was obtained by Esso Research and Engineering Company prior to the inception of this contract. The authors wish to acknowledge the efforts of their colleagues who contributed to this work, in particular Dr. A. W. Moerikofer, and to express their appreciation to Esso Research and Engineering Company for permitting its publication.

BIBLIOGRAPHY

- (1) Stein, B. R., "Status Report On Fuel Cells", p. 60-62, O.T.S. PB 151804 (1959)
- (2) Reneke, W. E., "Air Regeneration Of Bromine-Bromide Fuel Cell Catholyte" O.T.S. AD 273299 (1961)
- (3) Minc, S. and Jasielski, S., *Roczniki Chem*, 28, 109 (1954)
- (4) Ellingham, H. J. T., *J. Chem. Soc.*, 1565 (1932)
- (5) Monk, R. G., and Ellingham, H. J. T., *J. Chem. Soc.*, 125 (1935)
- (6) Vetter, K., *Z. physik. Chem.*, 194 199-206 (1950)
- (7) Delahay, P., "New Instrumental Methods In Electrochemistry", p. 184 New York, Interscience Publishers, (1954)
- (8) Beinert, H., and Bonhoeffer, K. F., *Z. Elektrochem. u. angew. physik. Chem.* 47, 538 (1941).
- (9) Chilton, T. H., "The Manufacture Of Nitric Acid by the Oxidation of Ammonia", *Chem. Eng. Progress Monograph*, No. 3, Vol. 56, A.I.Ch.E. (1960)

Figure 1 - Typical Performance Of HNO₃ Oxygen ElectrodeFigure 2 - Dependence of Limiting Currents on HNO₃ Concentration

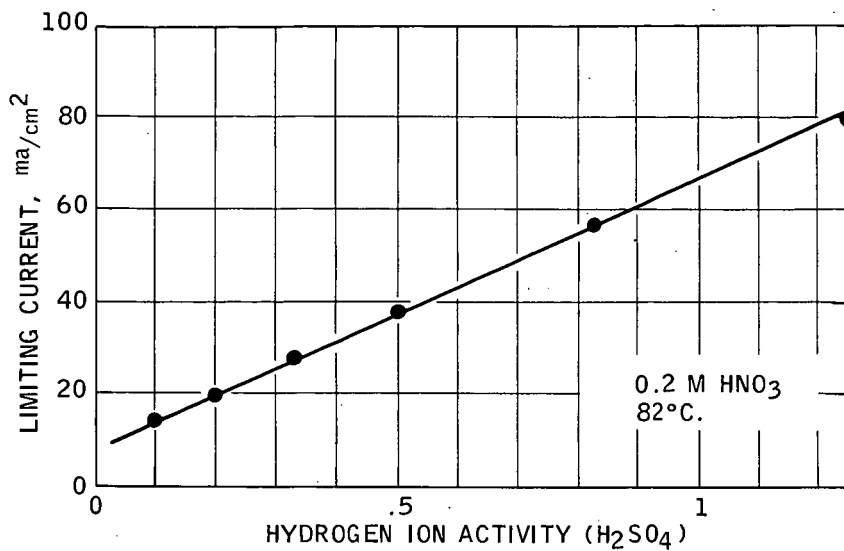


Figure 3 - Dependence of Limiting Currents on Hydrogen Ion Activity

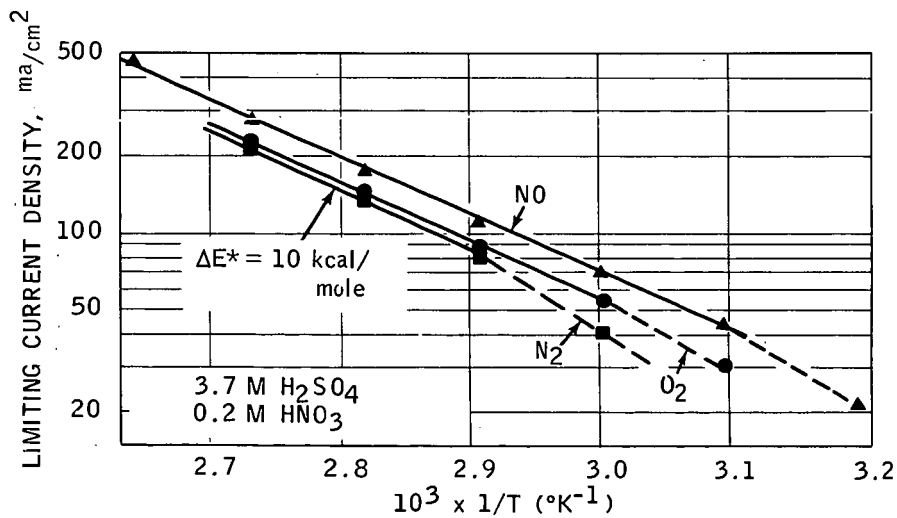


Figure 4 - Temperature Dependence of Limiting Current

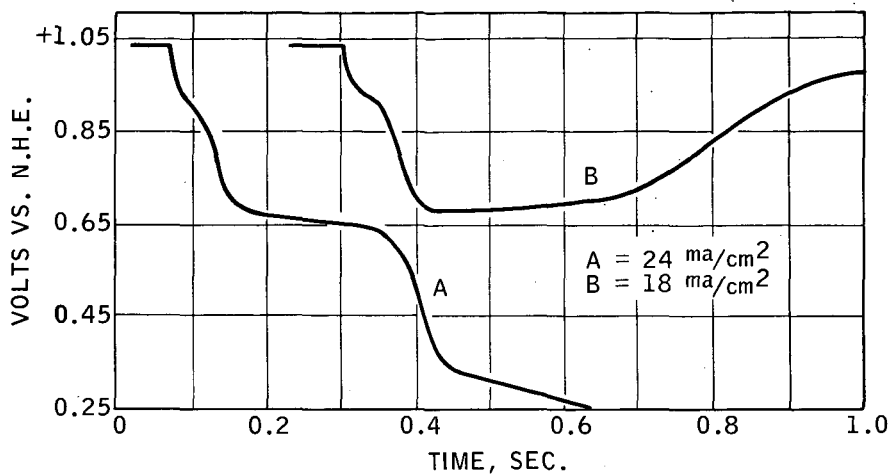


Figure 5 - Typical Voltage Transients at Constant Current

- A. Current in Excess of Limiting Current
- B. Current Less Than Limiting Current

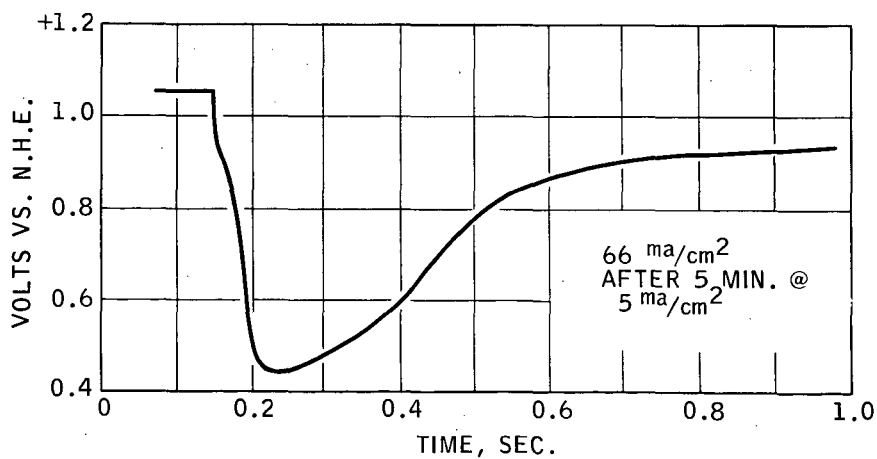


Figure 6 - Response to High Loads After Preconditioning

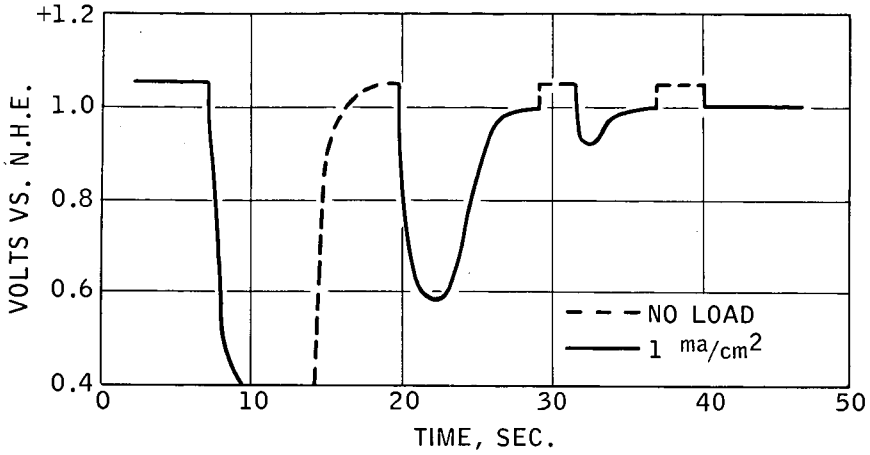


Figure 7 - Response to Repetitive Load

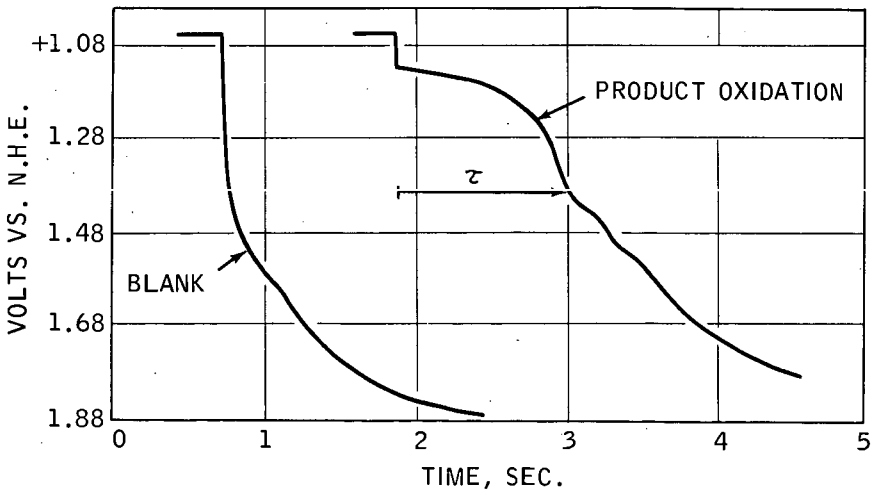


Figure 8 - Transient Observed During Product Reoxidation

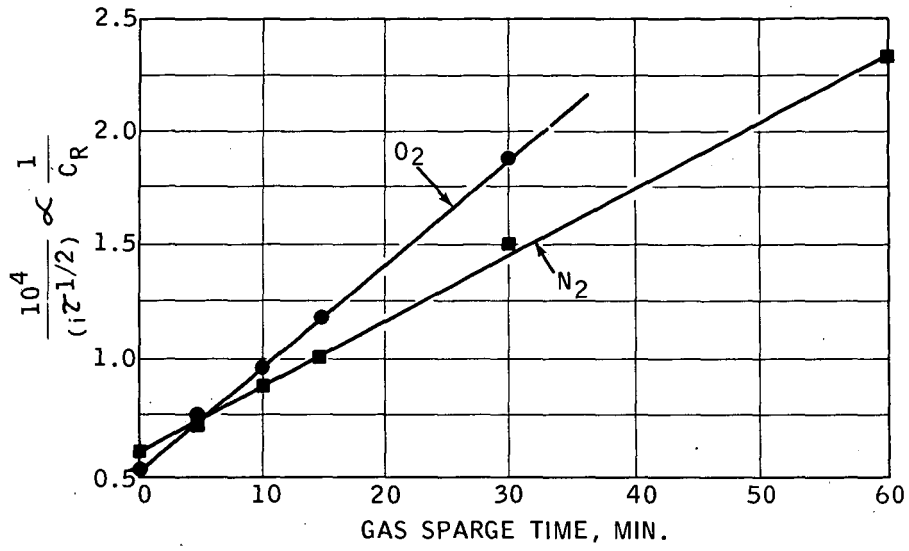


Figure 9 - Removal of Product by Gas Sparging

The Technology of Hydrogen-Oxygen Carbon Electrode Fuel Cells

Karl V. Kordesch and
Lawrence M. Litz

Advanced Developments Department,
Union Carbide Corporation, Parma, Ohio

Abstract*

Low temperature, low pressure hydrogen-oxygen fuel cells have emerged from the research state and are presently subject to very intensive development efforts. The performance characteristics of carbon electrode fuel cells, namely, high current density, flat discharge characteristics, long life and high overload capabilities are established.

Recent engineering studies have led to a definition of the operating and design requirements for proper distribution of the feed gases and electrolyte, for water removal by transpiration through the electrodes into the circulating streams and for proper heat balance. The broad operating range of the carbon electrode fuel cell has permitted simplification of the auxiliary control and circulation systems.

Considerable reduction in size and weight have been achieved by using electrodes of a new structural design. Reliability assurance can be extended by redundancy.

* Complete manuscript not received in time for inclusion in Division Preprints.

IONISATION OF HYDROGEN AND OXYGEN AT THE THREE
PHASE BOUNDARY FORMED BY THE CONTACT OF ALKALINE
SOLUTIONS WITH SMOOTH METALLIC SURFACES

by

N. A. Fedotov, V. I. Veselovsky, K. I. Rosenthal, and J. A. Masitov
Institute for Electrochemistry, Academy of Sciences, USSR

Abstract*

The ionisation of hydrogen and oxygen in concentrated alkaline solutions was studied at various temperatures with electrodes partly immersed in the electrolyte.

It was shown that the ionisation current increased by a factor of more than ten or even by a factor of more than a hundred if an electrolyte film wetting the electrode was formed. The width of the reaction zone of the oxygen ionisation depends on the temperature and potential of the electrode.

It was established that at temperatures lower than 30 C the speed of the process at a silver electrode is determined not only by diffusion but also by the true kinetics of the oxygen ionisation. At higher temperatures the limiting factor is diffusion. The energy of activation of oxygen diffusion in concentrated alkaline solutions was determined.

For a series of metals the temperature at which the true kinetics of oxygen ionisation changes over to diffusion kinetics was determined.

It was shown that the oxygen ionisation current depends on the nature of the metal, the temperature and the concentration of the solution; for a given temperature and concentration palladium shows a higher current than other metals.

* Complete manuscript not received in time for inclusion in Divisional Preprints.

The Current State of Development of Fuel Cells
Utilizing Semipermeable Membranes

Carl Berger

Astropower, Incorporated
2121 Paularino Avenue
Newport Beach, California

1.0 Introduction

The upsurge of interest in the last several years in fuel cell research is abundantly documented in the literature found in scientific, engineering and business articles. It may be of value to draw our thoughts together in one area of this field and to assess its accomplishments, its present status, and take a look at future development in that area.

In this paper we shall concentrate on the applications of semipermeable membranes, in particular, ion-membrane fuel cells. Most representative of this group are the single membrane fuel cell (Reference 1) the dual membrane fuel cell (Reference 2) and a significant hybrid, the gas-liquid single membrane fuel cell (Reference 3).

It may be of value to review briefly the advantages and disadvantages of an ion-membrane fuel cell in comparison with fuel cells with porous electrode and liquid electrolytes. Some of the advantages are:

1. The construction of electrode-catalyst configurations is non-critical - the exact sizing of electrode pores, the criticality of catalyst deposition and the requirements for water proofing are all minimized.
2. No loss of gaseous reactants due to pore inexactitude. The gaseous reactants cannot be lost to the electrolyte but simply rebound back into the gas chamber if they do not react.
3. Compactness.
4. Light weight.

The disadvantages in the ion-membrane fuel cell are:

1. Only moderate current densities have been achievable although the compactness of configurations mitigates this problem to some extent.
2. Heat removal is more difficult than in systems where an electrolyte can be circulated; for example, approximately 40-50% the realizable power in a fuel cell ends up as heat. The Hydrogen-Bromine Fuel Cell (HBFC) and the Dual Membrane Fuel Cell (DMFC) described later represent compromises instituted to overcome this problem.
3. The most highly developed ion-membrane fuel cells are organic and therefore sensitive to heat even when they are in an aqueous environment.
4. Water removal from electrode-catalyst site represents a variable

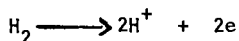
which is difficult to control quantitatively and directly influences voltage output.

The basic membrane used in the three generalized configurations described below are of two physical species - a homogeneous fabric supported polymer (Reference 4) and a grafted polymeric type (Reference, 5). In both cases the polymers are sulfonated polystyrenes cross linked to a greater or lesser extent. The mechanism of operation of the membrane, however, differs appreciably in the three type of fuel cells to be discussed. Sketches of the three types of fuel cells are represented in Figure 1.

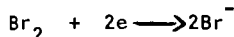
All of the fuel cells described in Figure 1 have been amply described in the literature (Reference 1, 2, 3, 6, 7, 8). Only brief descriptions will be given since the main purpose here is to delve more into the limiting factors inherent in the operation of such devices.

In Figure 1-A, the Single Membrane Fuel Cell which uses H_2 and O_2 as reactants is illustrated. H_2 is converted to H^+ at the anode, electromigrates through the membrane and unites with a reduced O_2 species at the cathode to form water which must be removed.

In Figure 1-B, the Hydrogen-Bromine Fuel Cell, the anode reaction is



and the cathode reaction



The net result of the reaction is the formation of HBr in the aqueous catholyte.

Finally in Figure 1-C, the Dual Membrane Fuel Cell, the anode and cathode reactions are identical to those in the Single Membrane Fuel Cell. The difference in these cells is that in the former a layer of H_2SO_4 is found between two membranes which serves to improve water balance problems and also functions as a heat transfer fluid.

1.1 Single Membrane Fuel Cell

The Single Membrane Fuel Cell (SMFC) is the system which has been most intensively investigated in the last few years. The membrane used in this case is a completely water leached ion-membrane where all of the electrical transport is due to the migration of H^+ ion formed at the anode from one sulfonic acid group to another until water is formed at the cathode.

If the ion exchange membrane is considered a polymer network of a linear or branched variety crosslinked at various sites and swollen with solvent, an adequate physical network can be envisioned for the transport of solute. It is apparent in envisioning this network as a "solid gel" that the velocity of H^+ ion in this network will be sterically hindered and if, as seems likely, the velocities of ions in "gel" structures is a function of the increased viscosity of the internal solvent phase (Reference 9) then it follows that the Stokes frictional resistance to flow

$$F = 6\pi\eta r \quad (1)$$

where

η = viscosity

r = radius of migrating particle

should be increased producing slower ionic migration whether the forces are purely

those of diffusion or electromigration. In the case of electromigration, this retardation will be manifested by lower ionic mobilities. For example, the ionic mobility of H^+ ion in an aqueous electrolyte is about 362×10^{-5} cm/sec. in contrast to a velocity of H^+ ion in sulfonated phenolformaldehyde resin of about 19×10^{-5} cm/sec. (Reference 9).

If one accepts as an operating basis that the SMFC is now utilizing the optimum catalysts obtainable for the $H_2 - O_2$ system and that operating voltages much greater than 0.93 V are not likely to be obtained (Reference 10), (a fact that the writer concurs in as a result of his experience in development of $H_2 - O_2$ fuel cells), then theoretically the net power that can be obtained will be a function of the ionic mobility of the H^+ ion over a given transit thickness.

Approximate calculations may be of some value in guiding us with respect to the limiting current densities that can be achieved in a leached H^+ transport system. Using the approach of Kortum and Bockris (Reference 11) and Spiegler and Coryell (Reference 12), the limiting current density of a leached membrane system may be defined as

$$\mathcal{J} = \frac{R}{Z_i F} \frac{\lambda TC}{i_L} \quad (2)$$

where

- \mathcal{J} = thickness of diffusion layer
- R = constant
- Z_i = valence
- F = Faraday
- λ = ionic mobility
- C = g. ions/mole
- i_L = limiting current

Substituting appropriate values

$$\begin{aligned} \mathcal{J} &= \text{thickness of diffusion layer} = \text{thickness of membrane} = 0.0165 \text{ cm.} \\ \lambda_{H^+ \text{ membrane}} &= 0.1 \lambda_{H^+ \text{ solution}} = 35 \text{ ohms}^{-1} \text{ cm}^2 \\ C &= 0.6 \text{ g. ion/liter} \end{aligned}$$

we find $i_L = c. 330 \text{ ma/cm}^2$

The writer recognizes that equation (2) holds strictly for cases at infinite dilution and that endosmotic transfer of water has not been considered, but, for our purposes the approximation is sufficient.

Another means of corroborating the order of magnitude of i_L is to use experimental data of resistances of membranes in the H^+ form in calculating achievable current density limits. The data presented by Grubb (Reference 13) on the specific resistance of ion exchange membranes yields on Ohms Law calculation for a membrane thickness of 0.0165 cm. current densities in the range of 400 ma/cm². Finally, it is of value to note that Maget (Reference 6), in his extrapolations of limiting current density for SMFC, projects values of the order of 500 ma/cm².

It can be assumed, based on the preceding approximations, that high current densities are achievable by the SMFC and indeed laboratory evidence (Reference 14) indicates that such is the case in single cell test units. It may then be valid to initiate thinking of thin ion membranes (<.02 cm) as diffusion barriers through which in theory, large amounts of current can flow in a fashion analogous to the thin diffusion barriers resulting from stirred electrolytes.

Candidly, while the preceding analysis is of interest in small, single cell test configurations, engineering factors have played a critical role in limiting the achievement of higher power densities in multiple fuel cell configurations. Firstly, the necessity of uniform rapid water removal at high current densities, which must be performed by gas circulation or a combination of condensation and capillary wick action is unsatisfactory. (Reference 8). Inability to remove water uniformly and rapidly enough can cause voltage fluctuations in individual cells and can in fact "drown" electrodes causing failure. Another important engineering problem is the removal of heat generated in the membrane. The removal of heat can be performed in a number of ways, but in all cases involves transit through a gaseous phase. In any case, it is our conviction that if the heat generated could be conducted into a fluid medium, the heat transfer considerations related to the rapidity of heat removal and energy expended for such transfer would be more favorable from overall systems considerations. It is interesting to note that in larger power sources, that heat transfer fluids will most likely be introduced to carry away large quantities of waste heat.

1.2 Hydrogen-Bromine Fuel Cell

The Hydrogen-Bromine Fuel Cell (HBFC), a secondary fuel cell device, (Reference 2) represents an attempt at overcoming the engineering difficulties inherent in one aspect of the SMFC, particularly heat transfer problems. A comparison of the heat transfer coefficients of O_2 , H_2 and H_2O in handbooks indicates the advantages of using an aqueous system such as the bromine - hydrobromic acid solution in water that serves as a catholyte for the HBFC.

In addition the Br_2/Br^- electrode is a highly reversible couple compared to the oxygen electrode in the SMFC. Oster (Reference 14) indicates that a certain activation loss of 0.35 V - 0.40 V occurs at the oxygen electrode in the SMFC. Calculations and experimental data (Reference 2, 15, 16) show that losses due to activation overvoltage for the HBFC on discharge should follow the equation

$$\eta = \frac{0.059}{0.6} \log i + \frac{0.059}{0.6} \log (3.10^{-3}) \quad (3)$$

where

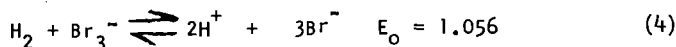
$$\begin{aligned} \eta &= \text{activation over voltage} \\ i &= \text{current density in amps/cm}^2 \end{aligned}$$

Therefore, at 100 amps/cm² on a plain electrode surface, the activation overvoltage for reduction of Br_2 to Bromide ion is equal to -.05 V.

It should be recognized however, that a disadvantage of the Br_2/Br^- couple is that the equivalent weight of Br_2 is considerably greater than O_2 , an important consideration in a practical engineering sense. This is mitigated to some extent by other considerations. For instance, when electrical regeneration of secondary fuel cells is called for, the higher voltage efficiency of the HBFC requires less weight of solar cells for recharging than a comparable secondary SMFC.

Once again our analysis of the maximum current density limitation will be based on the membrane as the limiting feature of the fuel cell and assuming that the anode and cathode are not limiting with respect to current densities.

A closer look at the ionic species involved in the performance of this cell is warranted before proceeding further inasmuch as this is an important factor in determining practical cell performance. The overall reaction of the cell is



The voltage of the cell is determined by the Nernst relationship

$$E = E^{\circ} - \frac{RT}{nF} \ln \frac{[H^+]^2 [Br^-]^3}{[H_2] [Br_3^-]} \quad (5)$$

Equation (5) implies that the major portion of the Br_2 exists in solution as Br_3^- . Since the equilibrium constant for $Br_2 + Br^- \rightleftharpoons Br_3^-$ is 17 and the equilibrium constant for $Br_3^- + Br_2 \rightleftharpoons Br_5^-$ is 0.055, it appears that at concentrations in the applicable catholyte range $H^+ = 6$, $Br^- = 6$, $Br_2 = 1 - 2$, the assumption is justified by a few simple calculations e.g., at $Br_2 = 1$, $Br_3^- = 0.99$ and $Br_5^- = 6 \cdot 10^{-4}$.

Proceeding onward to explore the nature of the discharge process at the anode, it can be seen that the ideal situation is where only H^+ and Br^- are in the membrane and Br_3^- is excluded. If this is the case $t_+ + t_- = 1$ and hydrogen ion formed at the anode is neutralized by Br^- . Clearly, if Br_3^- can diffuse into the membrane and migrate toward the anode, loss of electrical energy can result from the reaction of hydrogen and bromine complex at the noble metal catalyst electrode. It is exactly this problem that Berger and co-workers (Reference 2) found to be a limiting factor in cell life. A reformulation of the membrane in order to decrease the mean intramolecular diameter of the membrane was successful in limiting the diffusion of Br_3^- into the membrane and led to long cycling lines of greater than 9000 charge-discharge cycles.

One marked difference between the SMFC and the HBFC is that the major transport in the latter is a function of imbibed HBr rather than the H^+ ion in equilibrium with the fixed ionic sites in the ion exchange membrane. Let us assume that 6N HBr and 2N Br_3^- catholyte solution are in equilibrium with a cation membrane and if we assume that the migration of Br_2 into the membrane is strongly hindered, then an imbibition of 2-3 milliequivalents of HBr per milliliter of membrane volume can be assumed (Reference 17).

If we assume as previously discussed above that the limiting factor in i_d is the membrane itself then we can setup a series of limiting conditions. For the bromine electrode

$$i_d = \frac{DnF(C)}{(l - t_-)d} \quad (6)$$

or

$$i_d \approx 1.8 (10^{-1}) C \text{ amp/cm}^2, \text{ (Reference 16)} \quad (7)$$

where

$$\begin{aligned} D &= 4 \cdot 10^{-5} \text{ cm}^2/\text{sec} \\ n &= 2 \text{ electrons} \\ F &= 96,500 \text{ coulombs per equivalent} \\ t_- &\approx 0.15 \text{ (max)} \\ d &= 0.05 \text{ cm. (max)} \end{aligned}$$

At solution normality of 6N we have an activity of about 2-3 (Reference 18) and therefore could expect a limiting current density of about 360-540 ma/cm^2 even without considering surface roughness factors. The surface factor assumption is reasonable since smooth platinum was utilized for the cathode. We now turn to an analysis of the limiting current at the membrane-anode interface.

Presuming that the hydrogen electrode has its diffusion layer in the form of a membrane within which catalyst is imbedded, the diffusion barrier will be a membrane into which H^+ ion is discharged and which must be neutralized with electromigrating Br^- . The calculation of the limiting current for the hydrogen electrode may be expressed as

$$i_d = \frac{DnF(C)}{(1 - t_+) \delta} \quad (8)$$

or

$$i_d \approx \frac{4 \times 10^{-6} \times (1) 96,500 \times C}{(1 - .85) (.0165) 1000} = .156 C \quad (9)$$

where

$$\begin{aligned} D &= 4 \times 10^{-6} \text{ cm}^2/\text{sec} \text{ (Reference 16)} \\ n &= 1 \\ F &= \text{Faraday} \\ t_+ &= .85 \\ \delta &= .0165 \text{ cm.} \end{aligned}$$

Making the assumption that the concentration of HBr in the membrane has a limiting value of about 2.5 m.e. of HBr per ml of resin. The activity coefficient of 2.5 N HBr is about 1.2 and therefore an effective activity of 2.04. Substituting this value into (11) $i_d = 325 \text{ ma/cm}^2$.

Both of the limiting currents derived for the bromine electrode and the hydrogen electrode are deemed to be within conservative limits, e.g., the roughness factors have been assumed to be one.

1.3 Dual Membrane Fuel Cell

The ultimate extension of the combination of the membrane and electrolyte solution is found in the DMFC where the hydrogen and the oxygen electrodes are both placed against cation membranes and a 6N H_2SO_4 acid solution interposed between the membranes. It is clear that if we once again make the assumptions that ionic diffusion in the membrane is limiting, that limiting current calculations may be performed for both membranes.

$$i_d \approx \frac{4 \times 10^{-6} \times 1 \times 96,500 \times C}{0.15 \times 0.0165 \times 10^3} \quad (10)$$

or

$$i_d \leq .156 C$$

$$i_d \leq 94 \text{ ma/cm}^2$$

The assumptions made in this case are similar to those in the HBFC. It is assumed that the diffusion coefficient will be equivalent to or less than HBr, that the transference number of H^+ is slightly greater than for the HBFC, and we have also made the assumption that similar quantities of H_2SO_4 are imbibed but that the activity of 2-3N H_2SO_4 is much lower (Reference 20). There is one factor here however, which is not present in HBFC. A film of water forms at the oxygen cathode, the tendency of which is to migrate into the 6N liquid electrolyte between the membranes. In practice, interestingly enough this is borne out by the fact that all of the water formed is found ultimately in the central compartment. The film of water which forms can not be removed as rapidly as in the case of the SMFC because of the counter osmotic forces in the membrane tending to draw the water toward the central

electrolyte compartment. The presence of this water film causes significant IR losses and is a limiting factor in the operation of the DMFC.

2.0 Engineering Consideration

The approximations presented above with reference to current density limitations are no more than target areas which could be achieved if certain practical considerations are overcome. What then is the present stage of achievement of these three different fuel cells. A graph of attainable operating characteristics, based on available publications for these single fuel cells is shown in Figure 2. (References 14, 21, 22, 2, 23).

2.1 Single Membrane Fuel Cell

The SMFC shows the most advanced operational capability, one of the obvious reasons for this being that a great deal more research and development has been committed to this concept. Although current densities as high as 150 ma/cm² have been achieved, a number of practical limitations appear to limit gains for the SMFC in multiple fuel cell configurations.

1. Water removal from the area of the oxygen electrode must be carefully controlled so that enough water is removed from each cell of a multiple cell unit to keep the electrode from drowning or more practically to keep all single cell voltages in a multiple series configuration from widely diverging and tending to instability of cell output (Reference 24).

The removal of water from the electrode surface in the present apparatus is accomplished by the condensation on a bipolar cell separator of the moisture from the electrode surface. Mechanically, the potential for water removal is supplied by a difference in temperature (C. 5-10°F) between the electrode surface and the cell separator. It can be seen that the rate of product removal from the reaction site will vary with the temperature differential, the gas temperature and content of gas chamber and factors related to the heat removal system. In light of these complicated engineering problems, the writer projects that current densities of about 50-75 ma/cm² at 0.78-0.72 V appear to be achievable in multiple units within the next 18-24 months but it is not likely that operating current densities of greater than 100 ma/cm² will be achieved within the next 36 months unless important break-throughs in engineering know-how occurs. This does not appear to be an important limitation, since it is likely that operational current densities in the range of 25-35 ma/cm² will suffice for space missions such as orbital manned flights.

2. 40-50% of the total energy generated in the SMFC results in heat which must be dissipated. This can be effected by heat transfer through metal cell separators with radiative heat loss to space or the recirculation of fuel gas (H₂) to pickup heat and moisture with subsequent cooling and condensation and finally the use of a separate liquid circulation system to remove heat from the separator plate area. If the last approach is used for units in the 1-5 Kw range (Reference 25) then it appears that the weight and volume of the circulation system would at least equal the electrolyte inventory required in the HBFC or the DMFC. In addition, in contrast to the DMFC, the water recovery system for the SMFC requires a separate subsystem for transport and recovery of water, an important factor in decreasing overall reliability and in adding weight to the system.

3. Reproducibility and the quality control appears to be an important engineering area where more research must be performed. The leached membrane used in the SMFC must have an absolute homogeneity of physical and chemical characteristics in order to avoid areas of intense heating and uneven water formation and removal. This is avoided to a great extent by HBFC and DMFC since the electrolyte imbibed by the membranes in this system serves as a leveling factor for physical properties and water balance problems.

2.2 Hydrogen-Bromine Fuel Cell

The HBFC limiting diffusion current is high as indicated in 300 ma/cm^2 and when used, as is commonly the case, as a secondary battery charge, acceptance efficiency is high compared to the $\text{H}_2 - \text{O}_2$ system. This is due to the considerable irreversibilities encountered on charging a leached $\text{H}_2 - \text{O}_2$ SMFC system compared to the HBFC where overvoltage is a minor consideration.² In practicality this calls for 20-30% greater power requirement for recharging at a given current density (Reference 2). The major factor which has held back the rapid development of this concept has been the lack of solid advances in membrane technology. Recently, however, (Reference 2) advances have been made which auger well for the development of this cell. It will continue to suffer, however, from one basic limitation. In order to prevent the migration of Br_2 , or Br_3^- more accurately, the network of the ion membrane fuel cell must be made less porous, i.e., diffusivity must be decreased. This will lead to lower limiting current densities as a result of decreased ionic mobility and cause higher IR drops. It therefore seems unlikely that effective operation of greater than $50\text{-}60 \text{ ma/cm}^2$ at $0.62 \text{ V} - 0.57 \text{ V}$ will be achieved in multiple configurations of HBFC in the next 36 months. The maximums could probably be improved by 30-50% if substantially more effort is devoted to this type of device than is presently contemplated. It is likely in fact that fuel cell optimization studies will indicate that values of about 30 ma/cm^2 and 0.72 V are more appropriate for design considerations at the present time. Since, however, this output is good for a secondary battery, solid practical achievements (orbital unmanned missions) may be anticipated.

2.3 Dual Membrane Fuel Cell

A number of factors indicate the advantages possessed by the DMFC. The membranes are continually in equilibrium with $6\text{N } \text{H}_2\text{SO}_4$, thereby eliminating problems related to water balance and drying of membranes (Reference 21). Moreover, the removal of generated heat can be efficiently performed by circulation of the electrolyte. Finally, since water formed at the cathode migrates into the central electrolyte reservoir, (Reference 3) we essentially eliminate the water transfer system required in the SMFC, eliminate complexity and increase reliability.

Factors detrimental to the achievement of higher operating current densities in the device are the good probability of the low activity of equilibrated H_2SO_4 in the membrane thereby lowering the conductivity substantially as compared to HBr of the same concentration in the membrane and also, most importantly, the formation of a water film on the oxygen electrode-membrane interface, suggests a limiting factor, the diffusion rate of the water from the interface into the membrane and the central reservoir. The water film appears to have a definitive means of leaving the area of the oxygen electrode by ordinary mass diffusional processes. If one assumes a diffusion constant of an order equivalent to that used in calculating limiting currents in membranes and taking into account the ambiguities in working with activities at membrane interfaces, then a rate of migration of water or more properly H_2SO_4 up to the O_2 electrode of about $8\text{-}16 \text{ ma/cm}^2$ for a membrane .050 cm thick can be calculated, or values of about $24\text{-}48 \text{ ma/cm}^2$ for membranes .0165 cm thick. It is interesting to note that the former value agrees rather well with the results obtained during the course of a research program related to the DMFC (Reference 3). It appears likely that using thinner membranes and with sufficient development, current densities of $40\text{-}50 \text{ ma/cm}^2$ at $.67 - .63 \text{ V}$

can be achieved in multiple configuration within the next few years. Possible improvements in this area might result from operating at higher temperatures or the removal of water via gas circulation. Of note here, however, is that because of the simplicity and ruggedness of this fuel cell, that fuel cell units have been offered to industry and government since 1962, (Reference 21).

3.0 Summation

The writer has taken operating parameters that he feels may be achieved within the next 18 months for multiple fuel cells of the three general classes of devices discussed in this paper bearing in mind that one of them, HBFC, is fundamentally used as a secondary battery. Of particular interest are projections of approximate weight volumes and power density based on projections of reasonable voltage and current densities. These are found in Table 1.

Type	Voltage	Amp/ft	Thickness (inches)	Pounds/ft ²	Volume(ft ³)	watts/ft ²	Kw./ft ³	Watts/lb
SMFC	.72	75	.205	1.37	.0171	55.0	3.2	40.2
DMFC	.72	30	.194	1.97	.0162	21.6	1.33	10.97
HBFC	.72	30	.165	1.67	.0138	21.6	1.56	12.92

Table 1. Volume and Weight Factors

It is important to reiterate the basis on which the calculations were made.

1. The weights and dimensions refer to a unit cell with no instrumentation, electrolyte holdup, water removal or any other system factors considered. For instance, it is clear that in long missions requiring primary cells, the increased weight of fuel needed will tend to improve markedly the watt hours/lb obtained from the system. It is because of this variability of missions in space, on land, or in the sea that no attempt has been made to go beyond the unit cell structure in analysis. Table 2 however, should be of value as a general starting point for systems analysis and is presented in the non-metrical units for engineering convenience.
2. The SMFC and DMFC are primary cells and therefore not strictly comparable with HBFC.
3. The SMFC has been the subject of a far greater investment of time and effort than either the DMFC or the HBFC. It is almost certain that the values of watts/lb and Kwatts/ft³ for the latter, two would increase by a factor of 2-4 times with an intensive development effort. Projections made in this paper assume that the development of neither the DMFC nor HBFC will be at as high a level in the next three years as has been the case with the SMFC.

Little has been said about quasi-membrane systems, such as gelled electrolytes and electrolytes absorbed in materials such as asbestos. In general, it is our feeling that with regard to gas permeability, retention of electrolytes under accelerative or vibrational forces, removal of waste water and heat that such systems are as yet unproven compared to ion membrane fuel cells. This in no sense indicates however, that systems such as H₂ - O₂ regenerable fuel cell with asbestos electrolytes (Reference 26)

or other primary systems (Reference 27) may not come to fruition in the future.

It may be of value, hazardous though it always appears to be, to suggest possible research and development areas that appear promising over the next few years:

1. Firstly, it is of some value due to advances in producing thinner membranes (Reference 5) to regard the membrane as less of a structural electrolyte and more as a diffusion barrier up against an electrode. In this conceptual framework we find that the membrane for instance, can be regarded as a means for producing low cost porous electrodes since thin membrane barriers will lessen the need for the elegant procedures used at present for preparation of metal and carbon electrodes. Moreover, such combined electrode membrane systems could be used in various electrolytes. Finally, if very thin membranes are used (<0.01)cm., there should be little difficulty in eventually sustaining current densities in excess of 200 ma/cm² at reasonable voltage levels.
2. Inorganic membrane systems have strong potential as intermediate temperature range (100 - 200°C) solid electrolytes both as cationic and anionic systems. Recent results (References 28, 29) indicate that novel inorganic systems have achieved resistances of 2-3 ohm cm.² at 115°C.
3. Research relevant to attaining a high level of quality control for membranes and membrane electrode assemblies would appear to be of much value in promoting the commercial manufacture of multiple unit cells.
4. The exploration of the advantages in using liquid ion exchangers would appear to be of value.
5. Although considerable effort has been expended in recent years in basic membrane research (References 5, 9, 10, 12, 13, 17, 30) intensified and well planned efforts may yet bring important breakthroughs in this field.

ACKNOWLEDGEMENTS:

The writer wishes to acknowledge his debt to those individuals who have been his co-workers in the past on various fuel cell projects - R. Lurie, H. Viklund, V. Masse, F. Leitz, S. Jain, and H. Perry and to the agencies which have provided support for these activities, the National Aeronautics and Space Agency and the United States Air Force. The writer also wishes to acknowledge the useful discussions with Dr. D. H. McClelland of Astropower relevant to theoretical considerations.

REFERENCES:

- (1) Grubb, W. T. and Niedrach, L. W., J. Electrochem. Soc. 107, 133 (1960)
- (2) Berger, C., Lurie, M. R., Viklund, H. J., Contract AF 19(604)-8508 (1960-1962)
- (3) Berger, C., Perry, H., Jain, S., Leitz, F., TRW Subcontract RD 236560 to Ionics, Inc., (1962 -)
- (4) Nepton CR-61, Ionics, Inc.
- (5) AMFion C-60, American Machine and Foundry Co.
- (6) General Electric Co., Contract No. DA-36-039-AMC-00095 (E), (1 October 1962 -) U.S.A. ERDL, Ft. Monmouth, New Jersey
- (7) Berger, C., Lurie, M. R., Shuman, R. J., and Viklund, H. J., Contract No. DA-44-009-ENG-4554, Final Report U.S.A. Engineering Center, Ft. Belvoir, Va.
- (8) General Electric Co., AF 33(616)-8159, (1961 - 1962)
- (9) Despic, A. and Hills, J. C., Trans. Faraday Soc. 51, 1260 (1956)
- (10) Papat, P. V., Contract No. DA-44-009-ENG-3771, (Nov 1, 1959 - Nov. 30, 1961)
- (11) Kortum G., and Bockris, J. O'M., Textbook of Electrochemistry Vol. II, P. 403
- (12) Spiegler, K. S. and Coryell, C., J. Phys. Chem., 57, 687, (1953)
- (13) Grubb, W. T., J. Phys. Chem., 63, 55, (1959)
- (14) Oster, E. A., Ion Exchange Membrane Fuel Cells - 16th Annual Power Sources Conference, p. 22-24
- (15) Astropower Internal Report (1963)
- (16) Chang, F. L. and Wick, H., Z. Phys. Chem., A172, 448 (1935)
- (17) Juda, W., Rosenberg, N. W., Marinsky, J. A. and Kasper, A. A., J. Am. Chem. Soc. 74, 3736, (1952)
- (18) Kortum G., and Bockris, J. O'M., Textbook of Electrochemistry Vol. II, P. 661
- (19) Kortum G., and Bockris, J. O'M., Textbook of Electrochemistry Vol. II, Page 704
- (20) Harned, H. S., and Owen, B. B., The Physical Chemistry of Electrolytic Solutions 3rd Edition No. 137
- (21) Berger, C. - Sales Brochure - Ionics Inc., Bulletin FC-101
- (22) Curve Calculated Presuming Use of AMFion C-313 Membrane for DMFC
- (23) Curve Calculated Presuming Use of AMFion C-313 Membrane for HBFC
- (24) General Electric Co., AF 33(616)-8159, (1961 - 1962)
- (25) Schanz, J. L. and Bullock, E. K., ARS, Space Power System Conference, (Sept, 1962)
- (26) NASA Contract NAS 7-7, Electro-Optical Systems, Inc., Report 1584-IR-1
- (27) Wynveen, R. A. and Kirkland, T. G., 16th Annual Power Sources Conference, P. 24-28
- (28) Astropower Internal Project #8017-1
- (29) NASA Contract NAS 7-150, Astropower, Inc.
- (30) Gregor, H. P., J. Am. Chem. Soc., 73, 642, (1951)

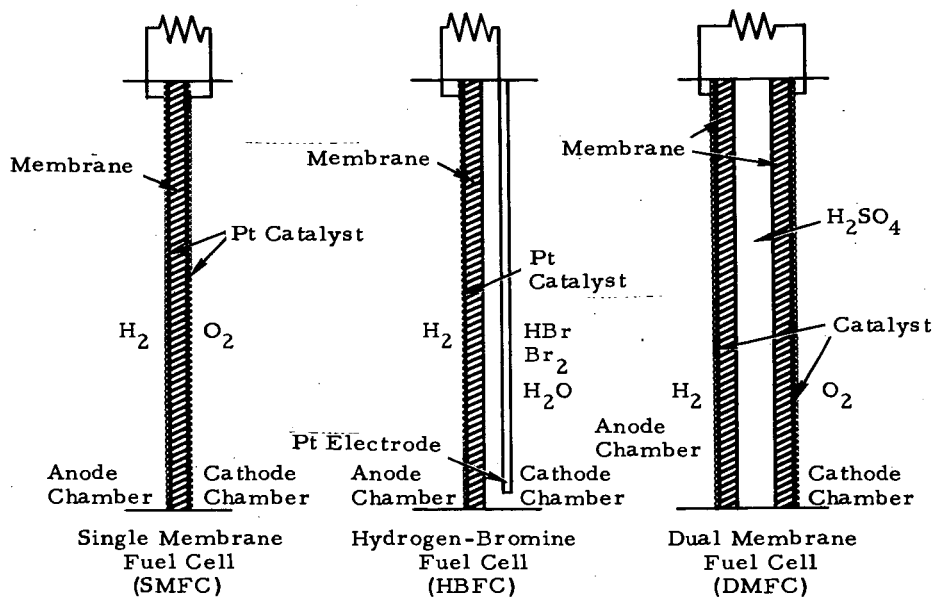


Figure 1. Three Representative Ion-Membrane Fuel Cells

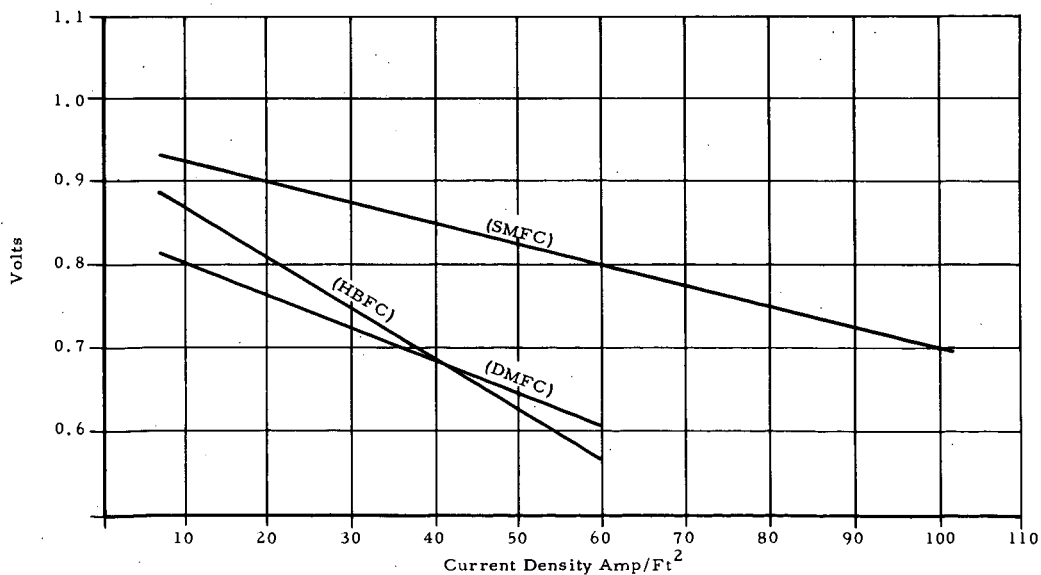


Figure 2. Comparison of Discharge Curves for SMFC, HBFC and DMFC

Performance of Hydrogen-Bromine Fuel Cells

W. B. Glass and
G. H. Boyle

Ionics Incorporated
152 Sixth Street
Cambridge 42, Mass.

Abstract*

One of the particular merits of the hydrogen-bromine ion exchange membrane regenerative fuel cell system is that the hydrogen-bromine couple is highly reversible. In early cells, bromine diffusion through the membrane caused deterioration of the hydrogen electrode. Data are presented on the successful development of a new membrane designed to overcome this problem. The effect of the brominating environment on the membrane is discussed.

Experimental data are also presented that demonstrate the effect of wide variations in the composition of the $\text{Br}_2\text{-HBr-H}_2\text{O}$ electrolyte on the voltage, cell resistance and performance capabilities of $\text{H}_2\text{-Br}_2$ cells at several temperature levels. Various inorganic bromide salts have also been investigated as possible bromine solubilizers and the resulting voltage and resistance data are presented and evaluated.

* Complete manuscript not received in time for inclusion in Division Preprints.

WESTINGHOUSE SOLID-ELECTROLYTE FUEL CELL

Fuel Design Group

D. H. Archer	L. Elikan
J. J. Alles	E. F. Sverdrup
W. A. English	R. L. Zahradnik

Westinghouse Electric Corporation
 Research & Development Center
 Pittsburgh 35, Pennsylvania

The basic component of the Westinghouse solid-electrolyte fuel cell is the $(\text{ZrO}_2)_{0.85} (\text{CaO})_{0.15}$ [or $(\text{ZrO}_2)_{0.9} (\text{Y}_2\text{O}_3)_{0.1}$] electrolyte. This material is an impervious ceramic which has the unique ability to conduct a current by the passage of O^- ions through the crystal lattice. The ease with which these ions pass through the electrolyte is measured by the electrical resistivity, ρ_b , of the electrolyte. Values of ρ_b for both $(\text{ZrO}_2)_{0.85} (\text{CaO})_{0.15}$ and $(\text{ZrO}_2)_{0.9} (\text{Y}_2\text{O}_3)_{0.1}$ as functions of temperature, T, are given in Figure 1. The resistance of a disc of $(\text{ZrO}_2)_{0.85} (\text{CaO})_{0.15}$ 2 in. in diameter and 15 mils thick is about 0.1 ohm at 1000°C.

FABRICATING THE CELL

To fabricate a cell from such a disc, porous platinum electrodes are applied to both sides. On the lower electrode of Figure 2 a molecule of O_2 gas from the surroundings acquires 4 electrons and forms 2 O^- ions, which enter the crystal lattice of the ceramic. At the upper electrode, 2 O^- ions emerge from the electrolyte, give up 4 electrons, and recombine to form O_2 . The lower electrode is positively charged; the upper is negatively charged if O_2 flows upward through the electrolyte.

The most direct method for bringing about this flow is to construct one chamber around the lower electrode in which O_2 is kept at a high partial pressure and another chamber around the upper electrode in which the partial pressure of O_2 is maintained at a low value. In this case, the observed open circuit voltage of the cell, E_t , can be computed from

$$E_t (4 \mathcal{F}) = RT \ln (P_{\text{O}_2, \text{H}} / P_{\text{O}_2, \text{L}}) \quad (1)$$

where $4 \mathcal{F} = 4$ (the Faraday number) = quantity of charge transferred per mol of O_2 passing through the electrolyte, 386,000 coulombs/mol
 R = universal gas constant, 8.134 watt-sec/°K mol
 T = absolute temperature of cell, °K

$P_{O_2,H}$; $P_{O_2,L}$ = O_2 partial pressures in lower and upper chambers
 $RT \ln (P_{O_2,H} / P_{O_2,L})$ = work per mol obtained from reversible, isothermal expansion of a gas at temperature T, watt-sec/mol

UTILIZATION AS FUEL CELL

The device can be utilized as a fuel cell by flowing oxygen or air to the lower chamber. If atmospheric air is used, the O_2 partial pressure in the lower chamber is maintained at about 0.2 atm. Fuel flows through the upper chamber, combines with any O_2 present, and reduces the O_2 partial pressure in the fuel chamber to about 10^{-16} atm. (The total pressure in both chambers is 1.0 atm.) The calculated value of E_t in this instance is approximately 1.0 volt.

When a current, I , is drawn from the terminals, the voltage V of the cell drops below the open circuit voltage E_t because of resistance losses in the electrolyte and electrodes.

$$V = E_t - IR \quad (2)$$

where E_t is the voltage computed from Equation 1 and R is the ohmic resistance of electrodes and electrolyte. An approximate expression for the resistance R of a cell is

$$R = \rho_b \delta_b / A_b + (\rho_e / \delta_e) (L_e / P_e) \quad (3)$$

where δ_b = electrolyte thickness

A_b = active cell area

ρ_e / δ_e = resistivity-thickness quotient for the cell electrodes

(See Figure 3)

L_e = mean distance travelled by the electronic current in the electrodes passing from the plus to the minus terminal of the cell

P_e = mean width of the electrode perpendicular to the direction of electronic current flow

For a cell operating at 1000°C using a $(ZrO_2)_{0.85} (CaO)_{0.15}$ electrolyte 5 cm in diameter and 0.04 cm thick,

$$\begin{aligned}
 R &\approx \frac{(60 \Omega\text{-cm}) (0.04 \text{ cm})}{(\pi/4) (5 \text{ cm})^2} + (0.44 \text{ ohm}) \frac{(2.5 \text{ cm})}{2\pi (2.5 \text{ cm})} \\
 &\approx 0.12 + 0.07 = 0.19 \text{ ohm}
 \end{aligned}$$

If the electrodes of the cell are sufficiently porous, the IR loss -- as indicated in Equation 2 -- is the only voltage loss in the cell; there are no appreciable voltage drops in the solid-electrolyte cell attributable to the slowness of diffusion or chemical reaction.

CHARACTERISTICS OF SINGLE CELLS

A number of single cells based on these principles have been constructed and tested. The components of a disc cell with an effective diameter of 1.3 inches are shown in Figure 4 and the performance of such a cell is shown in Figure 5. The open circuit voltage of the cell with H_2 fuel is 1.15 volts; its resistance is about 0.4 ohm. The maximum power delivered by the device is 0.85 watt, and the current density at these conditions is 150 amp/ft².

SOLID-ELECTROLYTE FUEL CELL BATTERIES

Solid-electrolyte fuel cell batteries have been investigated. One type of battery is constructed of short, cylindrical electrolyte segments shaped so that they can be fitted one into the other and connected into a long tube by bell-and spigot joints. Figure 6 shows an electrolyte segment. A mathematical analysis has been carried out to determine the active cell length L which maximizes the power per unit of cell volume for given values of (1) $\rho_b \delta_b$, the electrolyte resistivity-thickness product; (2) ρ_e / δ_e , the electrode resistivity-thickness quotient (see Figure 3); (3) l , the seal length; and (4) R_{eo} , the electrical resistance of the metal alloy joint which both makes the seal and connects the individual cell segments electrically in series.

An optimized three-cell battery with bell-and-spigot joints is shown in Figure 7. One of the platinum wires at each end of the cell stack is the current lead to the battery; the other wires are probes for measuring potentials throughout the battery.

PERFORMANCE OF BATTERY ON H_2 FUEL AND AIR

The performance of the battery on H_2 fuel and air is shown in Figure 8. The open circuit voltage of the device is below the expected 3.3 volts because of some shorting of the cells occurring in the seal region. Such shorting has been determined to draw about 100 ma in each cell; improved seal design will minimize this loss. In spite of this problem, a current

density greater than 450 ma/cm^2 has been achieved in this battery at the maximum power point -- about 1.2 volts. Three of the four joints required in the fabrication of the battery of Figure 8 have been demonstrated to be tight with a helium leak detector. The oxygen leak rate through the fourth joint was shown to be less than the oxygen added to the fuel by a current flow of 20 ma.

PERFORMANCE OF BATTERY ON H_2 FUEL AND PURE O_2

The performance of this same three-cell battery with H_2 fuel and pure O_2 is shown in Figure 9. The open circuit voltage is 2.9 volts. The current density at maximum power was 750 ma/cm^2 . At the maximum power point, the battery produces 2.1 watts; and each cell segment, 0.7 watt -- about the same as an ordinary flashlight battery.

The segmented-tube bell and spigot battery gives promise of providing a compact, lightweight power system.

CELL SEGMENT CHARACTERISTICS

The characteristics of the cell segments which make up this battery are given below.

Over-all length, $(L + \mathcal{L}) = 0.58 + 0.53 = 1.11 \text{ cm}$

Mean diameter, $D = 1.07 \text{ cm}$

Electrolyte material: $(\text{ZrO}_2)_{0.9} (\text{Y}_2\text{O}_3)_{0.1}$

Electrolyte resistivity-thickness parameter at 1000°C ,

$$\rho_b \delta_b = 0.4 \text{ ohm-cm}^2$$

Electrode material: porous platinum

Electrode resistivity/thickness at 1000°C $(\rho_e/\delta_e) =$

$$0.43 \text{ ohm-cm/cm}$$

Segment weight (including one joint) = 1.97 gm

Segment volume (including one joint) = 2.0 cm^3

The electrodes of the cell are quite light, and the total weight of the cell is also small -- about 2.0 gm. If the cells are operated at maximum power, the power produced is equivalent to 160 watts/lb of electrolyte and electrodes. (This figure does not include battery casing, insulation, and auxiliaries.) The power per unit volume of the cell unit is 9.5 kw/ft^3 .

These performance figures can still be improved by (1) the development of electrodes with lower ρ_e / δ_e values, (2) the use of electrolyte materials with lower ρ_b values, and (3) optimization of the seal dimensions. More power/volume can also be obtained by using smaller diameter cells.

SOLID-ELECTROLYTE FUEL CELL SYSTEMS FOR SPACE

In order to provide a useful power source it is necessary not only to combine the unit cells into batteries but also to provide manifolding, casing, and insulation. All these components must be integrated into a system. A series of 500 watt solid-electrolyte fuel cell systems have been designed for use in space. Stacks of cells connected by bell-and-spigot joints are contained in an insulated cylindrical can which is maintained at the 1027°C operating temperature by the heat generated in operating the system at the design power. The H_2 fuel flows inside each each tube stack and the O_2 oxidant fills the can housing the stacks (see Figure 10). The gas stream emerging from the stacks is water vapor with 4 mole % or less unburned H_2 ; this gas is exhausted to the surroundings.

Minimum-weight 500-watt systems have been determined for 10-hour, 100-hour and 1000-hour total mission lengths using 1-inch diameter stacks. A choice of 1/2-inch diameter stacks would have resulted in a smaller, lighter device. For a 100-hour mission, the estimated weight of the fuel-cell system (including the cell battery, casing, manifolding, insulation, radiator, and controls) is 25 pounds; the estimated weight of H_2 and O_2 reactants and reactant storage system is 115 pounds. For the 1000-hour mission, the estimated minimum fuel cell system weight is 47 pounds; the reactant and reactant storage weight is 643 pounds.

ADVANTAGES OF SOLID-ELECTROLYTE FUEL CELLS

Although particular solid electrolyte fuel cell systems have been considered, modifications can be made to meet other specific requirements. In addition to their light weight, solid-electrolyte fuel cell systems have distinct advantages over other fuel cells: They are compact; Their high operating temperature enables the heat generated in operating the cell to be radiated to the surroundings without weighty, complex cooling systems and radiators; The electrolyte is physically and chemically stable; There is no difficulty in removing water from the cell (it flows from the system in vapor form); The system operates independently of gravitational forces.

For all these reasons, the solid-electrolyte fuel cell system is a promising candidate for generating power in space.

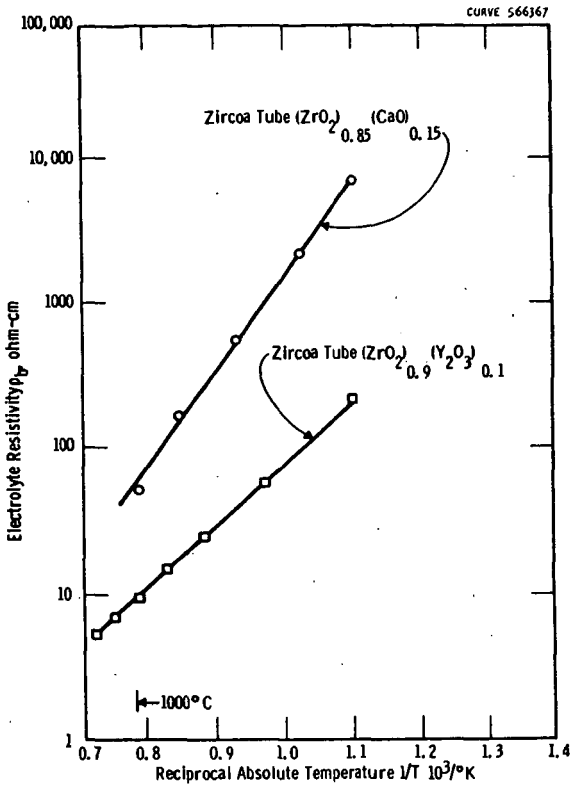


Fig. 1—Electrolyte resistivity-temperature characteristics (CaO and Y₂O₃ stabilized ZrO₂)

DWG. 626A088

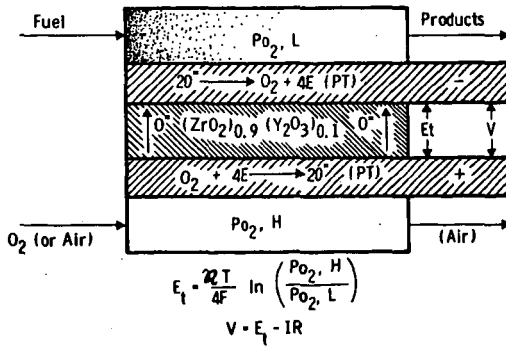


Fig. 2—Solid-electrolyte fuel cell

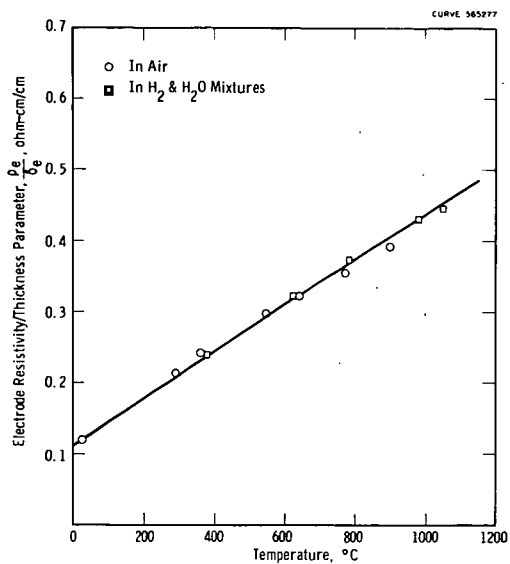


Fig. 3—Characteristics of air-sprayed platinum electrodes

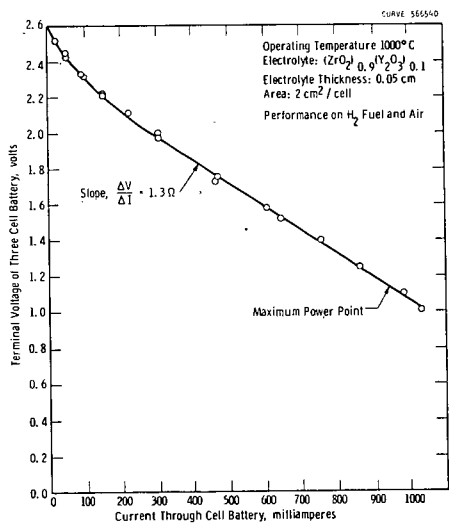


Fig. 8—Voltage-current characteristics of three-cell segmented tube battery with bell-and-spigot joints (H₂ fuel and air)

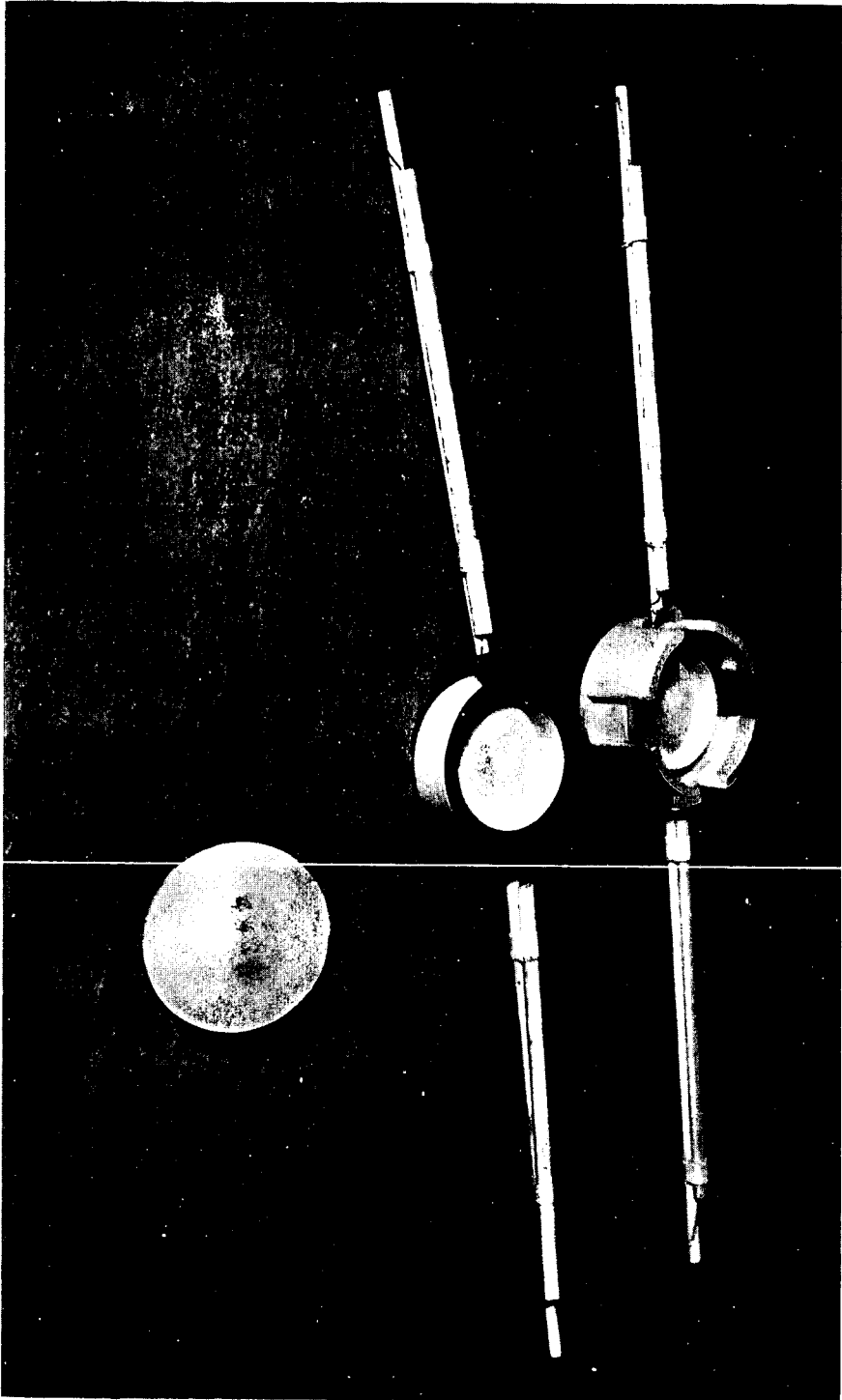


Figure 4. Single Cell Test Assembly

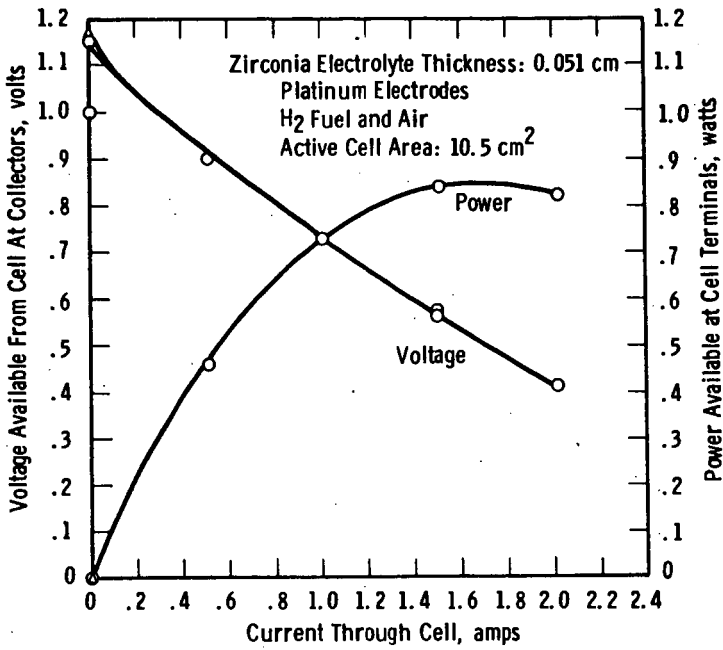


Fig. 5—Voltage and power output of Westinghouse solid-electrolyte fuel cell

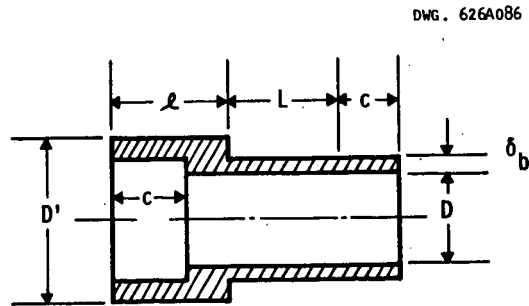


Fig. 6—Cross section of basic cell unit for bell-and-spigot design

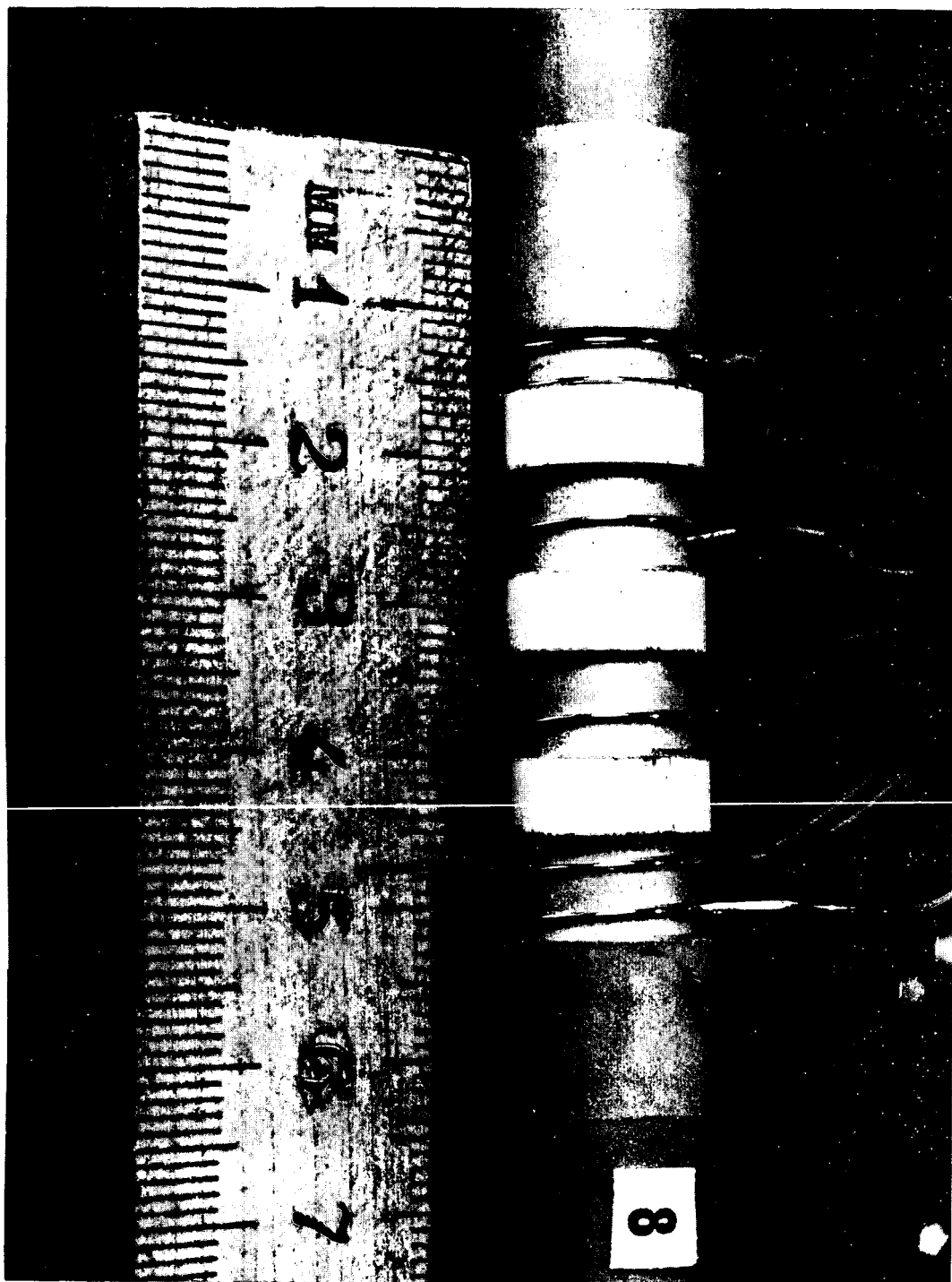


Figure 7. Three-cell segmented tube battery
with bell-and-spigot design.

R. Zahradnik
n. n. 5-15-63

CURVE 566827

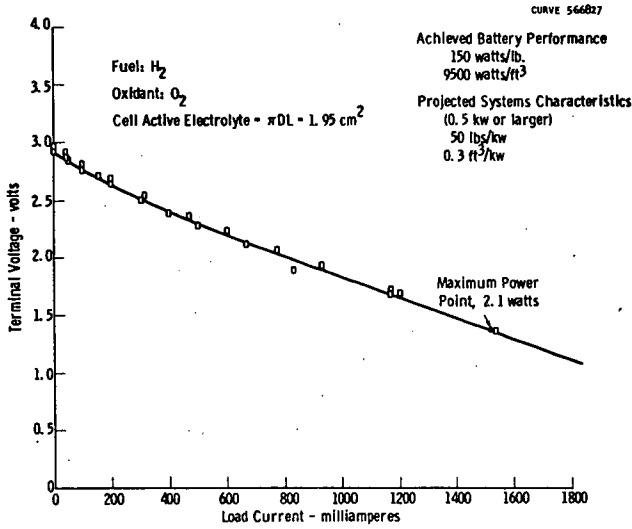


Fig. 9—Voltage-current characteristics of three-cell segmented tube battery with bell-and-spigot joints (H_2 fuel and O_2)

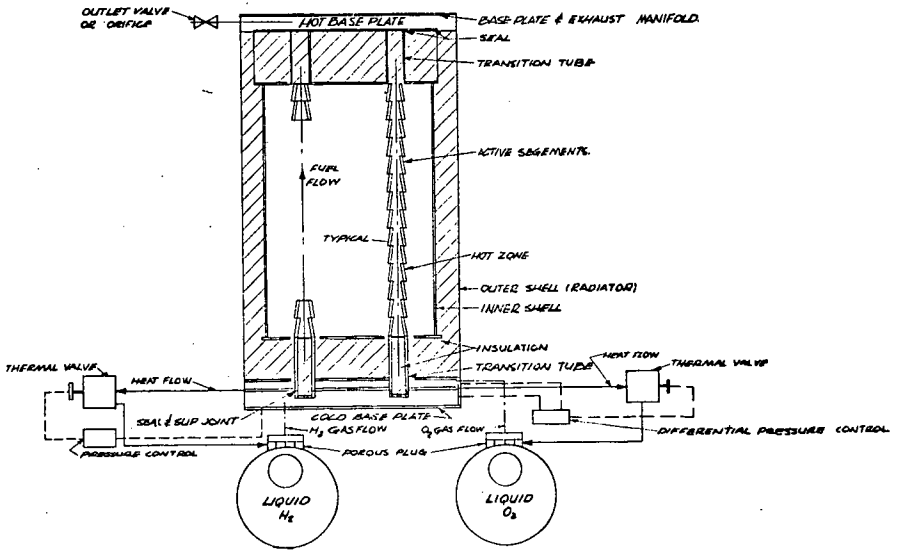


Fig. 10—Diagram of over-all fuel cell system

Electrode Processes in Molten Carbonate Fuel Cells

Isaac Trachtenberg

Corporate Research & Engineering, Texas Instruments Incorporated, P. O. Box 5474,
Dallas 22, Texas

Introduction

Many of the potential applications of fuel cells require operation on cheap, readily available fuels and air. These fuels in all probability will be hydrocarbons or impure fuel gases readily derived from hydrocarbons. Fuel cells employing molten carbonate electrolytes and operating above 500°C afford an early opportunity for rapid development of a system capable of satisfying these requirements. The material presented here is concerned with some of the more fundamental aspects of molten carbonate-magnesium oxide-matrix cells. The causes of electrode polarization are established and measured. Typical data for the effect of fuels on anode polarization are given. Based on the experimental observations, chemical and electrochemical reaction schemes are suggested. Theoretical voltage-fuel composition curves are illustrated and indicate that good utilization of fuel at reasonable voltages can be expected. Cells have actually operated on hydrocarbon fuels and air at acceptable power levels continuously over extended time intervals.

Fuel cells employing various eutectics of molten alkali carbonates as the electrolyte have been previously described.¹⁻⁴ Operating characteristics of magnesium oxide (MgO) matrix cells have also been reported.⁵⁻⁷ These cells have been thermally cycled a number of times and in some instances attained more than 4000 hours of continuous operation at 600°C. Power densities greater than 100 watts/ft² at 0.7 volts have been obtained with pure hydrogen fuel and 4:1 air: CO₂ mixtures as the cathode gas feed. These results have led to the initiation of design and development work on molten-carbonate hydrocarbon fuel cell batteries and systems. However, discussion of these engineering studies is beyond the scope of this paper.

Experimental

All of the experimental work reported here was performed on cells identical to that shown in Fig. 1. This illustration shows the cathode chamber of the cell with the third idling electrode. This small electrode is used to monitor the performance of the individual anode and cathode in a working fuel cell. The large electrode (15.6 cm² or 1/60 ft²) is the working cathode and is bonded to the MgO matrix. The matrix is impregnated with the binary LiNaCO₃ eutectic (m. p. ca. 500°C). Not shown is the anode bonded on the bottom side of the MgO matrix. The anode has the same geometrical configuration and area as the cathode. Cathodes for this study were pure silver; however, substrates of base metals containing catalyst are now being used successfully. The anode is made of either silver or base metal substrates containing a wide variety of inexpensive catalyst.

Electrical connections are made from the electrodes to the various insulated lead-throughs. The only electrical connection within the cell between the three electrodes is through the electrolyte contained in the MgO matrix. The lids are then welded on to make each chamber gas tight. The cell is placed vertically in a furnace and the necessary external gas and electrical connections are completed.

Current-voltage traces for the complete working cell and the individual electrodes were obtained with a Moseley Model 3S X-Y recorder. A transistor network is used to give a continuously variable, pure resistive, load for the cell. The current passed in this circuit is the X-input. The voltage between the non-working electrode and the particular working electrode to be studied, or the terminal voltage of the cell becomes the Y-input. In order to avoid polarization of the non-working electrode the Y-input or for that matter any voltage measuring device used with the non-working electrode must have a high input impedance. These current-voltage curves measure the total steady-state polarization of the individual electrodes and the complete cell under working conditions.

In order to establish the contributions of the various types of polarization, ohmic, activation, and concentration, to the total polarization, it is necessary to resort to a transient method. A single current interruption technique was used for this purpose. The three types of polarization of interest may be distinguished according to time intervals after removing the polarizing load. Ohmic polarization is removed immediately after current interruption for the present investigation in times less than a microsecond. Since removal of activation polarization requires the electrode potential to change, the time required for its decay is governed by the rate of charging of the electrical double layer or about 10^{-6} to 10^{-4} seconds. Polarization decay because of concentration effects requires times greater than 10^{-4} seconds since appreciable mass transport (either ions in the electrolyte or molecules in gas phase) must occur.

Figure 2 schematically shows the interruption circuit. The heart of this circuit is the mercury wetted Clare relay and its make before break operating feature. This latter feature permits triggering and use of the sweep delay circuits of the 545A oscilloscope. Voltage time curves are recorded from the oscilloscope from 10^{-6} to 1 second.⁷

Current-Voltage Curves for Operating Cell

The specific results presented are typical examples of the data obtained from a large number of experiments on many similar cells. Figure 3 is current-voltage curves for a cell operating at 600°C on pure H_2 fuel on the 25th day of operation. The cathode is supplied with a 4:1 mixture of air: CO_2 . The curve V_T represents the terminal voltage of the operating cell. The open circuit voltage is 1.40 volts. V_A and V_C curves are the voltage of the anode and cathode, respectively, versus the non-working electrode. The values of R_A and R_C , the ohmic resistances as determined by current interruption, were measured at several pre-interruption currents and found to be constant. Correction for the ohmic polarization is made and the curves $V_A + IR_A$ and $V_C - IR_C$ are the current-voltage curves due to concentration polarization. It is interesting to note that $R_A + R_C < R_T$. This difference is assumed to be the bulk electrolyte resistance, R_E . In addition to the ohmic resistance at the electrode-electrolyte-matrix interface, R_A and R_C contain the resistance of the individual electrode leads to the terminals just outside of the furnace. For the particular case of cell 117R at 600°C , R_A , R_C , and R_T are 0.075, 0.10, and 0.21 ohms, respectively; the lead resistance of the individual electrodes is about 0.025 ohms. R_E is calculated to be .035 ohms. The calculated resistance based on electrolyte conductivity, electrode size, and separation is .011 ohms. These calculations imply a factor due to porosity and tortuosity of the MgO disc of about 3.

The V_T curve indicates a power density equivalent to 60 w/ft² at 0.7 volts. If all ohmic factors with the exception of the bulk electrolyte resistance, R_E , could be removed, this cell would produce an equivalent of 120 watts/ft² at 0.7 volts.

Several features concerning the polarization of the individual electrodes should be pointed out. Limiting currents are not being approached even at current densities of 200 amps/ft². Ohmic polarization is a more important factor at the cathode, where oxide films may be formed. Concentration polarization is greater at the anode, since products must back diffuse.

Figure 4 shows additional current-voltage curves for cell 117R. In order to obtain these data, 200 cc/min of CO₂ were added to the original H₂ fuel supply. This fuel represents a reformed hydrocarbon. The cathode conditions were unchanged and the same polarization curves were obtained for it as in Fig. 3. The effect of additional flow rate by itself is negligible (H₂ rate was raised to 700 cc/min with no measurable change in the current-voltage curve). The effect of adding CO₂ was observed immediately even at open circuit. Considerable amounts of water were obtained in the fuel effluent. The values of R_A , R_C and R_T were not altered by the change in fuel composition. However, the open circuit voltage is markedly reduced and can be attributed to the introduction of CO₂ and the formation of H₂O from the water-gas shift equilibrium. These substances are products from the overall anode process.

The terminal power output is equivalent to 42 watts/ft² at 0.7 volts and if all ohmic factors excluding bulk electrolyte resistance were eliminated, an equivalent power of about 84 watts/ft² at 0.7 volts could be obtained. It should be noted in comparing figures 4 and 3 that the concentration polarization, 0.18 volts, at an equivalent of 100 amps/ft² for reformed hydrocarbon fuel is considerably lower than that of the pure H₂ fuel, 0.35 volts, at the same current density. However, the open circuit voltage and the operating voltage is lower for the reformed fuel, 1.06 volts open circuit, compared to 1.40 volts open circuit, for the pure H₂ fuel.

What has been referred to as concentration polarization until now is really total polarization minus ohmic polarization. From data such as these and current interruption studies, no activation polarization or evidence of any could be detected. As might be expected, the system is subject to less concentration polarization as product concentration of the incoming fuel increases.

Current Interruption Studies

As previously mentioned the various types, ohmic, activation, and concentration polarization may be distinguished and measured by voltage decay as a function of time after interruption of a steady state current. A previous publication⁷ was concerned only with pure H₂ fuel in this system. Comparison of hydrogen with simulated reformed hydrocarbon fuels is presented here.

Figure 5 illustrates anode current-voltage curves corrected for ohmic polarization. Open circuit voltage decreases with decreasing flow rate and increasing product (CO₂ and H₂O) concentration. However, polarization at any given current density decreases with increasing product concentration of the incoming fuel. The lower open circuit voltage of curve B compared to curve A is related to the amount of CO₂ continuously escaping from the electrolyte and the relative concentration of CO₂, H₂O and H₂ (see proposed reaction scheme).

Current interruption experiments were completed with the fuels indicated in Fig. 5. All measurements were made at a pre-interruption current equivalent to a current density of 60 amps/ft². Figure 6 illustrates the voltage-time curves for the two high fuel flow rates. The two straight lines are characteristic of this type measurement. The steady state polarization is represented by the symbols through the ordinate. The initial drop is the same for all fuels and flows studied. Data in the 10⁻⁶ range are somewhat distorted by the ring-back voltage which develops when the current drops instantly to zero. The horizontal line in the 10⁻⁵ to 10⁻⁴ second range indicates no measurable activation polarization. The polarization decay in times greater than 10⁻⁴ are attributed to concentration effects. The two curves are almost parallel. At the high flow rates used, any effect of flow rate has been removed. Since polarization for the H₂-CO₂ fuel is less than that for pure H₂, the H₂-CO₂ open circuit voltage is attained more rapidly.

Figure 7 illustrates the voltage time curves for the lower flow rates of Fig. 5. The same characteristic features are observed here as in Fig. 6. The ohmic polarization is constant and there is no measurable activation polarization. However, there is an effect of flow rate. The total flow of 360 cc/min for H₂-CO₂ case increases the rate of decay of concentration polarization over that observed for pure H₂ at 160 cc/min.

The effect of flow rate on anode polarization curves was studied in another series of experiments. In Fig. 8 anode polarization curves corrected for ohmic polarization at various fuels and flow rates are presented. Curve I illustrated that cells operating on reformed hydrocarbons at high flow rates perform better than on pure H₂ even though the open circuit voltage is higher for the pure fuel. The introduction of an inert gas to aid sweep, curve III, leads to high open circuit voltage but polarizes much more rapidly (compare curves II and III) when placed under load.

All of those data relating to flow rates indicate that the benefits of high open circuit voltage obtained by high flows of pure hydrogen or hydrogen diluted with inert gases is lost when significant quantities of the fuel are consumed. The effect of the high flow rates of gases is to reduce the concentration of non-electrochemically produced CO₂ and H₂O. When the electrochemical processes are functioning, this effectiveness of gas sweeping is greatly reduced.

Interruption studies were made on cathodes. Figure 9 is a typical voltage-time plot for a cathode operating on a 4:1 mixture of air:CO₂. The curves are very similar to those obtained for anodes. Cathodes exhibit higher ohmic polarization than anodes and less concentration polarization. Cathodes are not as sensitive to gas flows. Since concentration polarization is small, electrode steady state is rapidly attained.

Ohmic Polarization and Electrolyte Resistance

Ohmic resistance at the individual electrodes is calculated from the initial (10⁻⁶ second) voltage decay and the pre-interruption current. The values determined include lead resistance (.025 ohms). Bulk electrolyte resistance is determined by subtracting the sum of the anode and cathode resistance from the total cell resistance.

The temperature coefficients of the various resistances were measured. The coefficient of anode was nearly identical with that of bulk electrolyte, while the co-

efficient of the cathode was much higher (resistance decreased more than would be predicted on the basis of changes in electrolyte conductivity alone).

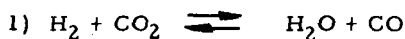
The relatively high ohmic polarization, the consequence of ohmic resistance, at the anode may be attributed to electrolyte restriction at the electrode-matrix interface. It is very unlikely that all pores of the electrode match the pores in the matrix. In fact, there is a great deal of masking. This masking greatly reduces the thickness and number of electrolyte paths between the active electrode sites and the bulk electrolyte and increases the ohmic resistance. Since the temperature coefficient of the ohmic resistance at the anode is the same as the bulk electrolyte, it is reasonable to assume that all of the ohmic polarization at this electrode is due to the electrolyte. Its relatively large value is directly attributable to the degree of electrolyte restriction.

At the cathode a similar situation exists. However, there is an additional contribution to the ohmic resistance which has a larger temperature coefficient. Although silver oxide is thermally unstable at 600°C there is a finite amount present on the electrodes. This oxide layer introduces some additional ohmic resistance. As the temperature is increased the amount of oxide is reduced and the ohmic polarization decreases.

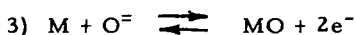
Reaction Scheme for Overall Electrode Processes

The foregoing experiments and results suggest that all reaction kinetics are very fast and equilibriums are established. The observed polarization is attributed to ohmic resistances and mass transport limitations. At the anode the same types of polarizations exist for pure H₂ fuel as for a variety of H₂-CO₂ fuels which represent reformed and partially consumed reformed hydrocarbon fuels.

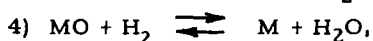
Two chemical reactions are assumed to always be in equilibrium:



The oxide ion is the active potential determining species present in the electrolyte. The electron-transfer reaction becomes



where M represents the active metal catalysts. Fuel is consumed in the chemical reduction of the metal oxide by H₂



thus regenerating the active metal catalysts. At 600°C and higher, this latter reaction proceeds rapidly and is always in equilibrium. The equilibrium being shifted very far toward metal-water.

On the basis of this model the anode potential may be represented as

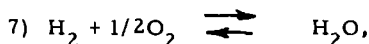
$$5) E_A = E_A^{\circ} - \frac{2.3 RT}{nF} \log \frac{[{}^a\text{H}_2\text{O}][{}^a\text{CO}_2]}{[{}^a\text{H}_2]}$$

where a_i represents the activity of the various reactants and products. The various activities are represented in terms of a contribution from electrochemical and chemical reaction. For example

$$6) a_{\text{H}_2\text{O}} = \Theta_{\text{H}_2\text{O}} (x + y)$$

where $\Theta_{\text{H}_2\text{O}}$ is a proportionality constant, x is partial pressure of water obtained from electrochemical conversion and y is the partial pressure of water obtained by shift conversion.

Figure 10 illustrates anode potential curves obtained assuming $\Theta_{\text{H}_2\text{O}}$, $\Theta_{\text{H}_2\text{O}}$ and Θ_{CO_2} all equal to 1. The initial fuel is pure H_2 . The potential is plotted as a function of the H_2 electrochemically consumed. The potential scale is meant to be a relative scale since E_A° was assumed to be standard potential for the reaction,

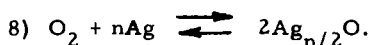


at the appropriate temperature. The dashed line is the same plot neglecting the shift reaction.

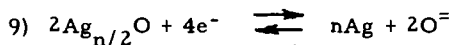
In Fig. 11 the value of $\Theta_{\text{H}_2\text{O}}$ was varied and a family of curves with the same potential variation with H_2 consumption was obtained. In all of these curves the cathode is invariant. $\Theta_{\text{H}_2\text{O}}$ represents a weighting factor for surface coverage. Since CO_2 pressure effects the potential by establishing the equilibrium concentration of O^- , its weighting factor is always unit. However, there is competition for metal sites between H_2 and H_2O . The weighting factor indicates the ratio of H_2O -coverage to H_2 -coverage when the partial pressure of the two components is equal. As figure 11 indicates, $\Theta_{\text{H}_2\text{O}}$ merely changes the absolute anode potential for a given E_A° . This value of $\Theta_{\text{H}_2\text{O}}$ for an electrode will depend upon the metal catalyst.

Figure 12 illustrates the effect of starting with fuels obtained from various hydrocarbon treating processes. Curves A and B represent steam reforming with limited purification of the raw reformat. Curve C represents completely reformed and shifted natural gas. Curve D represents partial oxidation of hydrocarbons of the class C_nH_{2n} . Curve E is a 80% consumed fuel in which all the water is removed. At low consumption there is appreciable benefit for initially supplying a pure H_2 . However, at more than 50% electrochemical consumption of the starting fuel there is very little advantage for the use of pure H_2 and various partially oxidized hydrocarbons may be used with equal effectiveness.

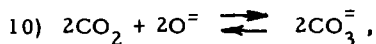
The proposed reaction scheme for cathodes⁷ is similar to anodes. The first step in the scheme is the adsorption of O_2 .



This oxide formation is responsible additional ohmic resistance observed at the cathode. The electrochemical reaction is



and finally the equilibrium between CO_2 and O^- ,



is established at the cathode. The potential of the cathode may be written as

$$11) E_C = E_C^\circ - \frac{2.3 RT}{nF} \log \left[\frac{1}{(a_{\text{O}_2}) (a_{\text{CO}_2})^2} \right]$$

where a_{O_2} and a_{CO_2} are the activities (partial pressures) of oxygen and CO_2 .

According to equation 11 the substitution of O_2 for air should increase the overall cell voltage about 30 millivolts. This predicted result has been verified experimentally.

Conclusion

Fuel cells employing molten-carbonate electrolytes can be operated successfully on air and a wide variety of fuels readily derived from hydrocarbons. At current densities up to 200 amps/ft² there is no kinetic limitation other than mass transport.

When hydrocarbon-derived fuels are initially supplied to the anode, open circuit voltage is lower than when pure H_2 is supplied. However, under appreciable load, anode polarization on impure fuel is much lower. Cathodes perform well on mixtures of air and CO_2 .

Although all of the electrodes investigated showed no activation polarization, electrode potential under operating conditions is dependent on the product-reactant adsorption equilibrium of the particular catalyst-electrode.

Acknowledgements

In part the work reported here received financial support from the United States Army Engineers Research and Development Laboratories, Fort Belvoir, Virginia

References

1. G. H. J. Broers, "High Temperature Galvanic Fuel Cells" Thesis, University of Amsterdam (1958).
2. G. H. J. Broers and J. A. A. Ketelaar in "Fuel Cells", G. J. Young, Editor, pp 79-93, Reinhold Publishing Co. (1960).
H. H. Chambers and A. D. S. Tantrum, *ibid.*, pp 94-100.
3. M. L. Kronenberg, *J. Electrochem. Soc.* 109, 753 (1962).
4. Y. L. Sandler, *ibid* 109, 1115 (1962).
5. C. G. Peattie, B. H. Barbee, K. W. Kreiselmaier, S. G. Parker, I. Trachtenberg, and A. H. White, "Performance Data for Molten-Electrolyte Fuel Cells Operating on Several Fuels", Conference Proceedings 1962, Pacific Energy Conversion Conference, San Francisco, Calif., Aug. 12-16, 1962.
6. C. G. Peattie, I. Trachtenberg, B. H. Barbee, K. W. Kreiselmaier, S. G. Parker and A. H. White, "Factors Involved in the Use of a High Temperature Fuel Cell as a Space Power Source", Vol. II, Progress in Astronautics and Rocketry "Power Systems for Space Flight" in press (1963).
7. I. Trachtenberg, *J. Electrochem. Soc.*, in press (1963).
8. H. Flood, T. Forland, and K. Motzfeldt, Acta. Chem. Scand. 6, 257, (1952).
9. S. Djordjevic and G. J. Hills, *Trans. Faraday Soc.* 56, 269 (1960).

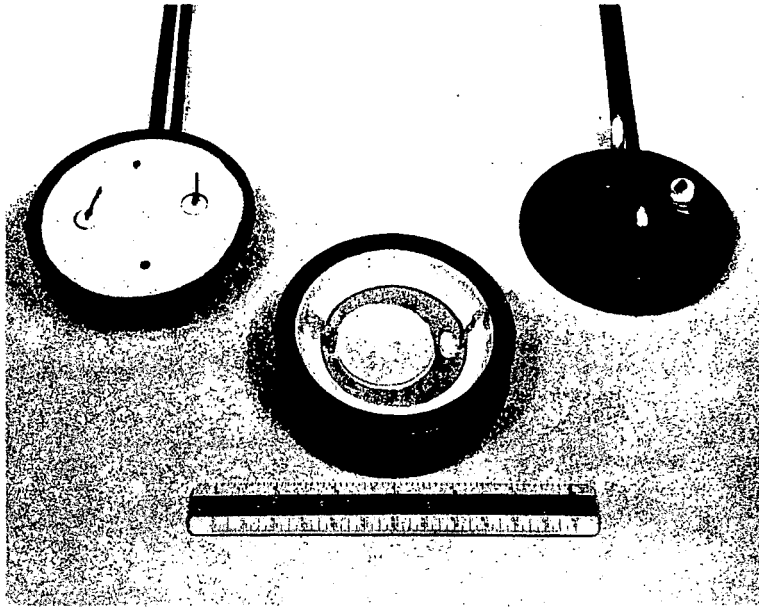
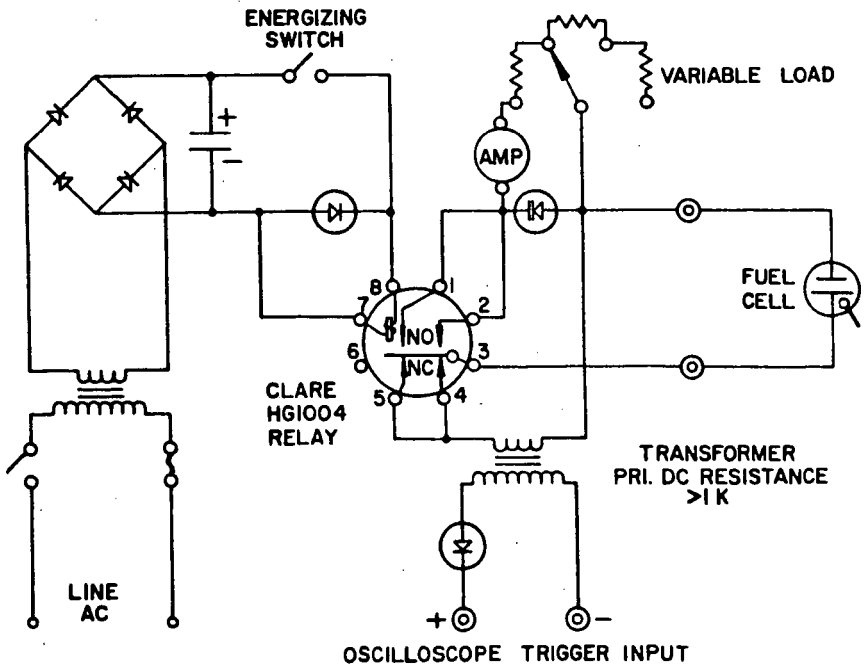


Fig. 1 Cathode chamber of a working fuel cell showing third idling electrode



Circuit used to obtain voltage-time curve < 1 sec.

Fig. 2 Interrupter circuit

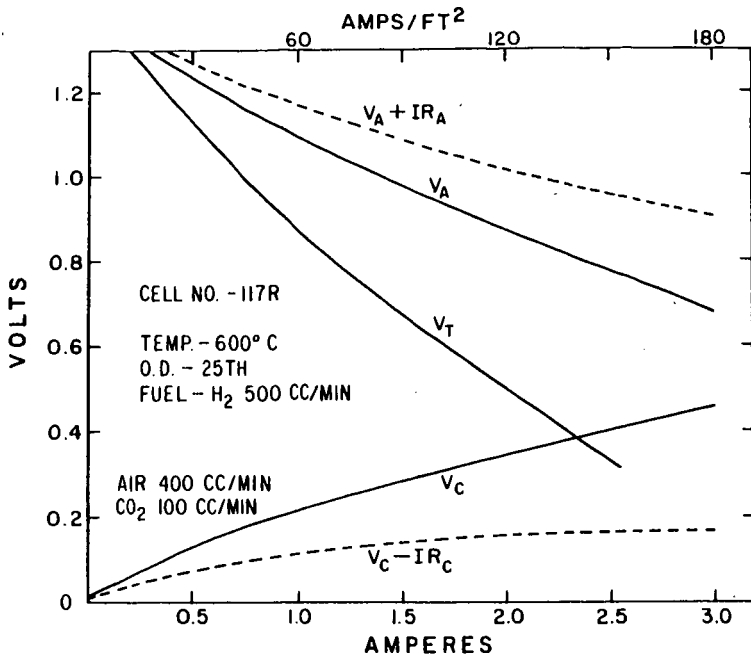


Fig. 3 Typical polarization curves for a cell and individual electrodes operating on H_2 and air- CO_2

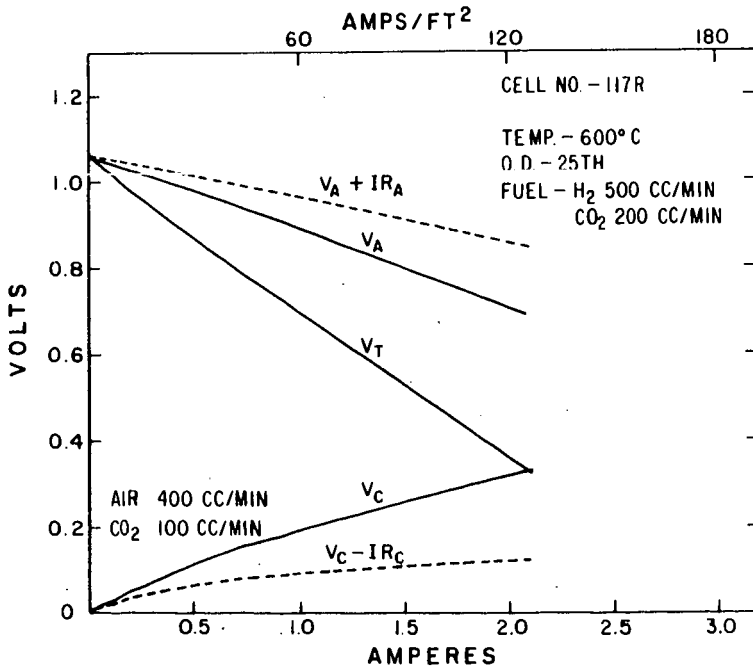


Fig. 4 Typical polarization curves for a cell and individual electrodes operating on a simulated reformed hydrocarbon and air- CO_2

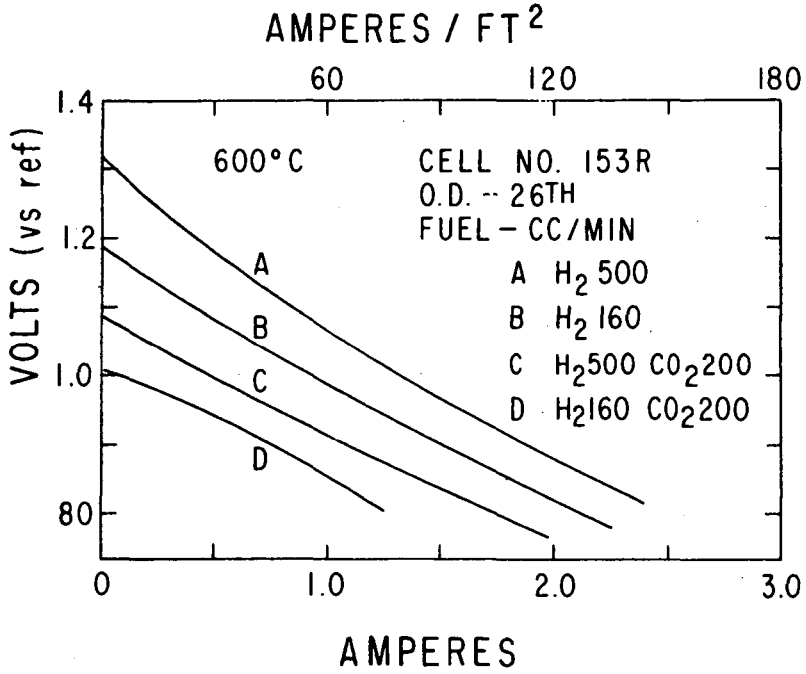


Fig. 5 Anode polarization curves corrected for ohmic polarization. Data obtained from operating cell.

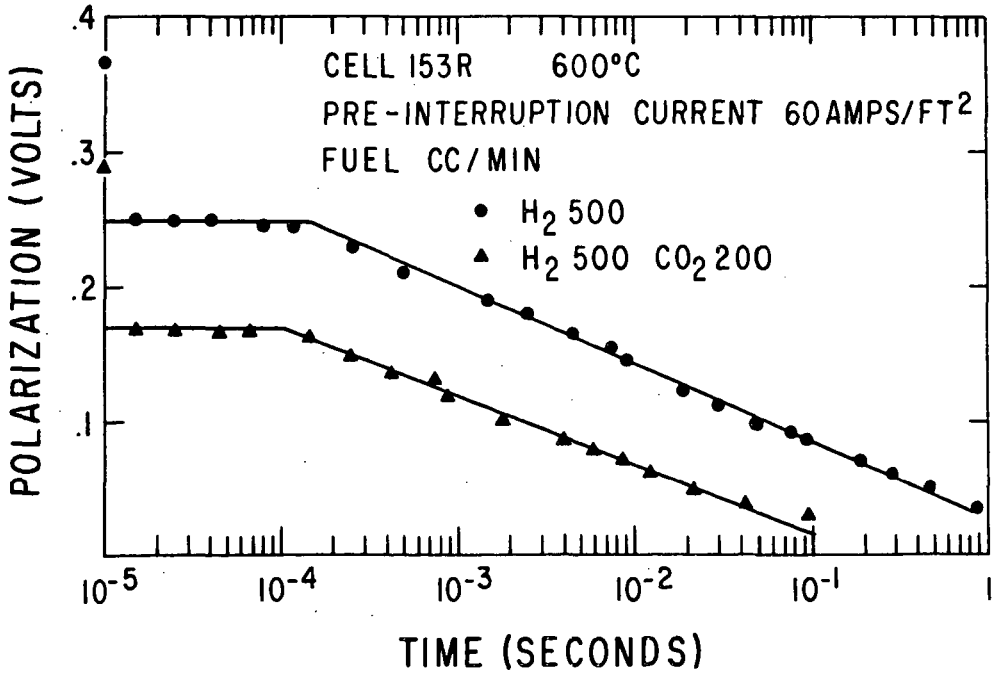


Fig. 6 Anode polarization-time curves after interruption of 1.0 amp.

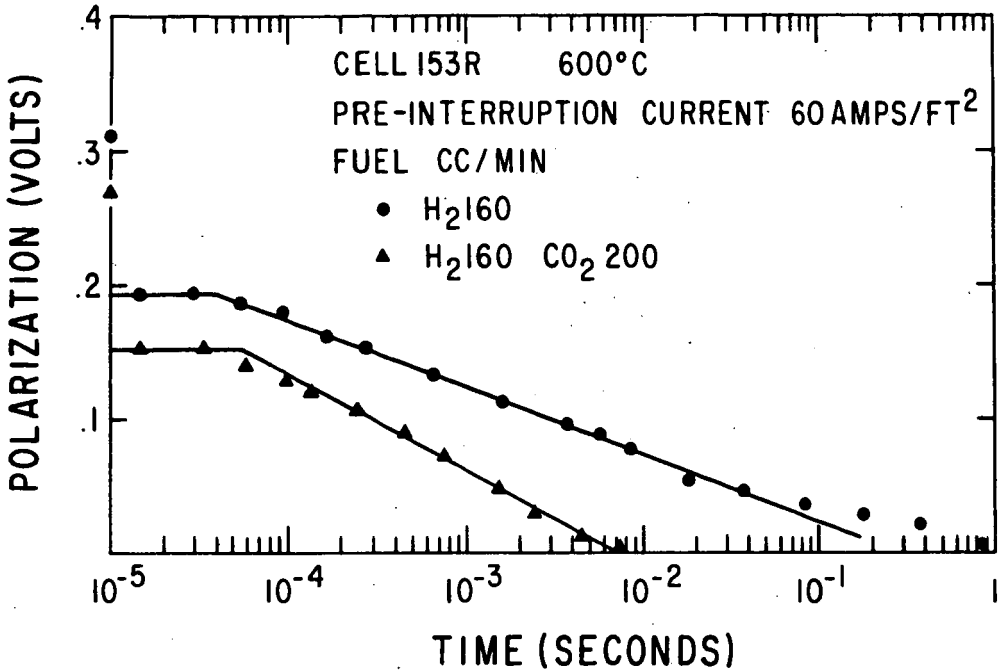


Fig. 7 Anode polarization-time curves after interruption of 1.0 amp.

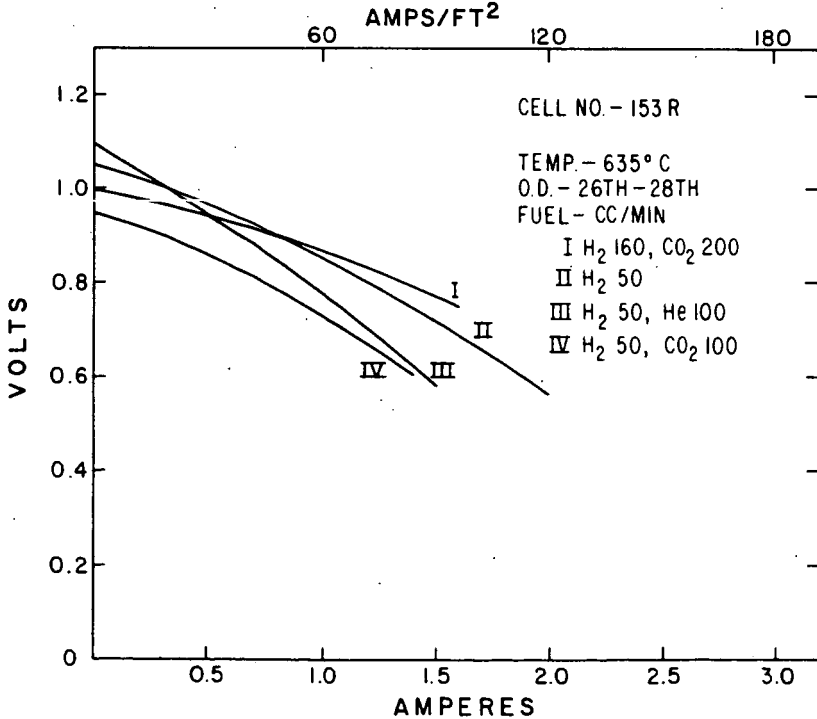


Fig. 8 Anode polarization curves corrected for ohmic polarization. Data obtained from operating cell varying fuel composition and flow rate.

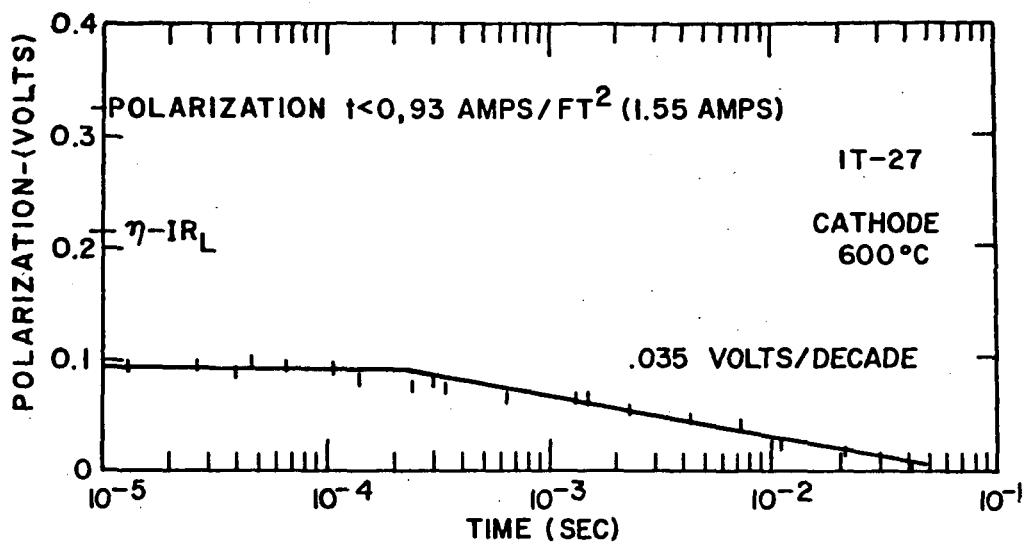


Fig. 9 Cathode polarization-time curve for typical cathode after interruption of 1.55 amps.

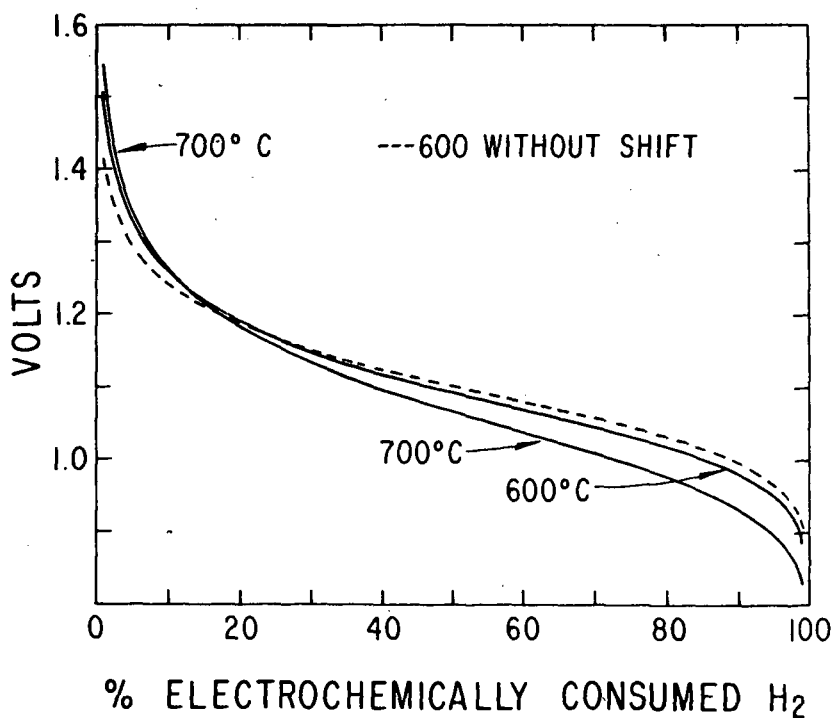


Fig. 10 Calculated potential-fuel consumption curves for anodes

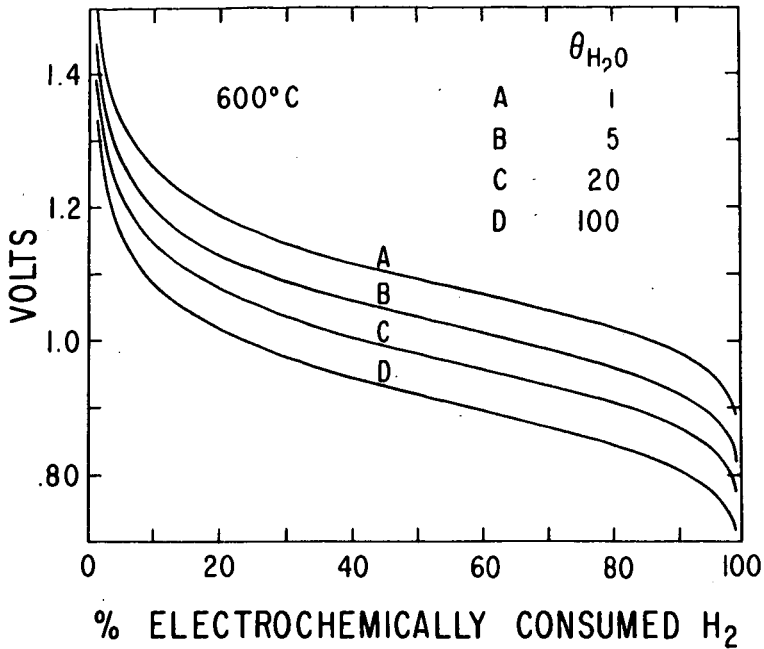


Fig. 11. Calculated potential-fuel composition curves for anodes assuming various ratio of H₂O:H₂ adsorption

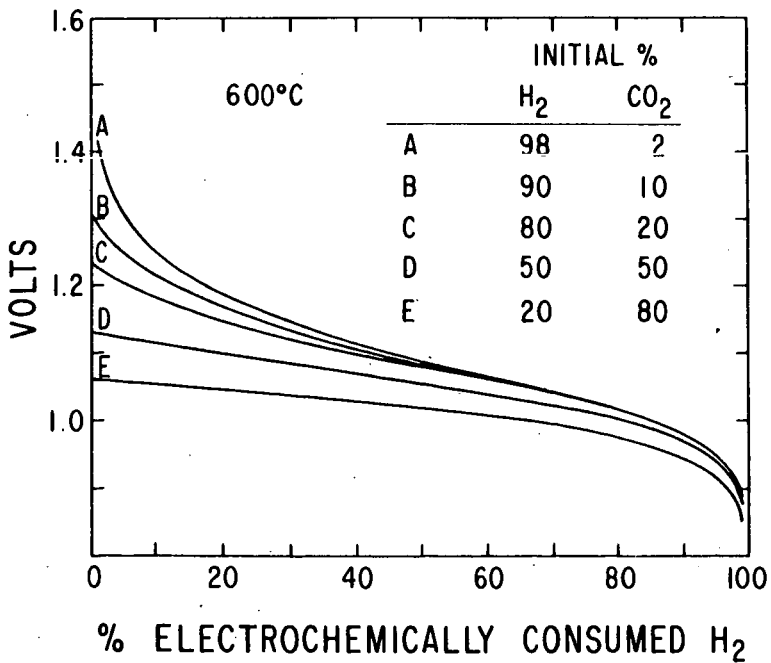


Fig. 12 Calculated potential-fuel composition curves for anodes varying composition of starting fuel

Further Developments in High-Temperature Natural Gas Fuel Cells

B. S. Baker, L. G. Marianowski
John Meek and H. R. Linden

Institute of Gas Technology
Chicago 16, Illinois

INTRODUCTION

Fuel cell research at the Institute of Gas Technology began in 1959. Using the work done by Broers (2) on the molten carbonate high-temperature fuel cell as a starting point, IGT has concentrated a large portion of its effort on further development of this system from both a fundamental and an engineering viewpoint. Background material and earlier work from this laboratory, through 1960, have been described elsewhere (11).

During the past 2 years the research and development effort of IGT on a natural gas operated, molten carbonate fuel cell system has been in five areas:

- Electrode evaluation and design
- Paste electrolyte development
- Natural gas reforming
- Battery design and scaleup
- Economic evaluation

In this paper the results in these five areas are summarized. All five areas are strongly interrelated and interdependent, and each combination of electrode, electrolyte, reformer, and battery design gives rise to different fundamental requirements for one or more of the individual components. Any given design will affect the economics of the fuel cell system.

In his economic analysis of domestic fuel cell systems, von Fredersdorff (12) has indicated some of the limitations on fuel cell hardware costs. It has been an important part of this research to establish the feasibility of economic hardware for natural gas operation.

ELECTRODE EVALUATION AND DESIGN

Almost all fuel cell electrodes must possess the same general characteristics of high electrocatalytic activity, good mass transport properties, and long-term physical and chemical stability. In the high-temperature molten carbonate system, the activity criterion is alleviated by the elevated operating temperatures, and the mass transfer problems are not unlike those associated with other types of fuel cells. However, the stability problems are in many respects unique because of the properties of the molten carbonate electrolyte and the operating temperatures.

At IGT a number of different types of electrodes have been studied from both a structural and chemical viewpoint in the last 2 years. Metal foil, thin film, sintered powder, and sintered fiber structures have been explored. Materials used in these investigations have been platinum, nickel, silver, palladium and alloys of silver and palladium.

Metal Foil Electrodes

Hydrogen permeable metal foils have been used for some time in conjunc-

tion with commercial hydrogen purification processes, and much technical literature on these materials is available (4,7). IGT was attracted to the concept of a metal foil anode early in its program as an expedient means for solving two problems associated with the molten carbonate fuel cell, electrode flooding and corrosion. The first foils studied were alloys of palladium and silver, of which typical performance is shown in Figure 1. Complete details of the IGT palladium foil fuel cell have been published (9). Since the anode in this cell is not permeable to the reaction products, the mass transport processes are very different from those associated with more conventional molten carbonate fuel cells. A variety of experiments indicated that the overall anode reaction is strongly limited by the diffusion of reaction products, carbon dioxide and water, away from the electrode. The fact that diffusion of hydrogen through the foil did not appear to be limiting led to experiments with pure palladium foils of poorer hydrogen diffusion characteristics. Somewhat better cell performance was observed (Figure 1), although a direct comparison could not be made, because improvements in other cell components were incorporated at the same time.

Silver-palladium diffusion foil electrodes have operated continuously under 25 ma. per sq. cm. load for over 7 months without apparent damage to the anodes. Unfortunately, these palladium diffusion foil electrodes are too expensive for gas industry use. At present other, less expensive, hydrogen permeable foil electrode materials are being investigated.

Thin Film Electrodes

The use of metal film electrodes is economically attractive, especially in those cases where noble metals are needed. With semisolid electrolyte molten carbonate fuel cells it is possible to use the electrolyte, which at suboperating temperature is a solid, as the support for applying the thin film. Electrodes were applied by vacuum deposition and simple painting techniques. In the latter, the metal to be deposited exists as a finely dispersed particle in an organic binder. All solutions used for the process were commercially available.

The first experiments were directed toward development of a thin film silver cathode. The major anticipated difficulty in this instance was the dissolution of the silver in the electrolyte. Douglas (5), Broers (3) and Janz (8) have discussed this problem. Silver film electrodes (0.001 cm. thick) prepared from commercial silver paints have performed over 4000 hours at 600°C. without apparent loss in performance although some dissolution of silver in the electrolyte did occur. The relatively long lifetime is attributed to the fact that the cells were operated at lower temperatures than those used in the work of others and were continuously under load; the oxygen electrode is always cathodically polarized, suppressing the dissolution reaction. Moreover, cathodes were not physically flooded to any significant extent.

The successes with the silver film cathodes led to experimentation with other metals in an effort to develop a similar type of anode structure. Little success was achieved in this area primarily because of electrode flooding. Results of various experiments are summarized in Table I. The best results were achieved with vacuum-deposited palladium; however, the cell lifetimes obtained were only about 300 hours.

Since performance decreases with load, anode flooding could have been caused either by carbonate ion transport, or by drag forces exerted on the electrolyte by the escaping reaction products. However, the reaction products do not cause cathode flooding when they are forced to escape through a film cathode (by using a foil anode, which is impermeable to the reaction products). Hence, flooding must be associated with the directional character of ionic transport phenomena. A more detailed investigation of these effects is now in progress.

Sintered Metal Electrodes

Two types of sintered metal electrodes have been investigated: 1) conventional nickel and silver powder electrodes available from Clevite Corporation; and 2) nickel and palladium fiber metal electrodes obtained from Armour Research Foundation of Illinois Institute of Technology. Early in the study, it was observed that similar performances were obtained from bulk sintered silver and silver film cathodes, and further research with the former was abandoned in favor of the more economic silver film electrode.

The high cost of palladium foil anodes indicated that a new look at non-noble metals was required. Early IGT attempts to use sintered nickel powder, described elsewhere (11), indicated that severe corrosion problems existed. The most serious difficulty arises from direct contact of the anode with the oxygen from the cathode because of air leakage through the electrolyte. A second problem arises when the anode is operated at polarization conditions such that electrochemical consumption of the nickel is possible. At 600°C., this polarization value is about 200 millivolts below the hydrogen consumption potential. This phenomenon has been discussed recently in some detail by Broers (3) for nickel and iron electrodes, and by Bloch (1) for these and other electrode materials. The most recent IGT experiments with nickel metal electrodes and improved electrolyte structures have been operated at 500°C. over 1500 hours at current densities between 15 and 25 ma. per sq. cm., without serious nickel corrosion. The lower operating temperature alleviates the direct chemical corrosion problem, but reduces the polarization zone in which the anode can be safely operated.

In order to determine the effect of electrode structure on cell performance, a number of recent experiments with sintered fiber metal electrodes have been made. Typical results comparing sintered powder and fiber metal electrodes are shown in Figure 2. So far, performance of fiber metal electrodes seems inferior to that of the sintered powder types. However, the possibilities of fiber metal structures have been only superficially explored, and more extensive research is now in progress.

The conclusions concerning electrode development are:

- ▶ Hydrogen permeable palladium-silver metal foil electrodes can be used for long periods of time (over 7 months) without apparent deterioration.
- ▶ Thin film silver cathodes, at 600°C., are relatively stable and make excellent low-cost structures for the molten-carbonate type fuel cell.
- ▶ Thin film anode structures are unstable, becoming rapidly flooded in proportion to the current drain on the cell.
- ▶ Sintered powder nickel anodes can be operated for at least 1500 hours without appreciable corrosion under the proper conditions.

PASTE ELECTROLYTE DEVELOPMENT

In molten carbonate fuel cells, the electrolyte can exist: 1) as a free liquid between appropriate electrode structures; 2) contained in a presintered porous inert matrix; 3) mixed with an inert powder to form a pasty structure above the melting point of the carbonate mixture. Because of technological problems associated with sealing, stability, contacting, and fabrication techniques, the first two approaches have been abandoned in favor of the paste electrolyte.

Paste electrolytes for the molten carbonate fuel cells can be prepared by cold-pressing, hot-pressing, hot injection or extrusion, and other special techniques, some of which have been described in some detail by other workers (10). In this paper, only variations in cold-pressing techniques will be explored, since these constituted the bulk of the IGT effort.

Binary and ternary eutectics of sodium-lithium carbonates and sodium-lithium-potassium carbonates were used in all experiments. The ternary

eutectic melts at about 100°C. below the binary mixture, and thus allows the construction of lower temperature cells. Typical 1000-cycle cell resistivities of 9 and 7 ohm-cm. were obtained for 50 weight % mixtures of ternary carbonate in magnesium oxide at 500° and 600°C., respectively. Thirty weight % mixtures of binary carbonate eutectic exhibited cell resistivities in the neighborhood of 11 ohm-cm. at 600°C. For the most part, cell resistances were dependent only on electrolyte mixtures and not on the electrode structure employed.

The electrolyte matrix employed was determined by the anode structure. In the case of the hydrogen-permeable foil anodes, 30 weight % molten carbonate disks were prepared with 70% coarsely grained magnesium oxide as inert constituent. This cold-pressed disk had a density of 70% of the theoretical after firing. Denser electrolyte compositions showed better open-circuit potential, but under load they polarized more heavily than the 70% density disk. Thus, in the case of foil anodes, where reaction products must escape through the electrolyte via the cathode, densification of electrolyte would be detrimental.

With the sintered metal electrodes, especially those consisting of non-noble metals, densification of the electrolyte is important and increases both lifetime and performance characteristics of the fuel cell. Initial experiments with nickel electrodes and 70% density paste electrolyte exhibited lifetimes of the order of 100 hours. By increasing the density of paste electrolyte to about 80% of the theoretical, IGT has achieved lifetimes of 1500 hours. Increasing electrolyte density also increases both the load and open circuit potential by about 200 millivolts. Electrolyte densification can be achieved by repeated crushing and grinding procedures if care is taken to avoid metallic contamination. Also, it is advantageous to increase the total carbonate content of the mixture by the use of small grained (less than 1 micron) magnesium oxide, which has a greater melt retention capacity.

Recent experiments, in which cold-pressed and fired disks are heated to within five degrees of the melting point of the carbonate eutectic and then hot-pressed at moderate pressures, indicate that disks with 96% of the theoretical density can be prepared.

The conclusions concerning paste electrolytes are:

- ▶ High-density electrolyte pastes are detrimental to the performance of fuel cells using hydrogen-permeable foil anodes.
- ▶ In all other cases high-density pastes are essential for achieving reasonable cell lifetimes.
- ▶ Cold-pressed disks can achieve a maximum density of about 85% by repetitive crushing and grinding techniques.
- ▶ Hot-pressing previously cold-pressed disks at a few degrees below the melting point causes significant densification to take place.

NATURAL GAS REFORMING

Four modes of operation are theoretically possible for natural gas utilization in a molten carbonate fuel cell system:

- 1) Direct electrochemical oxidation of methane.
- 2) In situ reforming of methane and steam on the anode, and electrochemical oxidation of the carbon monoxide and hydrogen thus formed.
- 3) In situ catalytic reforming of methane and steam in the anode chamber and electrochemical oxidation of the carbon monoxide and hydrogen thus formed.

4) External catalytic reforming of methane and steam, followed by electrochemical oxidation of hydrogen or hydrogen-carbon monoxide mixtures in the fuel cell.

Scheme 1 has been found unacceptable because of the electrochemical inertness of methane even at relatively high temperatures and the occurrence of carbon deposition when methane alone is present at these temperatures.

Scheme 2 is undesirable because the temperature required for the reforming (750°C.) is higher than that needed for electrochemical oxidation of hydrogen. This places an undesirable high operational temperature handicap on the fuel cell. Moreover, the presence of excess steam reduces the electrode performance (6). Finally, it is very difficult to design an electrode which is effective both as an electrochemical element and as a reforming catalyst.

Scheme 3 is relatively unexplored but would be characterized by the same drawbacks as Scheme 2, except that the electrode would not be required to function both electrochemically and as a reforming catalyst.

Scheme 4 has been adopted by IGT as the most feasible, since it permits separate optimization of fuel cell and reformer units. It permits accurate control of the composition of the input gas to the fuel cell and allows the cell to be operated effectively at substantially lower temperatures (between 500° and 600°C.). The lower operating temperatures for the fuel cell enhance electrode stability and the lifetimes of the materials of construction.

The drawback of separate fuel cell and reformer units is a reduction of the overall system efficiency in the case where the fuel cell is operated at a lower temperature than the reformer. Theoretically, this reduction can be shown to be about 10% for a reformer operating at 750°C. and a fuel cell operating at 500°C. The loss in efficiency for the dual temperature system arises from the unavailability of the low-quality waste heat of the fuel cell for supply of the heat of reaction for the reforming operation. In actual practice other losses might be incurred when two units are used because of the inefficiency of the heat transfer processes. However, since the 10% reduction figure quoted above is based on the comparison of maximum theoretical efficiencies for the two systems and since there is a large amount of unused low-quality heat (500°C.) in the dual-temperature model, it is more likely that an efficiency closer to the theoretical maximum can be achieved with this model.

The higher voltage efficiencies experimentally achieved with the reformed mixture more than compensate for the engineering and theoretical losses resulting from the dual system mode of operation. In Figure 3 a comparison is shown between the performances of a fuel cell at 500°C., supplied with externally reformed natural gas, and of a fuel cell at 750°C. with the equivalent methane-to-water ratio for in situ reforming. Also shown in this figure is the experimentally observed ratio of efficiencies of the two systems. This ratio was computed from the products of the experimental Faradaic efficiency and voltage efficiency of the two cells. Thermal inefficiency is not considered in this figure. It is significant that with external reforming, performance in terms of efficiency is almost 2.5 times greater at practical current densities.

Reformer design for natural gas is well known, and many excellent reforming catalysts are commercially available. The costs of these catalysts and the corresponding reformer units are only a small fraction of fuel cell hardware costs. The incorporation of the reformer into the natural gas fuel cell system is readily achieved.

It may be concluded that the use of external reforming with natural gas molten carbonate fuel cells seems justified on the basis of the improved experimental performance of this system over in situ reforming, as well as the more moderate operating temperatures it imposes on the fuel cell.

BATTERY DESIGN AND SCALEUP

The progress made in other areas of the molten carbonate fuel cell development indicated that some attention should be given to the problems associated with battery design and scaleup. The first step in the process was the assembly of a battery consisting of several small laboratory cells in series (Figure 4). No difficulties were encountered in this relatively simple transition, and next the more formidable problem of scaleup was attacked. The long-life performance of the silver film cathode and palladium-silver foil anode indicated that these particular compounds were the best adapted for scaleup techniques. The greatest problems were expected with increasing the size of the electrolyte disks from the 3-inch diameter laboratory disks to the 6-inch square dimensions chosen for the battery development program. In order to achieve the same electrolyte properties developed with the smaller cells a one million-pound press was required for the paste electrolyte fabrication. Special die fixtures were designed, and the larger electrolyte bodies were fabricated without difficulty.

Components for the new battery are shown in Figure 5, and a ten-cell battery built from the components is shown in Figure 6. The battery is assembled at room temperature and moderately tightened. It is then heated to 600°C., and the final sealing is accomplished when the paste electrolyte is in a semisolid state. The battery can now be thermally cycled between ambient and operating temperatures without damage or further adjustment. A 100% leak-tight assembly has not yet been achieved, but this represents only a slight loss in fuel efficiency. Complete sealing is anticipated in future designs.

As seen in Figure 5, the cathode compartment is open to the atmosphere. This design feature is essential for any practical molten carbonate fuel cell system. The mode of operation of the battery is a direct carryover from the laboratory models and is shown schematically in Figure 7. A portion of the incoming methane is burned directly in a burner underneath the fuel cell battery. Another portion of the methane is passed through activated carbon to remove sulfur compounds and, after steam addition, through the reformer containing commercial nickel catalyst.

The hot flue gas, containing excess air, carbon dioxide and water, rises by natural convection; in passing by the reformer, the flue gas drops in temperature to sustain the endothermic reforming reaction. The flue gas then enters the open cathode chambers, rises through the fuel cell, and supplies the oxygen and carbon dioxide needed to maintain the cathodic reaction. The water vapor in the flue gas has no adverse effect on the fuel cell reaction. To conserve fuel and carbon dioxide, the spent anode gases should be recycled to the burner.

Battery performance is shown in Figure 8. Faradaic efficiencies as high as 40% have been achieved in this apparatus although complete system efficiencies, as might be expected in such a small battery, are very low.

Some conclusions arrived at in battery design are:

- ▶ Operation of a multiple-cell battery molten carbonate fuel cell has been demonstrated.
- ▶ A mode of operation comprising a gas burner-reformer-open cathode fuel cell has been defined.

ECONOMIC EVALUATION

In order to evaluate the economics of a fuel cell system both its application and design must be considered. Von Fredersdorff (12) has outlined the economics of the domestic fuel cell application in considerable detail. In this section a brief description of the economics of fuel cell hardware as a function of its operating characteristics will be presented. The cost of fuel cell hardware depends on the cost of materials and cost of manufacturing.

Since manufacturing costs are difficult to estimate at this early stage of development, only the material costs for the most recent IGT design will be evaluated. The design model is similar to that described in the last section, with two significant changes. Nickel electrodes are used in place of the expensive silver-palladium foil and a parallel, dual element, geometry is chosen in place of the bipolar flange. The effect of this last change is to eliminate the flange completely from the fuel cell design, using the electrode itself as a structural element.

In Table II, the itemized cost of the various materials used in the IGT battery are given. These costs, plus the costs of fittings and an additional 10% of the total to cover miscellaneous materials, were used to compute the curves in Figure 9. In this figure battery material costs are plotted as a function of current density at constant voltage for various single-cell potentials. The dashed line represents the IGT fuel cell performance curve. Since fully manufactured batteries at \$300 per kilowatt are reasonable for domestic fuel cell applications, an increase in cell performance by a factor of about two is necessary.

It may be concluded that only moderate improvements in voltage-current characteristics of the molten carbonate fuel cells are required to bring them within the economic framework of domestic applications.

ACKNOWLEDGMENT

The Institute of Gas Technology work on development of high-temperature fuel cells discussed in this paper was sponsored by the General Research Planning Committee of the American Gas Association under the Association's PAR (Promotion-Advertising-Research) Plan.

LITERATURE CITED

- (1) Bloch, O. and Degobert, P., Bull. Soc. Chim. de France, 1887-92 (October 1962).
- (2) Broers, G. H. J., Ph.D. Thesis, University of Amsterdam, The Netherlands (1958).
- (3) Broers, G. H. J. and Schenke, M., "High Temperature Galvanic Fuel Cells," Final Report, File No. DA-91-591-EVC-1701 (April 1962).
- (4) de Rosset, A. J., Ind. Eng. Chem. 52, 525-28 (1960).
- (5) Douglas, D. L., "Molten Alkali Carbonate Cells with Gas Diffusion Electrodes," in Young, G. J., ed., "Fuel Cells," Vol. 1, 129-49. New York: Reinhold Publ. Corp. (1960).
- (6) Eisenberg, M. and Baker, B. S., Electrochemical Society Fall Meeting, Boston, Mass. (Sept. 16-20, 1962), Extended Abstract No. 46, Battery Division.
- (7) Hurlbert, R. C. and Konecny, J. O., J. Chem. Phys. 34, 655-58 (1961).
- (8) Janz, G. J. and Neuenschwander, E., "Corrosion Studies in Molten Alkali Carbonates." Part I "Silver Metal," Technical Report, No. 16, AD-289005. Washington, D.C.: Office of Technical Services (1962).
- (9) Marianowski, L. G., Meek, J., Shultz, E. B., Jr. and Baker, B. S., Paper presented at the 17th Annual Power Sources Conference, Atlantic City (May 21-23, 1963).
- (10) Schenke, M. and Broers, G. H. J., "High Temperature Galvanic Fuel Cells," Final Report, File No. DA-91-591-EUC-1398 (February 1961).

- (11) Shultz, E. B., Jr., Vorres, R. S., Marianowski, L. G. and Linden, H. R., "High Temperature Methane Fuel Cells," in Young, G. J., ed., "Fuel Cells," Vol. II, 24-36. New York: Reinhold Publ. Corp. (1963).
- (12) von Fredersdorff, C. G., "An Outline of the Economics of a Domestic Fuel Cell System," in Young, G. J., ed., "Fuel Cells," Vol. II, 50-67. New York: Reinhold Publ. Corp. (1963).

Table I.-PERFORMANCE OF POROUS NOBLE METAL ANODE FILMS

<u>Anode Material</u>	<u>Preparation Method</u>	<u>Performance Decay,*</u> hr.		<u>Cell Lifetime, hr.</u>
		<u>90%</u>	<u>75%</u>	
Pt	Paint	15	85	108
Ag-Pt	Paint	4	17	41
Pt	Paint	40	57	66
Pd	Paint	26	60	138
Pd	Paint	17	42	95
Pd	Paint	15	45	72
Pd	Vacuum Deposited	100	Not Determined	293

* Time to reach 90% and 75% of initial performance

Table II.-FUEL CELL HARDWARE COSTS

<u>Material</u>	<u>Cost</u>
Electrolyte paste - 100 mil thick ($MgO-Na_2CO_3-K_2CO_3-Li_2CO_3$)	\$ 0.37/sq. ft.
Nickel anode - 25 mil thick	0.14/sq. ft.
Silver cathode - 0.4 mil thick	0.43/sq. ft.
Carbon steel anode current collector - 18 GA.	0.16/sq. ft.
Stainless steel cathode current collector - 18 GA.	1.18/sq. ft.
Stainless steel frame - 125 mil thick	0.14/ft.

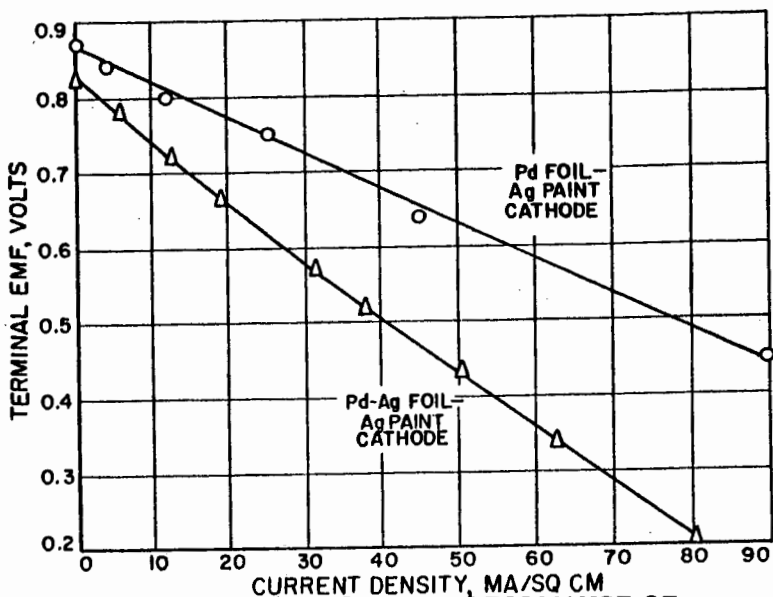


Fig. 1.-COMPARISON OF PERFORMANCE OF PURE PALLADIUM AND PALLADIUM-SILVER ANODE HIGH-TEMPERATURE FUEL CELLS AT 600°C

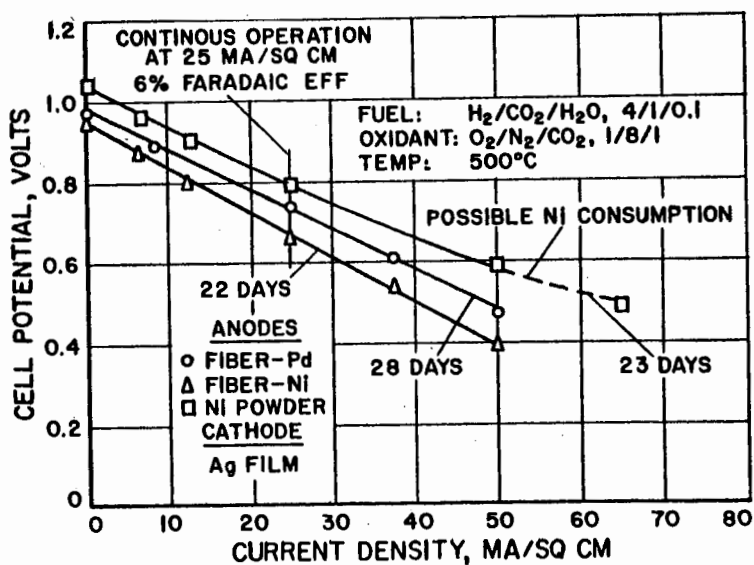


Fig. 2.-EFFECT OF DIFFERENT ANODES ON HIGH-TEMPERATURE FUEL CELL PERFORMANCE

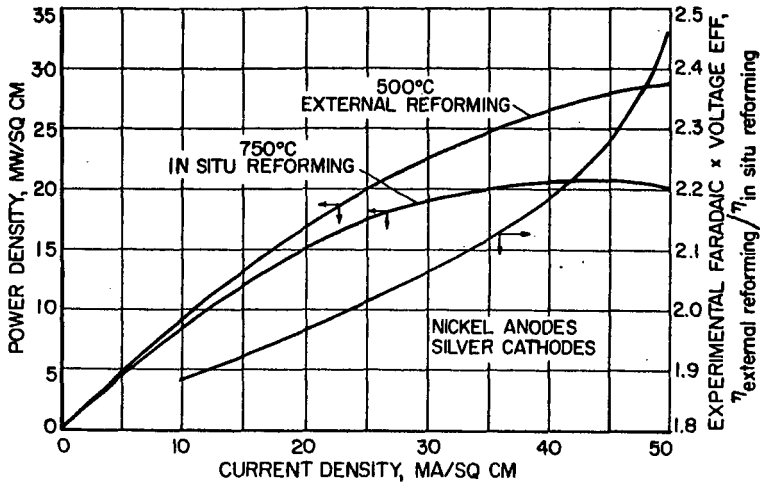


Fig. 3.- COMPARISON BETWEEN EXTERNAL AND IN SITU REFORMING ON FUEL CELL PERFORMANCE

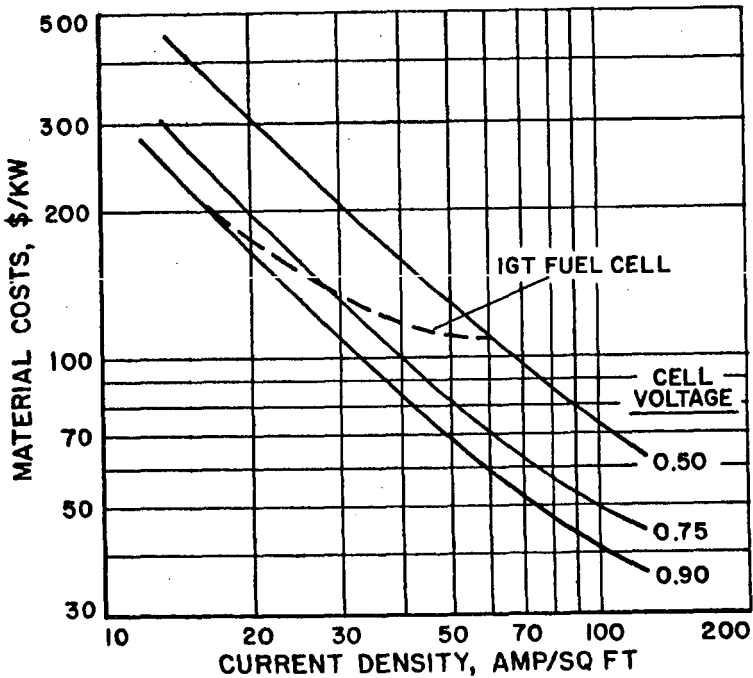


Fig. 9.- ECONOMICS OF IGT HIGH-TEMPERATURE MOLTEN CARBONATE FUEL CELL FOR CONSTANT BATTERY VOLTAGE

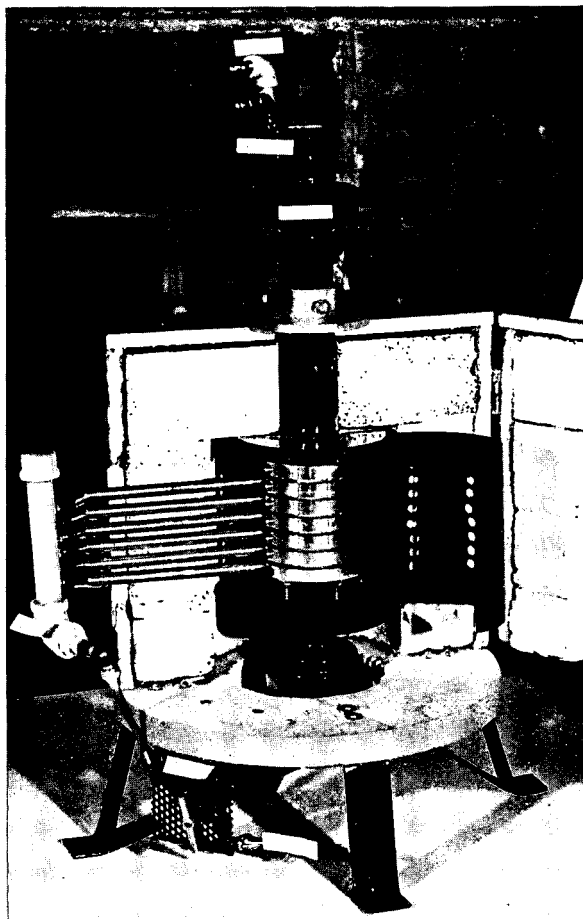


Fig. 4.-LABORATORY SIZE IGT HIGH-TEMPERATURE
FUEL CELL BATTERY

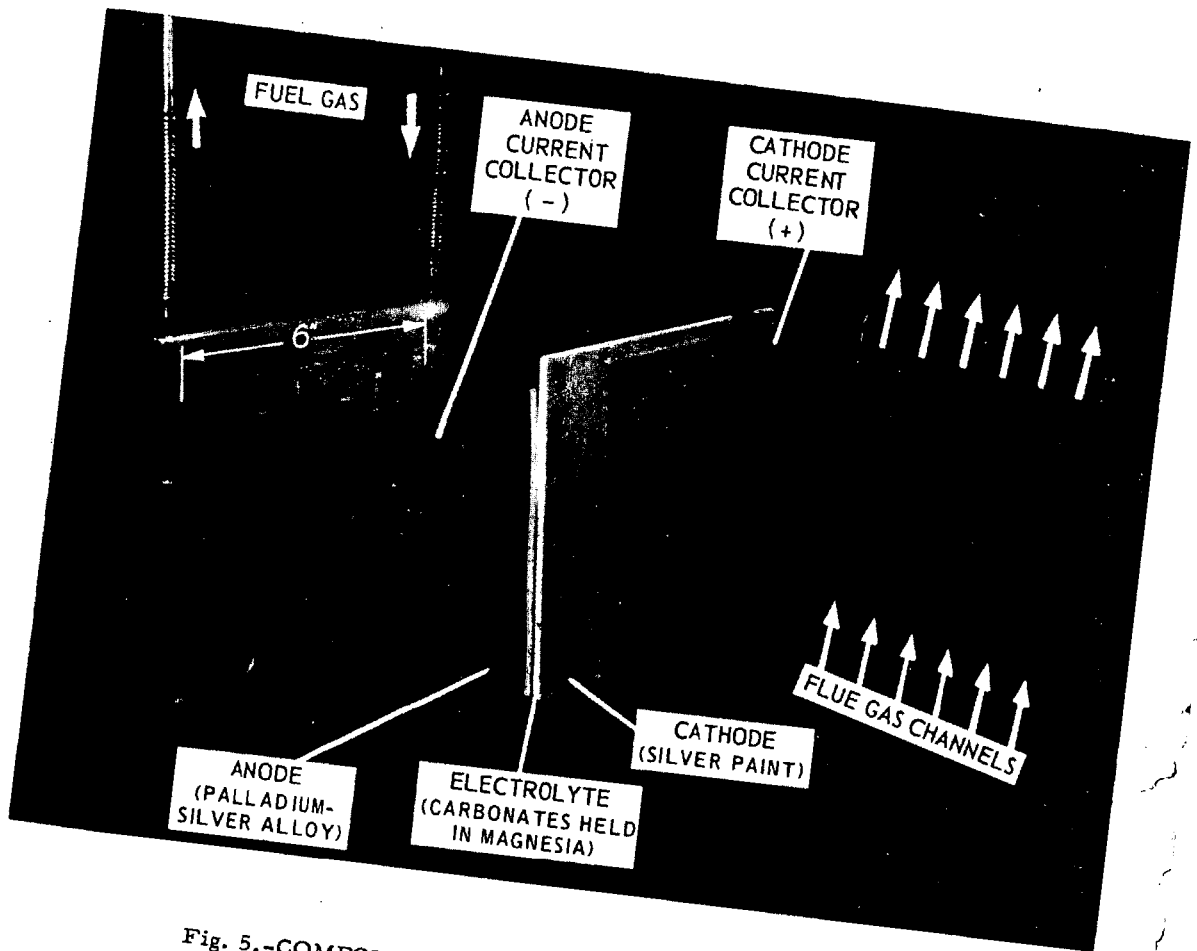


Fig. 5.-COMPONENTS USED IN CONSTRUCTION OF SCALED-UP IGT FUEL CELL BATTERY

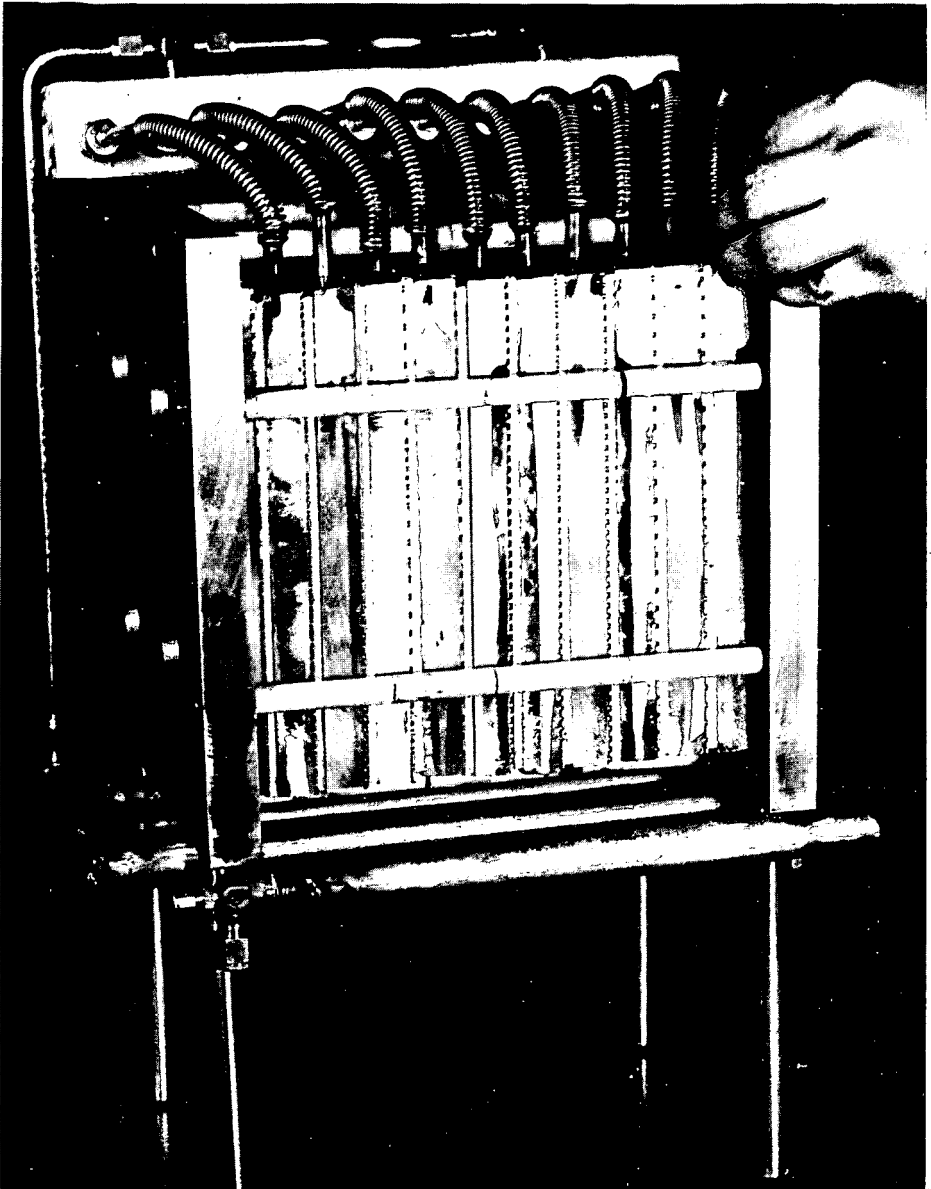


Fig. 6.-IGT HIGH-TEMPERATURE FUEL CELL BATTERY
AND REFORMER

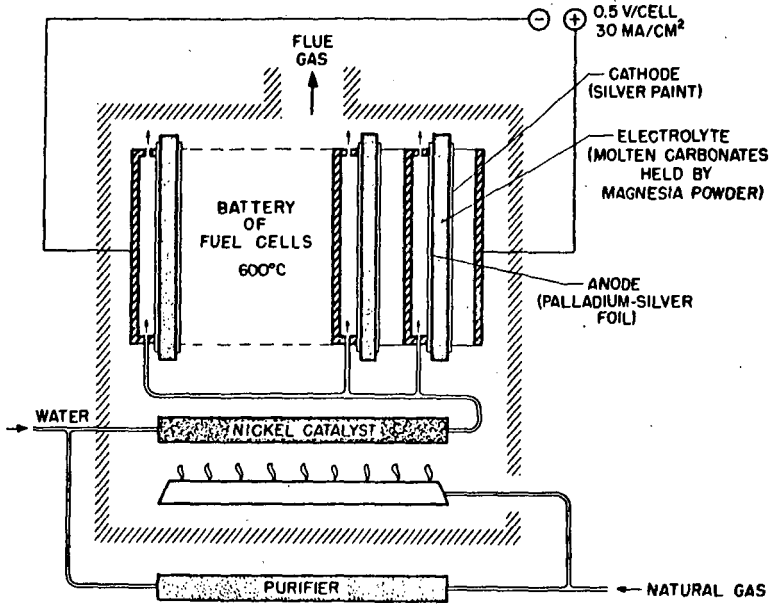


Fig. 7.-SCHEMATIC REPRESENTATION OF IGT HIGH-TEMPERATURE NATURAL GAS FUEL CELL SYSTEM

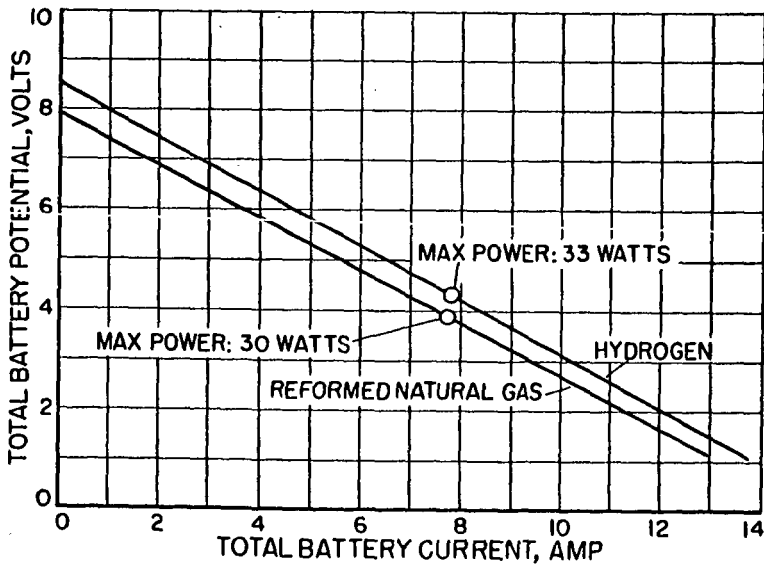


Fig. 8.-PERFORMANCE OF 10-CELL HIGH-TEMPERATURE FUEL CELL BATTERY

METHANOL FUEL CELLS WITH DISSOLVED OXIDANTS

D. B. Boies and A. Dravnieks

IIT Research Institute

(formerly Armour Research Foundation
of Illinois Institute of Technology)
Chicago, Illinois

I. INTRODUCTION

Among the desired characteristics of both fuel and oxidant for fuel cells are storability and high energy content per unit weight. The weight must include that of the container. Therefore, the best high-energy fuel and oxidant -- hydrogen and oxygen -- lose much of their advantage in transportable cells, especially if oxygen cannot be taken directly from the air. One of the most easily stored fuels is methanol, and recently the authors developed high-current-density electrodes for the electrochemical oxidation of methanol in alkaline solution (1). Since methanol is soluble in the electrolyte, no multiple porosity is required in the electrode and the active layer may be only 0.01-0.02 cm thick. Thus, as far as fuel is concerned, compact cells are feasible. Matching oxidant electrodes are, however, needed.

The customary porous carbon electrode that is operated with oxygen or air as the oxidant performs very poorly in the methanol-containing caustic since its waterproofing fails in the presence of methanol. In some applications, air may not be available at all and then the weight of bottled oxygen is a handicap; for instance, in the regular large-size oxygen cylinder, one gram equivalent (8 g) of oxygen requires an additional 80 g in the cylinder weight.

Even though all other oxidants have higher equivalent weights, many can be easily stored in solid, dissolved, or liquid form in light containers. Some also have higher oxidizing potentials. Oxidants supplied in dissolved form to the fuel-cell cathode should require only a thin porous layer of an electrocatalyst and no porous bulk electrode in addition to this layer. Thus, compact fuel cells should be possible if a sufficiently electrochemically active alkaline oxidant/electrode system were available.

To find an appropriate system, several oxidants and electrodes were investigated as half-cells. Complete methanol fuel cells were constructed with the most promising oxidant -- chlorite.

II. SELECTION OF OXIDANTS: THEORETICAL

Following requirements were formulated for the selection of soluble oxidants:

- (1) high electrode potential to provide for high cell potential when coupled with the methanol electrode.
- (2) low weight per ampere-hour
- (3) storability in concentrated form
- (4) freedom from obnoxious fumes
- (5) solubility of reduction products
- (6) lack of gas formation in reduction
- (7) electrochemical reactivity
- (8) low polarization.

The first six requirements can be checked by using literature data. The high electrode potential expected may not be realized when the electrode is not a good electrocatalyst. Hence the reactivity and low polarization requirements need experimental study.

Table I lists soluble oxidants with high Gibbs electrode potentials, V° .^{*} The weights are calculated on the basis of sodium salts of the corresponding anions, except for HO_2^- in which H_2O_2 is the oxidant. Since water is generated at the anode, the weight of water is not included in the calculation. Data for oxygen, with the theoretical V° for the four-electron process and for the more realistic two-electron Berl's reaction, are also listed. For comparison, data are shown for Ag_2O , the best solid oxidant used in commercial cells. Oxygen needs a container, and hence the weight per ampere-hour would actually be several times higher. Hypochlorite cannot be stored except in dilute form or as $\text{CaCl}_2 \cdot (\text{ClO})$; hence its weight index is much poorer than shown. Storage of hydrogen peroxide in concentrated form under normal conditions is undesirable. With the usual easily storable 30% peroxide solution, the weight index is much poorer.

Table I indicates that selection of soluble oxidants of an inorganic nature is rather limited. The open-circuit potential for our methanol electrodes in 5 N KOH is -0.79 volt. Therefore, iodate with $V^\circ = +0.26$ is the last that may be considered in the descending potential series if the complete cell must have a voltage of one volt or higher.

III. SELECTION OF OXIDANTS: EXPERIMENTAL

Although the theoretical electrode potentials for a given oxidant can be high, active low-polarization electrodes for the corresponding reactions may not exist. Soluble oxidants of Table I were studied experimentally in half-cell arrangements. Conventional half-cell polarization techniques, similar to those which have been reported previously, were used.

Polarization characteristics were measured potentiostatically by observing current densities that could be obtained at electronically controlled, preselected, polarized potentials.

* Sign convention recommended by Pitzer and Brewer in 1961 edition of Lewis and Randall "Thermodynamics," p. 356; cf. de Bethune, J. Electrochem. Soc. 102, 288C (1955).

Table I

SOLUBLE OXIDANTS FOR FUEL-CELL CATHODE IN ALKALINE SOLUTION

Calculated from Latimer's
"Oxidation States of Elements," Prentice Hall, 1952

Reaction	V ^o , Standard Electrode Potential Vs S.H.E.	Weight Relations	
		amp-hr/lb	gr/amp-hr
$\text{ClO}^- + \text{H}_2\text{O} + 2e \rightarrow \text{Cl}^- + 2\text{OH}^-$	0.89	325	1.4
$\text{HO}_2^- + \text{H}_2\text{O} + 2e \rightarrow 3\text{OH}^-$	0.88	700 210	0.65 2.15 for 30% soln.
$\text{ClO}_2^- + 2\text{H}_2\text{O} + 4e \rightarrow \text{Cl}^- + 4\text{OH}^-$	0.77	525	0.86
$\text{ClO}_3^- + 3\text{H}_2\text{O} + 6e \rightarrow \text{Cl}^- + 6\text{OH}^-$	0.62	670	0.67
$\text{BrO}_3^- + 3\text{H}_2\text{O} + 6e \rightarrow \text{Br}^- + 6\text{OH}^-$	0.61	470	0.98
$\text{ClO}_4^- + 4\text{H}_2\text{O} + 8e \rightarrow \text{Cl}^- + 8\text{OH}^-$	0.55	780	0.59
$\text{IO}_3^- + 3\text{H}_2\text{O} + 6e \rightarrow \text{I}^- + 6\text{OH}^-$	0.26	360	1.26
$\text{O}_2 + 2\text{H}_2\text{O} + 4e \rightarrow \text{OH}^-$	0.4	1500	0.3
$\text{O}_2 + \text{H}_2\text{O} + 2e \rightarrow \text{OH}^- + \text{HO}_2^-$	-0.08	1500	0.3
$2\text{HO}_2^- \rightarrow 2\text{OH}^- + \text{O}_2$			
$\text{AgO} + \text{H}_2\text{O} + 2e \rightarrow \text{Ag} + 2\text{OH}^-$	0.45	200	2.34

Electrodes included carbon and flame-sprayed thin layers of Raney nickel with or without further platinizing, flame sprayed Raney nickel-silver, and silver. The aluminum-rich phase of alloys was extracted by electrochemical leaching. The platinized Raney nickel corresponded to the high-performance methanol electrodes (1). The bases for the sprayed layers were either nickel sheets or porous sintered-nickel powder plates. Representative results are shown in Table II. None of the oxidants reached the theoretical electrode potentials. Only chlorite and hydrogen peroxide supplied practical current densities at acceptable polarization. Because the chlorite is easily stored and handled, this chemical was selected for further study.

IV. EXPLORATION OF CHLORITE ELECTRODES

Open-circuit potentials and polarization characteristics of flame-sprayed and other electrodes were measured in alkaline chlorite solutions. The effects of chlorite concentration and temperature were studied at the most promising electrodes, flame-sprayed silver, and flame-sprayed Raney nickel-silver. Representative data are summarized in Table II and Figure 1.

The highest values of the open-circuit potential of the chlorite electrode were +0.27 to +0.30 volt, much lower than the theoretical value of +0.77 (Table I). The theoretical value for the $\text{Ag}_2\text{O}/\text{Ag}$

Table II

EXPERIMENTAL EVALUATION OF OXIDANTS

Temperature, 23°C
Electrolyte, 5 N KOH

Oxidant	NaClO	NaClO	H ₂ O ₂	NaClO ₂	NaClO ₃	KBrO ₃	NaClO ₄	KIO ₄
Concentration, %	3.8	3.8	3.0	3.0	3.0	5.0	3.0	3.0
Open-Circuit Potential, volts vs SHE	0.48	0.29	0.10	0.29	0.28	0.28	0.15	0.22
Electrode Surface	Carbon	Raney Ni-Ag	Sprayed Ag	Sprayed Ag	Raney Ni-Ag	Raney Ni-Ag	Raney Ni-Ag	Raney Ni-Ag
Current Density, ma/sq cm	1.2							
At + 0.30 volts vs SHE	4.7	41		30		23		
At + 0.20 volts	13.2	55	90	53		27		2.5
At + 0.10 volts	23.0	57	133	83	0.1	28	0.1	7.0
At - 0.00 volts	38.0		140	108	0.2	29	0.1	10.0
At - 0.10 volts			140	137	0.3	30	0.1	
At - 0.20 volts					0.4		0.1	

electrode in 5 N KOH is +0.306; hence, it is likely that the reaction mechanism involves chemical oxidation of silver to Ag_2O by chlorite and electrochemical reduction of Ag_2O . In anodic polarization of the Raney nickel-silver electrode in chlorite solution, heavy currents were accepted with low polarization, apparently with formation of silver oxide. When current was then reversed to begin reduction, approximately equivalent high currents at low polarization could be drawn for a limited time. At continued cathodic polarization, the curves returned to the normal shape of Figure 1. This behavior indirectly supports the $\text{Ag}_2\text{O}/\text{Ag}$ mechanism of the alkaline chlorite electrode.

The data in Table III show that the flame-sprayed silver and Raney nickel-silver gave comparable results. However, the silver electrode appeared to be susceptible to poisoning. The performance often fell after a period of time and could only be restored by electrolytic evolution of hydrogen from the surface. The Raney nickel-silver electrodes were not affected in this manner and were, therefore, chosen for the methanol-chlorite full-cell tests.

Since chloride is the end product of chlorite reduction, the effect of this material on the electrode operation was studied. An electrolyte containing 10% sodium chlorite and 20% sodium chloride was tested and at 55°C showed only a slight decrease in performance due to the chloride. However, at 23°C, the solubility limit was exceeded. Some precipitate was formed, and a severe (75%) decrease in performance was noted.

Addition of small amounts of methanol to a chlorite half-cell did not decrease its performance. Chlorite reduced the performance of a methanol half-cell in a manner similar to that previously noted for chloride (1). It is probable that the chlorite is immediately reduced to chloride by the methanol and then acts as such.

V. EXPLORATION OF METHANOL-CHLORITE FUEL CELL

A. Experimental Work

Full-cell tests were conducted with the following conditions:

Fuel:	160 g methanol/liter 270 g KOH/liter
Fuel electrode:	Flame-sprayed Raney nickel, platinized
Oxidant:	370 g NaClO_2 /liter 270 g KOH/liter
Oxidant electrode:	Flame-sprayed Raney nickel-silver
Temperature:	55°C

The fuel and oxidant compartments were 3 mm thick and were separated by a dialysis membrane (D-30, Nalco Chemical Company, Chicago). The fuel and oxidant were circulated through the cell and were heated externally.

The results of a full-cell test are shown in Figure 2. For comparison, the predicted performance based on the combined best methanol

Table III

EXPERIMENTAL EVALUATION OF CHLORITE ELECTRODES

Electrolyte: 10% NaClO₂ in 5 N KOH
 Temperature: 23°C

Electrode	Sprayed Raney Ag-Ni	Sprayed Silver	Platinized Sprayed Raney Ni*	Platinized Platinum*	Carbon
Open-Circuit Potential, volts	0.26	0.27	0.30	0.30	0.10
Current Density, ma/sq cm					
At + 0.20 volts	35	48	1.1	3	
At + 0.10 volts	92	118	6	13	
At 0.00 volts	170	172	25	50	
At - 0.10 volts	280	215	90	104	0.03
At - 0.20 volts		245		200	0.08

* These electrodes are electrochemically active also with methanol.

and chlorite half-cell data is shown. The lower performance of the full cell is probably due to the IR drop in the electrolyte and membrane and possible variations in electrodes. The cell output was 144 ma/sq cm at 0.6 volt.

The efficiency of methanol utilization in this cell was studied in long-term tests. It was found that the number of electrons obtained per methanol molecule approached four at high current densities and fell as current density lowered. This drop is caused by an approximately constant loss of methanol by chemical reaction with the chlorite as a result of diffusion of these across the membrane. At lower current densities this loss became an appreciable part of the total methanol consumption and thus led to a lowered current efficiency for both chlorite and methanol.

B. Weight Projections

The possible utility of the methanol-chlorite cell can be seen from Table IV, in which the output of several types of cells is given in terms of watt-hour/lb. The fuel-cell performance figures are based on the weight of the fuel and containers only. Therefore, the performance figure is a limiting figure approached for long-term use in which the weight of the cell itself becomes small compared with that of the reactants. For short-term, high current-drain applications, the conventional cells occupy a more favorable position than indicated by the table.

Table IV

ENERGY-TO-WEIGHT PROJECTIONS

<u>Conventional Cells</u>	<u>Watt-hour/lb</u>
Lead Storage	10-20
Nickel-Iron (Edison) Storage	15
Silver-Zinc	65
<u>Fuel Cells (weight of reactants and containers only)</u>	
Hydrogen Cell, Air Breathing (hydrogen from sodium borohydride and sulfuric acid)	102
Hydrogen Cell, Air Breathing (hydrogen in light-weight steel container)	70
Methanol Cell - Air Breathing*	300
Methanol Cell - Pressurized Oxygen *	70
Methanol -Chlorite*	140

* Based on 0.7 volt polarized working voltage, 70% current efficiency with 4-electron methanol reaction and with methanol + NaOH as fuel mixture.

It can be seen that the methanol cells show a potential advantage in the weight:energy ratio when compared with the conventional galvanic cells or the hydrogen fuel cells. This advantage exists despite the need for caustic as a fuel component in the alkaline methanol cells. Also compared with cylinder oxygen, chlorite is a more compact form of oxidant. The air-breathing cell is more advantageous on a weight basis but at present suffers from a lower current density.

VI. CONCLUSION

Sodium chlorite has low equivalent weight and favorable electrode potential that combine to make it an interesting oxidant for fuel cell use. It gives useful current densities in alkaline solution at silver-containing electrodes. A methanol-chlorite fuel cell can operate at a current density in excess of 100 ma/sq cm. The easy storability of the fuel and oxidant for such cell results in energy-to-weight ratios that are higher than for cells based on stored gaseous reactants.

VII. ACKNOWLEDGMENT

This work was conducted under a contract with the K W Battery Company and the Joslyn Manufacturing and Supply Company. Their permission to publish this material is gratefully acknowledged. The authors wish to thank Mr. F. Child who performed much of the experimental work.

LITERATURE CITED

- (1) Boies, D. B. and Dravnieks, A., "New High-Performance Methanol Fuel-Cell Electrodes," presented at the Boston meeting of the Electrochemical Society, Sept. 1962. At press.

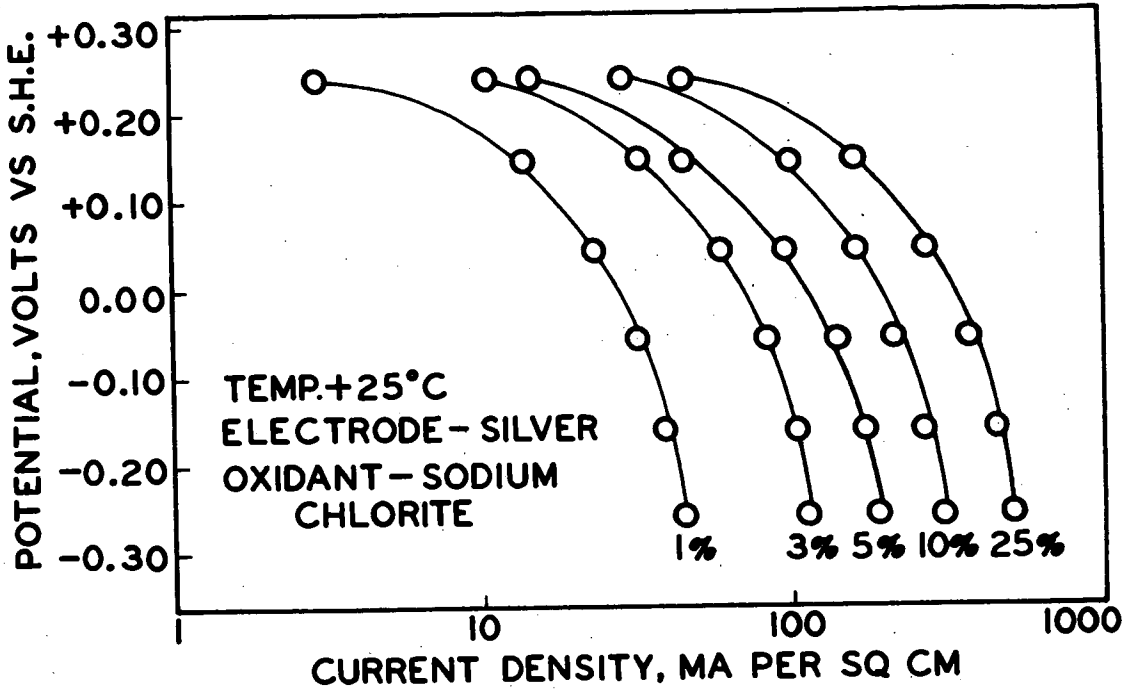


FIGURE 1
EFFECT OF CONCENTRATION

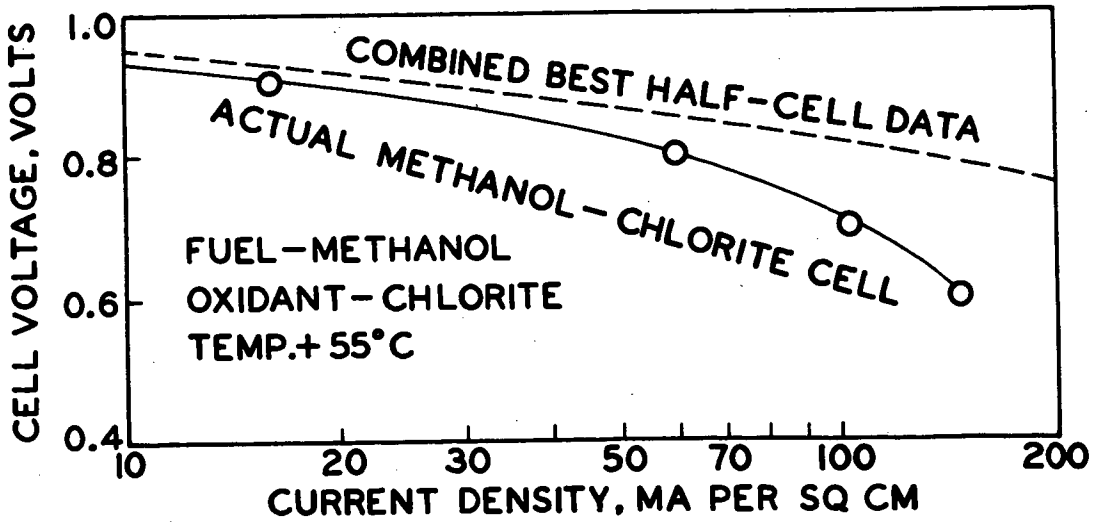


FIGURE 2
FUEL CELL POLARIZATION CURVES

Anodic Oxidation of Derivatives of Methane, Ethane and
Propane in Aqueous Electrolytes

H. Binder,
A. Kohling,
R. Krupp,
K. Richter, and
G. Sandstede

Battelle-Institut e.V., Frankfurt/Main, W. Germany

Abstract*

The behavior of twelve partially oxidized hydrocarbons of the paraffin series during anodic oxidation was studied at temperatures of 25° C and 80° C using an immersed Raney platinum electrode in 5 N sulfuric acid and 5 N potassium hydroxide. Galvanostatic potential-current density curves gave information on the differences in reactivity of the individual substances; the degree of conversion was determined from potentiostatic-coulometric measurements.

With Raney platinum electrodes anodic oxidation of carboxylic acids was observed only in sulfuric acid at 80° C to give carbon dioxide and water. With sulfuric acid at 25° C and with potassium hydroxide electrolyte practically no reaction was observed. One exception was formic acid which is the only carboxylic acid that, as a reduction product of carbon dioxide, still contains a reactive hydrogen atom attached to the carbonyl-C atom. Even at room temperature, it is oxidized at a considerable rate both in sulfuric acid and potassium hydroxide solution.

At a temperature of 80° C, the polarization involved in the conversion of alcohols is generally smaller in potassium solution than in sulfuric acid. With the exception of methanol, the reaction in 5 N potassium hydroxide proceeds up to the step of carboxylic acid.

Methanol can be oxidized to carbon dioxide in alkalies as well as in acids. Oxidation of ethanol in sulfuric acid leads to complete conversion to carbon dioxide; the evaporation of acetaldehyde formed as an intermediate must be prevented.

In the case of isopropanol, the reaction proceeds only to acetone; this in turn is nearly inactive. At reasonable potentials only small current densities are observed both in alkalies and in acids even at 80° C. The oxidation of acetone probably only proceeds via its condensation products.

The polyvalent alcohols glycol and glycerol can be converted at considerable current densities both in sulfuric acid and potassium hydroxide solution even at room temperature. In acid solutions, the oxidation proceeds up to carbon dioxide.

* Complete manuscript not received in time for inclusion in Division Preprints.

MECHANISM OF ANODIC OXIDATION OF ORGANIC
COMPOUNDS ON PLATINUM

by

V. S. Bagotzky

Institute for Electrochemistry
Academy of Sciences, USSR

Abstract*

The oxidation of organic compounds (alcohols, aldehydes, formic acid, etc.) on platinum electrodes is greatly affected by adsorption phenomena. Adsorption of reacting species on the inhomogeneous surface leads to a fractional reaction order, which is valid over a large concentration range. Increasing oxygen-coverage of the surface lowers the reaction-rate by an exponential law. Three arrests on the oxygen part of the charging curve on platinum correspond to three regions of current decrease on anodic current-potential curves.

Oxidation and reduction reactions are also affected by adsorption of surface active ions or molecules. In some cases this influence can be attributed to blocking action and to desorption of reacting species from the surface.

The experimental results are interpreted on the bases of a nonelectrochemical rate-determining step - dehydrogenization with formation of adsorbed H-atoms or oxidation by adsorbed OH-radicals.

* Complete manuscript not received in time for inclusion in the Divisional Preprints.

The Oxidation of Olefins and Paraffins In Low Temperature Fuel Cells

M. J. Schlatter

California Research Corporation, Richmond, California

We concluded that a low temperature hydrocarbon fuel cell might be feasible when we found that current could be drawn from an ethylene or propane depolarized platinized porous carbon electrode for a sustained period at 80°C and that under these conditions the hydrocarbon was completely oxidized.¹ Similar results with these and some other hydrocarbons have since been reported from other laboratories.^{2,3}

Further studies of the behavior of hydrocarbons on platinized porous carbon electrodes in aqueous sulfuric acid electrolytes are discussed in this paper. Results from rotating disk and small platinum foil electrodes have been reported by other members of our group.⁴

We chose to use platinized porous carbon electrodes for hydrocarbon product studies in order to make enough product for quantitative determination. Porous carbon and graphite are electrically conducting, resistant to acidic and basic electrolytes, and are available in a variety of porosities and surface areas. Further modification by chemical treatment is also possible.

The use of porous electrodes for electrochemical measurements and for electrocatalyst studies does result in some problems. These difficulties are shared by those working with "practical" fuel cell electrodes. The theory of porous electrodes is inadequate at present. However, it is receiving much attention because it is probable that the practical fuel cell electrodes will be porous structures. This is necessary if large electrocatalyst surface areas and high fuel cell power densities are to be attained.

Time-dependent polarization leading to unstable current-potential behavior complicates the use of current-potential measurements in the evaluation of porous electrodes which are depolarized with saturated hydrocarbons. These difficulties can be avoided by using pseudo steady-state currents after step changes in electrode potential. This procedure gives current-potential curves similar to those obtainable by potential-sweep methods with small electrodes and shows promise for use in the detailed comparison of very different electrodes and systems. From these curves, large differences in behavior of olefins and paraffins can be seen. It is clear that the unstable current-potential behavior with paraffins at high constant currents is not due to inadequate mass transfer immediately adjacent to the electrode but rather to the lower currents that can be supported by paraffins as the electrode potential is polarized above peak current potentials. Electrode poisoning occurs in this potential region with the formation of an oxide film on the electrode. This could inhibit adsorption of the paraffins and reduce the number of

effective catalyst sites for the paraffin oxidation. The potential at which this effect will dominate over the tendency for the current to increase with increasing potential differs with different fuels and probably depends on their ability to inhibit formation of the oxide film or to remove it as it is formed. With olefins, the potential of peak current is more positive than that of an oxygen counterelectrode.

Hydrocarbon depolarized electrodes were also found to be much more sensitive to inhibiting influences than electrodes depolarized with more reactive fuels. Different types of inhibition by air and oxygen and by extreme polarization of a fuel cell anode were observed and interpreted. When carbon monoxide was injected into the feed stream to a propane or propylene depolarized electrode, an improvement of performance resulted. No effect was evident when carbon dioxide was injected in this way. Preliminary experiments were made to evaluate the possibility of using inhibition data in the study of porous electrode activity and behavior. However, the factors affecting the shape and size of these inhibition peaks are complex; and more study will be required before they are completely understood or before significant application of these techniques can be expected.

Apparatus and Methods

1. Product Studies

The apparatus used for our new hydrocarbon product studies is shown in Figure 1. It differs slightly from that described before.¹ Fritted-glass separators fused in place are used instead of ion exchange membranes to separate the three cell compartments. A means of equalizing pressure is provided to minimize flow of electrolyte from one compartment to another. The Ascarite "carbon dioxide" absorption tube is preceded by a condensate trap, Drierite and Anhydron, to remove sulfuric acid spray and water. Ascarite and Drierite follow the Ascarite "carbon dioxide" absorption tube to exclude moisture and atmospheric carbon dioxide.

The apparatus was thoroughly flushed with the hydrocarbon used before weighing the Ascarite tube at the beginning of each experiment. At the end of an experiment, hydrocarbon flow was continued until at least 2 liters of gas passed through the anode in order to remove all carbon dioxide product from the cell. Additional flushing for an equal period gave changes in the weight of the Ascarite tube of the order of ± 0.5 mg.

Constant cell currents were maintained by automatically varying the load resistance as was previously described.

Current and anode potential versus SCE at 25°C were recorded on a calibrated dual-pen Varian recorder. The reference electrode was a Beckman saturated calomel electrode maintained at room temperature (25°C) and connected to a Luggin capillary through a long, small-diameter bridge filled with the fuel cell electrolyte. The anode potential versus the saturated calomel electrode (SCE) was sensed by a Keithley Model 600A electrometer with recorder output. Potentials in this paper are reported versus NHE with the sign of the oxygen electrode positive relative to the hydrogen electrode.

2. Potential-Step Voltammetry

In its simplest form the apparatus used for potential-step voltammetry consisted of a cell like that used for the product studies but modified for half-cell studies by substituting a platinum gauze cathode for the oxygen electrode. Current through the cell was provided by a storage battery in series with variable resistors. Anode potential was controlled by manually adjusting these resistors. Current and potential were sensed and simultaneously recorded as previously described.

Recently we have used one function of a versatile two-stage constant potential/constant current d.c. power source in place of the manually controlled system. The preregulator uses a magnetic amplifier and controlled rectifiers. The second regulator stage uses power transistors with an adjustable gain amplifier for control.

In the constant potential mode, the potential difference between the fuel cell anode and a reference electrode is sensed by an electrometer amplifier. The output of this is compared with an adjustable reference voltage. The difference is then used, through an operational amplifier, to maintain the anode at constant potential.

Slow response of the fuel cell anode potential with changes in cell current requires time delay circuits to limit the rate of change of the power supply output. This is accomplished through variable capacitor feedback to the operational amplifier which controls the power to the test cell.

3. Air and Oxygen Inhibition Experiments

The apparatus used was similar to that for potential-step voltammetry. Current was supplied to the cell from a storage battery through variable resistors. Control circuits provided for automatic constant current operation.

Inhibition data were obtained by injecting 2.48-ml portions of air, oxygen, and other gases into the fuel gas stream before it passed through a platinized porous carbon anode. This was done by means of a Wilkins XA-202 gas sampling valve.* Propane and propylene were each used as fuels. Flow rates were measured on the exit gas from the anode compartment using a soap film flowmeter.

4. Electrodes

The electrodes used were similar in form to those previously described.¹ Each consists of a porous carbon cylinder 2-1/2 inches long, 3/4-inch OD, and 1/2-inch ID which is fitted tightly to a 1/2-inch OD impervious graphite tube. This tube serves as electrical conductor and gas conduit. The lower end of the cylinder is closed with a graphite plug, and the joints are sealed with an Epon resin.**

* Wilkins Instrument and Research, Inc.,
P.O. Box 313, Walnut Creek, California.

** Epon 828-2, Shell Chemical Company.

As used in the experiments described here, the electrodes were sometimes new; in other cases they had been used extensively with various fuels and electrolytes at different conditions.

The platinum was applied to the electrode by two general methods:

Method A

The electrode was electroplated for 20 minutes at ambient temperature and at a current density of 40 ma/cm² in a 1.25- or 1.5-inch diameter graphite cup which served as the counter electrode. The plating solution was drawn into and forced out of the electrode every 2 minutes during the plating period. Sometimes this procedure was repeated. Different plating solutions were used as shown in Table I.

More active electrodes were obtained by Method B:

Method B

The porous carbon electrode blank was impregnated with chloroplatinic acid solution containing 10 weight per cent platinum. It was dried on a rotating graphite mandrel in an air oven at 140°C and was reduced for 3 hours in a stream of hydrogen at 400°C. It was then mounted and sealed.

The preparation and geometric areas of the electrodes are summarized in Table I.

New Product Studies

Product data which we reported previously¹ showed that ethylene and propane can be completely oxidized in fuel cells at 80°C. New data for propane reconfirm this result, but data from n-butane suggest that incomplete oxidation of this hydrocarbon can occur under some conditions that give complete oxidation with propane.

The new results were obtained using a platinized porous carbon electrode (Electrode A, Table I) with sulfuric acid at 80°C. In this series, the cell was operated at 25.2 ma (0.84 ma/cm²). A slow decrease in cell voltage occurred with time. When the cell voltage dropped close to the point where the current could no longer be maintained, a short period at open circuit restored the electrode activity for further operation under load. Initial anode potentials for propane and n-butane under load were of the order of 0.45-0.50 volt (versus NHE) increasing with time to 0.74-0.84 volt.

The present series consisted of two propane experiments followed by three n-butane experiments and another propane experiment. The product results are summarized in Table II.

The "carbon dioxide" values for n-butane are 6-8% above theory based on the ampere-hours produced during the experiments. This excess could come from direct chemical oxidation of n-butane by oxygen transported through the electrolyte from the cathode chamber or from some electrooxidation of the electrode carbon. This would give more carbon dioxide per coulomb than can be obtained from a hydrocarbon. However, similar oxygen transport or carbon oxidation would

be expected in the propane experiments which gave the theoretical amount of "carbon dioxide." Partial oxidation products absorbed from the fuel cell exit gas stream with the carbon dioxide could also account for a high "carbon dioxide" value. Calculations were made for Experiment No. 4 (Table II) which gave 108.2% of the theoretical amount of "carbon dioxide." Cases were considered where the partial oxidation product was butanol, butanone, butyric acid, or acetic acid. Assuming complete recovery of the products, values of 9 to 14 weight per cent of partially oxidized n-butane in the "carbon dioxide" product were calculated. As it is improbable that all of the partially oxidized materials reached and were retained in the Ascarite tube, even higher percentages of partially oxidized products are possible.

The Evaluation of Hydrocarbon Depolarized Electrodes

As part of a program to improve the performance of platinized porous carbon electrodes, propane was chosen as a test material. With this hydrocarbon we had considerable difficulty in using conventional potential-current plots because of time-dependent polarization.

The nature of these difficulties can be seen more clearly from curves showing the change in electrode potential with time at constant current. This is illustrated in Figure 2. Here the over-all cell voltage is plotted against time. Sequence numbers and current are shown on each curve. Curves 1 and 2 were both recorded at 10 ma current and show the effect of the removal of active products from preelectrochemical reactions. Curve 6, also at this current, may illustrate further removal of active materials or the formation of inhibitors during the intermediate experiments. The rapid decrease in potential at the end of the 100-ma curve is characteristic of time-potential curves at higher currents and would be accentuated at still higher currents.

Another example of the effect of preelectrochemical reactions on time-dependent polarization is seen in Figure 3. Here an attempt to remove impurities and intermediates from an electrode was made by use of a repetitive test cycle. The anode was caused to cycle from 0.44 to 0.84 volt under load with return from 0.84 to 0.44 volt at open circuit. In the course of several cycles, it was expected that impurities would be removed and reproducible cycles obtained. In practice, variations in treatment of the electrode immediately before test caused more change in the first few cycles than later; but a continuing decrease in polarization time and increase in recovery time occurred as each series progressed. Preliminary tests were made in order to select appropriate current ranges for each cycle test series. The curves in Figure 4 are derived from these data. The upper curve represents the time in minutes for the anode to polarize from 0.44 to 0.84 volt plotted against the number of test cycles. The lower curve shows the corresponding data for recovery times from 0.84 to 0.44 volt.

Data like these were used by us in some cases for comparing electrodes or for investigating the effects of pretreatments on the behavior of a particular electrode.

Potential-Step Voltammetry

In an effort to simplify the interpretation of electrochemical

data from porous electrodes, we attempted to establish steady-state conditions by prolonged operation of bubbling hydrocarbon depolarized electrodes at a series of fixed potentials.

If no change in the catalytic activity of a fuel cell anode occurs, it should be possible to establish a steady-state current at constant potential for each set of conditions. In this situation current would be determined by the catalytic activity of the electrode surface and the steady state concentrations of reactants and products at the electrode surface.

With our platinized porous-carbon anodes depolarized with propane, this steady state is not reached in 4 hours at 80°C at 0.74 volt; though in many cases the current was decreasing very slowly at this time. A curve obtained using automatic potential control is shown in Figure 5.

Many experiments were carried out to determine the reproducibility of constant potential-current data and to provide a basis for selecting test sequences which would give satisfactory, comparable data in the least time. These curves appear to consist of two sections. In the first part, the current is changing rapidly. This section of the curve appears to be affected considerably by recent electrode history and is sometimes difficult to reproduce. After a period which varies in length, depending on the recent history of the electrode, a steady state is approached. With some fuels, such as ethylene and propylene, the current will remain constant for long periods; with others, such as propane, a gradual, slow decline in current is observed. With the electrodes listed in Table I, 20 to 60 minutes was ordinarily used at each controlled anode potential.

Fuel Cell Oxidation of Propane, Isobutane, Propylene, Ethylene, and Hydrogen in 5 N H₂SO₄ at 80°C

The anode current densities corresponding to different anode potentials were measured by a constant-potential technique for propane, isobutane, and propylene. These data are shown in Figure 6. The points shown correspond to current densities 20 minutes after the indicated potential was established. A current-potential curve for hydrogen on this electrode is included for reference.

Curves showing ethylene and propylene performances are plotted in Figure 7. These data were taken from constant-current experiments, but in these cases the rates of polarization with time were so slow that the data actually were obtained at nearly constant potentials. The ethylene curve is similar to the propylene curve but is displaced slightly toward more favorable lower anode potentials.

The shapes of the propane and propylene curves correspond fairly closely with potential-sweep data obtained using a platinum-foil electrode and 2 N sulfuric acid electrolyte. These data are plotted in Figure 8.

From Figure 6 it is seen that with the saturated hydrocarbons, propane and isobutane, the anode current increases to a maximum between 0.6 to 0.7 volt and then decreases as the anode is polarized further. This type of behavior appears to be general for

saturated hydrocarbons. It is also found with saturated hydrocarbons that at anode potentials above those for maximum current, the rate of decay of current increases as the anode potential increases; and "steady-state" currents require more time to establish. Up to a point it is possible to draw more current temporarily by decreasing the load resistance but at the expense of rapidly increasing polarization. Thus, with the constant-current methods ordinarily used in determining electrode current-dependent polarization, a "limiting" current is found beyond which unstable electrode behavior is observed.

Olefins differ from paraffins in their current-potential behavior (Figures 6, 7). They give higher "steady-state" currents as the potential is increased beyond the region of interest for hydrocarbon-oxygen fuel cells. Therefore, they do not give the "limiting" currents found with saturated hydrocarbons.

Air and Oxygen Inhibition of Hydrocarbon-Depolarized Electrodes

The study of hydrocarbon-depolarized electrodes is complicated by their susceptibility to various inhibiting influences. Such effects were much less apparent with hydrogen, methanol, and other more active fuels.

Inhibition by air or oxygen is one such effect. It is also one of practical interest as there is always some possibility that air or oxygen may contact a fuel cell anode.

Typical inhibition behavior is observed when a little air enters the feed line to a hydrocarbon fuel cell anode. A severe polarization occurs resulting in a very sharp increase in anode potential. This change in potential can amount to several tenths of a volt, and the electrode potential can approach that of an oxygen cathode.* Recovery of the original anode potential may require a minute or two or several minutes, depending on the hydrocarbon involved, the amount of air admitted, and the temperature.

Variable "induction" periods which often occur on startup with saturated hydrocarbons are also probably due to air inhibition. Examples with propane are shown in Figure 9. Curves 1 and 2 were obtained on successive days with Electrode A (Table I). The exposure to air differed, and Curve 1 shows less inhibition than Curve 2. In other cases "induction" periods from a few minutes to several hours have been observed. All of the curves show a gradual initial drop in potential followed by a rapid transition to a potential minimum and then a gradual increase to a constant open-circuit potential. These open-circuit potentials, although reasonably constant in a particular experiment, do vary a little from one experiment to another.

Similar behavior is noted when enough oxygen is injected into the propane stream to bring the potential of the electrode above 0.8 volt. Inhibition curves obtained with Electrode F (Table I)

* In our equipment, open-circuit potentials of 1.058 to 1.081 volt were observed with platinized porous carbon electrodes at 80°C in 5 N sulfuric acid electrolyte with oxygen at 1 atmosphere pressure. Lower potentials are, of course, obtained under load.

resulting from the injection of different amounts of oxygen are shown in Figure 10. Here the transitions are less abrupt than those in Figure 9. The electrodes are quite different, but there may also be some differences in the nature of the inhibition.

Polarization of a propane-depolarized platinized porous carbon electrode under load until potentials above approximately 0.94 volt are attained also inhibits the electrode. Operation at open circuit then gives a gradual initial drop in potential followed by a rapid transition to open-circuit potential. The effect of the electrode potential on the potential recovery curves at open circuit for Electrode G (Table I) is shown in Figure 11. In these experiments the cell was operated at 100 ma current until the anode polarized to the test potential. The current was then manually adjusted as required to hold this potential for 7 minutes. The circuit was then opened, and the potential recovery curve was recorded. The single exception to this is the highest potential case. Here the circuit was opened as soon as the 1.14-volt potential was reached.

A slight convex shape of the recovery curve is seen after operation at potentials as low as 0.64 volt. Pronounced effects, however, are not observed until 0.94 volt or more is reached.

The possibility that hydrocarbon fuel cell anodes can be inhibited by polarization may be of practical concern. With present oxygen-propane fuel cells, anode recovery at open circuit is rapid even after brief short circuit because the potential of the anode cannot exceed the relatively low potential of the polarized oxygen counterelectrode. However, if oxygen electrode efficiencies are improved, their potentials could be high enough to substantially inhibit some saturated hydrocarbon depolarized anodes. These potentials can also be attained in a multiple fuel cell arrangement or in a fuel cell where the anode half cell is coupled with a halogen-depolarized electrode or other high potential system.

The inhibited electrode is restored by contact with propane in due time. The activity toward propane can also be restored rapidly by injecting small amounts of more reactive fuels into the propane stream. Reactivation of Electrode F (Table I), which had been polarized under load, can be seen in Figure 12. Here hydrogen was used as the reactive fuel.

The experiments described in the following section were carried out to obtain more information about the characteristics and the nature of the air and oxygen inhibition. In this series some factors were maintained constant. The same seasoned electrode (Electrode D, Table I) was used in all experiments. The air or oxygen volume injected into the hydrocarbon feed stream was 2.48 ml in each case. The electrolyte was nominally 5 N sulfuric acid. It was changed at intervals, but some variation in concentration occurred because of evaporation of water by the gases passing through the anode compartment.

Variables studied are temperature (40-80°C), hydrocarbon fuel (propane, propylene), hydrocarbon flow rate (5-15 ml/min), oxygen content of the injected inhibiting gas (air, oxygen), anode current (including open-circuit studies), and anode potential at the time of injection of the inhibiting gas.

Temperature Effects

The effect of temperature on the inhibition of propane-depolarized anodes was studied by repeated injections of air into the propane feed stream at 40°C, 60°C, and 80°C at flow rates of 5, 10, and 15 ml/min. Single representative curves are shown in Figure 13. These data show that the rate of inhibition is so rapid that any effects of temperature are masked by other factors which control the shape of the ascending inhibition part of the anode potential curve. The slightly slower increase of the 40°C curve suggests that inhibition may be more rapid at higher temperatures, but this observed difference is within the limits of experimental error. The inhibition peak potentials are close to the same value in these series. The height and shape of the peaks do differ, however, with different electrodes and with changing activity of the same electrode.

After the initial break, the anode potential recovers logarithmically with half recovery at 8.0, 1.72, and 0.82 minutes at 40°C, 60°C, and 80°C, respectively.

a. Effects of Hydrocarbon Flow Rate Through the Anode

The effects of hydrocarbon flow rate through the anode on the inhibition and recovery of propane anode potential were investigated at 40°C, 60°C, and 80°C. The data for the series at 80°C are typical and are shown in Figure 14. Comparable oxygen inhibition data for propane at 80°C are shown in Figure 15, while Figures 16 and 17 give corresponding curves for propylene.

One effect of the threefold increase in hydrocarbon flow rates in these experiments is to increase rate of inhibition of the electrode. The time from the beginning to maximum inhibition is very little more than the time required to sweep the air or oxygen into the electrode. The amount of inhibition in a given series was not affected by flow rate to any great extent. This is seen in the relatively constant height of the peaks in the anode potential curves. The greatest variations occurred in the experiments at the lowest flow rates. These were the first experiments in each series, and they were often carried out before the propane open-circuit potential had stabilized. The variations of this potential are seen at the extreme left on the curves. The recovery times, as well as the rates of the initial inhibition of the anode, are decreased by increasing the rate of hydrocarbon flow through the anode. Data illustrating this are plotted in Figure 18. These data were taken from curves such as those shown in Figures 14 to 17. A decrease in recovery time with increase in hydrocarbon rate is common to all of the experiments. The effect is less with propane than with propylene. Decreasing the temperature of a propane-depolarized anode from 80°C to 60°C slowed the recovery time after air poisoning. However, the two curves showing the recovery time, as a function of propane flow rates through the electrode, are parallel and show a comparatively small effect. Recovery times after poisoning with oxygen are much more dependent on the propane flow rate. This is most pronounced as the rate is increased from 5 to 10 ml/min.

b. Effects of Load Current During Air Poisoning

The effects of operating a propane anode under load when air is injected are seen in Figure 19. These curves show the same rapid

response obtained at open circuit. The higher the anode potential at the time of air injection, the higher the inhibition peak. The incremental difference in peak height, however, is not linearly related to the difference in potentials at the time of injection. As the inhibition peak potentials increase, the recovery times also increase.

c. Effects of Oxygen Compared With Air and the Amount of Oxygen in Anode Poisoning

Direct comparisons of Figures 14 with 15 and 16 with 17 show the effects of substituting an equal volume of oxygen for air in poisoning a platinized porous carbon anode which is depolarized with propane or with propylene. In general, the peak heights in a given series are about the same. Even though peak heights are greater with oxygen, recovery times are only slightly longer than for air; and recovery time decreases more with increased hydrocarbon flow rate than is the case after air inhibition. The relative increase in the inhibition peaks for oxygen compared with air is less for propylene than for propane.

Other experiments carried out with Electrode F (Table I) show that the same peak heights are obtained if air or an amount of oxygen equal to that contained in the air is injected. The difference in peak heights with air and oxygen inhibition is due only to the fivefold difference in the amount of oxygen injected. Data showing the effects of amount of oxygen and air injected on the height of the inhibition peaks are plotted in Figure 20. The effect on the shape of the curves is seen in Figure 10. With this electrode, when the inhibition peak potentials get above 0.54 volt, there is a residual effect from one oxygen injection on the next. In a series of four injections of 4 ml of oxygen at 20-minute intervals, the peak potentials increased successively from 0.54 to 0.60 volt, even though the electrode potential returned to the same value between injections. The scatter of points in Figure 20 is due largely to such residual effects as the points were obtained at different times and in different sequence over a period of 3 days.

Discussion

1. Products from Hydrocarbon Oxidation

The new product work reported here confirms our earlier conclusion that propane can be completely oxidized in a fuel cell at 80°C. The n-butane data suggest, however, that hydrocarbon oxidation need not be complete and that higher molecular weight hydrocarbons may have a greater tendency to give isolatable intermediates. We have also observed odors tentatively identified as acetic acid and acetaldehyde from some ethylene "fuel cell" oxidations at potentials approximating those of the oxygen electrode. Such odors have also been reported by Young and Rozelle.⁵

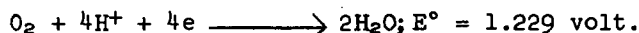
Small amounts of side products would not be detectable by our analytical method, but we have ample electrochemical evidence for preelectrochemical reactions at open circuit with saturated hydrocarbons. We also see effects of a buildup of some inhibitors on our electrodes after prolonged experiments with various hydrocarbons. These can often be largely removed by drawing hot distilled water through the electrode, cleaning the cell, and using fresh electrolyte.

It is apparent that more product work should be done, especially at constant anode potentials and with some higher hydrocarbons. There appears to be a good chance of isolating intermediates which may provide clues to the hydrocarbon oxidation reaction mechanisms.

2. Oxygen Electrode Potentials

Although in this paper we are concerned mainly with the hydrocarbon fuel cell anode, oxygen and oxide films play an important part in inhibition behavior and in affecting hydrocarbon electrode performance at high polarizations.

The over-all oxygen half-cell reaction in acid is:



The equilibrium potential for this reaction can only be established on platinum when extreme care is used in preparing the electrode surface and in eliminating impurities from the test cell.^{6,7} Usually, mixed potentials are obtained which give open-circuit voltages of the order of 1.06-1.09 volts versus NHE. In our equipment we have observed open-circuit potentials of 1.058-1.081 volt at 80°C in 5 N sulfuric acid. At the present state of development of the oxygen electrode in acid, therefore, there is an inherent loss of at least 0.18 volt before any current is drawn.

By present standards an oxygen electrode that will operate at 0.85 volt at 100 ma/cm² would be considered quite good. This corresponds to a 35% loss in efficiency due to the oxygen electrode alone in a hydrocarbon-oxygen fuel cell.

3. Hydrocarbon Electrode Potentials

Reaction potentials calculated from free energy changes for the complete oxidation of some hydrocarbons with oxygen are shown in the following table. Theoretical reversible half-cell potentials were calculated from thermodynamic data.

	Theoretical Reversible Potential for Complete Oxidation, Volts	Hydrocarbon Half-Cell Potential*
		Volt Versus NHE
Ethane	1.079	0.150
Ethylene	1.136	0.093
Propane	1.091	0.138
Propylene	1.127	0.102

* Calculated O₂ half-cell potential in acid, 1.229 volts vs NHE.

With ethane and propane the actual half-cell potential may go as low as or even lower than the calculated values. The actual processes occurring at the anode, however, are different from those represented by the theoretical reversible hydrocarbon half cells.

Thus, the saturated hydrocarbon potentials are probably determined largely by the concentration of hydrogen atoms resulting from dissociative adsorption of the hydrocarbons on the electrocatalyst. The open-circuit potentials observed with the olefins are always more positive than those from the paraffins. It may be that with olefins the adsorbed hydrogen atoms react to hydrogenate unsaturated species, giving paraffins which are then displaced by the more strongly adsorbed olefins.² During our air and oxygen inhibition experiments, when the feed to the electrode was changed from propane to propylene, the open-circuit potential gradually changed from about 0.29 volt to 0.50-0.55 volt. The reverse change occurred when propane was supplied to the electrode again.

Under load the polarization behavior of olefins and paraffins is very different. Even structures as closely related as ethane and propane can show large differences. This is revealed clearly by comparison of plots of pseudo steady-state current densities at constant potential versus potential (Figure 6). At low potentials the paraffins will often support higher currents than the olefins. With the paraffins, "steady-state" currents increase to maxima between 0.6 and 0.7 volt. This is well below the potential of an oxygen fuel cell cathode. With olefins, the current rises rapidly with potential beyond the fuel cell range. These differences are probably due to differences in the relative rates of reactions of paraffins and olefins at or with the oxide film on platinum. All electrodes are not alike in their detailed behavior, and we believe that pseudo steady-state current-potential curves should be valuable in more searching evaluations of electrodes, in studying the behavior of different fuels, and in determining the effects of operating variables.

The importance of oxygen and oxide films in determining the behavior of platinized porous carbon electrodes is also seen when inhibition behavior is considered.

4. Air and Oxygen Inhibition of Hydrocarbon Depolarized Electrodes

Three general types of inhibition of hydrocarbon depolarized porous carbon electrodes have been described in this paper. These are (1) inhibition of hydrocarbon oxidation at an oxygen or air saturated electrode, (2) inhibition of a hydrocarbon saturated electrode by injected oxygen or air, and (3) inhibition of a hydrocarbon depolarized electrode by extreme polarization. All of these are probably due to adsorbed oxygen or catalytically inactive oxide films, yet they differ in detail. Recovery of electrode activity depends on the removal of the inhibitor. The rate at which this occurs will depend on the nature of the inhibitor but also on the fuel and operating conditions. Some factors affecting electrode potential and inhibition behavior will be discussed in the following section.

a. Nature of Mixed Anode Potentials

Initially, when two electrochemically active species contact different sites on the surface of an electrode, potentials characteristic of the processes involved tend to develop at these two points. This causes electrons to move in the conducting electrode in order to equalize the potential of the electrode surface. If a net transfer of electrons from one species to the other can occur, reactions proceed.

The net anode potential observed will be intermediate between the open-circuit potentials that would be observed for the two reactants separately. Its magnitude will depend on the polarization of the two processes which, in turn, will be determined by the polarizability and effective "current density" as determined by relative surface coverage for each reactant. To a lesser extent, it will depend on the geometry of the electrode, on the way in which the two species are distributed on the surface, and on the location of the connections of the potential-measuring device to the electrode.

From this picture, it is obvious that the coupled oxidation-reduction of a hydrocarbon and oxygen at a platinized electrode in contact with electrolyte can be purely "electrochemical." There need be no direct contact of the reacting species. In this sense this oxidation-reduction differs from direct chemical reaction. It differs also from heterogeneous catalytic oxidation-reduction processes where an electrolyte is not present. These, in general, are believed to require that the reactants contact or at least be adsorbed close to one another. Direct chemical reaction can, of course, also be involved in the electrode recovery process.

b. Selective Adsorption and the
Relative Strengths of Adsorption
of Reactants and Inhibitors on Platinum

(1) Induction Period Due
to Oxygen Adsorption

Oxygen is known to adsorb rapidly and completely to give a 1:1 ratio of oxygen atoms to surface platinum atoms.⁸ On the other hand, coulometric methods show that only about 10% of the surface platinum atoms which will adsorb oxygen are covered with propane at 1 atmosphere pressure in the presence of dilute sulfuric acid electrolytes. Similar coverages are obtained with ethane. Only slightly higher coverages were obtained with ethylene and probably with propylene.⁴ Thus, when an electrode is exposed to air or oxygen before contacting with hydrocarbon, the catalyst sites which can catalyze the electrochemical oxidation of propane or propylene are covered. When placed in an electrolyte, this electrode develops the oxygen potential. When propane or propylene is passed through this electrode, the potential is not affected to any extent at first. Gradually, a few molecules of oxygen leave the electrode surface and are removed by the hydrocarbon stream; or they are removed by a catalyzed chemical reduction. This allows the hydrocarbon access to the catalyst sites. The amount of hydrocarbon reacting increases as oxygen is removed; and then suddenly, as the amount of oxygen is reduced to a low level, the hydrocarbon potential resulting from chemisorption becomes dominant; and there is a sudden decrease in net anode potential. After the oxide layer has been removed (approximately 0.55 volt), the potential approaches the open-circuit potential logarithmically with time. The rate is determined by the rate of oxidation of the hydrocarbon and by the capacitance of the ionic double layer.

Following inhibition of this kind (Figure 9), the potential drops below the open-circuit hydrocarbon potential and then gradually rises to the open-circuit potential. This may be due to formation of a particularly active catalyst surface as the oxide film is reduced.

This may survive long enough to dissociate more propane than the usual catalyst, giving a higher hydrogen atom concentration than is normal for the electrode surface.

Behavior after polarization under load to the oxygen potential is very similar to that from oxygen inhibition after standing for several hours in the presence of air and absence of propane (Figure 11). Recovery after polarization and presumably after the other similar inhibition processes can be assisted by injecting hydrogen into the hydrocarbon feed (Figure 12).

Inhibition to the oxygen potential by oxygen injection into a propane stream passing through the electrode does have some different characteristics (Figure 10). This type of inhibition requires a comparatively large amount of oxygen. The propane adsorbed on this electrode must be displaced by oxygen, and this may be a comparatively slow process. More than a monolayer of oxygen may also be retained on the platinum or loosely adsorbed on the graphite. This may result in the more gradual transition to the open-circuit propane potential observed with this system.

If inhibition results from injection of a small amount of air or oxygen which is added to a stream of hydrocarbon passing through an electrode, the effect is immediate because open sites on the catalyst surface are available. If the amount of air or oxygen is not enough to displace all of the hydrocarbon, electrochemical reduction and elimination of the added oxygen begins immediately and hydrocarbon potential is soon established again.

A detailed understanding of the factors which determine the shape, height, and inhibition peak potentials might lead to useful methods for evaluating and studying the behavior of porous electrodes. However, the situation is complex; and more study will be required before complete understanding or useful application of inhibition techniques can be expected.

Acknowledgment

The author gratefully acknowledges the support of the Army Materiel Command, Harry Diamond Laboratories, and the Advanced Research Projects Agency, Washington, D.C., and wishes to thank Drs. G. H. Denison, D. R. Rhodes, L. R. Griffith, and R. T. Macdonald for helpful discussions of this work.

Literature Cited

1. M. J. Schlatter, American Chemical Society, "Symposium on Recent Advances in Fuel Cells," Division of Petroleum Chemistry Preprints, 6, No. 4, B-149 to 168, September 3-9, 1961; Chapter 15, "Fuel Cells"; Vol. II, G. J. Young, editor, Reinhold Publishing Corporation, New York, 1963.
2. W. T. Grubb, "Low Temperature Hydrocarbon Cells," 17th Annual Power Sources Conference, Atlantic City, New Jersey, May 21-23, 1963.
3. C. E. Heath and C. H. Worsham, Chapter 14, "Fuel Cells," Vol. II, G. J. Young, editor, Reinhold Publishing Corporation, New York, 1963.

4. L. R. Griffith and D. R. Rhodes, presented at the Buffalo Meeting of the American Institute of Chemical Engineers, May 6-8, 1963. To be published.
5. G. J. Young and R. B. Rozelle, Chapter 3 in "Fuel Cells," G. J. Young, editor, Reinhold Publishing Corporation, New York, 1960.
6. J. P. Hoare, Extended Abstracts of the Theoretical Division, Abstract No. 165, The Electrochemical Society, April 15-18, 1963.
7. J. O'M. Bockris and A. K. M. S. Huq, Proc. Roy. Soc. London, 237A, 277 (1956).
8. M. Breiter, C. A. Knorr, and W. Völkl, Z. Elektrochemie, 59, 681 (1955).

:vld

TABLE I
PREPARATION AND GEOMETRIC AREAS OF SOME PLATINIZED POROUS CARBON ELECTRODES

Electrode	Carbon Base Material*	Geometric Area, cm ²	Platinum Solution (H ₂ PtCl ₆)		Method	Number of Times Plated
			Wt % Pt	Other Components		
A	139	29.9	0.5	0.12 N HCl	A	6
B	139	31.8	0.5	0.12 N HCl	A	1
C	139	30.0	0.5		A	2
D	139	30.6	0.5	0.12 N HCl	A	2
E	139	35.4	0.5	0.12 N HCl	A	3
			0.5		A	2
F	FC-14	24.0	10.0	0.12 N HCl	A	1
G	139	33.0	0.5	0.04 wt % Pb Acetate	B	1
					A	1

* No. 139, Stackpole Carbon Company,
 St. Mary's, Pennsylvania
 No. FC-14, Pure Carbon Company,
 St. Mary's, Pennsylvania

TABLE II
 CARBON DIOXIDE PRODUCED BY FUEL CELL
 OXIDATION OF HYDROCARBONS

Expt. No.	Fuel	Current, ma	Current Density, ma/cm ²	Time, hr	Energy, amp-hr	Carbon Dioxide		
						Theory, mg	Found, mg	Per Cent of Theory
1	Propane	25.2	0.84	18.37	0.463	114.2	113.7	99.4
2	Propane	25.2	0.84	18.00	0.453	111.8	112.3	100.5
3	n-Butane	10.0	0.84	6.53	0.169	42.6	45.4	106.6
4	n-Butane	25.2	0.84	41.75	1.053	266.0	287.7	108.2
5	n-Butane	25.2	0.84	14.17	0.356	90.3	96.7	107.1
6	Propane	25.2	0.84	14.67	0.369	91.0	90.1	99.0

Propane: $C_3H_8 + 5 O_2 \longrightarrow 3CO_2 + 4H_2O$ (20-electron change)
 $3/20$ mole CO_2 per faraday = 246.5 mg CO_2 per amp-hr.

Butane: $C_4H_{10} + 6-1/2 O_2 \longrightarrow 4CO_2 + 5H_2O$ (26-electron change)
 $4/26$ mole CO_2 per faraday = 252.7 mg CO_2 per amp-hr.

FIGURE 1
APPARATUS FOR HYDROCARBON PRODUCT STUDIES

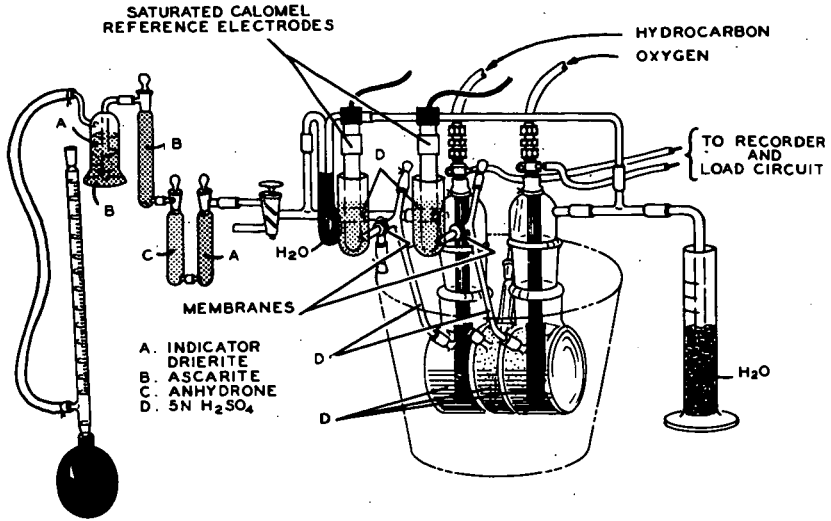


FIGURE 2
PROPANE-OXYGEN FUEL CELL POLARIZATION WITH TIME AS A FUNCTION OF LOAD.
PLATINIZED POROUS CARBON ELECTRODES (TABLE I, ANODE B; CATHODE C)
5N SULFURIC ACID ELECTROLYTE, 80°C

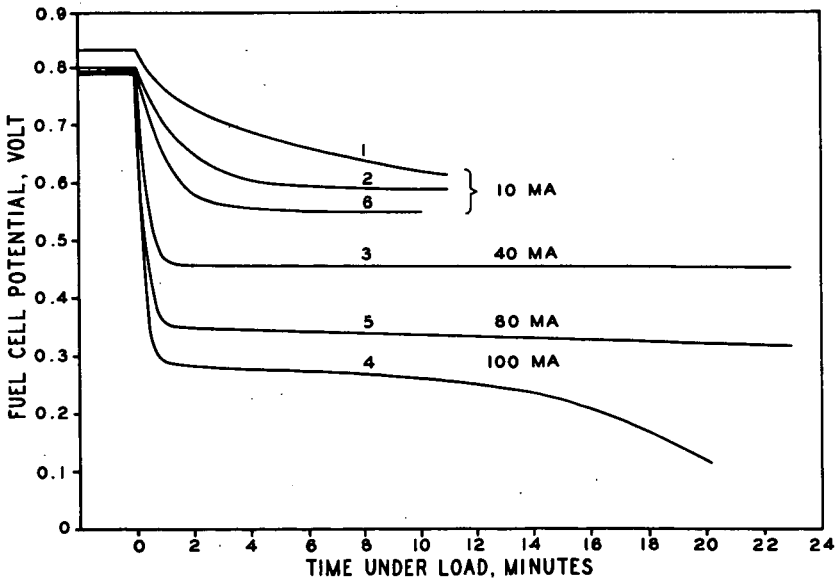


FIGURE 3

FUEL CELL ANODE POLARIZATION DATA WITH PROPANE AT 80°C
 PLATINIZED POROUS CARBON ANODE (TABLE I, ELECTRODE C)
 5N SULFURIC ACID ELECTROLYTE

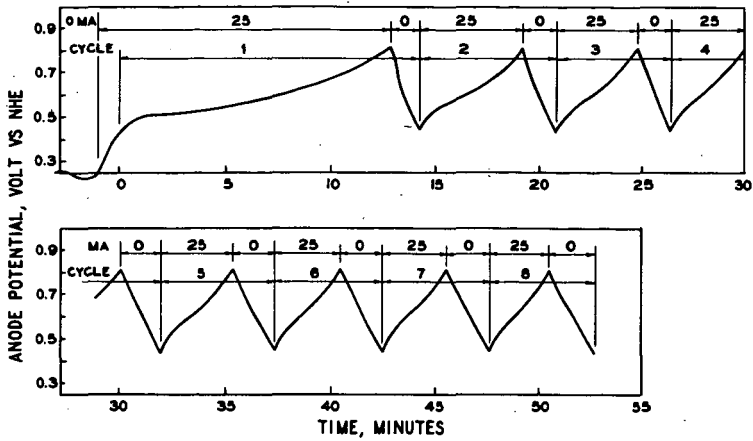


FIGURE 4

THE EFFECT OF THE NUMBER OF LOAD-RECOVERY CYCLES ON POLARIZATION TIME AND
 RECOVERY TIME OF A PROPANE DEPOLARIZED ELECTRODE AT 80°C
 PLATINIZED POROUS CARBON ANODE (TABLE I, ELECTRODE C)
 5N SULFURIC ACID ELECTROLYTE

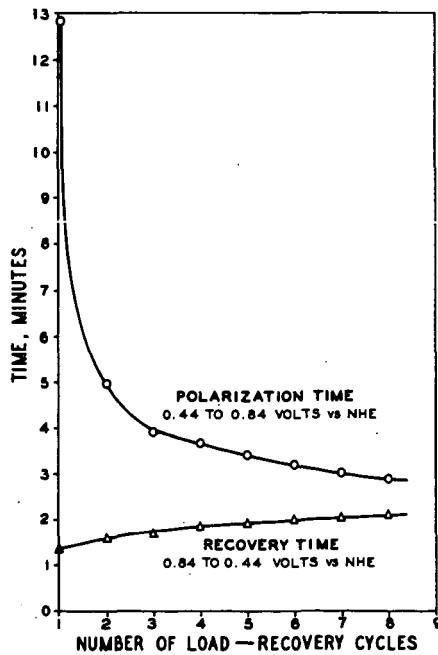


FIGURE 5

CURRENT DECREASE WITH TIME FOR PROPANE-DEPOLARIZED FUEL CELL ANODE AT CONSTANT POTENTIAL
 POTENTIAL AUTOMATICALLY CONTROLLED AT 0.74 VOLT VS NHE
 PLATINIZED POROUS CARBON ANODE (TABLE I, ELECTRODE D)
 5N SULFURIC ACID ELECTROLYTE, 80°C

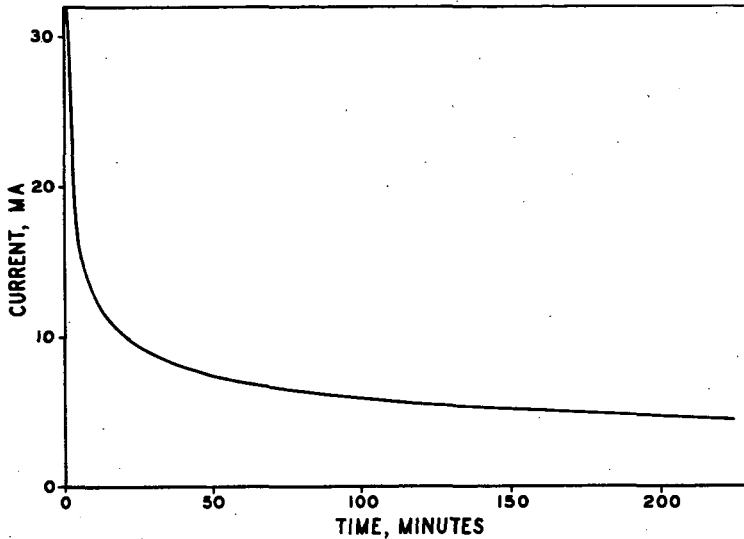
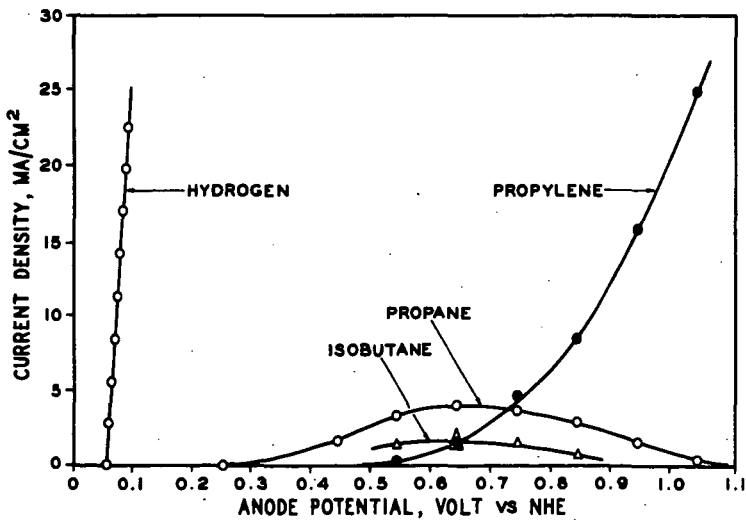


FIGURE 6

THE EFFECT OF ANODE POTENTIALS ON FUEL CELL "STEADY STATE" CURRENT DENSITIES FOR
 HYDROGEN, ISOBUTANE, PROPANE AND PROPYLENE
 PLATINIZED POROUS CARBON ANODE (TABLE I, ELECTRODE E)
 5N SULFURIC ACID ELECTROLYTE, FUEL RATE 10 ml./MINUTE, 80°C



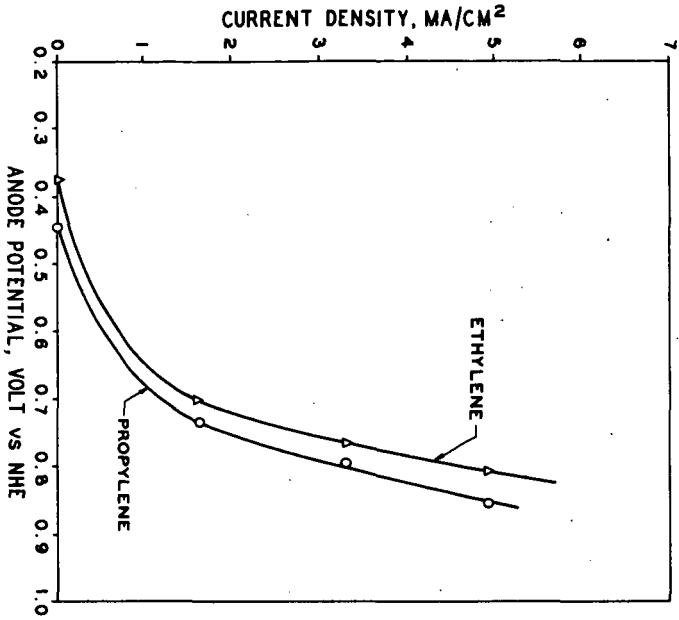


FIGURE 7
 THE EFFECT OF ANODE POTENTIALS ON FUEL CELL "STEADY STATE" CURRENT DENSITIES FOR ETHYLENE AND PROPYLENE PLATINIZED POROUS CARBON ANODE (TABLE I, ELECTRODE D) IN SULFURIC ACID ELECTROLYTE, FUEL RATE 10 ml/MINUTE, 80°C

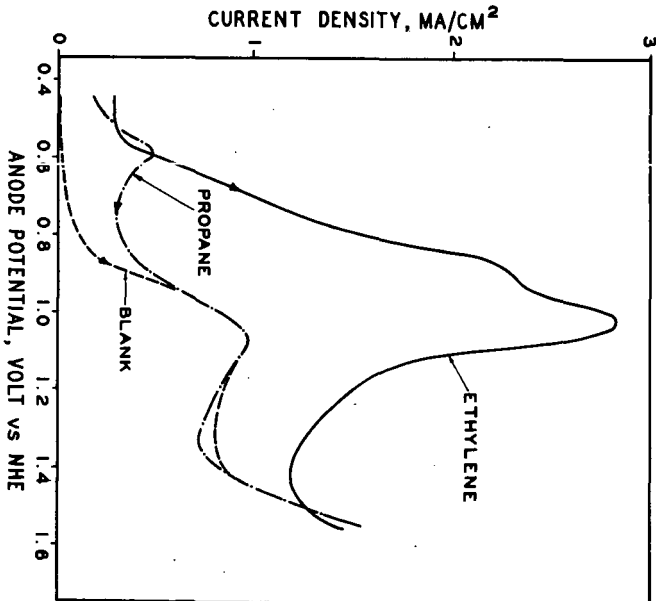


FIGURE 8
 CURRENT POTENTIAL CURVES FOR ANODIC OXIDATION OF PROPANE AND PROPYLENE ON PLATINIZED PLATINUM FOIL SATURATED SOLUTIONS, 2N SULFURIC ACID ELECTROLYTE, SWEEP RATE 16.7 mV/SEC, 80°C

FIGURE 9

INDUCTION PERIODS BEFORE ESTABLISHING THE PROPANE OPEN CIRCUIT POTENTIAL OF AN AIR POISONED PLATINIZED POROUS CARBON ELECTRODE (TABLE I, ELECTRODE A) 5N SULFURIC ACID ELECTROLYTE, 80°C

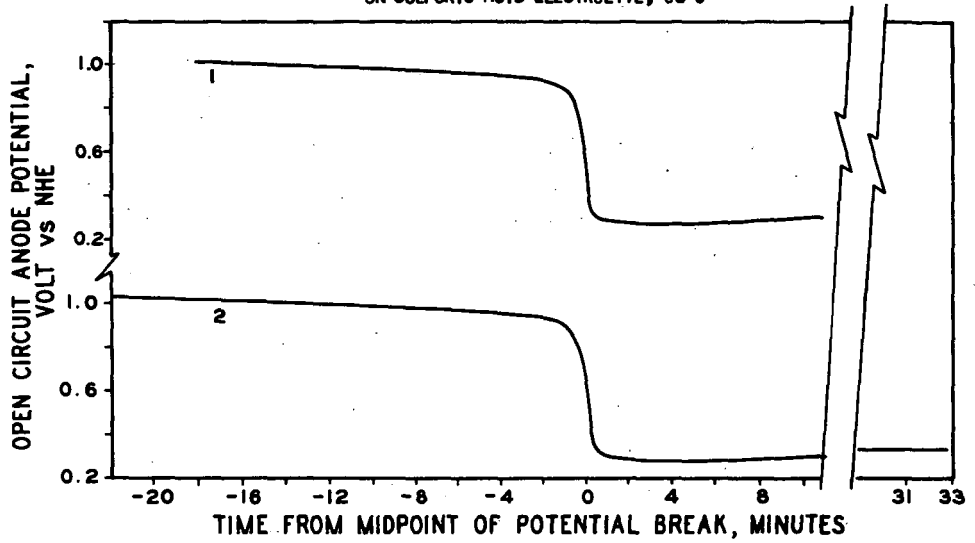


FIGURE 10

OXYGEN INHIBITION OF A PROPANE DEPOLARIZED ELECTRODE PLATINIZED POROUS CARBON ELECTRODE (TABLE I, ELECTRODE F) 1N SULFURIC ACID, 80°C

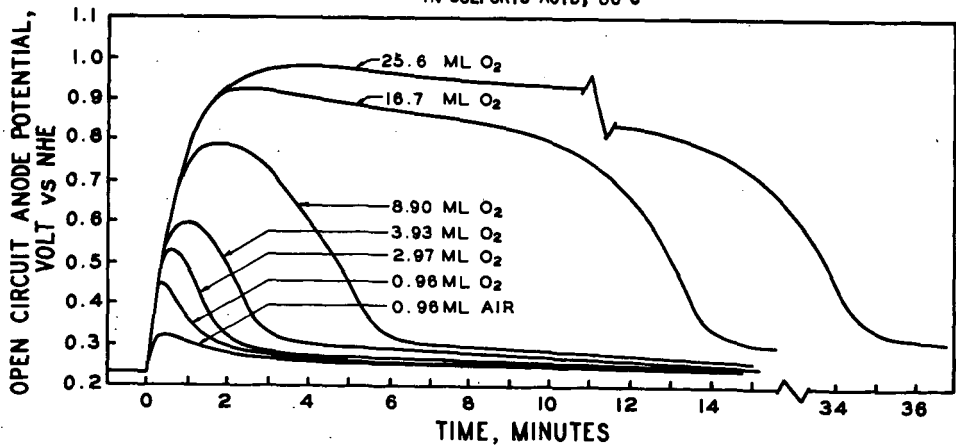


FIGURE 11

EFFECT OF ANODE POTENTIAL OF A PROPANE DEPOLARIZED ANODE ON
 RECOVERY AT OPEN CIRCUIT
 PLATINIZED POROUS CARBON ELECTRODE (TABLE I, ELECTRODE G)
 5N SULFURIC ACID ELECTROLYTE, 80°C
 AT 0.54 TO 0.94 VOLTS, LOAD ADJUSTED TO MAINTAIN POTENTIAL CONSTANT FOR
 7 MINUTES BEFORE RECORDING OPEN-CIRCUIT POTENTIAL

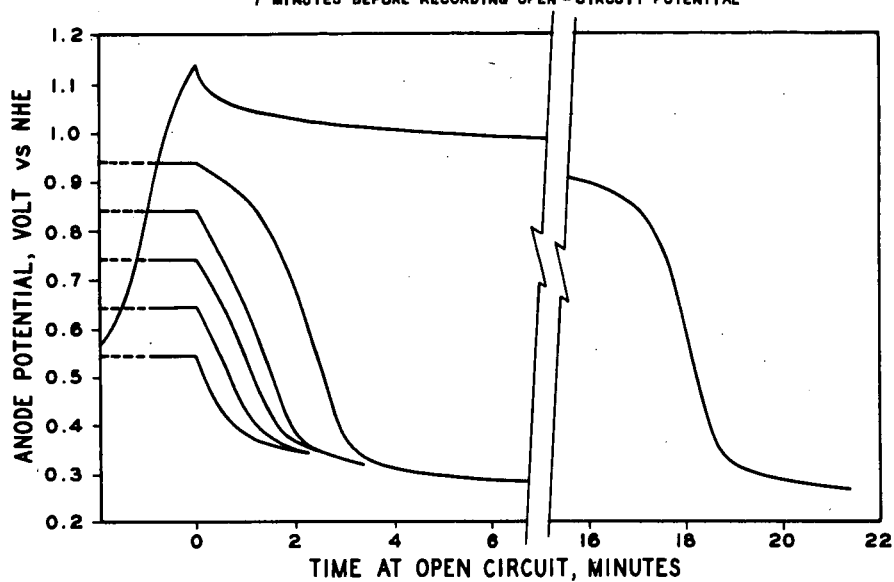
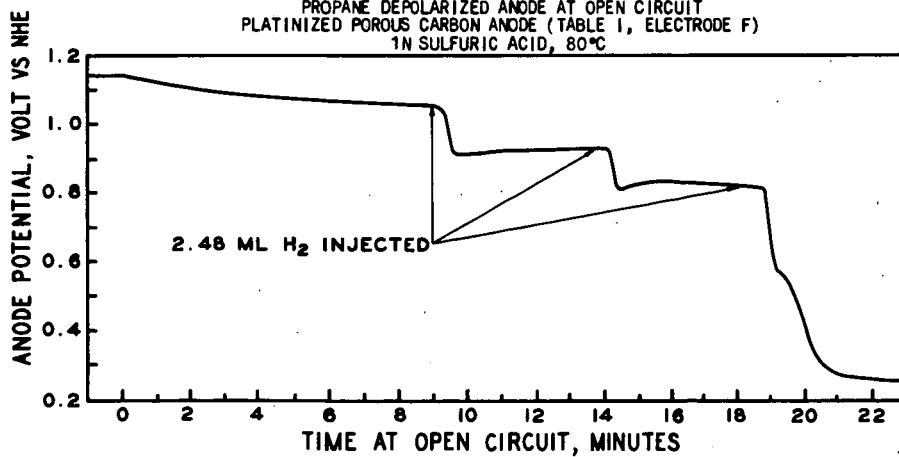


FIGURE 12

EFFECT OF INJECTED HYDROGEN ON THE RECOVERY OF A
 PROPANE DEPOLARIZED ANODE AT OPEN CIRCUIT
 PLATINIZED POROUS CARBON ANODE (TABLE I, ELECTRODE F)
 1N SULFURIC ACID, 80°C



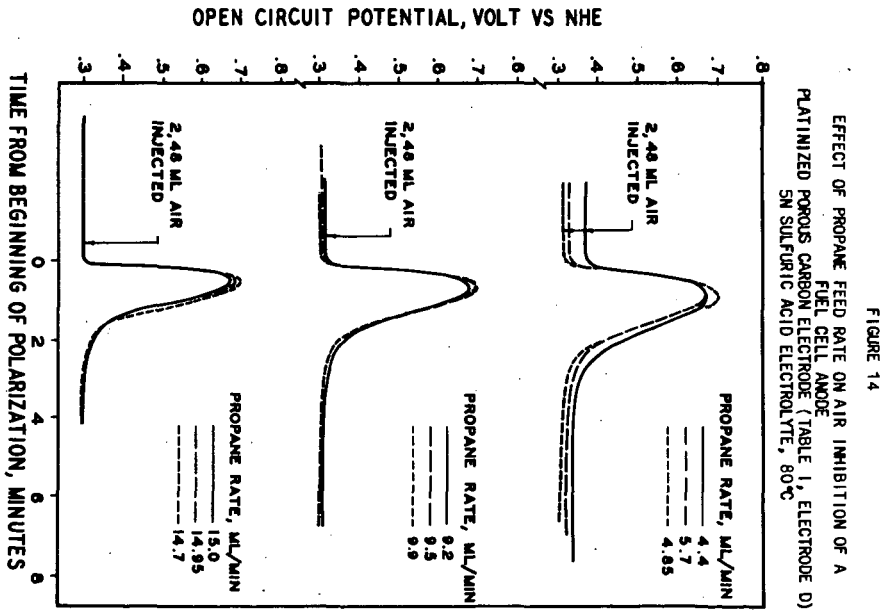
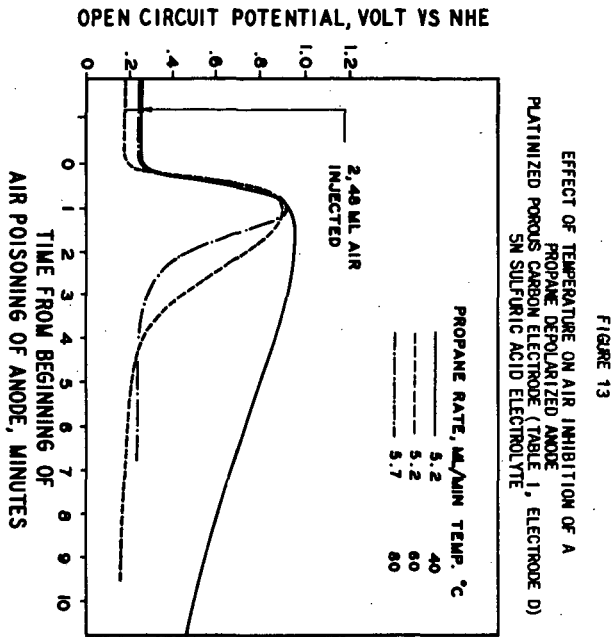


FIGURE 15
EFFECT OF PROPANE FEED RATE ON AIR INHIBITION OF A
FUEL CELL ANODE
PLATINIZED POROUS CARBON ELECTRODE (TABLE I, ELECTRODE D)
5N SULFURIC ACID ELECTROLYTE, 80°C

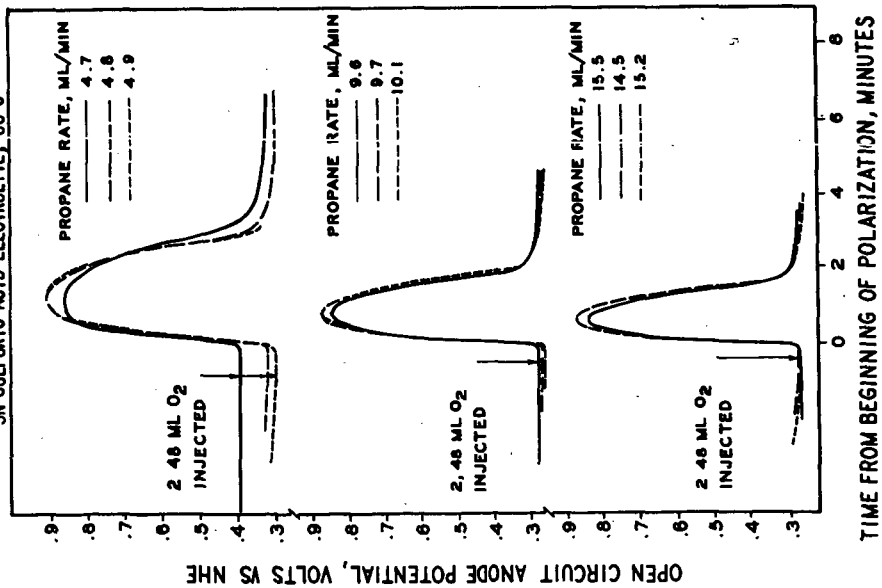


FIGURE 16
EFFECT OF PROPYLENE FEED RATE ON AIR INHIBITION OF A
FUEL CELL ANODE
PLATINIZED POROUS CARBON ELECTRODE (TABLE I, ELECTRODE D)
5N SULFURIC ACID ELECTROLYTE, 80°C

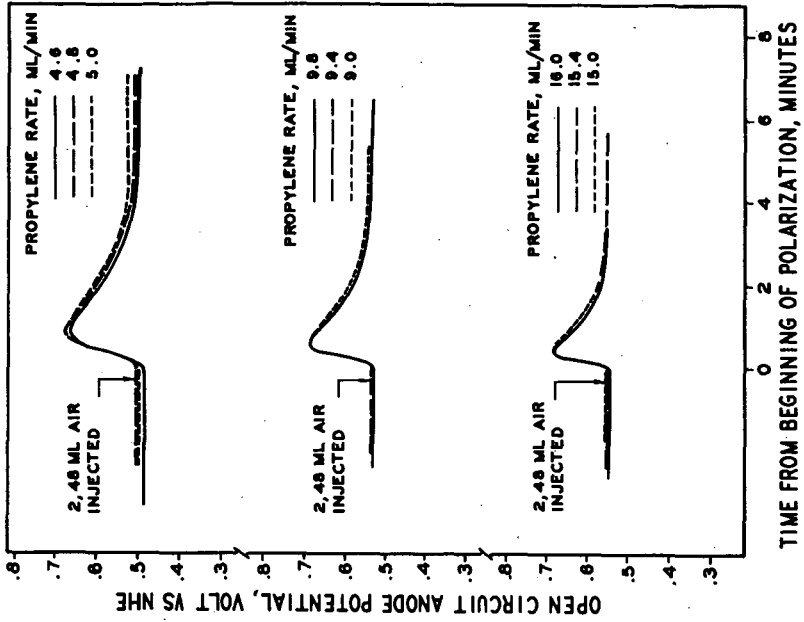


FIGURE 17

EFFECT OF PROPYLENE FEED RATE ON OXYGEN INHIBITION OF FUEL CELL ANODE PLATINIZED POROUS CARBON ELECTRODE (TABLE 1, ELECTRODE D) 5N SULFURIC ACID ELECTROLYTE, 80°C

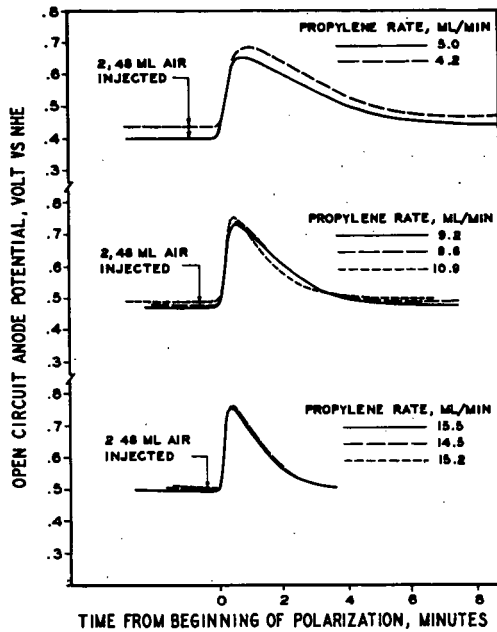


FIGURE 18

EFFECT OF HYDROCARBON FLOW RATE ON THE RECOVERY TIMES FOR A FUEL CELL ANODE AFTER INHIBITION WITH AIR OR OXYGEN PLATINIZED POROUS CARBON ELECTRODE (TABLE 1, ELECTRODE D) 5N SULFURIC ACID ELECTROLYTE, 80°C

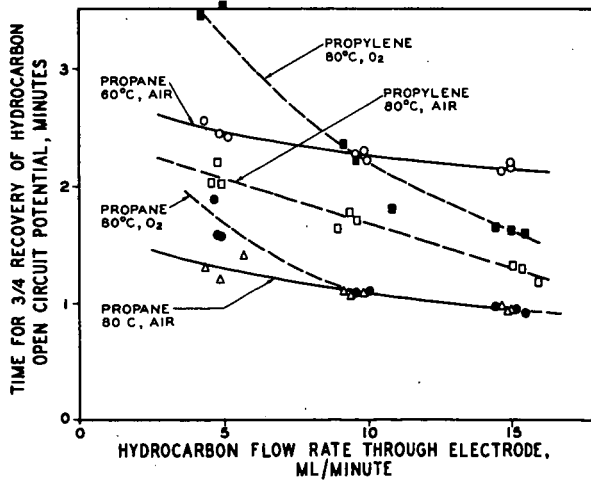


FIGURE 19

EFFECT OF LOAD CURRENT ON AIR POISONING OF A FUEL CELL ANODE
 DEPOLARIZED WITH PROPANE
 PLATINIZED POROUS CARBON ELECTRODE (TABLE I, ELECTRODE D)
 5N SULFURIC ACID, 80°C, PROPANE RATE 15 ml/MINUTE

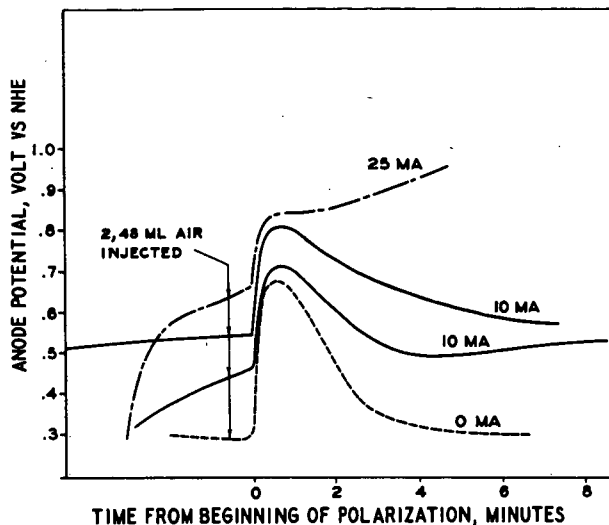


FIGURE 20

EFFECT OF THE AMOUNT OF AIR OR OXYGEN INJECTED ON THE INHIBITION OF
 A PROPANE DEPOLARIZED FUEL CELL ANODE
 PLATINIZED POROUS CARBON ELECTRODE (TABLE I, ELECTRODE F)
 1N SULFURIC ACID ELECTROLYTE, 80°C, PROPANE RATE 10 ml/MINUTE

